

**Fate of veterinary pharmaceuticals in  
soil: An experimental and numerical  
study on the mobility, sorption and  
transformation of sulfadiazine.**

**Inaugural-Dissertation**

zur  
Erlangung des Grades  
Doktor der Agrarwissenschaften (Dr.agr.)

der  
Hohen Landwirtschaftlichen Fakultät  
der  
Rheinischen Friedrich-Wilhelms-Universität  
zu Bonn

Vorgelegt im März 2006  
von  
Diplom Geoökologin  
Anne Wehrhan  
aus Jena

Referent: Prof. Dr. Harry Vereecken

1. Korreferent: Prof. Dr. Wulf Amelung

2. Korreferent: Prof. Dr. Thilo Streck

Tag der mündlichen Prüfung: 26.06.2006

Gedruckt bei: Betriebsdirektion - Graphische Betriebe FZ-Jülich

Erscheinungsjahr: 2006

Diese Dissertation ist auf dem Hochschulschriftenserver der ULB Bonn

[http://hss.ulb.uni-bonn.de/diss\\_online](http://hss.ulb.uni-bonn.de/diss_online) elektronisch publiziert.

## Abstract

Among other veterinary pharmaceuticals sulfadiazine (SDZ) is a widely used antimicrobial substance in intensive livestock production to prevent and treat diseases. Up to 40 % of the administered sulfonamides are eliminated as microbial active substances with the excretions. Antibiotics such as sulfadiazine reach agricultural soils directly through grazing livestock or indirectly through the spreading of manure or sewage sludge on the field. Knowledge about the fate of antibiotics in soil is crucial to assess the environmental risk of these compounds, including possible transport to groundwater. Sorption, transport and transformation of  $^{14}\text{C}$ -labelled SDZ in a silty loam were investigated using batch-type and column experiments. The batch sorption/desorption experiments were conducted at various concentration levels (0.044 to 13 mg L $^{-1}$  initial solute concentration) and time-scales (0.75 to 272 days). Sorption of SDZ in the investigated soil was time-dependent and strongly non-linear with regard to the concentration. The time to reach the apparent sorption equilibrium was about 20 days. However, desorption was very slow and 41 days were insufficient to reach the desorption equilibrium. In annealed soil the sorption affinity was lower and the desorption was also very slow. Transport of  $^{14}\text{C}$ -labelled SDZ was investigated in disturbed soil columns at a constant flow rate of 0.26 cm h $^{-1}$  near saturation.  $^{14}\text{C}$ -SDZ was applied in different concentrations (5.7 or 0.57 mg L $^{-1}$ ) for either a short or a long pulse duration (7 or 70 hours). Breakthrough curves (BTCs) of  $^{14}\text{C}$ -SDZ and the non-reactive tracer chloride were measured. At the end of the leaching period the soil concentration profiles were determined. The peak maxima of the BTCs were delayed by a factor of 2 to 5 compared to chloride and the decreasing limbs are characterized by an extended tailing. The maximum relative concentrations differed as well as the eluted mass fractions, ranging from 18 to 83 % after 500 hours of leaching. Mineralization of SDZ during the batch and column experiments was neglectable. Inverse modelling techniques were used to identify relevant sorption processes of SDZ and its transformation products during the batch and column experiments. One-, two- and three-domain sorption models were tested, involving linear or non-linear, instantaneous equilibrium, rate-limited reversible and irreversible sorption. The various sorption concepts were included in a convective-dispersive transport model for the description of the column experiments. Models involving similar processes and complexity were necessary to describe the characteristic features of the batch and transport experiments. The non-linear sorption in the batch experiments was best described by the Freundlich sorption isotherm and may also be one reason for the pronounced tailing of the BTCs in the transport experiments. Rate-limited sorption accounts for the slow attainment of the apparent sorption equilibrium during the batch experiments and can also contribute to the tailing of the BTCs. However, sorption sites exhibiting instantaneous equilibrium sorption were required in addition to the kinetic sorption to describe both, the one-day adsorption and the BTCs of the column transport experiments with the long pulse duration. Only the consideration of irreversible sorption enabled

the description of the very slow desorption at the various experimental time scales as well as the description of the mass retained in the columns. Three-site sorption models exhibiting fast and slow equilibrium sorption as well as irreversible sorption were required for the description of the batch and transport experiments. Despite the high flexibility of the proposed model concept, the description of the soil concentration profiles in the soil columns failed. The optimal parameter set differed among the three transport experiments and were also different from the set describing the sorption experiments best. In soil-water systems SDZ was transformed into N<sup>4</sup>-acetylsulfadiazine, hydroxysulfadiazine and an unidentified, polar transformation product. In the peak of the BTCs, 12 to 43 % of the leached radioactivity was composed of the transformation products. The investigation of the underlying transformation pathways and their concentration- and time-dependency was impeded, because of the limitation to experimentally separate the sorption and transformation processes and because of the high detection limit of the analytical method. A further modelling approach was tested to investigate whether transformation of SDZ can explain the unexpected transport behavior. Common transformation assumptions were combined to the previous sorption concepts in the transport model. A model that considers reversible and irreversible kinetic sorption of SDZ with subsequent transformation of the reversibly bound species into a reversibly sorbing transformation product was able to describe the characteristic features of the BTCs and soil concentrations profiles. However, BTCs and soil concentration profiles could not be described simultaneously. Despite this incomplete process description, the obtained results have implications for the transport behavior of sulfadiazine in the field. Its leaching may be enhanced if it is frequently applied at higher concentrations.

## Kurzfassung

Sulfadiazin wird neben vielen anderen Veterinärpharmaka häufig in der intensiven Tierhaltung präventiv und therapeutisch als Antibiotikum eingesetzt. Bis zu 40 % der verabreichten Sulfonamide werden als aktive Substanzen vom Organismus wieder ausgeschieden. Durch weidende Tiere, Gülle- oder Klärschlammausbringung gelangen Antibiotika auf landwirtschaftlich genutzte Flächen. Kenntnisse über das Schicksal der Antibiotika im Boden sind entscheidend, um das Umweltrisiko und einen möglichen Austrag ins Grundwasser abschätzen zu können. Sorption, Transport und Transformation von  $^{14}\text{C}$ -markiertem Sulfadiazin in einem schluffigen Lehm wurden in Batch- und Säulenexperimenten untersucht. Die Sorptions/Desorptionsexperimente wurden in verschiedenen Konzentrationsstufen (0.044 bis  $13 \text{ mg L}^{-1}$ ) und mit verschiedenen Kontaktzeiten (0.75 bis 272 Tage) durchgeführt. Die Sorption von SDZ im untersuchten Boden war zeitabhängig und bezüglich der Konzentration stark nicht-linear. Nach ca. 20 Tagen stellte sich ein scheinbares Sorptionsgleichgewicht ein. Die Desorption verlief ebenfalls sehr langsam. 41 Tage reichten nicht aus, um ein Desorptionsgleichgewicht zu erreichen. Die Sorptionsaffinität von geblühtem Boden für SDZ war niedriger als in Boden mit organischer Substanz, aber auch hier war die Desorption sehr langsam. Der Transport von  $^{14}\text{C}$ -markiertem SDZ wurde in gestörten Bodensäulen nahe Sättigung bei konstanter Flußrate von  $0.26 \text{ cm h}^{-1}$  untersucht. Die Applikation von Sulfadiazin erfolgte in verschiedenen Konzentrationen ( $5.7$  oder  $0.57 \text{ mg L}^{-1}$ ) über eine lange oder kurze Pulsdauer (7 oder 70 h). Die Durchbruchkurven von Sulfadiazin und dem konservativen Tracer  $\text{Cl}^-$  wurden über 500 h aufgenommen. Nach Beendigung des Beregnungsexperiments wurde das Konzentrationsprofil im Boden bestimmt. Im Vergleich zu  $\text{Cl}^-$  waren die Peakmaxima der Durchbrüche von SDZ um einen Faktor 2 bis 5 verzögert. Die Durchbruchkurven sind durch ein ausgeprägtes Tailing gekennzeichnet. Die Maxima der relativen Konzentrationen variieren zwischen den verschiedenen Experimenten ebenso wie die eluierten Massenanteile nach 500 Stunden Beregnung (18 bis 83 %). Die Mineralisierung von SDZ während der Batch- und Säulenexperimente war vernachlässigbar gering. Die inverse Modellierung wurde eingesetzt, um relevante Sorptionsprozesse von SDZ und seinen Transformationsprodukten während der Batch- und Säulenexperimente zu identifizieren. Sorptionsmodelle mit ein, zwei und drei Domänen wurden getestet, wobei lineare oder nicht-lineare Sorptionsisothermen, instantane Gleichgewichtssorption oder Ratenlimitierte reversible oder irreversible Sorption berücksichtigt wurden. Zur Beschreibung der Transportexperimente wurden diese verschiedenen Sorptionskonzepte in ein konvektiv-dispersives Transportmodell eingebaut. Modelle ähnlicher Komplexität waren notwendig, um die Charakteristika der Batch- und Säulenexperimente zu beschreiben. Die Freundlich Sorptionsisotherme beschrieb die nicht-lineare Sorption in den Batchexperimenten am besten. Nicht-lineare Sorption kann auch eine Ursache für das ausgeprägte Tailing der Durchbruchkurven sein. Ratenlimitierte Sorption ist für das langsame Erreichen des scheinbaren Sorptionsgleichgewichtes verantwortlich und kann ebenso zum Tailing der Durchbruchkurven beitragen. Jedoch waren auch Sorptionsplätze mit instantanem Gleichgewicht notwendig, um die Sorp-

tion nach kurzer Kontaktzeit und die Durchbruchskurven der Transportexperimente mit langem Applikationspuls zu beschreiben. Nur die zusätzliche Berücksichtigung von irreversibler Sorption erlaubte sowohl eine Beschreibung der sehr langsamen Desorption während der verschiedenen Kontaktzeiten als auch die Beschreibung der in den Säulen verbliebenen Massenanteile. Drei Sorptionsdomänen mit schneller und langsamer reversibler sowie irreversibler Sorption waren für die Beschreibung der Batch- und Säulenexperimente notwendig. Trotz der grossen Flexibilität dieses vorgeschlagenen Modellkonzeptes konnten die Konzentrationsprofile in den Bodensäulen nicht beschrieben werden. Die optimalen Parametersätze variierten sowohl zwischen den drei Säulenexperimenten als auch zwischen Säulen- und Batchexperimenten. In Boden-Wasser Systemen wurde SDZ zu N<sup>4</sup>-Acetylsulfadiazin, Hydroxysulfadiazin und einem unidentifizierten, polaren Produkt transformiert. Diese Transformationsprodukte hatten einen Anteil von 12 bis 43 % an der elluierten Stoffmenge in den Peaks der Durchbruchskurven. Die Untersuchung der Konzentrations- und Zeitabhängigkeit der zu Grunde liegenden Transformationspfade wurde erschwert, da Sorption und Transformation experimentell nicht getrennt werden konnten und da die Nachweisgrenze der analytischen Methode sehr hoch war. Ein weiterer Modellansatz wurde getestet, um zu untersuchen, ob die Transformation von SDZ das unerwartete Transportverhalten erklären kann. Gängige Transformationsannahmen wurden in einem Transportmodell mit dem vorherigen Sorptionskonzept kombiniert. Ein Model, das reversible und irreversible kinetische Sorption von SDZ mit anschliessender Transformation des reversibel gebundenen Anteils in ein reversibel sorbierendes Transformationsprodukt berücksichtigt, war in der Lage, die Charakteristika der Durchbruchskurven und Konzentrationsprofile zu beschreiben. Jedoch konnten Durchbruchskurven und Konzentrationsprofile nie gleichzeitig beschrieben werden. Trotz dieser unvollständigen Prozessbeschreibung sind die erzielten Ergebnisse relevant für die Abschätzung des Feldverhaltens von SDZ. Sein Transport im Boden könnte verstärkt werden, wenn SDZ häufiger in höherer Konzentration appliziert wird.

# Contents

<b>Abstract</b>	<b>i</b>
<b>Kurzfassung</b>	<b>iii</b>
<b>List of Figures</b>	<b>ix</b>
<b>List of Tables</b>	<b>xvii</b>
<b>Abbreviations and Symbols</b>	<b>xix</b>
<b>1 General introduction</b>	<b>1</b>
1.1 Rationale . . . . .	1
1.2 Experimental and model approaches . . . . .	2
1.3 General objectives and outline of the thesis . . . . .	3
<b>2 Sorption of sulfadiazine in soil</b>	<b>5</b>
2.1 Introduction . . . . .	5
2.2 Sorption Theory . . . . .	8
2.2.1 One-domain sorption . . . . .	8
2.2.2 Two domain sorption . . . . .	10
2.2.3 Three domain sorption . . . . .	13
2.3 Materials and methods . . . . .	15
2.3.1 Experimental setup . . . . .	15
2.3.2 Sampling and analysis . . . . .	15
2.3.3 Data analysis and parameter estimation . . . . .	17
2.4 Results . . . . .	17
2.4.1 Experimental results . . . . .	17
2.4.2 Modelling results . . . . .	23
2.5 Discussion . . . . .	35
2.6 Conclusions . . . . .	40
<b>3 Transport of sulfadiazine</b>	<b>41</b>
3.1 Introduction . . . . .	41
3.2 Theory of solute transport . . . . .	43
3.2.1 Sorption models . . . . .	44
3.2.2 Isotherm-based models . . . . .	44

3.2.3	Attachment/detachment models . . . . .	47
3.3	Materials and Methods . . . . .	48
3.3.1	Soil columns . . . . .	48
3.3.2	Transport experiments . . . . .	49
3.3.3	Parameter estimation . . . . .	50
3.4	Results . . . . .	51
3.4.1	Transport and breakthrough curves of chloride . . . . .	51
3.4.2	Transport of SDZ - experimental results . . . . .	52
3.4.3	Transport of SDZ - modelling results . . . . .	54
3.5	Discussion . . . . .	64
3.6	Conclusions . . . . .	68
<b>4</b>	<b>Transformation and transport</b>	<b>71</b>
4.1	Introduction . . . . .	71
4.2	Materials and Methods . . . . .	74
4.2.1	Experiments . . . . .	74
4.2.2	Model approaches . . . . .	74
4.3	Results . . . . .	80
4.3.1	Experimental results . . . . .	80
4.3.2	Modelling results . . . . .	81
4.4	Discussion . . . . .	99
4.5	Conclusions . . . . .	100
<b>5</b>	<b>Final remarks</b>	<b>101</b>
5.1	Synthesis of results . . . . .	101
5.2	General conclusions . . . . .	104
5.3	Outlook . . . . .	105
	<b>Bibliography</b>	<b>107</b>
	<b>A Properties of sulfadiazine</b>	<b>115</b>
	<b>B Soil properties</b>	<b>116</b>
	<b>C Analysis of <sup>14</sup>C in liquid samples</b>	<b>118</b>
	<b>D Analysis of <sup>14</sup>C in soil samples</b>	<b>119</b>
	<b>E Transformation products</b>	<b>120</b>
E.1	Detection of the transformation products . . . . .	120
E.2	Identification of the transformation products . . . . .	121
E.3	Conclusions . . . . .	125



<b>F Mineralization of <math>^{14}\text{C}</math>-SDZ in wet soil</b>	<b>127</b>
F.1 Experimental setup . . . . .	127
F.2 Sampling and analysis . . . . .	128
F.3 Results . . . . .	128
F.4 Conclusions . . . . .	129
<b>G Occurrence of transformation</b>	<b>130</b>
G.1 Experimental setup . . . . .	130
G.2 Results . . . . .	131
G.3 Conclusion . . . . .	131
<b>H Chemicals and Instruments</b>	<b>133</b>
H.1 Chemicals . . . . .	133
H.2 Instruments . . . . .	134



# List of Figures

2.1	Sorption/desorption of SDZ in the short-term batch experiments A and B. Concentrations were measured after 1, 2, 4, 7 and 14 days for adsorption kinetics (A). Desorption steps (B) were carried out after 1, 2, 3, 4, 7 and 14 days. Time proceeded in the direction of the arrows. The fitted Freundlich isotherm for the adsorption after one day is given. . . . .	18
2.2	Sorption/desorption of SDZ in the intermediate-term batch experiment C. Concentrations were measured after 0.75, 2, 4, 7, 9 and 14 days for adsorption kinetics (filled symbols), desorption steps were carried out after 14, 21, 28, 35 and 42 days (empty symbols). Time proceeded in the direction of the arrows. The fitted Freundlich isotherm for the adsorption after 0.75 days is given. . . . .	19
2.3	Sorption/desorption of SDZ in the long-term batch experiment D. Desorption steps were carried out after 41, 84, 124, 163, 204 and 272 days. Time proceeded in the direction of the arrow. The fitted Freundlich isotherm for the adsorption after 41 days is given. . . . .	20
2.4	Desorption kinetics of SDZ in the long-term batch desorption experiment D. Sorbed concentrations $S(t)$ were normalized by the corresponding equilibrium adsorption concentration $S_{\text{adsorption}}(41\text{d})$ to illustrate the slow decrease. . . . .	20
2.5	Freundlich parameters a) $K_f$ and b) $m$ from adsorption and desorption experiments D and E. . . . .	21
2.6	Adsorption of SDZ in the long-term batch adsorption experiment E. Concentrations were measured after 1, 5, 11, 18, 25, 40 and 153 days. Time proceeded in the direction of the arrows. The fitted Freundlich isotherm for the adsorption after one day is given. . . . .	22
2.7	Adsorption kinetics of SDZ in the long-term batch adsorption experiment E. . . . .	22
2.8	Sorption/desorption of SDZ in annealed soil in batch experiment F. Concentrations were measured after 0.75, 2, 4, 7, 9 and 14 days for adsorption kinetics (filled symbols), desorption steps were carried out after 14, 21, 28, 35 and 42 days (empty symbols). Time proceeded in the direction of the arrows. The fitted Freundlich isotherm for the adsorption after 0.75 days is given. . . . .	23

2.9	Measured and optimized sorption in experiment E using the kinetic sorption model (RLS: rate-limited sorption). The dashed line is the equilibrium isotherm resulting from the optimized parameters. . . . .	24
2.10	Solute distribution among the various domains in a batch-system according to the 2S1R model at different concentration levels. Initial total solute concentrations were 0.038, 0.38 and 3.8 mg L <sup>-1</sup> from the top to the bottom figures. Experimental conditions A, B and their best fit parameters were used. The desorption step was conducted after 1 day by exchanging the solution phase completely. Solute concentrations are given in column a) as mass of solute in the domain per total batch volume [mg L <sup>-1</sup> ]. Normalized solute concentrations are given in column b), where solute concentrations in each domain are divided by the total solute concentration in the system ( $C_t$ ). . . . .	26
2.11	Solute distribution among the various domains in a batch-system according to the 2S1R model at different concentration levels. Initial total solute concentrations were 0.038, 0.38 and 3.8 mg L <sup>-1</sup> from the top to the bottom figures. Experimental conditions A, B and their best fit parameters were assumed. The desorption step was conducted after 10 days by exchanging the solution phase completely. Solute concentrations are given in column a) as mass of solute in the domain per total batch volume [mg L <sup>-1</sup> ]. Normalized solute concentrations are given in column b), where solute concentrations in each domain are divided by the total solute concentration in the system ( $C_t$ ). . . . .	27
2.12	Measured data of sorption experiments A, B, C, D, E with model predictions using the two-stage-one-rate sorption model (2S1R) and the best fit parameters of experiments A and B. . . . .	29
2.13	Measured data of sorption experiments A, B, C, D, E with model predictions using the two-stage-one-rate sorption model (2S1R) and the best fit parameters of experiment C. . . . .	29
2.14	Measured data of sorption experiments A, B, C, D, E with model predictions using the two-stage-one-rate sorption model (2S1R) and the best fit parameters of experiment D. . . . .	30
2.15	Measured data of sorption experiments A, B, C, D, E with model predictions using the two-stage-one-rate sorption model (2S1R) and the best fit parameters of experiment E. . . . .	30
2.16	Measured data of sorption experiments A, B, C, D, E and model predictions using the two-site-two-rate irreversible sorption model (2S2Rirx). The last three desorption steps of D and the last adsorption point of E were not involved in the inverse solution. The corresponding model values were determined by forward simulation. . . . .	32
2.17	Measured data of sorption experiments A, B, C, D, E with model predictions using the three-stage two-rate irreversible sorption model (3S2Rirx). . . . .	33

2.18 Measured data of sorption experiments A, B, C, D, E with model predictions using the three-stage two-rate irreversible sorption model, where irreversible sorption is independent of the sorption isotherm of the reversible sorption domain (3S2Rirrev). . . . . 34

2.19 Solute distribution among the various domains in a batch-system according to the 3S2Rirrev-model at different concentration levels. The initial total solute concentrations were 0.0089, 0.089, 0.89, 8.9 mg L<sup>-1</sup> from the top to the bottom figures. Experimental conditions D and the best fit parameters (Table 2.5) were used. Solute concentrations are given as mass of solute in the domain per total batch volume normalized by the total solute concentration in the system ( $C_t$ ). Adsorption kinetics during 200 days are given in column a). The desorption steps in column b) were conducted after 2 and 7 days by exchanging the solution phase completely. . . . . 36

2.20 Solute distribution among the various domains in a batch-system according to the 3S2Rirrev model at different concentration levels. The initial total solute concentrations were 0.0089, 0.089, 0.89, 8.9 mg L<sup>-1</sup> from the top to the bottom figures. Experimental conditions D and the best fit parameters (Table 2.5) were used. The desorption steps were conducted after 41 and 84 days by exchanging the solution phase completely. Solute concentrations are given as mass of solute in the domain per total batch volume [mg L<sup>-1</sup>] in column a). Normalized solute concentrations (divided by the total solute concentration in the system ( $C_t$ )) are given in column b). . . . . 37

2.21 Measured data of sorption experiment F with model predictions using the rate-limited sorption model (RLS: rate-limited sorption). The model parameters are:  $K_f = 5.023\text{mg}^{1-m}\text{L}^m\text{kg}^{-1}$ ,  $m = 1.11$ ,  $\alpha = 0.0046d^{-1}$ . . . . . 38

2.22 Measured data of sorption experiment F with model predictions using the two-site-one-rate sorption model (2S1R). The fitting parameters are given in Table 2.4. . . . . 38

3.1 The applied solute-soil-water distribution models. The boxes labelled with  $C$  represent the liquid phase with concentration  $C$ , the boxes  $S_i$ , with  $i=1,2,3$  represent the three sorption sites with the respective concentrations  $S$ . The arrows indicate the sorption process, where  $K_d$  is the distribution coefficient,  $K_f$  and  $m$  are the Freundlich coefficient and exponent,  $\alpha_2$  is the reversible ad- and desorption rate,  $\beta_i$  and  $\gamma_i$  are the one-way attachment and detachment rates, respectively. Less complex versions of each model were derived by omitting one or two sorption sites: The possible combinations for reversible and irreversible models are given below the models. The model names are composed of the number of sites, S (1 - 3), number of rates, R (0 - 5), sorption concept (lin: linear and Freu: Freundlich sorption isotherms, att: attachment/detachment model) and reversibility (rev: reversible, irrev: irreversible). . . . . 45

3.2	Breakthrough curves of chloride in the three columns with the fitted physical physical equilibrium curves. . . . .	52
3.3	Breakthrough curves of SDZ in the three columns plotted on a linear (a) and a logarithmic (b) scale. . . . .	53
3.4	Soil concentration profiles of resident $^{14}\text{C}$ concentrations in the three columns. . . . .	56
3.5	Normal (a) and semi-log (b) plots of the BTC for column A and different fits of the one-site models. The models with Freundlich sorption were fitted to the $\log_{10}$ -transformed data. . . . .	57
3.6	Semi-log plot of the BTC of column A and different model fits with a) two-site reversible and b) two- or three-site irreversible sorption models. For each model in Figure 3.6a both fits to the non-transformed (solid lines) and to the $\log_{10}$ -transformed (dashed or dotted lines) are given. In Figure 3.6b the 2S1R-lin-irrev, 2S2R-lin-irrev, 2S1R-Freu-irrev, 2S3R-att-irrev models were fitted to the non-transformed data, the other four models to the $\log_{10}$ -transformed data. . . . .	59
3.7	Semi-log plot of the BTC of column B (a) and C (b) and different fits of two- or three-site irreversible models. For column B (a) the 3S2R-Freu-irrev and the 3S5R-att-irrev models were fitted to the $\log_{10}$ -transformed data, while the other two models to the non-transformed data. For column C (b) the models 2S2R-lin-irrev and 2S3R-att-irrev were fitted to the non-transformed data, while the other two models to the $\log_{10}$ -transformed data. . . . .	60
3.8	Measured and modelled soil profiles of resident $^{14}\text{C}$ concentrations in column A. The reversible models are given in Figure 3.8a, the irreversible models in Figure 3.8b. . . . .	62
3.9	Measured and modelled soil profiles of resident $^{14}\text{C}$ concentrations in column B (a) and C (b). . . . .	63
3.10	Measured, fitted and predicted BTCs with the 3S5R-att-irrev model for experimental conditions A (a), B (b) and C (c). . . . .	67
4.1	Conceptual model involving isotherm-based sorption. The boxes labelled with $C_i$ represent the liquid phase concentration $C$ , the boxes $S_{ij}$ represent the sorbed concentrations at the separate sorption sites. The index $i = 1, 2$ indicates the solute number, the index $j = 1, 2, 3$ the sorption sites number. $K_{f,i}$ and $m_i$ are the Freundlich distribution coefficient and the Freundlich exponent, respectively, $f$ indicates the fraction of equilibrium sorption sites, $\alpha_i$ is the kinetic sorption rate coefficient, $\beta_{13}$ is the irreversible sorption rate coefficient and $\mu_1$ is the transformation rate coefficient. . . . .	75

4.2	Conceptual model involving attachment/detachment-based sorption. The boxes labelled with $C_i$ represent the liquid phase concentration $C$ , the boxes $S_{ij}$ represent the sorbed concentrations at the separate sorption sites. The index $i = 1, 2$ indicates the solute number, the index $j = 1, 2, 3$ the attachment/detachment sites number. Parameters $\beta_{ij}$ and $\gamma_{ij}$ are the attachment and detachment rate coefficients of solute $i$ at sorption sites $j$ , respectively, and $\mu_1$ is the transformation rate coefficient. . . . .	77
4.3	Conceptual model involving attachment/detachment-based sorption and three solutes. The boxes labelled with $C_i$ represent the liquid phase concentration of solute $i$ , the boxes $S_{ij}$ represent the sorbed concentration of solute $i$ at the separate sorption sites $j$ . Parameters $\beta_{ij}$ and $\gamma_{ij}$ are the attachment and detachment rate coefficients of solute $i$ at sorption sites $j$ , respectively, and $\mu_i$ is the transformation rate coefficient of solute $i$ . . . . .	79
4.4	BTCs of total $^{14}\text{C}$ , SDZ and its transformation products in column A.	80
4.5	BTCs of total $^{14}\text{C}$ , SDZ and its transformation products in column B.	81
4.6	Breakthrough curves of total $^{14}\text{C}$ , SDZ and one transformation product in column A. The symbols represent measurements and the lines (solid, dashed and dotted) model calculations. The Freundlich equilibrium sorption model (model I in Table 4.1) was fitted to the BTC data. The corresponding soil concentration profiles are given in Figure 4.14. . . . .	84
4.7	Breakthrough curves of total $^{14}\text{C}$ , SDZ and one transformation product in column B. The symbols represent measurements and the lines (solid, dashed and dotted) model calculations. The Freundlich equilibrium sorption model (model I in Table 4.1) was fitted only to the $^{14}\text{C}$ BTC data. The corresponding soil concentration profiles are given in Figure 4.15. . . . .	85
4.8	Breakthrough curves of total $^{14}\text{C}$ , SDZ and one transformation product in column B. The symbols represent measurements and the lines (solid, dashed and dotted) model calculations. The kinetic Freundlich sorption model (model II in Table 4.1) was fitted to the BTC and profile data. The corresponding soil concentration profiles are given in Figure 4.16. . . . .	87
4.9	Breakthrough curves of total $^{14}\text{C}$ , SDZ and one transformation product in column A. The symbols represent measurements and the lines (solid, dashed and dotted) model calculations. The attachment/detachment sorption model (model III in Table 4.1) was fitted to the BTC and profile data. The corresponding soil concentration profiles are given in Figure 4.17. . . . .	88

4.10	Breakthrough curves of total $^{14}\text{C}$ , SDZ and one transformation product in column A. The symbols represent measurements and the lines (solid, dashed and dotted) model calculations. The attachment/detachment sorption model (model III in Table 4.1) was fitted to the profile and $\log_{10}$ -transformed BTC data. The corresponding soil concentration profiles are given in Figure 4.18. . . . .	89
4.11	Breakthrough curves of total $^{14}\text{C}$ , SDZ and one transformation product in column B. The symbols represent measurements and the lines (solid, dashed and dotted) model calculations. The attachment/detachment sorption model (model IV in Table 4.1) was fitted to the BTC and profile data. The corresponding soil concentration profiles are given in Figure 4.20. . . . .	91
4.12	Breakthrough curves of total $^{14}\text{C}$ , SDZ and one transformation product in column B. The symbols represent measurements and the lines (solid, dashed and dotted) model calculations. The attachment/detachment sorption model (model IV in Table 4.1) was fitted to the profile and $\log_{10}$ -transformed BTC data. The corresponding soil concentration profiles are given in Figure 4.21. . . . .	92
4.13	Breakthrough curves of total $^{14}\text{C}$ , SDZ and one transformation product in column C. The symbols represent measurements and the lines (solid, dashed and dotted) model calculations. The attachment/detachment sorption model (model IV in Table 4.1) was fitted to the BTC and profile data. The corresponding soil concentration profiles are given in Figure 4.19. . . . .	93
4.14	Resident soil concentration profiles of total $^{14}\text{C}$ , SDZ and one transformation product in column A. The symbols represent measurements and the lines (solid, dashed and dotted) model calculations. The Freundlich equilibrium sorption model (model I in Table 4.1) was fitted to the BTC data. . . . .	94
4.15	Soil resident concentration profiles of total $^{14}\text{C}$ , SDZ and one transformation product in column B. The symbols represent measurements and the lines (solid, dashed and dotted) model calculations. The Freundlich equilibrium sorption model (model I in Table 4.1) was fitted only to the $^{14}\text{C}$ BTC data. . . . .	94
4.16	Soil resident concentration profiles of total $^{14}\text{C}$ , SDZ and one transformation product in column B. The symbols represent measurements and the lines (solid, dashed and dotted) model calculations. The kinetic Freundlich sorption model (model II in Table 4.1) was fitted to the BTC and profile data. . . . .	95
4.17	Soil resident concentration profiles of total $^{14}\text{C}$ , SDZ and one transformation product in column A. The symbols represent measurements and the lines (solid, dashed and dotted) model calculations. The attachment/detachment sorption model (model III in Table 4.1) was fitted to the BTC and profile data. . . . .	95



4.18	Soil resident concentration profiles of total $^{14}\text{C}$ , SDZ and one transformation product in column A. The symbols represent measurements and the lines (solid, dashed and dotted) model calculations. The attachment/detachment sorption model (model III in Table 4.1) was fitted to the profile and $\log_{10}$ -transformed BTC data. . . . .	96
4.19	Soil resident concentration profiles of total $^{14}\text{C}$ , SDZ and one transformation product in column C. The symbols represent measurements and the lines (solid, dashed and dotted) model calculations. The attachment/detachment sorption model (model IV in Table 4.1) was fitted to the BTC and profile data. . . . .	97
4.20	Soil resident concentration profiles Breakthrough curves of total $^{14}\text{C}$ , SDZ and one transformation product in column B. The symbols represent measurements and the lines (solid, dashed and dotted) model calculations. The attachment/detachment sorption model (model IV in Table 4.1) was fitted to the BTC and profile data. . . . .	97
4.21	Soil resident concentration profiles of total $^{14}\text{C}$ , SDZ and one transformation product in column B. The symbols represent measurements and the lines (solid, dashed and dotted) model calculations. The attachment/detachment sorption model (model IV in Table 4.1) was fitted to the profile and $\log_{10}$ -transformed BTC data. . . . .	98
5.1	Measured and predicted BTCs and soil concentration profiles. The applied model was the 3S2Rirrev with the sorption parameters gained from fitting the model to the sorption experiments A, B, C, D and E.	103
A.1	Chemical structure of sulfadiazine (SDZ). . . . .	115
E.1	Radio-HPLC-chromatograms of selected samples determined with method I (top left), method II (top right) and method III (bottom). .	123
E.2	Chemical structure of the identified transformation products of sulfadiazine, $^4\text{N}$ -acetylsulfadiazine (top) and hydroxy-sulfadiazine (bottom).	124
F.1	Mineralization of $^{14}\text{C}$ -SDZ in wet soil (Figure a). Decrease of extractable fraction of $^{14}\text{C}$ residues in wet soil (Figure b). Vertical bars indicate the standard error of the three replicates. . . . .	129
G.1	Transformation of SDZ in batch systems with fresh and sterilized soil. The symbols indicate the two replicates, the lines the respective mean values. $C_{\text{in}}$ is the initial concentration in the liquid phase in the batch systems (solid phase concentrations are initially zero). No radio-HPLC data are available in the lower concentration range. . . .	132



# List of Tables

2.1	The applied sorption models. The boxes labelled with $C$ represent the liquid phase with concentration $C$ . The boxes $S_i$ , with $i=1,2,3$ represent the three possible sorption domains with the respective concentrations $S_i$ . The arrows indicate the sorption process, $K_f$ and $m$ are the Freundlich coefficient and exponent, $\alpha_i$ is the reversible ad- and desorption rate for the assigned sorption domain, $\alpha_{\text{rev}}$ and $\alpha_{\text{irrev}}$ are the reversible or irreversible sorption rates between solution and bulk soil, respectively. $\beta_3$ is the irreversible sorption rate independent of the sorption isotherm. Parameters assigned with an apostrophe, as well as $K_x$ and $g$ are derived by calculation from model parameters.	9
2.2	Experimental conditions for the batch experiments. . . . .	16
2.3	Sampling schedule for the batch experiments. . . . .	16
2.4	Best fit parameters for the sorption experiments A-F using the 2S1R sorption model. . . . .	28
2.5	Best fit parameters for the sorption experiments A-E using the irreversible sorption models 2S2Rirx, 3S2Rirx and 3S2Rirrev. Models were simultaneously fitted to all experiments. In the upper panel the fithyst-parameters are given. The lower panel shows the recalculated parameters after elimination of one parameter. . . . .	28
3.1	Experimental conditions of the column experiments. . . . .	48
3.2	Properties of the soil columns and the experimental conditions. The irrigation rate, $j_w$ , and the soil bulk density, $\rho$ , were determined experimentally. The pore water velocity, $\nu$ , and the dispersion coefficient, $D$ , were fitted to the BTCs of chloride. The volumetric water content, $\theta$ , and the dispersivity, $\lambda$ , were calculated. . . . .	49
3.3	Mass recovery of SDZ after the column experiments. . . . .	54
3.4	Fitting parameters of the different isotherm-based (upper part) and attachment/detachment (lower part) models for column A. The eluted mass fraction in the experiment was 82.7 %. . . . .	55
3.5	Fitting parameters of the different isotherm-based (upper part) and attachment/detachment (lower part) models for column B. The eluted mass fraction in the experiment was 60.7 %. . . . .	65

3.6	Fitting parameters of the different isotherm-based (upper part) and attachment/detachment (lower part) models for column C. The eluted mass fraction in the experiment was 17.8 %. . . . .	66
4.1	Model assumptions for the isotherm-based (upper part) and the attachment/detachment-based (lower part) sorption and transformation models for two solutes. The relevant equations as well as the assumptions for the involved parameters are given. . . . .	82
4.2	Fitting parameters of the different isotherm-based (upper part) and attachment/detachment-based (lower part) sorption and transformation models for two solutes. . . . .	83
5.1	Best fit parameters for the sorption experiments A-E and column experiments A, B, C using the 3S2Rirrev or 3S2R-Freu-irrev model, respectively. . . . .	102
A.1	Selected physicochemical properties of sulfadiazine according to the supplier of the non-labelled SDZ, Sigma Aldrich, Taufkirchen, Germany.	115
B.1	Selected physical and chemical properties of the soil material. . . . .	117
E.1	HPLC-methods for chromatographic separation of SDZ and its transformation products. Methods I and II were routinely applied for the sample analysis of the batch and BTC samples, respectively, method III should be considered for further investigations. . . . .	122
E.2	Retention time (given in minutes after injection) of SDZ and its transformation products during HPLC. . . . .	123
E.3	Characteristic fragment ions of SDZ, acetyl-SDZ and hydroxy-SDZ for tandem mass spectrometry and the respective collision energies. . . . .	125

# Abbreviations and symbols

## Abbreviations

att	attachment/detachment concept
BTC	breakthrough curve
CAS	Chemical Abstracts Service
CDE	convective dispersive equation
D <sub>4</sub> -SDZ	deuterized SDZ (as internal standard for LC-MS-MS)
Freu	Freundlich (sorption isotherm)
HPLC	high performance liquid chromatography
irrev	irreversible (independent of sorption isotherm)
irx	irreversible (following sorption isotherm)
IUPAC	International Union of Pure and Applied Chemistry
LC-MS-MS	liquid chromatography with coupled tandem mass spectrometry
lin	linear (sorption isotherm)
LSC	liquid scintillation counting
LUFA	Landwirtschaftliche Untersuchungs- und Forschungsanstalt
m	mass related
MB <sub><i>i</i></sub>	transformation product <i>i</i>
rev	reversible
RP	reversed phase (HPLC-column)
SE	standard error of estimate
SDZ	sulfadiazine
SIM	selected ion monitoring (LC-MS-MS)
SRM	selected reaction mode (LC-MS-MS)
SSQ	sum of squares
v	volume related

## Symbols

$A$	$[T^{-1}]$	radioactivity
$A_{\text{spec}}$	$[T^{-1}L^{-3}; T^{-1}M^{-1}]$	specific radioactivity
$C$	$[ML^{-3}]$	solute concentration in the liquid phase
$C_{\text{initial}}, C_{\text{in}}$	$[ML^{-3}]$	initial solute concentration in the liquid phase
$C_i$	$[ML^{-3}]$	concentration of solute $i$
$C_{\text{org}}$	$[\%]$	organic carbon content
$C_t$	$[ML^{-3}]$	total solute mass per batch volume
$C_0$	$[ML^{-3}]$	input concentration
CEC	$[\text{charge}M^{-1}]$	cation exchange capacity
$D$	$[L^2T^{-1}]$	hydrodynamic dispersion coefficient
$f_i$	$[-]$	fraction of $i$ -th sorption domain on total soil mass
$g$	$[-]$	fraction of instantaneous on reversible sorption sites (3S2Rirx and 3S2Rirrev sorption models)
$i, j$		running indices
$j_w$	$[LT^{-1}]$	water flow density
$k$	$[-]$	total number of sorption sites
$K_d$	$[L^3M^{-1}]$	soil-water distribution coefficient
$K_f$	$[M_{\text{solute}}^{1-m} L^{3m} M_{\text{soil}}^{-1}]$	Freundlich soil-water distribution coefficient
$K_{f,i}$	$[M_{\text{solute}}^{1-m} L^{3m} M_{\text{soil}}^{-1}]$	Freundlich soil-water distribution coefficient of solute $i$
$K_x$	$[M_{\text{solute}}^{1-m} L^{3m} M_{\text{soil}}^{-1}]$	transformed Freundlich coefficient in 3S2Rirx and 3S2Rirrev sorption models
$L$	$[\text{mm}; \text{cm}]$	length
$m$	$[-]$	Freundlich exponent
$m_i$	$[-]$	Freundlich exponent of solute $i$
$M$	$[\mu\text{g}; \text{mg}; \text{g}; \text{kg}]$	mass
$m_{\text{initial}}$	$[M]$	initial solute mass
$m_{\text{soil}}$	$[M]$	mass of soil
$[M + H]^+$		mass of ionized parent compound
$m/z$		mass-charge ratio
$N_{\text{tot}}$	$[\%]$	total nitrogen content
$P_{\text{tot}}$	$[M M^{-1}]$	total phosphorus content

pH		negative decadic logarithm of the hydronium ion concentration
pK <sub>a</sub>		acidity constant
$R$	[-]	retardation factor
$S$	[MM <sup>-1</sup> ]	solute concentration in the solid phase
$S_i$	[MM <sup>-1</sup> ]	local sorbed concentration in $i$ -th sorption domain
$S'_i$	[MM <sup>-1</sup> ]	bulk sorbed concentration in $i$ -th sorption domain related to total soil mass
$S_{ij}$	[MM <sup>-1</sup> ]	sorbed concentration of solute $i$ in $j$ -th sorption domain
$t$	[T]	time
T	[s; min; h; d]	time
u		atomic mass unit
$V$	[L <sup>3</sup> ]	volume
$V_{\text{liquid}}$	[L <sup>3</sup> ]	volume of liquid
$z$	[L]	depth
$\alpha_i$	[T <sup>-1</sup> ]	sorption rate coefficient in $i$ -th sorption domain
$\alpha'_i$	[T <sup>-1</sup> ]	sorption rate coefficient in $i$ -th sorption domain (in rewritten models)
$\alpha_{ij}$	[T <sup>-1</sup> ]	sorption rate coefficient of solute $i$ in $j$ -th sorption domain
$\beta$	[T <sup>-1</sup> ]	irreversible sorption rate coefficient
$\beta_i$	[T <sup>-1</sup> ]	attachment rate coefficient towards $i$ -th sorption site
$\beta_{ij}$	[T <sup>-1</sup> ]	attachment rate coefficient of solute $i$ towards $j$ -th sorption site
$\gamma_i$	[T <sup>-1</sup> ]	detachment rate coefficient from $i$ -th sorption site
$\gamma_{ij}$	[T <sup>-1</sup> ]	detachment rate coefficient of solute $i$ from $j$ -th sorption site
$\lambda$	[L]	dispersivity
$\mu_i$	[T <sup>-1</sup> ]	transformation rate coefficient of solute $i$
$\rho$	[ML <sup>-3</sup> ]	soil bulk density
$\theta$	[L <sup>3</sup> L <sup>-3</sup> ]	volumetric water content
$\theta_{\text{initial}}$	[L <sup>3</sup> L <sup>-3</sup> ]	initial volumetric water content
$\nu$	[LT <sup>-1</sup> ]	pore water velocity

# Model descriptions

## sorption models

LEQ	local equilibrium assumption
RLS	rate-limited sorption model
2S1R	two-stage one-rate sorption model
2S1R (sites)	two-sites one-rate sorption model
2S2R	two-stage two-rate sorption model
2S2R (sites)	two-sites two-rate sorption model
2S2Rirx (sites)	two-sites two-rate sorption model with irreversible sorption
3S2Rirx	three-sites two-rate sorption model with irreversible sorption
3S2Rirrev	three-sites two-rate sorption model, irreversible sorption as independent sink

## transport models

1S0R-lin-rev	one-site zero rate sorption model, linear isotherm (equivalent to LEQ model)
1S0R-Freu-rev	one-site zero rate sorption model, Freundlich isotherm (equivalent to LEQ model)
1S1R-lin-rev	one-site one-rate sorption model, linear isotherm (equivalent to RLS model)
1S1R-Freu-rev	one-site one-rate sorption model, Freundlich isotherm (equivalent to RLS model)
1S2R-att-rev	one-site two-rate reversible attachment/detachment model
2S1R-lin-rev	two-site one-rate sorption model, linear isotherm
2S1R-Freu-rev	two-site one-rate sorption model, Freundlich isotherm
2S2R-lin-irrev	two-site two-rate irreversible sorption model, linear isotherm
2S2R-Freu-irrev	two-site two-rate irreversible sorption model, Freundlich isotherm
2S3R-att-irrev	two-site three-rate irreversible attachment/detachment model
2S4R-att-rev	two-site four-rate reversible attachment/detachment model
3S2R-lin-irrev	three-site two-rate irreversible sorption model, linear isotherm (equivalent to 3S2Rirrev model)
3S2R-Freu-irrev	three-site two-rate irreversible sorption model, Freundlich isotherm (equivalent to 3S2Rirrev model)
3S5R-att-irrev	three-site five-rate irreversible attachment/detachment model



# Chapter 1

## General introduction

### 1.1 Rationale

Antibiotic substances are used in human and veterinary medicines to treat and prevent bacterial infections (*Thiele-Bruhn*, 2003; *Boxall et al.*, 2004). After medication these drugs are almost completely excreted as parent substances or in a metabolized form with the feces or the urine (*Kroger*, 1983). The human waste water passes sewage treatment plants before its release into the environment. The animal excreta on the contrary are either directly dropped onto the pasture by grazing livestock, or are applied onto arable soil as fertilizer after storage (*Jørgensen and Halling-Sørensen*, 2000). Since the antibiotics<sup>1</sup> and their metabolites are not completely removed or degraded during sewage treatment or storage, they reach soils and surface waters (*Christian et al.*, 2003; *Kay et al.*, 2004). Here, they are subjected to various processes such as further biotic, abiotic or photo-induced degradation and transformation, sorption onto soil or sediment particles, transport by the moving water in the dissolved or particle-bound form, water and wind erosion and uptake by plants or microorganisms. Depending on their persistence and affinity to the soil particles, they can be widely distributed and eventually even reach the groundwater.

Antibiotics are drugs that kill or inhibit the growth of the bacteria which are sensitive to the substances. The effect of an antibiotic is not restricted to the target organisms, but especially wide-spectrum antibiotics affect a larger range of bacterial species. Also in low concentration levels antibiotic substances may be effective (*Thiele-Bruhn*, 2005). Furthermore, the omnipresence of antibiotics may accelerate the development of antibiotic resistances, which is the ability of a microorganism to withstand the effects of an antibiotic. Antibiotic resistances develop via natural selection through random mutation and plasmid exchange between bacteria. However, the successful treatment of infections in human and veterinary medicines depends on the effectiveness of the administered antibiotics. It is thus desirable to limit the dispersion of antibiotics in the environment in order to reduce the environmental pressure due to natural selection of resistant strains.

---

<sup>1</sup>For reasons of simplicity the term antibiotics is used in this thesis for all antimicrobial agents, i.e. microbially and synthetically produced antibiotic substances (*Haller et al.*, 2002).

As a consequence, antibiotic food-additives serving as growth promoters in intensive livestock production were banned in the European Union in 2006 (*EMEA*, 2000). However, antibiotics are used therapeutically and therefore their fate and effects in the environment need investigation to estimate the risk of soil and groundwater contamination. The objective defined by the European Medicine Agency is to stay below the trigger values for veterinary pharmaceuticals in soil ( $100 \mu\text{g kg}^{-1}$ ) and groundwater ( $1 \mu\text{g L}^{-1}$ ) (*EMEA*, 2000).

In order to take the appropriate precautions to maintain clean soil and groundwater resources, the processes governing the environmental fate of the veterinary pharmaceuticals need to be understood. The input of veterinary medicines into the environment is estimated from information such as the administered amount and the agricultural practice for the application of manure. The characteristic pathways of xenobiotics such as pharmaceuticals in the environment may be roughly approximated according to their physicochemical properties. However, experimental investigations are required to quantify sorption, transformation, degradation and mineralization as well as the effect of the substance and its transformation products on selected target organisms. Transport experiments are conducted especially with substances anticipated to be persistent and mobile. In combination with the estimated exposure data the determined characteristic sorption and degradation parameters are then included in mathematical models to predict the concentration of the target substance under defined environmental conditions. The thus developed models can be validated by various experimental approaches such as lysimeter, plot or field studies.

## 1.2 Experimental and model approaches

Apart from field- or lysimeter-scale experiments, the fate of xenobiotics in the soil environment is commonly assessed in small-scale laboratory experiments. The persistence of a chemical in the environment is typically characterized by its half-life time, assuming first-order kinetics for the dissipation. The dissipation of the parent substance in a closed system may be attributed to mineralization, abiotic transformation, microbial decomposition or volatilization. In addition the formation of non-extractable residues, which are not available for many analytical procedures, is a further dissipation pathway. These processes may strongly depend on environmental conditions such as water content, temperature, light, redox potential and microbial activity in a certain soil but also on the concentration of the target substance. The overall dissipation of the parent substance is investigated, when the non-labelled substance is applied and its concentration in soil is observed over time. The application of a  $^{14}\text{C}$ -labelled substance allows the assessment of the mineralization to  $^{14}\text{CO}_2$  and the formation of non-extractable residues in soil microcosms.

Batch or column experiments are used to characterize the sorption behavior. Whereas batch systems are well mixed and run at an elevated water content compared to field conditions, soil columns are more realistic experimental setups. However, the interaction of soil and solute in the soil columns is additionally governed by

the flowing water. The observed breakthrough curves and soil concentration profiles are the result of combined physical and chemical processes. To account for flow related effects on solute transport, the transport of a reactive substance is usually compared to a simultaneously applied conservative tracer. The difference in the transport behavior (e.g. retardation and tailing) of the two tracers is then assigned to sorption of the reactive tracer.

However, sorption characteristics determined by batch and column techniques are not always in agreement. The differences are attributed to various causes, such as loss of sorbent from the column, variations in column flow, immobile water in the column, differences in flow or mixing regime between the two methods, different soil/water ratios and possible soil abrasion in the batch systems (*Altfelder et al.*, 2001). Since pesticide sorption equilibrium is reached faster in well-stirred batch systems than under flow conditions, *Kookana et al.* (1992) concluded that a large fraction of sorption sites is not readily available to pesticides under flow conditions due to physical hindrance. Despite these limitations, they found that batch experiments were a suitable method to estimate the sorption equilibrium and chemical sorption kinetics. In contrast, only apparent rate laws can be estimated in flow experiments due to the combined effect of chemical and physical processes. However, if kinetic two-site sorption concepts were considered for the parametrization of batch experiments, the fitted parameters successfully predicted the transport of various organic chemicals at the lysimeter and field scale (e.g. *Larsen et al.*, 1992; *Ma and Selim*, 1994a; *Streck et al.*, 1995; *Streck and Richter*, 1999). *Altfelder et al.* (2001) reevaluated the compatibility of batch and column experiments. They demonstrated that the consideration of slow kinetic sorption (two-stage model) enabled the prediction of the transport of dimethylphthalate from batch experiments, which was impossible assuming local equilibrium (*Maraqqa et al.*, 1998).

### 1.3 General objectives and outline of the thesis

The objective of the thesis was to improve our understanding of the behavior of sulfadiazine, a wide-spectrum antibiotic substance used in human and veterinary medicines, in the soil environment under laboratory conditions.  $^{14}\text{C}$ -labelled sulfadiazine was used in the experiments to ensure complete mass balances, independent of unknown transformation, mineralization or matrix effects during chemical analysis. Although antibiotics enter the soil environment typically as ingredient of manure, the experiments were conducted without manure, to circumvent any changes in the soil properties and their effect on the fate of sulfadiazine. To identify relevant processes, inverse parameter estimation methods were used.

Batch and column experiments were conducted to characterize the sorption and transport behavior of sulfadiazine. The experimental and modelling approaches are discussed in Chapter 2 and 3, respectively. Accompanying experiments assess the mineralization and transformation as environmental fate pathways of sulfadiazine in the soil environment (Appendices F and G). Whereas the investigations discussed in Chapters 2 and 3 focus on the total  $^{14}\text{C}$ -measurements, i.e. do not differentiate

between SDZ and its transformation products, Chapter 4 investigates the effect of transformation on the transport behavior. Chapter 5 synthesizes the experimental and modelling results and provides the conclusions of the presented thesis as well as an outlook on future experimental and modelling strategies.

# Chapter 2

## Sorption of sulfadiazine in soil - experiments and modelling approaches

### 2.1 Introduction

Sulfadiazine (SDZ) is one among many antibiotic substances used in intensive livestock production to treat and prevent diseases. Since these substances are only partially resorbed by the animals, the non-resorbed fraction is excreted (*Kroger, 1983*). Thus, the pharmaceuticals and their metabolites may reach the soil environment through grazing livestock or manure application (*Jørgensen and Halling-Sørensen, 2000*). Fate and transport of a contaminant in the soil environment depends largely on its interaction with the soil solids (e.g. *Kleineidam et al., 2004*). Understanding the governing sorption processes is crucial to estimate the leaching potential of the contaminant (e.g. *Pignatello and Xing, 1996; Altfelder et al., 2001*).

Because of the complex nature of the soil matrix and the wide variety of organic and inorganic chemicals, numerous processes on the molecular level contribute to overall sorption. However, suitable experimental and analytical methods are lacking to determine the processes at the molecular level. Therefore, macroscopic evidence usually by means of batch experiments is used to validate the proposed sorption concepts (*Luthy et al., 1997*).

Sorption of an organic substance in a certain soil is characterized by the equilibrium sorption isotherm, and the information about adsorption and desorption kinetics. The equilibrium sorption isotherms describe the relationship between the concentration in the solid and the liquid phase at sorption equilibrium. Depending on their shape, various mathematical equations are proposed to describe the isotherms (*Hinz, 2001*). However, they are often approximated by relatively simple mathematical functions, such as the Freundlich or Langmuir equations. The slow approach of equilibrium distribution is attributed to diffusion into soil particles (e.g. *Streck et al., 1995; Pignatello and Xing, 1996*). Hence, the rate-limited solute uptake (and release) by the sorbent is described by diffusion equations in some models (e.g.

*Zhao et al.*, 2001; *Gamst et al.*, 2003, 2004). Spherical particles are often assumed to approximate the soil matrix. Since the geometry of the sorbent is mostly unknown, other model approaches use the difference between actual and equilibrium concentration as driving force for rate-limited solute transfer between the liquid and the sorbed phases or among the various sorption domains (e.g. *Cameron and Klute*, 1977; *Brusseau*, 1991; *Streck et al.*, 1995; *Schwarzenbach et al.*, 2003). To address the heterogeneity of the sorbent and the variable accessibilities of sorption sites, sorption models with multiple sorption domains exhibiting characteristic rate laws or domains with distinct sorption properties were developed (*Cameron and Klute*, 1977; *Brusseau*, 1991; *Ma and Selim*, 1994a, 1997; *Zhao et al.*, 2001). Although the importance of slow sorption kinetics is widely accepted (e.g. *Cameron and Klute*, 1977; *Brusseau*, 1991; *Ma et al.*, 1993; *Ma and Selim*, 1994b; *Kan et al.*, 1994; *Streck et al.*, 1995; *Pignatello and Xing*, 1996; *Luthy et al.*, 1997; *Altfelder et al.*, 2000; *Gamst et al.*, 2001, 2004), available sorption data are often limited to short term adsorption isotherms (e.g. *Thiele*, 2000; *Kreuzig et al.*, 2003). Differences between the adsorption and desorption isotherms might be partly explained by kinetic effects (*Altfelder et al.*, 2000) and can result from not fully understood equilibrium conditions (*Sabbah et al.*, 2005).

For some organic contaminants sorption in soil was proved to be a completely reversible process, provided that there is enough time to approach the equilibrium (e.g. *Altfelder et al.*, 2000). True sorption hysteresis occurs, if adsorption and desorption isotherms differ and experimental artifacts can be ruled out (*Sander and Pignatello*, 2005a,b). This true hysteresis results in an irreversible sorption. The sorption hysteresis is postulated to be due to conditioning of the sorbent by repeated sorption of the same solute. For naphthalene in lignite it occurred only at elevated concentration levels due to "swelling" of the sorbate (*Sander and Pignatello*, 2005b). Irreversible sorption is also discussed as causation for bound residues in soil, which reduce the bioavailability and leaching risk of soil contaminants (*Northcott and Jones*, 2000).

Apart from the sorbent properties such as hydration status, grain size, surface coatings of the grains and surface charge also pH, ionic strength, temperature of the solution and the presence of co-solutes influence the overall sorption (e.g. *Luthy et al.*, 1997; *Gao and Pedersen*, 2005). All effects on sorption might be investigated separately for process elucidation. However, the combined sorption extend in the soil environment is unlikely to be the sum of the separate processes (*Addiscott et al.*, 1995).

*Gao and Pedersen* (2005) investigated the influence of the pH-value (and ionic strength) on the sorption of sulfonamides to clay minerals. Since sulfonamides possess two ionizable functional groups, their charge is pH-dependent. The cation at low pH-values showed the highest sorption affinity, whereas the anionic species (pH = 9) showed little or no sorption at the investigated smectite or kaolinite. However, in the pH-range where the neutral species dominates ( $pK_{a,1} < \text{pH} < pK_{a,2}$ ), sorption is relatively insensitive to pH-variations. The same pH-dependency of the sorption affinity of sulfathiazole was reported for compost and manure as model sorbents for soil organic substances by *Kahle et al.* (2005) and for soils by *Boxall et al.* (2002);

*Langhammer and Büning-Pfaue* (1989). In contrast the sorption affinity on the iron-oxide ferrihydrite was highest around neutral pH, presumably due to anion sorption (*Kahle et al.*, 2005).

Sorption was generally higher for organic sorbents than for mineral soil components although the affinity varied between the various soil organic substances (*Thiele-Bruhn and Aust*, 2003; *Kahle et al.*, 2005). Extrapolation of sorption characteristics of model sorbents to real soils or sediments must be done with caution, as for instance clays in the natural systems are often coated with organic matter (*Gao and Pedersen*, 2005). Investigations with the model substances demonstrate, the importance of the surface charge densities on the sorption of sulfonamides (*Gao and Pedersen*, 2005). The important role of the quality of soil organic matter on sulfonamide sorption was also indicated by *Thiele-Bruhn et al.* (2004), who found higher sorption affinities in fertilized than in unfertilized soils. Attributing sorption of polar pharmaceuticals solely to hydrophobic partitioning to soil organic matter is, thus, an unsuitable concept (*Tolls*, 2001; *Thiele-Bruhn et al.*, 2004), as is also shown for other organic compounds (e.g. *Ahmad et al.*, 2001).

Non-linear sorption isotherms for sulfonamides were previously reported by *Thiele-Bruhn and Aust* (2003); *Gao and Pedersen* (2005). The Freundlich sorption isotherm was a suitable model to describe the sorption characteristics. However, the estimated Freundlich exponents differed widely from 0.48 to 1.21. Moreover, sorption affinity was higher after 14 days than after one day of equilibration time for all investigated organic and oxidic sorbents (*Kahle et al.*, 2005), indicating slow sorption kinetics. Apart from that, little is known about adsorption and desorption kinetics of sulfonamides. However, the frequently reported low extraction efficiencies especially for aged soil residues (*Langhammer and Büning-Pfaue*, 1989; *Hartmann*, 2003; *Kreuzig et al.*, 2003; *Hamscher et al.*, 2005) hint towards an apparent sorption hysteresis and possible formation of bound residues due to irreversible sorption or very slow desorption.

Sulfadiazine showed the most non-linear sorption isotherm in soil and soil-manure slurries among the five sulfonamides tested by *Thiele-Bruhn and Aust* (2003). The sorption affinity of all sulfonamides was lower in the soil-manure slurries compared to soil-water slurries. However, the addition of manure reduced the pH in the batches during this study, due to the unusual low pH of the applied manure (pH = 4). In the presence of the normally alkaline manure, sorption affinity might further decrease due to the combined effect of manure and pH (*Thiele-Bruhn and Aust*, 2003).

The objective of this study was to assess the sorption properties of  $^{14}\text{C}$ -labelled sulfadiazine (SDZ) in the top soil of an Eutric Cambisol, collected from a grassland near lake Greifensee, Switzerland. The batch equilibrium technique was used to determine the distribution of SDZ between the solid and the liquid phase, depending on time and initial concentration. Since the solute analysis was restricted to  $^{14}\text{C}$ , we investigated the lumped sorption behavior of SDZ and its transformation products. An inverse parameter estimation method was used to identify relevant processes. One-, two- and three-domain reversible and irreversible kinetic sorption models were tested and their assumptions and limitations are discussed.

## 2.2 Sorption Theory

In this section a mathematical derivation for various one-, two- and three-domain sorption models is given.

The total mass in a batch system is given by Equation 2.1 and is assumed to be constant in time (Equation 2.2):

$$C_t = \theta C + \rho S \quad (2.1)$$

$$\frac{dC_t}{dt} = 0 \quad , \quad (2.2)$$

where  $C_t$  is total solute mass per total batch volume [ $M L^{-3}$ ],  $\rho$  is soil bulk density [ $M L^{-3}$ ],  $\theta$  is the volumetric water content [ $L^3 L^{-3}$ ] and  $C$  and  $S$  are the solute concentration in the liquid [ $M L^{-3}$ ] and the solid phases [ $M M^{-1}$ ], respectively. In case of multiple sorption domains the total sorbed concentration  $S$  is calculated from the sorbed concentrations in the separate domains. The sorbed concentration in one domain is either expressed as local or bulk concentration (Equation 2.3). The local concentration is defined as sorbed solute mass per mass of soil in the respective sorption domain [ $M M^{-1}$ ]. The sorbed solute mass is related to the total mass of soil in the definition of the bulk concentration [ $M M^{-1}$ ]. The bulk concentrations are indicated with an apostrophe. The general relationship between the local and the bulk concentrations is given by:

$$S'_i = f_i S_i \quad , \quad 0 \leq f_i \leq 1 \quad , \quad \sum_{i=1}^k f_i = 1 \quad , \quad (2.3)$$

where the subscript  $i$  indicates the domain number,  $f_i$  is the fraction of the  $i$ -th domain on total soil mass and  $k$  is the total number of sorption domains. The total sorbed concentration is, thus, expressed by:

$$S = \sum_{i=1}^k f_i S_i = \sum_{i=1}^k S'_i \quad , \quad (2.4)$$

for local and bulk concentrations, respectively.

### 2.2.1 One-domain sorption

#### Local equilibrium sorption (LEQ)

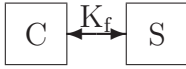
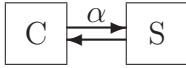
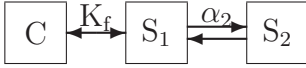
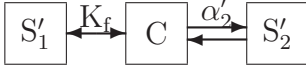
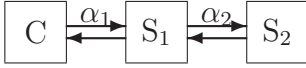
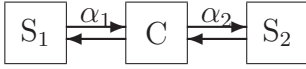
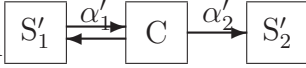
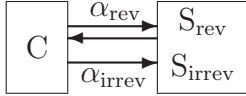
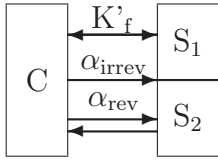
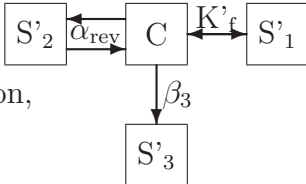
Concentration-dependent, equilibrium sorption of organic compounds is often described by the Freundlich equation (*Schwarzenbach et al.*, 2003):

$$S = K_f C^m \quad , \quad (2.5)$$

where  $K_f$  is the Freundlich distribution coefficient [ $M_{\text{solute}}^{1-m} L^{3m} M_{\text{soil}}^{-1}$ ] and  $m$  is the dimensionless Freundlich exponent. This form of local equilibrium sorption (LEQ) is called 1SOR-Freu-rev in the transport section, indicating that the sorption process is reversible and not rate-limited. Note that linear sorption is a special case of Freundlich sorption with  $m = 1$ .



Table 2.1: The applied sorption models. The boxes labelled with  $C$  represent the liquid phase with concentration  $C$ . The boxes  $S_i$ , with  $i=1,2,3$  represent the three possible sorption domains with the respective concentrations  $S_i$ . The arrows indicate the sorption process,  $K_f$  and  $m$  are the Freundlich coefficient and exponent,  $\alpha_i$  is the reversible ad- and desorption rate for the assigned sorption domain,  $\alpha_{\text{rev}}$  and  $\alpha_{\text{irrev}}$  are the reversible or irreversible sorption rates between solution and bulk soil, respectively.  $\beta_3$  is the irreversible sorption rate independent of the sorption isotherm. Parameters assigned with an apostrophe, as well as  $K_x$  and  $g$  are derived by calculation from model parameters.

Model	Concept	Parameters
<b>One domain models</b>		
LEQ local equilibrium sorption		$K_f, m$
RLS rate-limited sorption		$K_f, m, \alpha$
<b>Two domain models</b>		
2S1R two-stage one-rate sorption		$K_f, m, \alpha_2, f_1$
2S1R (sites) two-site one-rate sorption		$K_f, m, \alpha'_2, f_1$
2S2R two-stage two-rate sorption		$K_f, m, \alpha_1, \alpha_2, f_1$
2S2R (sites) two-site two-rate sorption		$K_f, m, \alpha'_1, \alpha'_2, f_1$
2S2Rirx (sites) two-site two-rate irreversible sorption		$K_f, m, \alpha'_1, \alpha'_2, f_1$
2S2Rirx two-site two-rate irreversible sorption		$K_x, m, \alpha_{\text{rev}}, \alpha_{\text{irrev}}$
<b>Three domain models</b>		
3S2Rirx three-site two-rate irreversible sorption		$K'_f, m, \alpha_{\text{rev}}, \alpha_{\text{irrev}}, g$
3S2Rirrev three-site two-rate irreversible sorption, independent sink		$K'_f, m, \alpha_{\text{rev}}, \beta_3, g$

### Rate-limited sorption (RLS)

If the equilibrium distribution of a substance is not reached instantaneously, a rate-limited solute uptake by the soil needs to be considered. This is described by the following equation:

$$\frac{dS}{dt} = \alpha(K_f C^m - S) \quad , \quad (2.6)$$

where  $\alpha$  is the sorption rate coefficient [ $T^{-1}$ ]. The sorption isotherm for the equilibrium distribution is given by Equation 2.5. The mass balance is given by Equations 2.1 and 2.2. The change of solute concentration in the liquid phase with time is expressed as:

$$\theta \frac{dC}{dt} = \alpha(C_t - \theta C - \rho K_f C^m) \quad . \quad (2.7)$$

The rate-limited sorption concept (RLS) is referred to as 1S1R-Freu-rev model in the transport section.

## 2.2.2 Two domain sorption

Another widely used approach is to assume two different types of sorption domains in soil, one with instantaneous sorption and one with rate-limited sorption (*Brusseau et al.*, 1989; *Ma et al.*, 1993; *Streck et al.*, 1995). The different sorption domains can either be arranged in series or parallel, further referred to as two-stage or two-site models, respectively (Table 2.1).

### Two-stage one-rate sorption (2S1R)

The two-stage one-rate approach (2S1R) assumes non-linear (Freundlich) sorption, with instantaneous equilibrium between the aqueous solution and one sorption region with local concentration  $S_1$ , whereas the other sorption region with local concentration  $S_2$  takes up the solute rate-limited from the instantaneous region (Table 2.1). Sorption is then described by the following equations:

$$S_1 = K_f C^m \quad (2.8)$$

$$(1 - f_1) \frac{dS_2}{dt} = \alpha_2 (K_f C^m - S_2) \quad (2.9)$$

$$S = f_1 S_1 + (1 - f_1) S_2 \quad , \quad (2.10)$$

where  $f_1$  is the dimensionless fraction of the total soil that exhibits equilibrium sorption, and  $\alpha_2$  is the sorption rate coefficient [ $T^{-1}$ ]. With the assumption of mass conservation (Equations 2.1, 2.2 and 2.4) the change of solute concentration in the liquid phase with time is expressed as:

$$(\rho f_1 m K_f C^{m-1} + \theta) \frac{dC}{dt} = \frac{\alpha_2}{1 - f_1} (C_t - \theta C - \rho K_f C^m) \quad . \quad (2.11)$$

**Two-site one-rate sorption (2S1R, sites)**

The two-site one-rate approach (2S1R, sites) assumes that both, the instantaneous and the rate-limited sorption domains are in direct contact with the aqueous solution (Table 2.1). The 2S1R (sites) model here is identical to the 2S1R-Freu-rev model in the transport section. The sorption equations are given by:

$$S'_1 = f_1 K_f C^m \quad (2.12)$$

$$\frac{dS'_2}{dt} = \alpha'_2((1 - f_1)K_f C^m - S'_2) \quad (2.13)$$

$$S = S'_1 + S'_2 \quad , \quad (2.14)$$

where  $\alpha'_2$  is the sorption rate coefficient [ $T^{-1}$ ] and  $S'_1$  and  $S'_2$  the bulk solid phase concentrations of the equilibrium and non-equilibrium domain, respectively. With the assumption of mass conservation (Equations 2.1, 2.2 and 2.4) the following equation describes the change of the concentration in the liquid phase with time:

$$(\rho f_1 m K_f C^{m-1} + \theta) \frac{dC}{dt} = \alpha'_2 (C_t - \theta C - \rho K_f C^m) \quad . \quad (2.15)$$

The two-stage one-rate (2S1R) and the two-site one-rate sorption (2S1R, sites) models are mathematically equal with  $\alpha_2 = (1 - f_1)\alpha'_2$  for linear ( $m = 1$ ) (*Altfielder et al.*, 2001) and nonlinear ( $m \neq 1$ ) sorption.

**Two-stage two-rate sorption (2S2R)**

For slow sorption processes instantaneous sorption might not occur. In this case both domains may sorb the solute kinetically (*Streck and Piehler*, 1998). If those two sorption regions are arranged in series (Table 2.1), the equations for the resulting two-stage two-rate sorption (2S2R) are:

$$f_1 \frac{dS_1}{dt} = \alpha_1 (K_f C^m - S_1) - \alpha_2 (S_1 - S_2) \quad (2.16)$$

$$(1 - f_1) \frac{dS_2}{dt} = \alpha_2 (S_1 - S_2) \quad , \quad (2.17)$$

where  $\alpha_1$  is the sorption rate coefficient of the first sorption stage in direct contact with the soil solution. Combining Equations 2.1, 2.2, 2.4, 2.16 and 2.17 results in:

$$\theta \frac{dC}{dt} = \frac{\alpha_1}{f_1} (C_t - \theta C - \rho f_1 K_f C^m - \rho(1 - f_1)S_2) \quad . \quad (2.18)$$

**Two-site two-rate sorption (2S2R, sites)**

Similarly the equations for the two-site two-rate sorption (2S2R (sites), Table 2.1) are written as:

$$\frac{dS'_1}{dt} = \alpha'_1 (f_1 K_f C^m - S'_1) \quad (2.19)$$

$$\frac{dS'_2}{dt} = \alpha'_2((1 - f_1)K_f C^m - S'_2) \quad (2.20)$$

$$\theta \frac{dC}{dt} = \alpha'_1(C_t - \theta C - \rho K_f C^m (f_1 + (1 - f_1) \frac{\alpha'_2}{\alpha'_1}) - \rho(1 + \frac{\alpha'_2}{\alpha'_1})S'_2) \quad (2.21)$$

Reformulating Equations 2.19 to 2.21 with  $\alpha'_1 = \alpha_1/f_1$ ,  $\alpha'_2 = \alpha_2/(1 - f_1)$  and Equation 2.3 leads to the two-site two-rate sorption model formulation with local concentrations  $S_1$  and  $S_2$ :

$$f_1 \frac{dS_1}{dt} = \alpha_1(K_f C^m - S_1) \quad (2.22)$$

$$(1 - f_1) \frac{dS_2}{dt} = \alpha_2(K_f C^m - S_2) \quad (2.23)$$

$$\theta \frac{dC}{dt} = \frac{\alpha_1}{f_1}(C_t - \theta C - \rho f_1 K_f C^m (1 + \frac{\alpha_2}{\alpha_1}) - \rho((1 - f_1) + f_1 \frac{\alpha_2}{\alpha_1})S_2) \quad (2.24)$$

Note that the two-stage and the two-site model are different in case of two kinetic sorption domains. Solute uptake and release of both sorption sites in the two-site model (2S2R, sites) is driven by the difference between the actual and the potential equilibrium sorbed concentration for the actual liquid concentration  $C$ .  $S_1$  and  $S_2$  of the two-site model, thus, depend only on  $C$ , whereas solute uptake and release is driven by the concentration gradient between the local concentrations  $S_1$  and  $S_2$  for the second sorption stage in the two-stage model (2S2R). The 2S2R (sites) model is equivalent to the 2S2R-Freu-rev model in the transport section.

### Two-site two-rate sorption – irreversible (2S2Rirx, sites)

Until now reversible sorption was assumed, which means that, depending on the direction of the concentration gradient, solute can be transferred in both directions: from the solution to the sorption sites or vice versa. Sorption velocities were equal in either direction.

In case desorption of a solute from the second sorption sites is impossible (2S2Rirx (sites) in Table 2.1), Equations 2.22 to 2.24 reduce to:

$$f_1 \frac{dS_1}{dt} = \alpha_1(K_f C^m - S_1) \quad (2.25)$$

$$(1 - f_1) \frac{dS_2}{dt} = \alpha_2 K_f C^m \quad (2.26)$$

$$\theta \frac{dC}{dt} = \frac{\alpha_1}{f_1}(C_t - \theta C - \rho f_1 K_f C^m (1 + \frac{\alpha_2}{\alpha_1}) - \rho(1 - f_1)S_2) \quad (2.27)$$

where  $\alpha_2$  now is the sorption rate coefficient for the irreversible sorption sites ( $S_2$ ). This formulation of irreversible sorption implies that there will not be an equilibrium distribution of solute between soil and solution for long sorption times: For  $t \rightarrow \infty$  all solute will accumulate at the irreversible sorption sites. Contrary to reversible sorption, solute transfer will continue until all solute is removed from the liquid phase

( $C = 0$ ). Therefore, the definition of local concentrations is no longer necessary for the calculation of the concentration gradients. Thus, we can omit the definition of two separate sorption sites. The mathematical derivation is given below and is based on the following assumptions:

$$S_{\text{tot}} = S'_{\text{rev}} + S'_{\text{irrev}} = S \quad (2.28)$$

$$S'_{\text{rev}} = f_1 S_1 = S'_1 \quad (2.29)$$

$$S'_{\text{irrev}} = (1 - f_1) S_2 = S'_2 \quad (2.30)$$

$$\alpha_{\text{rev}} = f_1 \alpha'_1 = \alpha_1 \quad (2.31)$$

$$\alpha_{\text{irrev}} = (1 - f_1) \alpha'_1 = \alpha_2 \quad (2.32)$$

$$K_x = f_1 K_f \quad (2.33)$$

where  $S'_{\text{rev}}$  and  $S'_{\text{irrev}}$  are reversibly and irreversibly bound bulk solute concentrations, respectively,  $\alpha_{\text{rev}}$  and  $\alpha_{\text{irrev}}$  are sorption rate coefficients and  $K_x$  is the distribution coefficient in the new model. Inserting Equations 2.28 to 2.33 in Equations 2.25 to 2.27 the two-site two-rate irreversible sorption model is defined as:

$$\frac{dS'_{\text{rev}}}{dt} = \alpha_{\text{rev}}(K_x C^m - S'_{\text{rev}}) \quad (2.34)$$

$$\frac{dS'_{\text{irrev}}}{dt} = \alpha_{\text{irrev}} K_x C^m \quad (2.35)$$

$$\theta \frac{dC}{dt} = \alpha_{\text{rev}}(C_t - \theta C - \rho K_x C^m (1 + \frac{\alpha_{\text{irrev}}}{\alpha_{\text{rev}}}) - \rho S'_{\text{irrev}}) \quad (2.36)$$

Note that  $f_1$  is eliminated and the reversible and the irreversible sorption now occur towards the bulk soil (2S2Rirx in Table 2.1).

### 2.2.3 Three domain sorption

#### Three-site two-rate sorption – irreversible (3S2Rirx)

The three-site two-rate irreversible sorption model (3S2Rirx, Table 2.1) consists of three different sorption domains: an equilibrium sorption domain with concentration  $S_1$ , a rate-limited, reversible sorption domain with concentration  $S_2$  and a rate-limited, irreversible sorption domain with concentration  $S_3$ . The 3S2Rirx model is given by the following set of equations:

$$S_1 = K_f C^m \quad (2.37)$$

$$f_2 \frac{dS_2}{dt} = \alpha_2 (K_f C^m - S_2) \quad (2.38)$$

$$f_3 \frac{dS_3}{dt} = \alpha_3 K_f C^m \quad (2.39)$$

$$(\theta + \rho f_1 K_f m C^{m-1}) \frac{dC}{dt} = \frac{\alpha_2}{f_2} [C_t - \theta C - \rho (1 + \frac{f_1}{f_2} + \frac{\alpha_3}{\alpha_2}) f_2 K_f C^m - \rho f_3 S_3] \quad (2.40)$$

Similar to the two-site two-rate irreversible model Equations 2.37-2.40 can be simplified, because the definition of local concentrations is only needed for the two reversible sorption sites  $S_1$  and  $S_2$ . Total sorbed concentration is given by Equation 2.28, where:

$$S'_{\text{rev}} = f_1 S_1 + f_2 S_2 \quad (2.41)$$

$$S'_{\text{irrev}} = f_3 S_3 = S'_3 \quad . \quad (2.42)$$

Rewriting Equations 2.37 to 2.40 results in:

$$S'_1 = f_1 K_f C^m = \frac{f_1}{f_1 + f_2} (f_1 + f_2) K_f C^m \quad (2.43)$$

$$\frac{dS'_2}{dt} = \alpha_2 (K_f C^m - \frac{S'_2}{f_2}) = \frac{\alpha_2}{f_2} (\frac{f_2}{f_1 + f_2} (f_1 + f_2) K_f C^m - S'_2) \quad (2.44)$$

$$(\theta + \rho f_1 K_f m C^{m-1}) \frac{dC}{dt} = \frac{\alpha_2}{f_2} [C_t - \theta C - \rho (1 + \frac{f_1}{f_2} + \frac{\alpha_3}{\alpha_2}) f_2 K_f C^m - \rho S'_3] \quad . \quad (2.45)$$

The following definitions are used:  $\alpha_{\text{rev}} = \alpha_2/f_2$ ,  $\alpha_{\text{irrev}} = \alpha_3/(f_1 + f_2)$ ,  $K'_f = (f_1 + f_2)K_f$  and  $g = f_1/(f_1 + f_2)$ , where  $g$  is the fraction of instantaneous sites on reversible sites. The number of parameters in the model is reduced from six to five:

$$S'_1 = g K'_f C^m \quad (2.46)$$

$$\frac{dS'_2}{dt} = \alpha_{\text{rev}} ((1 - g) K'_f C^m - S'_2) \quad (2.47)$$

$$\frac{dS'_3}{dt} = \alpha_{\text{irrev}} K'_f C^m \quad (2.48)$$

$$(\theta + \rho g K'_f m C^{m-1}) \frac{dC}{dt} = \alpha_{\text{rev}} [C_t - \theta C - \rho (1 + \frac{\alpha_{\text{irrev}}}{\alpha_{\text{rev}}}) K'_f C^m - \rho S'_3] \quad . \quad (2.49)$$

### Three-site two-rate sorption – irreversible sorption as independent sink (3S2Rirrev)

In the previously discussed irreversible sorption models, irreversible sorption followed the same isotherm as was used for reversible sorption. But irreversible sorption can also be defined independently of the sorption isotherm (3S2Rirrev in Table 2.1). Equations 2.48 and 2.49 then change to:

$$\frac{dS'_3}{dt} = \frac{\theta}{\rho} \beta_3 C \quad (2.50)$$

$$(\theta + \rho g K'_f m C^{m-1}) \frac{dC}{dt} = \alpha_{\text{rev}} [C_t - \theta C (1 - \frac{\beta_3}{\alpha_{\text{rev}}}) - \rho K'_{\text{rev}} C^m - \rho S'_3] \quad , \quad (2.51)$$

where  $\beta_3$  is the irreversible sorption rate coefficient for solute transfer from the liquid phase into the irreversible sorption domain. This 3S2Rirrev model is equal to the 3S2R-Freu-irrev model discussed in the transport section. Note that the factor  $\theta/\rho$  was introduced in the model in order to be comparable with the *HYDRUS-1D*-model (Simunek *et al.*, 1998) in the transport section. It would, however, be more appropriate to exclude the experimental conditions from the conceptual model for a better parameter comparison between the various experiments.

## 2.3 Materials and methods

All sorption experiments were performed with a mixed top-soil sample and sulfadiazine ( $^{14}\text{C}$ -SDZ) characterized in Appendix A and B.

### 2.3.1 Experimental setup

Six series (A-F) of adsorption/desorption studies were conducted using the batch equilibrium technique. The main procedure was identical for all experiments. Differences between the six series were in the time-scale, the soil-water ratio and the solute concentration levels (Tables 2.2 and 2.3). Contrary to the experiments A to E, experiment F was performed with annealed soil (48 h at 450°C) to test the influence of soil organic matter on the sorption behavior.

For all experiments, except F, field moist soil was weighted into 50 mL centrifugation vials and mixed with a 0.01 M  $\text{CaCl}_2$  solution. All batch systems were shaken in the dark at 20-22°C for one week prior to application of SDZ. Different amounts of  $^{14}\text{C}$ -SDZ were spiked (Table 2.2), using the corresponding volume of a stock solution (0.5 g  $\text{L}^{-1}$  dissolved in acetonitrile). The volume of acetonitrile was small compared to the volume of water. We therefore assumed no adverse effects of the organic solvent on the sorption behavior of SDZ. After spiking the batch systems were shaken again according to the time scale for ad- and desorption (Table 2.3).

Control systems containing only  $\text{CaCl}_2$  solution and  $^{14}\text{C}$ -SDZ at the highest spiking level were run simultaneously to check the stability of SDZ. Batch systems without SDZ (blanks) were run to check for cross contamination during the sample processing. pH-variations in the solution were monitored in the blanks and in the spiked batch systems. SDZ did not influence the pH in the soil suspensions. The pH in the batch systems changed with time from initially 6.0 - 6.5 to approximately 7.0 - 7.5 after one week of equilibration.

### 2.3.2 Sampling and analysis

The batch systems were centrifuged at 20°C with 3000 g for 45 minutes prior to sampling. To determine the adsorption kinetics the required measuring volume of the supernatant was removed (0.3 to 0.8 mL). In the desorption experiments the clear supernatant was removed at each desorption step and replaced by an equal volume of a fresh 0.01 M  $\text{CaCl}_2$  solution and shaken again.  $^{14}\text{C}$ -concentrations

Table 2.2: Experimental conditions for the batch experiments.

Experiment	$m_{\text{soil}}^{\dagger}$ [g]	$\theta_{\text{initial}}^{\dagger}$ [g g <sup>-1</sup> ]	$V_{\text{liquid}}^{\S}$ [mL]	$m_{\text{soil}}:V_{\text{liquid}}^{\parallel}$ [g mL <sup>-1</sup> ]	$C_{\text{initial}}^{\ddagger}$ [mg L <sup>-1</sup> ]	$m_{\text{initial}}^{\dagger\dagger}$ [ $\mu$ g]	replicates
A	8.25	0.21	21.75	0.38	0.044, 0.44, 4.4	0.95, 9.48, 94.8	2
B	8.25	0.21	21.75	0.38	0.044, 0.44, 4.4	0.95, 9.48, 94.8	2
C	3.00	0.31	20.80	0.14	1.3, 2.6, 5.0, 12.4	26.2, 52.4, 104.8, 261.9	1
D	3.00	0.31	20.93	0.14	0.09, 0.22, 0.99, 2.54, 10.3	1.8, 4.48, 19.8, 50.7, 205.0	3
E	8.55	0.17	24.00	0.36	0.29, 0.56, 1.48, 2.95	7.03, 14.03, 35.55, 70.67	2
F	3.00	0.00 <sup>##</sup>	20.00	0.15	1.33, 2.64, 5.25, 12.94	26.2, 52.39, 104.78, 261.96	1

Average values are given; calculations were based on the precise values for each batch container. <sup>†</sup>Mass of dry soil, <sup>‡</sup>initial water content in soil (field moist), <sup>§</sup>solution volume (volume of water in moist soil, CaCl<sub>2</sub> and SDZ stock solution), <sup>||</sup>soil to solution ratio, <sup>¶</sup>initial SDZ concentration levels, <sup>††</sup>total <sup>14</sup>C-SDZ mass per batch system. <sup>##</sup>Soil was dry after annealing in experiment F.

Table 2.3: Sampling schedule for the batch experiments.

Experiment	time-scale	sampling times [days]		sampling volume <sup>†</sup> [mL]
		adsorption	desorption	
A	short	1, 2, 4, 7, 14	<sup>‡</sup>	0.3 <sup>‡</sup>
B	short	1 <sup>§</sup>	1, 2, 3, 4, 7, 14	0.8
C	intermediate	0.75, 2, 4, 7, 9, 14	14, 21, 28, 35, 42	0.8
D	long	41 <sup>§</sup>	41, 84, 124, 163, 204, 272	0.8
E	long	1, 5, 11, 18, 25, 40, 153	<sup>‡</sup>	1.5 <sup>‡</sup>
F	intermediate	0.75, 2, 4, 7, 9, 14	14, 21, 35, 42	0.8

<sup>†</sup>Average values are given here; calculations were based on the precise values for each batch container.

<sup>‡</sup>No desorption conducted. <sup>§</sup>Time of first desorption step.



were measured by liquid scintillation counting (LSC) using the method given in Appendix C. After each ad- or desorption step the batch system was weighted to monitor all changes in solution volume, assuming that the total weight of soil was constant.

Sorbed concentrations were calculated based on mass balance considerations. The difference between the initial total mass and measured mass in the soil solution was assumed to be sorbed. In the calculation of the sorbed concentrations solvent removal during sampling (adsorption kinetics) and desorption steps was taken into account.

After the last centrifugation and sampling step the solution was completely decanted. The remaining wet soil was dried in an oven at 105°C for two to three days until the mass remained constant. The water content was determined from the weight difference before and after drying. The oven-dried soil was ground and mixed homogeneously prior to determination of  $^{14}\text{C}$  (Appendix D). The sorbed concentrations were calculated after correction for the SDZ mass in the liquid phase. To check mass balances, those concentrations were compared to the values calculated based on mass differences.

### 2.3.3 Data analysis and parameter estimation

Sorption processes were identified by testing the ability of various kinetic sorption models (Section 2.2) to describe the observed data. The sorption models were fitted to the measured data using the *fithyst*-programme (Streck *et al.*, 1995). It numerically solves the model equations and uses the Levenberg-Marquardt algorithm for the inverse parameter optimization. The required boundary conditions were given by the setup of the experiment (total solute mass, mass of soil, total volume of solution after each sampling time, removed and added volumes of solution at each sampling time) and the assumption that the total solute mass is constant over time (no decay). Initial parameter values for the model calculations were best guess values for the sorption parameters, which were derived from preliminary forward calculations. The concentration data were  $\log_{10}$ -transformed in the fitting procedure, to distribute the weight more evenly within the concentration range.

## 2.4 Results

### 2.4.1 Experimental results

The experiments A and B were short-term experiments, investigating the adsorption (A) and desorption (B) kinetics within 14 days. After one day of equilibration the adsorption data of both experiments can be described by a linear function in a  $\log C$ - $\log S$ -plot (Figure 2.1). This functional relationship is given by the Freundlich sorption isotherm (Equation 2.5), where the parameters  $\log K_f = 0.39$  (equals  $K_f = 2.46 \text{ mg}^{1-m} \text{ L}^m \text{ kg}^{-1}$ ) and  $m = 0.66$  are the intercept and the slope of the function, respectively. A decrease in  $^{14}\text{C}$  concentration in the solution with time was observed

in experiment A, which indicates that the adsorption of SDZ is a kinetic process within the time-scale of observation. In the desorption experiment B the sorbed concentrations did not significantly decrease (Figure 2.1), despite the strong concentration gradient between soil and solution imposed by the five desorption steps. Hence, desorption of SDZ is also rate-limited, but appears to occur on a much slower time scale than the adsorption kinetics.

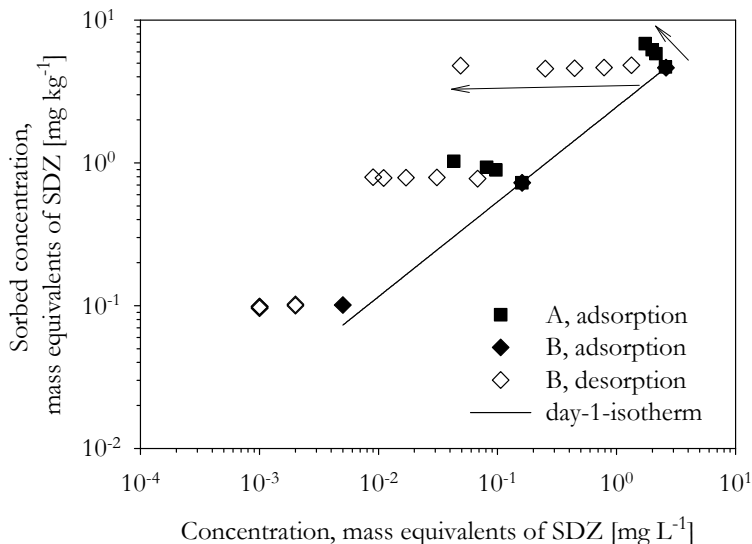


Figure 2.1: Sorption/desorption of SDZ in the short-term batch experiments A and B. Concentrations were measured after 1, 2, 4, 7 and 14 days for adsorption kinetics (A). Desorption steps (B) were carried out after 1, 2, 3, 4, 7 and 14 days. Time proceeded in the direction of the arrows. The fitted Freundlich isotherm for the adsorption after one day is given.

We decreased the amount of sorbent and increased the equilibration time to avoid the effect of incomplete adsorption during the desorption steps in experiment C. Since the soil-solution ratio was now lower, the observed changes in the sorbed concentration were more pronounced during adsorption (Figure 2.2). The parameter of the 0.75-day adsorption isotherm are similar to the previous experiments ( $K_f = 2.13 \text{ mg}^{1-m} \text{L}^m \text{kg}^{-1}$ ,  $m = 0.81$ ), indicating that the influence of the soil-solution ratio on sorption is negligible. Because of the slow desorption kinetics in experiment B, desorption intervals of one week were chosen in experiment C to increase the desorbed amount of solute. Nevertheless, the observed desorption was still very slow (Figure 2.2).

Since an equilibrium distribution of SDZ between the soil and the solution was not achieved in the experiments A, B or C, the experimental time scale was further increased in the experiments D and E (Table 2.3). Long-term desorption kinetics were studied in experiment D, after one adsorption step of 41 days (Figure 2.3). The 41 days adsorption isotherm is parameterized with  $K_f = 9.14 \text{ mg}^{1-m} \text{L}^m \text{kg}^{-1}$  and  $m = 0.52$ . For the following desorption steps (about 41 days equilibration time each)

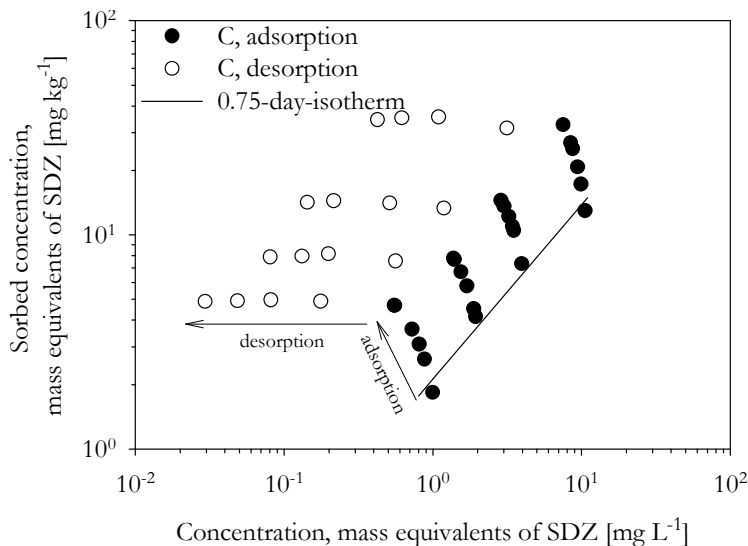


Figure 2.2: Sorption/desorption of SDZ in the intermediate-term batch experiment C. Concentrations were measured after 0.75, 2, 4, 7, 9 and 14 days for adsorption kinetics (filled symbols), desorption steps were carried out after 14, 21, 28, 35 and 42 days (empty symbols). Time proceeded in the direction of the arrows. The fitted Freundlich isotherm for the adsorption after 0.75 days is given.

again only little desorption was observed. Figure 2.4 shows the normalized sorbed concentrations  $S(t)/S_{\text{adsorption}}(41\text{d})$  with time, indicating very slow desorption kinetics. The decrease of the normalized sorbed concentrations,  $S(t)/S_{\text{adsorption}}(41\text{d})$ , was most pronounced during the first desorption steps and for the higher concentration levels, but was independent of concentration for the last desorption steps (equal slopes of the curves after 84 days). For each observation time, the Freundlich parameters were determined by curve fitting (Figure 2.5). A shift from a non-linear to a more linear desorption behavior with time was observed since the Freundlich exponent  $m$  increased from 0.52 after 41 days of adsorption to 1.03 for the last desorption step (Figure 2.5b).  $K_f$  increased with each desorption step from 9.14 to  $672 \text{ mg}^{1-m}\text{L}^m\text{kg}^{-1}$ , indicating that the adsorption outweighs the desorption within the experimental time frame (Figure 2.5a).

Long-term adsorption kinetics were studied in experiment E for 153 days (Figure 2.6). An apparent sorption equilibrium was reached within approximately 20 days. After this time the solute concentration did not change anymore with time (Figure 2.7). Thus, sorption equilibrium was already achieved at the first desorption step in experiment D (after 41 days), which was previously assumed. Fitting the Freundlich equation for each observation time revealed that the Freundlich coefficient  $K_f$  increased with time from 3 to  $9 \text{ mg}^{1-m}\text{L}^m\text{kg}^{-1}$  and the Freundlich exponent was approximately constant at a value of  $m = 0.63$  (Figure 2.5). This indicates a time-dependent, non-linear sorption behavior.

Experiment F indirectly showed the influence of organic matter on the sorption

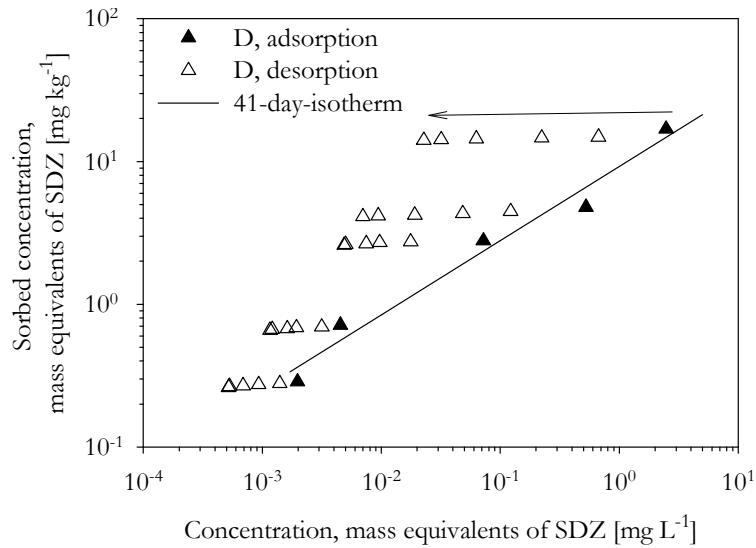


Figure 2.3: Sorption/desorption of SDZ in the long-term batch experiment D. Desorption steps were carried out after 41, 84, 124, 163, 204 and 272 days. Time proceeded in the direction of the arrow. The fitted Freundlich isotherm for the adsorption after 41 days is given.

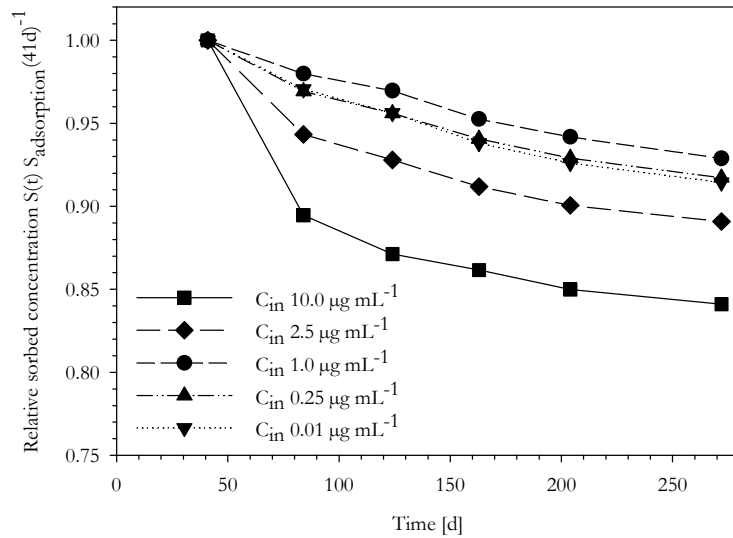


Figure 2.4: Desorption kinetics of SDZ in the long-term batch desorption experiment D. Sorbed concentrations  $S(t)$  were normalized by the corresponding equilibrium adsorption concentration  $S_{\text{adsorption}}(41\text{d})$  to illustrate the slow decrease.

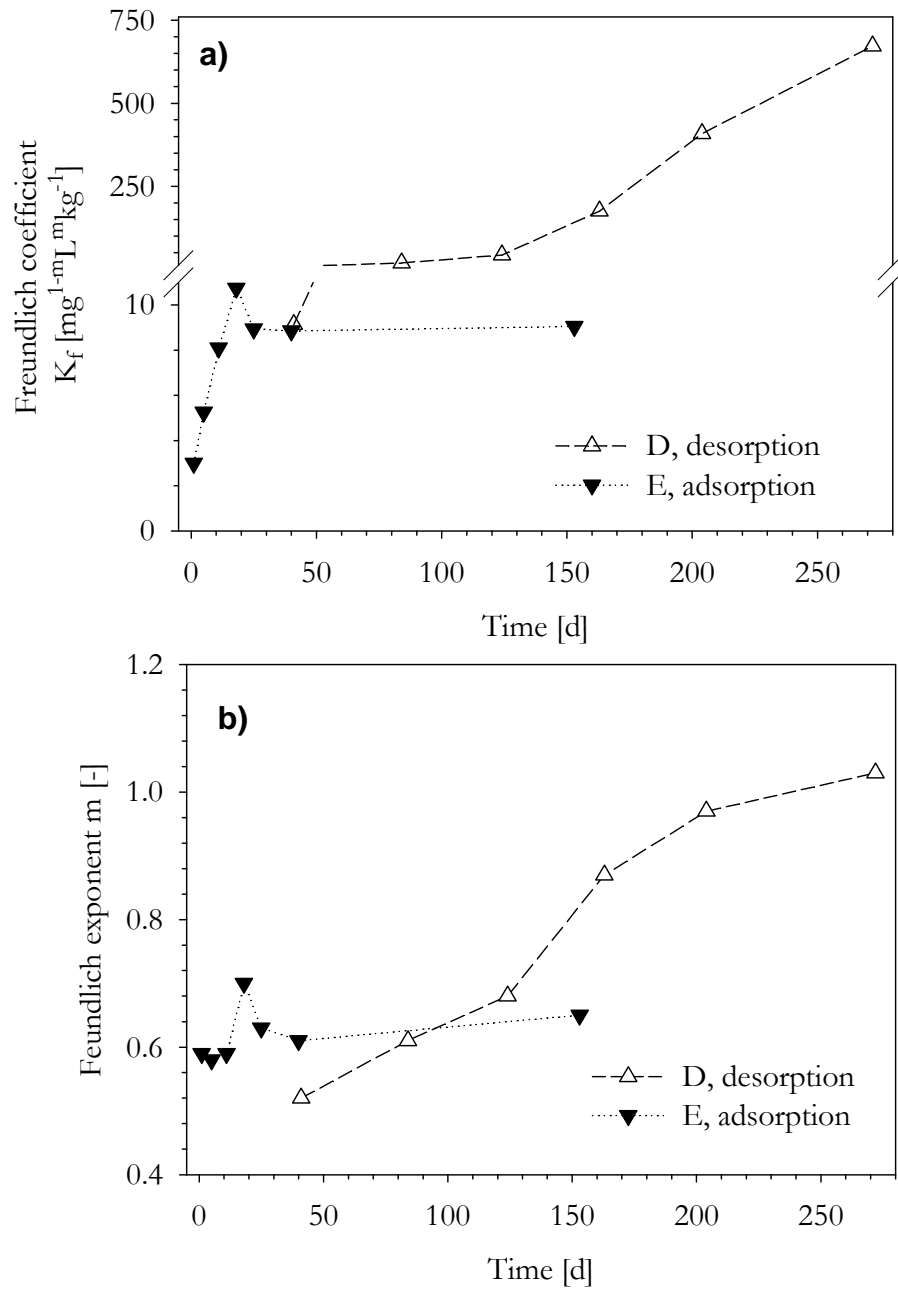


Figure 2.5: Freundlich parameters a)  $K_f$  and b)  $m$  from adsorption and desorption experiments D and E.

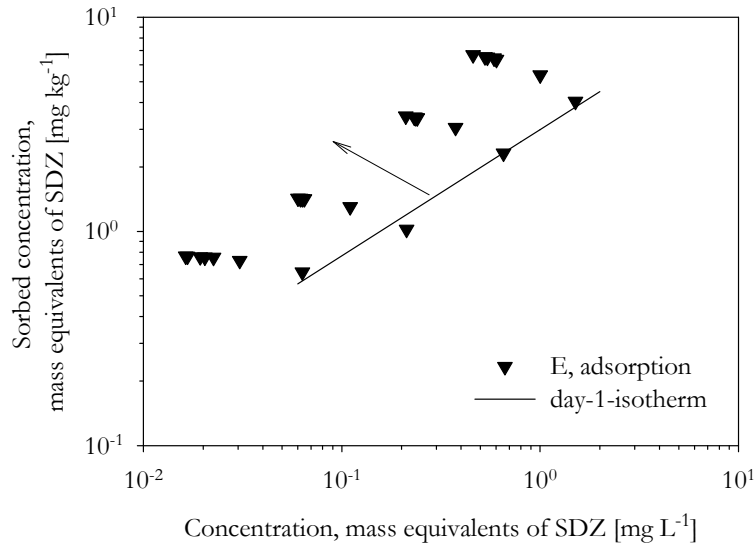


Figure 2.6: Adsorption of SDZ in the long-term batch adsorption experiment E. Concentrations were measured after 1, 5, 11, 18, 25, 40 and 153 days. Time proceeded in the direction of the arrows. The fitted Freundlich isotherm for the adsorption after one day is given.

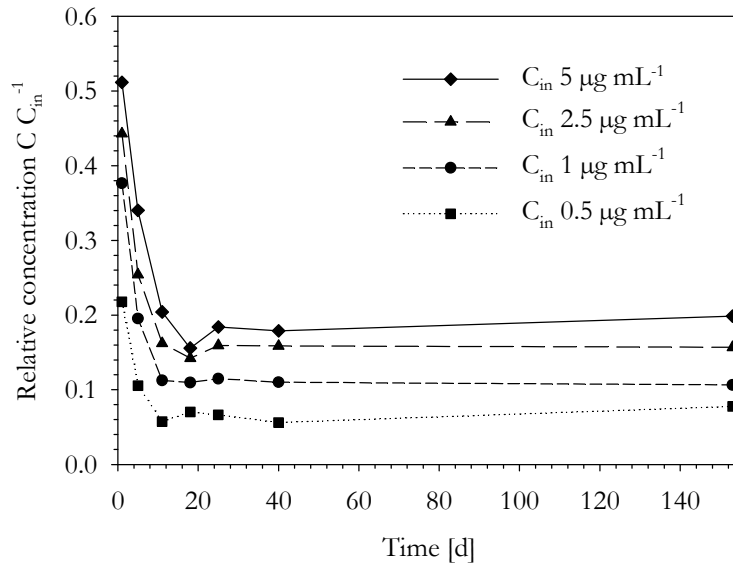


Figure 2.7: Adsorption kinetics of SDZ in the long-term batch adsorption experiment E.

behavior of SDZ in soil by the use of annealed soil. The experimental conditions were identical to those of experiment C (Tables 2.2 and 2.3). SDZ sorbed less to the annealed soil compared to the fresh soil (day-one Freundlich isotherm parameters:  $K_f=0.15 \text{ mg}^{1-m}\text{L}^m\text{kg}^{-1}$  with an  $m$  larger than 1,  $m = 1.18$ , Figure 2.8). However, slow desorption kinetics were also observed in the annealed soil and therefore the mineral phase is likely to cause this slow desorption.

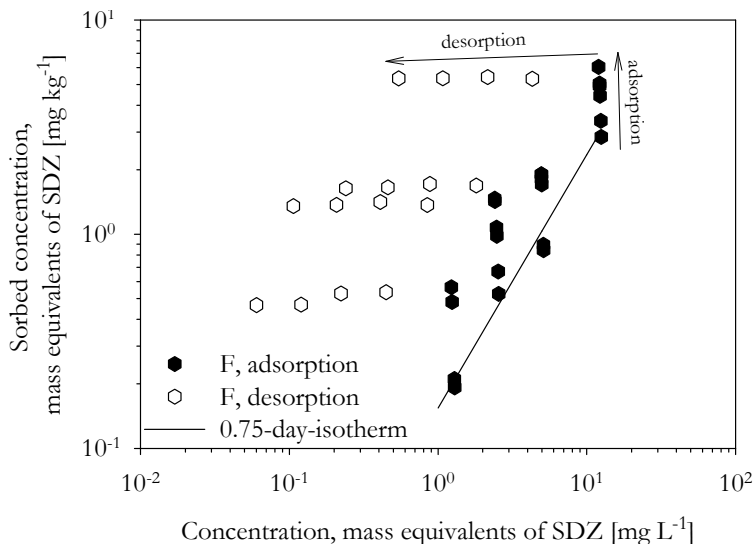


Figure 2.8: Sorption/desorption of SDZ in annealed soil in batch experiment F. Concentrations were measured after 0.75, 2, 4, 7, 9 and 14 days for adsorption kinetics (filled symbols), desorption steps were carried out after 14, 21, 28, 35 and 42 days (empty symbols). Time proceeded in the direction of the arrows. The fitted Freundlich isotherm for the adsorption after 0.75 days is given.

## 2.4.2 Modelling results

The experimentally determined sorption behavior of SDZ in soil was parameterized with various sorption models. Starting with the simplest model that accounts for the observed rate-limited, non-linear sorption (Section 2.2.1, Equation 2.6), model complexity was gradually enhanced to find an appropriate description of the experimental results with the smallest number of model parameters.

### Rate-limited sorption model

As a first estimate, a simple rate-limited sorption model (Equation 2.6) was used to describe the slow adsorption. The best fit of the rate-limited sorption model to experiment E shows (Figure 2.9) that the model was not able to describe the experimental data: Despite the relatively good description of the equilibrium sorption ( $K_f=8.38 \text{ mg}^{1-m}\text{L}^m\text{kg}^{-1}$  and  $m=0.64$ ), the initial sorption behavior is not correctly

reflected. To be able to fit the last time steps in the experiment, the rate parameter  $\alpha$  had to be very small ( $\alpha = 0.30 \text{ d}^{-1}$ ). This results in an underestimation of the observed initial sorbed concentrations. Higher values for either  $K_f$  or  $\alpha$  result in a better fit for the initial sorption but also in an overestimation of the equilibrium sorption or in faster adsorption kinetics, respectively.

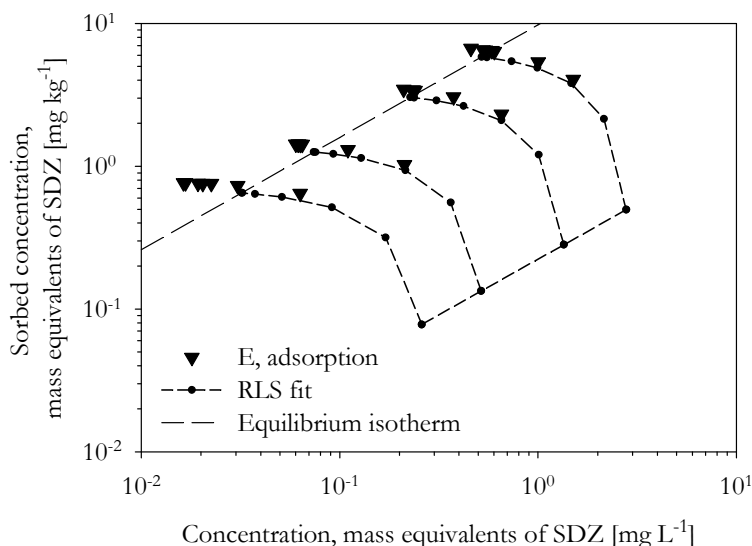


Figure 2.9: Measured and optimized sorption in experiment E using the kinetic sorption model (RLS: rate-limited sorption). The dashed line is the equilibrium isotherm resulting from the optimized parameters.

The rate-limited sorption model assumes equal transfer rates for both adsorption and desorption. From experiments D and E we know that desorption is much slower than adsorption because the time to reach an apparent adsorption equilibrium was not sufficient to reach a desorption equilibrium, too. Models with various sorption domains were introduced (Section 2.2.1) to account for different sorption processes in soil.

### Two-stage one-rate sorption model

The two-stages one-rate model (2S1R, Section 2.2.2) was used to individually parameterize the sorption behavior of SDZ in the various experimental series (Table 2.4). The solute mass transfer between the different domains in a batch system is illustrated for the parameter combination of the experiments A and B. Using the mathematical model, the contribution of all phases to the redistribution of the initially applied mass can be easily calculated. Experimentally it is impossible to measure the concentration in the various sub-domains.

Figures 2.10 and 2.11 show the theoretical solute distribution during sorption and desorption for the experimental conditions A, B. Three concentration levels (varying by two orders of magnitude) were plotted to demonstrate the effect of non-linear



sorption isotherms ( $m = 0.65$ ). Relatively more mass is removed by the desorption step at higher concentration levels. Sorption equilibrium is reached faster at lower concentration levels ( $C$  reaches constant values within ten days, Figure 2.11) due to the combined effect of sorption non-linearity and kinetics. The desorption step was performed after one or ten days in Figures 2.10 or 2.11, respectively. Since sorption kinetics are slow, more mass is removed by the desorption step after one day than after ten days (change in  $C_t$ , left hand side Figures 2.10 and 2.11). If sorption equilibrium is not reached at the time of desorption, a desorption step only further decreases the solute concentration in the liquid phase. Because of the mass removal and the dilution, solute concentration in the equilibrium domain  $S_1$  is also reduced, since it is directly linked to the solute concentration by instantaneous sorption. However, the kinetic sorption domain  $S_2$  keeps taking up solute, as long as the local sorbed concentration  $S_1$  is higher than  $S_2$ . Consequently, the concentration in the liquid phase decreases. Hence, only the desorption step after ten days of equilibration induced a reversed concentration gradient and  $C$  increased (Figure 2.11). Note that the bulk concentrations are plotted in Figures 2.10 and 2.11.

In Figures 2.12, 2.13, 2.14 and 2.15 the measured and fitted or predicted sorption data are plotted for each parameter set of the experiments with the fresh soil. Although the 2S1R-model was flexible enough to describe the various experiments, the optimized parameters depend on the experimental schedule. Whereas the Freundlich coefficients,  $K_f$ , were higher for the intermediate- or long-term desorption experiments C and D, the fitted rate parameters were smaller than for the other experiments (Table 2.4). The adsorption kinetics of experiments A, C, and E was well described with the best fit parameters of either experiments A and B (Figure 2.12) or E (Figure 2.15). The instantaneous sorption showed relatively high initial total sorbed concentrations, despite low values for  $\alpha$  and  $K_f$ . Fitted parameters for the equilibrium isotherm are within the range of the observations in experiment E (Table 2.4). The fitted model for experiments A and B or E overestimate the observed long-term desorption in experiments C and D (empty symbols in Figure 2.12 or 2.15). Therefore, the observation of adsorption kinetics and short-term desorption is insufficient for process identification of long-term desorption. This further indicates that the 2S1R-model concept itself is inappropriate to describe the experimental data.

Figure 2.13 demonstrates that it is possible to describe the intermediate-term desorption (experiment C) with the 2S1R model. To account for the slow desorption,  $\alpha$  is very small, whereas  $K_f$  in return needed to be higher to describe the initial sorption. But the forward calculations for the experimental conditions A, B, D and E do not match the data: Sorbed concentrations at sorption equilibrium (dashed line in Figure 2.13) are overestimated for experiment E due to the high  $K_f$ . The small adsorption rate results in lower predicted sorbed concentrations in experiment A than observed. For the short-term desorption in experiment B also lower sorbed concentrations are predicted. Because of the low transfer rate coefficient,  $\alpha$ , the total solute mass in the second sorption stage is still very low after one day of equilibration. With each desorption step mass is only removed from the instantaneous domain ( $C$  and  $S_1$ ), resulting in a decrease in total sorbed concentration  $S$ . Total sorbed

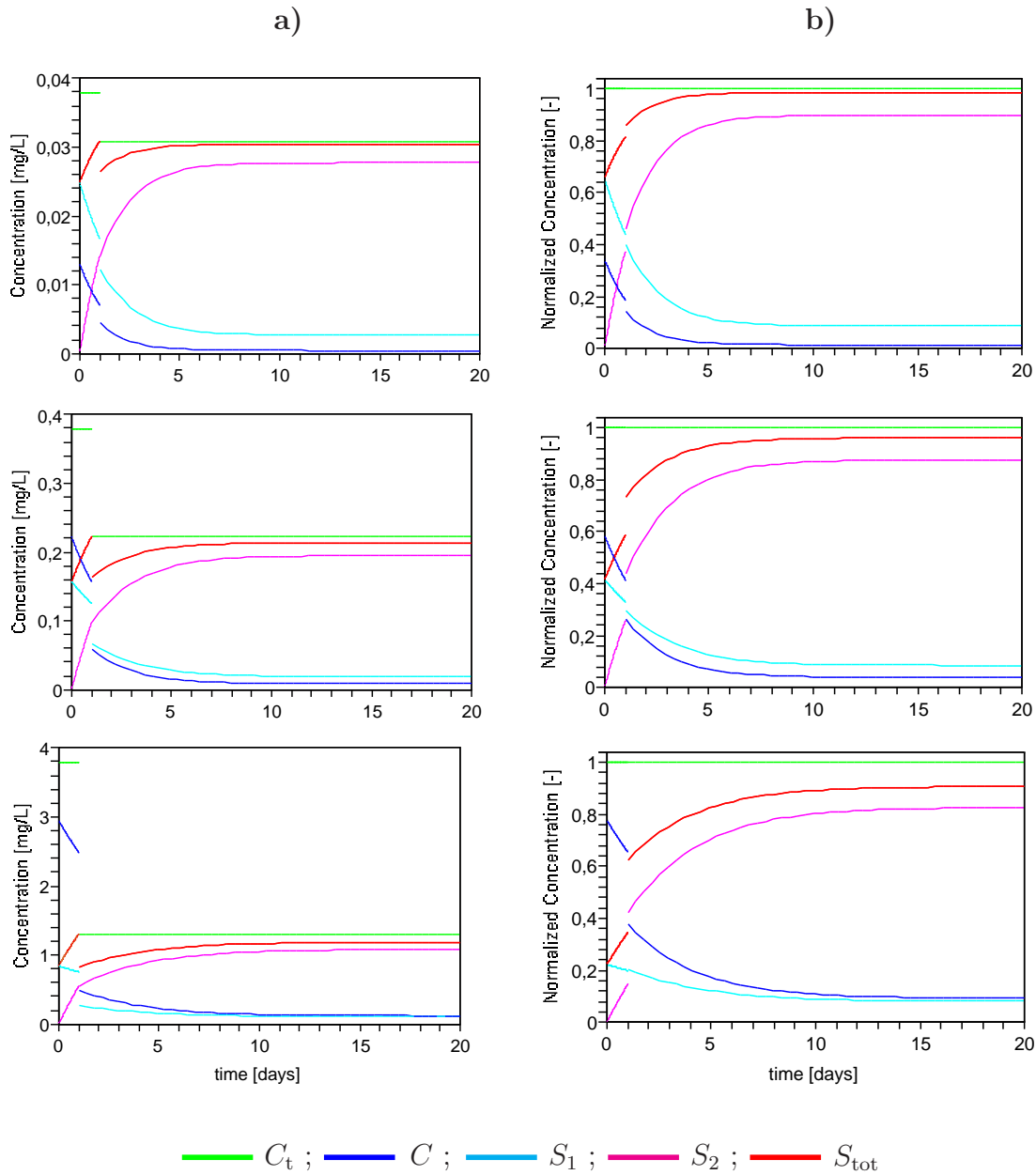


Figure 2.10: Solute distribution among the various domains in a batch-system according to the 2S1R model at different concentration levels. Initial total solute concentrations were 0.038, 0.38 and 3.8 mg L<sup>-1</sup> from the top to the bottom figures. Experimental conditions A, B and their best fit parameters were used. The desorption step was conducted after 1 day by exchanging the solution phase completely. Solute concentrations are given in column a) as mass of solute in the domain per total batch volume [mg L<sup>-1</sup>]. Normalized solute concentrations are given in column b), where solute concentrations in each domain are divided by the total solute concentration in the system ( $C_t$ ).

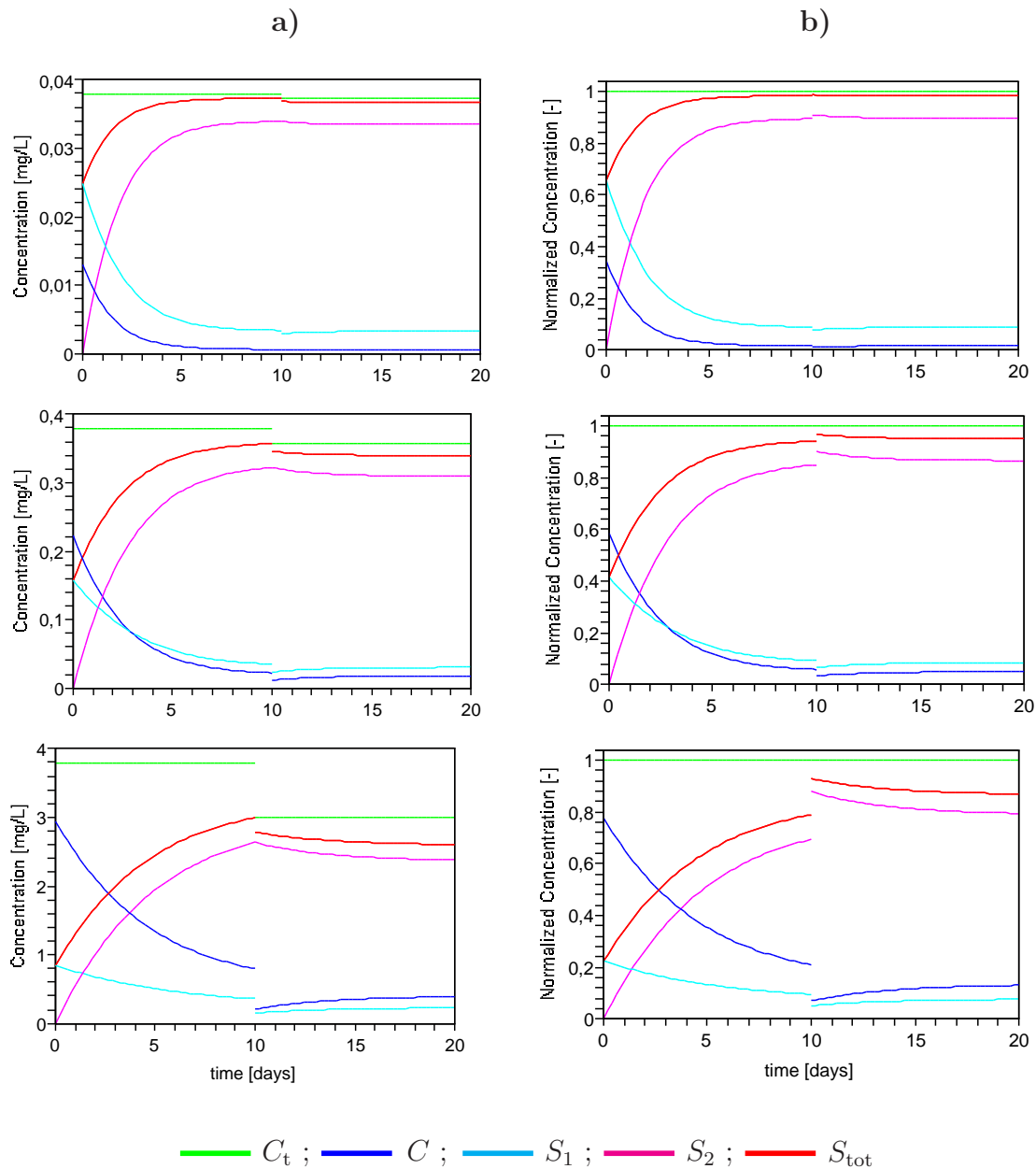


Figure 2.11: Solute distribution among the various domains in a batch-system according to the 2S1R model at different concentration levels. Initial total solute concentrations were 0.038, 0.38 and 3.8  $\text{mg L}^{-1}$  from the top to the bottom figures. Experimental conditions A, B and their best fit parameters were assumed. The desorption step was conducted after 10 days by exchanging the solution phase completely. Solute concentrations are given in column a) as mass of solute in the domain per total batch volume [ $\text{mg L}^{-1}$ ]. Normalized solute concentrations are given in column b), where solute concentrations in each domain are divided by the total solute concentration in the system ( $C_t$ ).

Table 2.4: Best fit parameters for the sorption experiments A-F using the 2S1R sorption model.

Experiment	$\alpha_2$	$SE_{\alpha_2}^{\dagger}$	$f_1$	$SE_{f_1}^{\dagger}$	$m$	$SE_m^{\dagger}$	$K_f$	$SE_{K_f}^{\dagger}$	$SSQ^{\ddagger}$
	$\text{d}^{-1}$						$\text{mg}^{-1-m}\text{L}^m\text{kg}^{-1}$		
A + B	$6.4 \times 10^{-2}$	$1.6 \times 10^{-2}$	$9.0 \times 10^{-2}$	$2.9 \times 10^{-2}$	$6.5 \times 10^{-1}$	$2.9 \times 10^{-2}$	$1.3 \times 10^{+1}$	$3.5 \times 10^{+0}$	$7.0 \times 10^{-1}$
C	$4.4 \times 10^{-3}$	$9.3 \times 10^{-4}$	$2.9 \times 10^{-2}$	$5.2 \times 10^{-3}$	$7.6 \times 10^{-1}$	$3.8 \times 10^{-2}$	$7.8 \times 10^{+1}$	$1.4 \times 10^{+1}$	$7.9 \times 10^{-2}$
D	$9.4 \times 10^{-4}$	$2.9 \times 10^{-4}$	$5.1 \times 10^{-2}$	$1.6 \times 10^{-2}$	$8.1 \times 10^{-1}$	$5.9 \times 10^{-2}$	$2.3 \times 10^{+2}$	$9.9 \times 10^{+1}$	$1.4 \times 10^{+0}$
E	$8.7 \times 10^{-2}$	$8.5 \times 10^{-3}$	$2.5 \times 10^{-1}$	$2.4 \times 10^{-2}$	$6.3 \times 10^{-1}$	$1.2 \times 10^{-2}$	$9.0 \times 10^{+0}$	$3.1 \times 10^{-1}$	$1.8 \times 10^{-1}$
F	$2.3 \times 10^{-3}$	$1.1 \times 10^{-3}$	$6.2 \times 10^{-3}$	$2.3 \times 10^{-3}$	$1.1 \times 10^{+0}$	$6.7 \times 10^{-2}$	$1.1 \times 10^{+1}$	$4.8 \times 10^{+0}$	$3.0 \times 10^{-3}$

<sup>†</sup>standard error of estimate; <sup>‡</sup>sum of squares. Since the data base is different for each set of parameters, the SSQ-values are not comparable.

Table 2.5: Best fit parameters for the sorption experiments A-E using the irreversible sorption models 2S2Rirx, 3S2Rirx and 3S2Rirrev. Models were simultaneously fitted to all experiments. In the upper panel the fitlyst-parameters are given. The lower panel shows the recalculated parameters after elimination of one parameter.

Model	$\alpha_1$	$SE_{\alpha_1}^{\dagger}$	$\alpha_2$	$SE_{\alpha_2}^{\dagger}$	$\alpha_3$	$SE_{\alpha_3}^{\dagger}$	$f_1$	$SE_{f_1}^{\dagger}$	$f_2$	$K_f$	$SE_{K_f}^{\dagger}$	$m$	$SE_m^{\dagger}$	$SSQ^{\ddagger}$
	$\text{d}^{-1}$									$\text{mg}^{-1-m}\text{L}^m\text{kg}^{-1}$				
2S2Rirx <sup>§</sup>	$7.8 \times 10^{-2}$	$1.2 \times 10^{-2}$	$8.6 \times 10^{-3}$	$1.0 \times 10^{-3}$	-	-	0.5 <sup>‡</sup>	-	-	12	1.1	0.66	$2.4 \times 10^{-2}$	3.9
3S2Rirx	-	-	$6.1 \times 10^{-2}$	$1.3 \times 10^{-2}$	$3.7 \times 10^{-3}$	$5.0 \times 10^{-4}$	0.12	$4.7 \times 10^{-2}$	0.5 <sup>‡</sup>	9.8	1.4	0.56	$2.7 \times 10^{-2}$	7.1
3S2Rirrev	-	-	$4.8 \times 10^{-2}$	$7.0 \times 10^{-3}$	$3.2 \times 10^{-2}$	$2.5 \times 10^{-3}$	0.12	$3.3 \times 10^{-2}$	0.5 <sup>‡</sup>	10	1.1	0.53	$2.2 \times 10^{-1}$	4.1

Model	$\alpha_{\text{rev}}$	$\alpha_{\text{irrev}}$	$g$	$m$	$K_f^{\#}$
	$\text{d}^{-1}$				$\text{mg}^{-1-m}\text{L}^m\text{kg}^{-1}$
2S2Rirx <sup>§</sup>	$7.8 \times 10^{-2}$	$8.6 \times 10^{-3}$	-	0.66	$6.2 \times 10^{+0}$
3S2Rirx	$1.2 \times 10^{-1}$	$6.1 \times 10^{-3}$	$1.9 \times 10^{-1}$	0.56	$6.0 \times 10^{+0}$
3S2Rirrev	$9.6 \times 10^{-2}$	$3.2 \times 10^{-2}$	$2.0 \times 10^{-1}$	0.53	$6.4 \times 10^{+0}$

<sup>†</sup>standard error of estimate; <sup>‡</sup>sum of squares; <sup>§</sup>long-term data of experiments D and E were not included in the fitting procedure; <sup>#</sup> $K_x$  in case of 2S2Rirx-model; <sup>‡</sup>fixed value in fitting procedure.

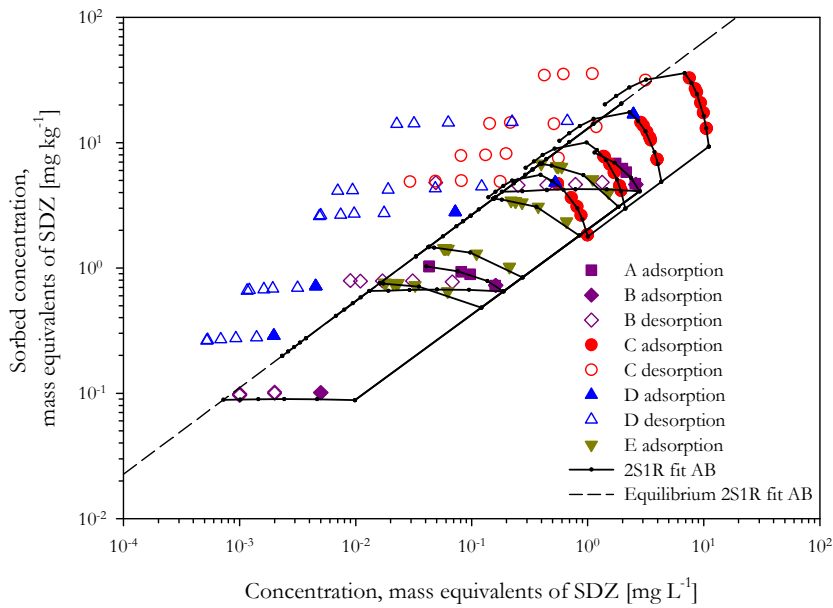


Figure 2.12: Measured data of sorption experiments A, B, C, D, E with model predictions using the two-stage-one-rate sorption model (2S1R) and the best fit parameters of experiments A and B.

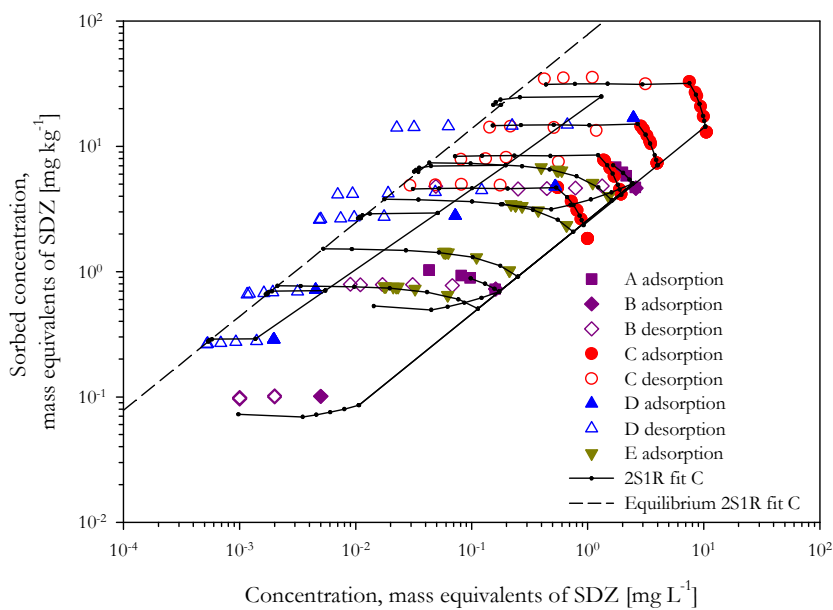


Figure 2.13: Measured data of sorption experiments A, B, C, D, E with model predictions using the two-stage-one-rate sorption model (2S1R) and the best fit parameters of experiment C.

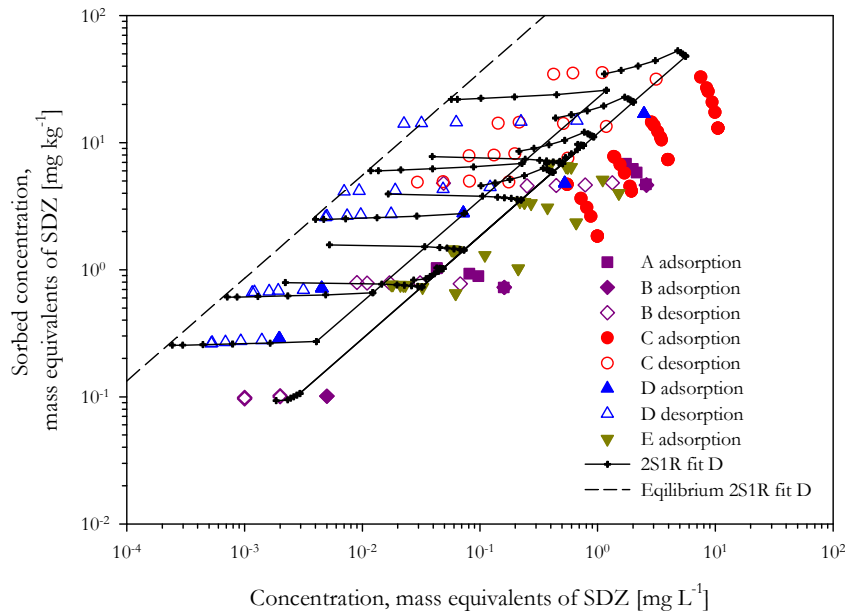


Figure 2.14: Measured data of sorption experiments A, B, C, D, E with model predictions using the two-stage-one-rate sorption model (2S1R) and the best fit parameters of experiment D.

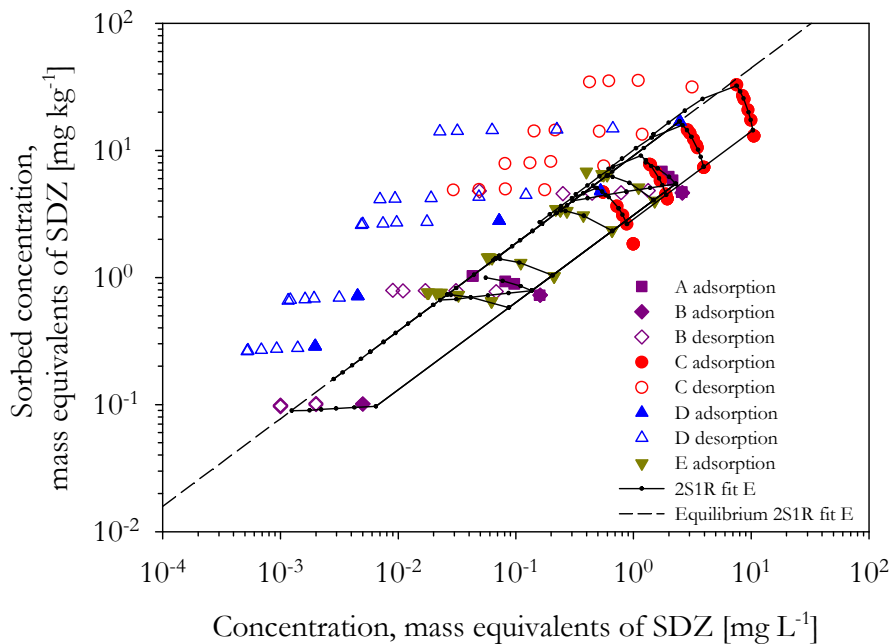


Figure 2.15: Measured data of sorption experiments A, B, C, D, E with model predictions using the two-stage-one-rate sorption model (2S1R) and the best fit parameters of experiment E.

concentration  $S$  is lowest directly after the instantaneous redistribution of solute between the equilibrium sorption stage and the fresh solution. With time the solute transfer from stage one to stage two carries on due to the concentration gradient. Since the fraction of stage two ( $1 - f_1$ ) is large, a slow increase in  $S_2$  results in a fast decrease in  $S_1$ . This is instantaneously compensated by an uptake of solute from solution, thus,  $C$  decreases. Because sorption equilibrium is reached faster in the lower concentration levels, the slope of the sorption isotherm,  $m$ , changes with time. In the beginning of the sorption process, the slope is equal to the equilibrium value, because kinetic sorption is still negligible. During the sorption process the slope of the isotherm decreases. Finally, the equilibrium isotherm will be reached. This explains the different slopes of the solid lines for the predicted initial concentrations of experiments A, B, C and E (0.75 or 1 day adsorption) compared to experiment D (41 day adsorption) in Figure 2.13.

A parametrization for the 2S1R-model was found to describe the very slow desorption in the long-term desorption experiment D (Figure 2.14). Since the time scale is longer in experiment D than in C, the fitted rate parameter is even smaller (Table 2.4). In combination with the small fraction of the equilibrium sorption stage and the large  $K_f$ , short-term adsorption is overestimated. Also for the long-term adsorption experiment E the predicted sorbed concentrations are higher than the observed, but the calculated equilibrium is not reached within this experimental schedule (final time 153 days). The predicted fast desorption for experiments B and C is caused by solute removal from the instantaneous stage only, whereas  $S_2$  still increases with time due to the very slow mass transfer.

Since no parametrization of the 2S1R-model was able to describe all the experimental data, not all relevant processes are included in the 2S1R-model. A major mismatch of the 2S1R model descriptions was observed in the different adsorption and desorption rates. Therefore, sorption models were tested, which considered one additional kinetic sorption domain instead of the instantaneous sorption domain.

### **Two-stage two-rate sorption model (2S2R, sites)**

However, no parameter combination was found for the two-stage two-rate reversible sorption model (2S2R (sites), Section 2.2.2) to describe all experiments simultaneously. The data are not presented here, because the model calculations for the single experiments were comparable to the 2S1R-models discussed before. Large rate coefficients for the mass transfer between solution and the first sorption stage enabled a high initial sorption. This fast kinetic process is, however, well approximated by the instantaneous sorption equilibrium in the 2S1R-model. In order to describe the slow desorption, the next model approach involves an irreversible kinetic process (Section 2.2.2) in the second sorption domain.

### **Two-site two-rate irreversible sorption model (2S2Rirx)**

It was impossible to describe all experimental data with the 2S2Rirx model using one set of parameters. However, if the long-term data points are not included in

the inverse calculation, the model is flexible enough to describe the remaining data (Figure 2.16, Table 2.5). Major differences between model and data were in the initial sorption of the short-term adsorption values and in the prediction of the long-term desorption of experiment D. Since solute uptake was assumed to be only kinetic, the initial adsorption in experiments A, B, C, and E was underestimated. For long times total mass will be irreversibly sorbed in the second sorption sites. Therefore, this model could not describe the equilibrium distribution observed in experiment E, or the slow desorption of experiment D. To overcome the mismatch in the prediction of the high initial sorption a further sorption site was added to the previous model. This third sorption domain is in instantaneous equilibrium with the soil solution.

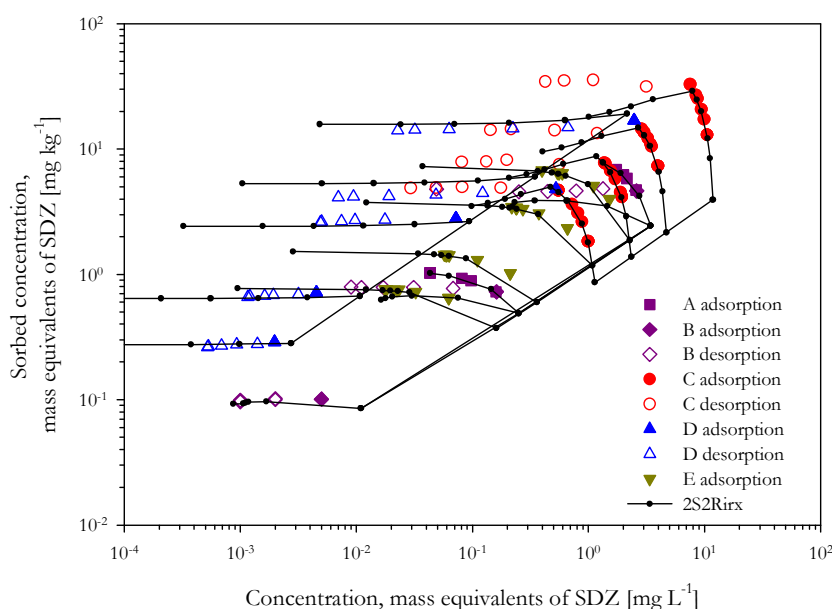


Figure 2.16: Measured data of sorption experiments A, B, C, D, E and model predictions using the two-site-two-rate irreversible sorption model (2S2Rirx). The last three desorption steps of D and the last adsorption point of E were not involved in the inverse solution. The corresponding model values were determined by forward simulation.

### Three-site two-rate irreversible sorption model (3S2Rirx)

The 3S2Rirx-model was flexible enough to describe all experimental data satisfyingly using one set of parameters (Figure 2.17, Table 2.5). The initial adsorption was better described in the lower concentration range, but underestimated in the higher concentration levels due to the small Freundlich exponent. The 3S2Rirx-model also predicted a larger sorption than observed for the short-term desorption experiments, caused by desorption from the instantaneous sorption sites.



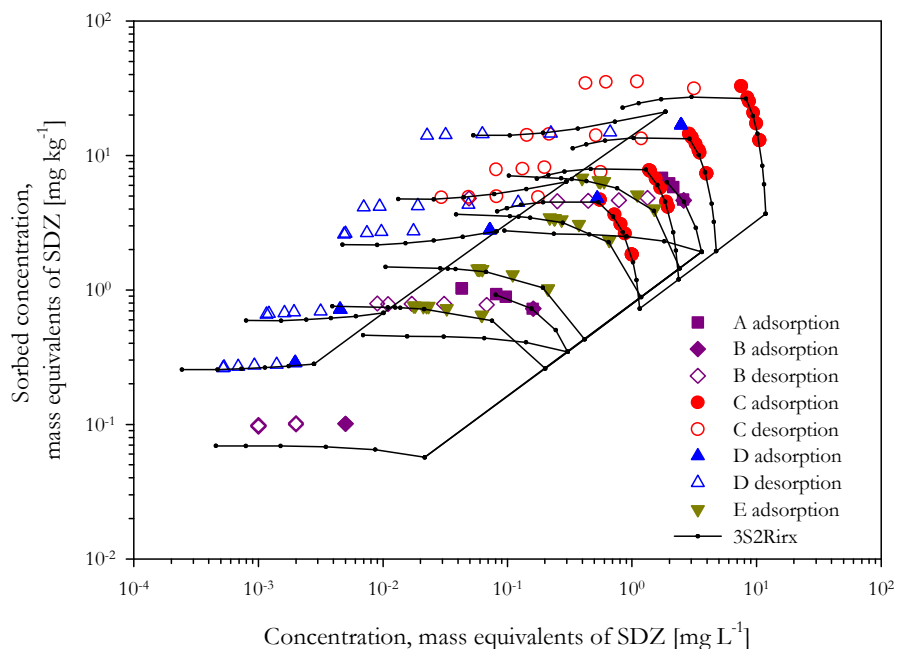


Figure 2.17: Measured data of sorption experiments A, B, C, D, E with model predictions using the three-stage two-rate irreversible sorption model (3S2Rirx).

### Three-site two-rate irreversible sorption model (3S2Rirrev)

Another approach to include an irreversible sorption process is to consider an infinite sink term, where the solute is removed from solution following first-order kinetics (3S2Rirrev). This model successfully described all sorption data (experiments A-E, Figure 2.18). The 3S2Rirrev-model describes the characteristic features of the experiments best (lowest SSQ of all models in Table 2.5) and is therefore discussed in more detail.

The solute distribution between the various sorption domains during ad- and desorption at four different concentration levels (varying by three orders of magnitude) is presented in Figures 2.19 and 2.20. The best fit parameters for all experimental data (Table 2.5) were used to calculate adsorption kinetics and a short-term and a long-term desorption experiment. Apparent equilibrium, characterized by an approximately constant concentration in the liquid phase, is reached faster at lower concentration levels (Figures 2.19a). However, despite this apparent constant  $C$ , the system is not equilibrated. Mass transfer between the sorbed phases will continue until the solute is completely stored in the irreversible domain. Two processes are responsible for solute uptake: i. reversible sorption (non-linear equilibrium and non-equilibrium), ii. irreversible sorption following first-order kinetics. Whereas the first process leads to a high sorption affinity at lower concentration levels, the second process is more effective at higher concentration levels. At the intermediate concen-

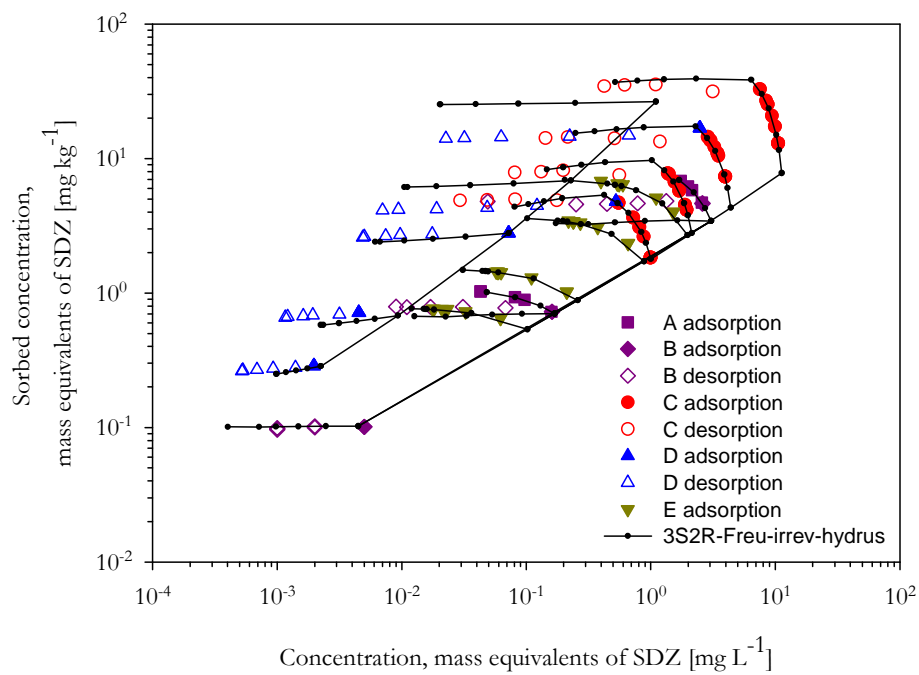


Figure 2.18: Measured data of sorption experiments A, B, C, D, E with model predictions using the three-stage two-rate irreversible sorption model, where irreversible sorption is independent of the sorption isotherm of the reversible sorption domain (3S2Rirrev).

tration levels the normalized total sorbed concentrations are, therefore, lower than at lower or higher concentration levels in Figure 2.19a. This effect causes the curvature of the predicted 41 day adsorption isotherm of experiment D in Figure 2.18. Desorption steps remove relatively more mass in the higher concentration levels (Figures 2.19 and 2.20). However, if the desorption steps were conducted after only two days of adsorption, the solute concentrations will further decrease, due to the slow sorption processes (Figure 2.19b). The second desorption step after five more days of equilibration results in increasing dissolved concentrations for the higher concentration levels. Desorption (mass transfer from the sorbed to the dissolved phase) occurs, if the desorption step is carried out after 41 days of equilibration. However, after approximately 10 days  $C$  decreases again, due to the ongoing irreversible sorption (Figure 2.20).

The fitted 3S2Rirrev-model described the short-term adsorption kinetics well (Figure 2.18). The 3S2Rirrev-model did not overestimate the long-term adsorption as much as the 3S2Rirx-model, because the irreversible sorption in this model proceeds slower at lower concentration levels. But long-term adsorption is still overestimated, especially at higher concentration levels. Very slow desorption at the various time scales is best described with the 3S2Rirrev model, although not perfectly. The observed rather linear desorption behavior in the long-term experiment D (Figure 2.4) is reflected in the irreversible sorption Equation 2.50. This results in shorter desorption branches at lower concentration levels for experiment D.

### Sorption in annealed soil

Sorption data of experiment F with annealed soil were investigated using the kinetic sorption model (RLS) as well as the one-stage two-rate model (2S1R). Both models were able to describe the observed very slow desorption at the experimental time scale (Figures 2.21, 2.22). The initial adsorption is better described with the 2S1R-model, because of the equilibrium stage, even though the fraction of equilibrium sites is very small ( $f_1 = 0.006$ ). Compared to the 2S1R fitting parameters from experiment C, the adsorption/desorption rate  $\alpha_2$  in annealed soil is smaller than in fresh soil as well as the equilibrium fraction  $f_1$  (Table 2.4).

The experiment with annealed soil can thus be taken as a hint that soil organic matter influences the extent of sorption ( $K_f$ ) and linearity of the isotherm ( $m$ ), whereas the sorption kinetic is not solely due to organic matter. Notice that the thermal treatment not only burns the organic matter, but may also change clay minerals and the accessibility of the sorption sites.

## 2.5 Discussion

The observed short-term sorption behavior of  $^{14}\text{C}$ -SDZ confirmed the results of previous studies by *Kreuzig et al.* (2003); *Thiele-Bruhn and Aust* (2003). A slow sorption process was also observed for other sulfonamides such as sulfathiazole and sulfadimidine (*Langhammer and Büning-Pfaue*, 1989; *Kahle et al.*, 2005). *Kahle et al.* (2005),

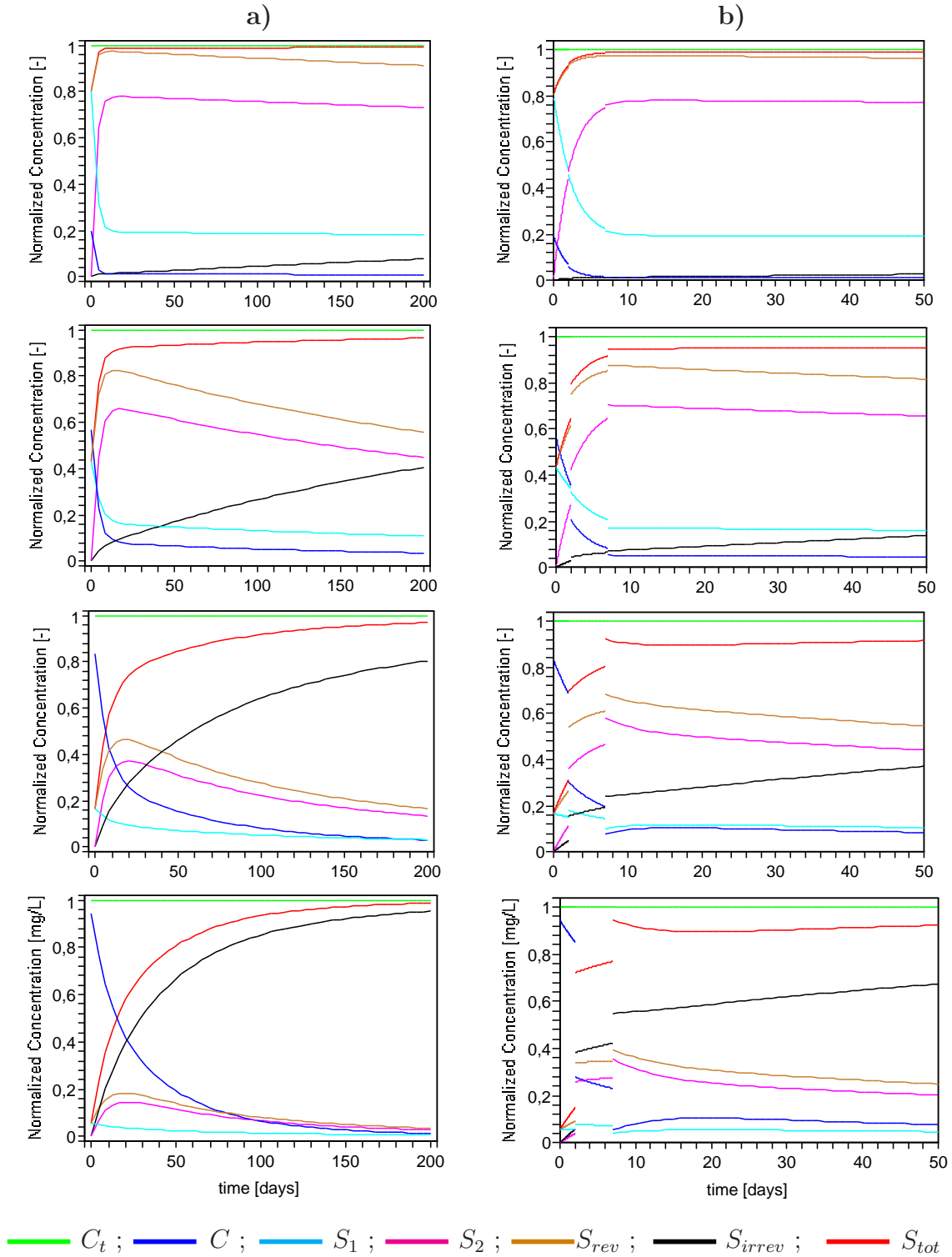


Figure 2.19: Solute distribution among the various domains in a batch-system according to the 3S2Rirrev-model at different concentration levels. The initial total solute concentrations were 0.0089, 0.089, 0.89, 8.9 mg L<sup>-1</sup> from the top to the bottom figures. Experimental conditions D and the best fit parameters (Table 2.5) were used. Solute concentrations are given as mass of solute in the domain per total batch volume normalized by the total solute concentration in the system ( $C_t$ ). Adsorption kinetics during 200 days are given in column a). The desorption steps in column b) were conducted after 2 and 7 days by exchanging the solution phase completely.

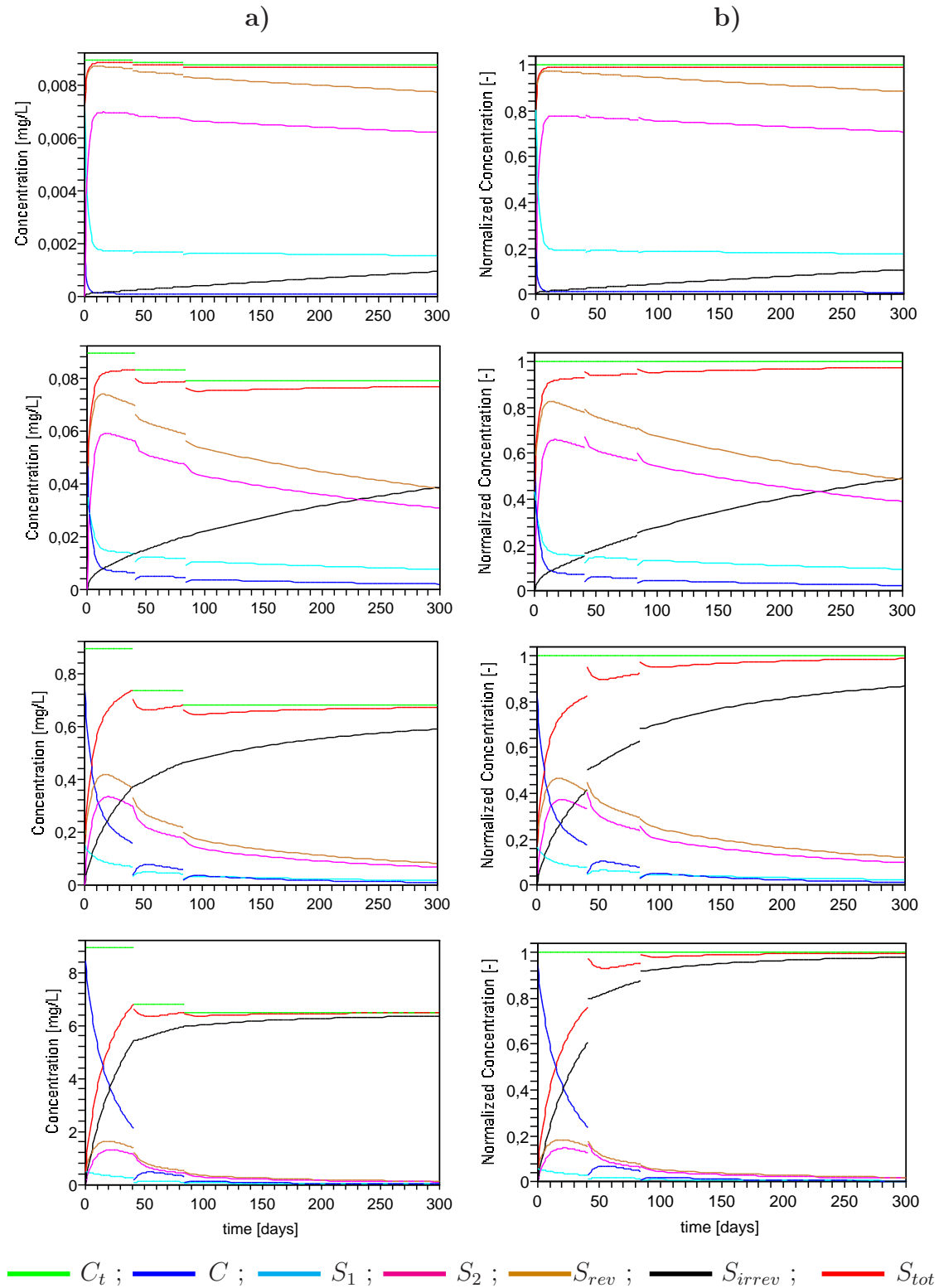


Figure 2.20: Solute distribution among the various domains in a batch-system according to the 3S2Rirrev model at different concentration levels. The initial total solute concentrations were 0.0089, 0.089, 0.89, 8.9 mg L<sup>-1</sup> from the top to the bottom figures. Experimental conditions D and the best fit parameters (Table 2.5) were used. The desorption steps were conducted after 41 and 84 days by exchanging the solution phase completely. Solute concentrations are given as mass of solute in the domain per total batch volume [mg L<sup>-1</sup>] in column a). Normalized solute concentrations (divided by the total solute concentration in the system ( $C_t$ )) are given in column b).

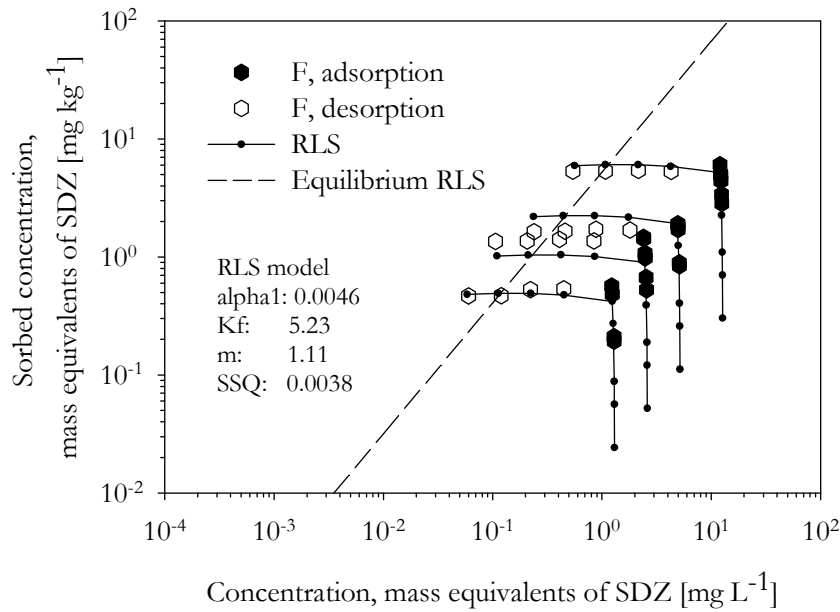


Figure 2.21: Measured data of sorption experiment F with model predictions using the rate-limited sorption model (RLS: rate-limited sorption). The model parameters are:  $K_f = 5.023 \text{mg}^{1-m} \text{L}^m \text{kg}^{-1}$ ,  $m = 1.11$ ,  $\alpha = 0.0046 \text{d}^{-1}$ .

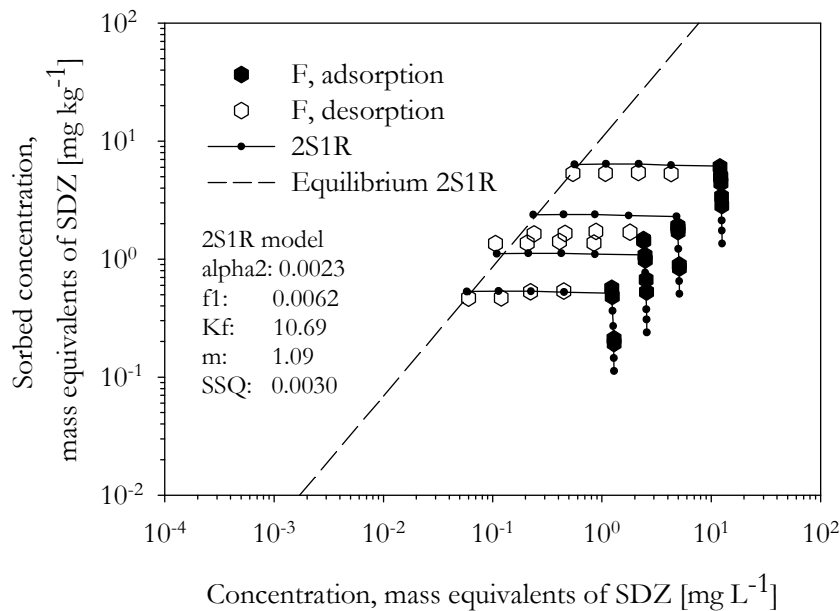


Figure 2.22: Measured data of sorption experiment F with model predictions using the two-site-one-rate sorption model (2S1R). The fitting parameters are given in Table 2.4.

*Gao and Pedersen (2005)* and *Thiele-Bruhn et al. (2004)* investigated the sorption mechanisms focusing on model sorbents or soil fractions. Our comparison between sorption in fresh and annealed soil confirmed the major contribution of soil organic matter to sorption affinity described by *Thiele-Bruhn and Aust (2003)*. While the previous studies aimed at the qualitative characterization of sorption mechanisms with certain soil components, our goal was to find a suitable model concept for the description of the observed sorption behavior of SDZ in soil. The properties of the batch systems were kept constant in our study, to restrict the investigations to the concentration- and time-dependency of sorption.

The reversible multiple-domain sorption models were previously used to describe the sorption behavior of pesticides in soil (e.g. *Brusseau et al., 1989; Brusseau, 1991; Ma et al., 1993; Ma and Selim, 1994a; Altfelder et al., 2000*). In comparison to these models, an irreversible sorption process was included in our model approach to account for the apparently very slow desorption of SDZ. Irreversible sorption is frequently characterized by first-order kinetics in the literature (e.g. *Kan et al., 1997, 1998; Baek et al., 2003; Prata et al., 2003*). However, even the most flexible model concepts (3S2Rirx or 3S2Rirrev) were not able to describe all observed features of the SDZ sorption.

The contradiction between the apparent sorption equilibrium after approximately 20 days and the very slow desorption is not solved by the irreversible sorption model concept. Irreversible sorption does not allow an equilibrium distribution. However, in combination with the non-linear sorption in the 3S2Rirrev-model, solute uptake is slowed down considerably at lower concentration levels. This results in fairly constant concentrations in the liquid phase over time, despite the ongoing mass fluxes between the various sorbed phases. However, the experimental error at low concentration levels complicates the determination of the true equilibration time. Data scattering in the long-term adsorption experiment E (Figure 2.7) reveals no information on the impact of concentration on equilibration time.

To investigate the concentration dependence of the sorption kinetics in more detail, different experimental protocols are needed. Observing the solution phase concentrations in smaller time intervals between two consecutive desorption steps, provides an experimental approach to test the proposed model concept (Section 2.4.2). However, the changes in the dissolved phase concentration might be small compared to the experimental uncertainties. Furthermore, the multiple-site sorption models are only conceptual. The existence and size of the various sorption domains cannot be determined experimentally. Furthermore, the model parameters provide only a description of the decrease of the concentration in the liquid phase, which might be a lumped effect of many processes (*van der Zee, 1991*).

Our sample analysis was restricted to total  $^{14}\text{C}$ -radioactivity. However, transformation of SDZ might occur (*Kreuzig and Hölting, 2005*). The measured total  $^{14}\text{C}$  concentrations would then include all, SDZ and its transformation products. Consequently, sorption characteristics of all species are lumped in the model calculations. The complexity of the sorption process in our model concepts might, thus, mask the influence of transformation on the overall sorption behavior. This issue will be

addressed in Section 4 for the transport experiments.

## 2.6 Conclusions

Sorption of SDZ in the investigated soil is non-linear and time-dependent. The equilibration time for the adsorption process was about 20 days. The Freundlich sorption isotherm was an adequate model to determine this sorption behavior. However, even 41 days were insufficient to establish a desorption equilibrium distribution of SDZ in the batch systems. Experimental observations and model exercises hint towards a complex sorption behavior of SDZ in soil. Since the slow desorption was also observed in annealed soil, sorption is not only attributed to soil organic matter. Although the conceptual models involve multiple sorption domains, these domains are not linked to any soil constituent.

Multiple-domain sorption models were used for process identification in combination with an inverse optimization algorithm. The sorption models consider non-linear, equilibrium and rate-limited reversible or irreversible sorption. Only a complex sorption model involving non-linear equilibrium and rate-limited reversible or irreversible sorption was flexible enough to describe all experimental data with one set of parameters. Despite the considerable deviations between the modelled and the experimental data, the wide ranges in concentration and time scale of the experiments should be noted. However, important processes affecting the sorption behavior of SDZ in soil might still be lacking in the proposed models.

In the presented study, only the effective behavior of  $^{14}\text{C}$  of the initially applied SDZ was investigated. Transformation reactions and the effect of different species with different sorption characteristics on overall sorption needs further investigation. A main obstacle for the quantification of the transformation processes is that the identity of the transformation products is partially not known. At present there is no analytical method to quantify the single species at lower concentration levels (Appendix E). Moreover, due to the low extraction efficiencies of SDZ residues in soil, there is no information about the concentration of SDZ and its transformation products in the soil. It was not possible to exclude the transformation in the batch systems for instance by the use of sterilized soil (Appendix G). Therefore, batch experiments with the single transformation products seem favorable to investigate the complex combination of sorption and transformation of SDZ in soil.

Our experiments showed that long-term sorption/desorption experiments are essential for the investigation of SDZ sorption in soil. The slow sorption kinetics and apparent irreversible sorption might be overlooked if common short-term experimental protocols (*OECD*, 1981) are used.



# Chapter 3

## Transport of sulfadiazine in soil columns – experiments and modelling approaches

### 3.1 Introduction

Among other veterinary pharmaceuticals sulfadiazine (SDZ) is a widely used antimicrobial substance in intensive livestock production to treat and prevent diseases (Boxall *et al.*, 2004; Thiele-Bruhn, 2003). Up to 40 % of the administered sulfonamides are eliminated as microbial active parent substances with the animal excretions (Kroeker, 1983). Manure is dropped directly onto the pastures by grazing livestock or spread onto agricultural soils after storage as fertilizer (Jørgensen and Halling-Sørensen, 2000). Concentrations of SDZ measured in pig manure range between 0.3 and 198 mg of SDZ per kg depending on medication, dilution and age of the manure (Hamscher *et al.*, 2005; Grote *et al.*, 2004; Höper *et al.*, 2002). As a result of the wide distribution of manure in the environment, sulfonamides are frequently found at concentration levels between a few and 100 ng L<sup>-1</sup> in surface waters of Northwestern Germany (Christian *et al.*, 2003). Due to low extraction efficiencies (Kreuzig *et al.*, 2003; Hamscher *et al.*, 2005), there are no reliable data for typical SDZ concentrations in soils. The risk of surface water contamination is enhanced by surface runoff from manured fields (Burkhardt *et al.*, 2005; Kay *et al.*, 2005a) or in drained arable lands. Peak concentrations of about 0.6 mg L<sup>-1</sup> of sulfachloropyridazine and 0.03 mg L<sup>-1</sup> of oxytetracycline were found in drainage water after the application of contaminated pig manure (Kay *et al.*, 2004).

SDZ has not yet been detected in the soil or groundwater during monitoring after the application of contaminated pig manure to a field site, in contrast to another sulfonamide (sulfamethazine) or tetracyclines (Hamscher *et al.*, 2005). Possible reasons for the fast dissipation of SDZ compared to the other substances are either a faster degradation or transformation, strong sorption in non-extractable fractions or low extraction efficiencies of soil analysis (Hamscher *et al.*, 2005). It is known that the recovery of SDZ from spiked soil samples decreases with time from 74 % to 18

% for samples extracted 5 minutes or 7 days after spiking (*Hamscher et al.*, 2005). The contact times of the antibiotics and the soil matrix are typically far longer in the field, provided that very fast degradation can be excluded.

Mineralization of  $^{14}\text{C}$ -labelled SDZ to  $^{14}\text{CO}_2$  in bovine manure, soil or soil manure slurries is less than 2 % after 102 days (*Kreuzig and Hölftge*, 2005), which we also found in separate investigations with the same soil without manure (data not shown). However, *Kreuzig and Hölftge* (2005) found that the dissipation of SDZ in the extracts was much faster (after one week only 40, 20 or 5 % of the initially applied  $^{14}\text{C}$  was detectable in manure, soil or soil manure slurries, respectively). They attributed this to the fixation of SDZ or its transformation products as non-extractable residues. They also detected up to four unidentified transformation products by radio thin layer chromatography in the remaining extractable fraction. This study was in contrast to another investigation, where no substances other than SDZ were found in comparable extracts (*Kreuzig et al.*, 2003).

Looking into the pharmacokinetics, one of these metabolites might be acetyl-SDZ. Within treated pigs, SDZ is metabolized to the N4-acetyl-sulfadiazine and both substances are mainly eliminated by renal excretion (*Kroker*, 1983; *Grote et al.*, 2004) and thus found in manure. However, de-acylation leads to an increasing concentration of SDZ in stored manure (*Berger et al.*, 1986; *Grote et al.*, 2004). Although those studies focused on the metabolism in manure, the results of *Kreuzig and Hölftge* (2005) and our separate experiments indicate that transformation reactions might also occur in soils. It is therefore essential to investigate the fate of both, the parent and possible transformation products in case of re-transformation.

To prevent further environmental contamination and possible adverse effects of the antimicrobial substances on soil microbial populations, an understanding of the environmental fate of these compounds is necessary (*Jørgensen and Halling-Sørensen*, 2000). Apart from the route of entry, the fate of the pharmaceuticals in the environment is comparable to other organic chemicals, such as pesticides. To assess the mobility of pollutants in the environment, knowledge about their persistence and sorption behavior is crucial. Until now the sorption/desorption processes of SDZ in soils are not thoroughly investigated. Sorption studies with sulfadiazine and other sulfonamides and different soils showed a Freundlich-type behavior with typical equilibrium times of 16 hours (*Thiele-Bruhn and Aust*, 2003). Formation of non-extractable residues of  $^{14}\text{C}$ -labelled SDZ was observed in a clayey silt (*Kreuzig et al.*, 2003). Whereas about 50 % of SDZ was not extractable after three days of incubation in this study, this fraction increased to about 90 % after 28 days. Therefore, concentration- and time-dependent and possibly also irreversible sorption can be expected in soils.

Process-oriented studies are scarce in literature concerning the transport of SDZ in soils. The mobility of sulfonamides in soils is assumed to be high, based on their physicochemical properties (*Tolls*, 2001). However, incomplete breakthrough of SDZ was observed in several transport studies. SDZ was rarely found in the leachate of column and plot studies, and most of the applied SDZ was retained in the upper part of the soil (*Kreuzig and Hölftge*, 2005). Fast sorption of SDZ into non-extractable

pools was reported in leaching experiments with undisturbed soil columns, after application of contaminated manure (*Kreuzig and Hölting, 2005*). Sulfachloropyridazine, which is a sulfonamide similar to SDZ, was found to be quite mobile, but also readily degradable (*Boxall et al., 2002; Kay et al., 2004, 2005a,b*). The component was classified as being mobile in different soils from two-days batch sorption experiments, which was additionally verified in column studies (*Boxall et al., 2002*). However, the leached mass fraction was lower than expected, and the non-recovered mass in the experiments was attributed to degradation (*Boxall et al., 2002; Kay et al., 2005b*). Similar observations were also reported for sulfamethoxazole: Leaching was shown to depend on (i) the applied mass, (ii) irrigation intensity and (iii) soil type (*Drillia et al., 2005*), which hints towards a soil dependent, non-linear and time-dependent sorption of the investigated sulfonamide.

To our knowledge transport and sorption mechanisms of sulfadiazine have not yet been systematically analyzed in column experiments. The objective of this study was to investigate the transport behavior of sulfadiazine in disturbed soil columns at a constant flow rate near saturation. We especially focus on the effect of concentration on the fate of SDZ, by changing the input concentration and/or pulse duration. Although the antibiotics enter the soil environment typically as ingredients of manure, the experiments were performed without manure to circumvent any changes in soil properties (e.g. pH, ionic strength, dissolved and particulate organic matter) and their effects on solute transport.  $^{14}\text{C}$ -labelled SDZ was used to ensure complete mass balances. To identify relevant sorption processes, measured breakthrough curves (BTCs) and soil concentration profiles of SDZ were fitted with a convective–dispersive transport model considering different sorption concepts.

## 3.2 Theory of solute transport

The transport of non-degradable dissolved substances in homogeneous soils with a constant water content and steady state flow conditions is typically described by the convection–dispersion equation (CDE) (e.g. *Hillel, 1998*):

$$\frac{\partial C_t}{\partial t} = D\theta \frac{\partial^2 C}{\partial z^2} - j_w \frac{\partial C}{\partial z} \quad , \quad (3.1)$$

where  $t$  is time [T],  $z$  is depth [L],  $D$  is the hydrodynamic dispersion coefficient [ $\text{L}^2\text{T}^{-1}$ ],  $\theta$  is the volumetric water content [ $\text{L}^3\text{L}^{-3}$ ],  $j_w$  is the water flow density [ $\text{L T}^{-1}$ ],  $C$  is the solute concentration in the liquid phase [ $\text{M L}^{-3}$ ] and  $C_t$  is the total mass of solute per unit volume of soil [ $\text{M L}^{-3}$ ]. For non-volatile compounds  $C_t$  is given as the sum of concentrations in the dissolved and sorbed phase:

$$C_t = \theta C + \rho S \quad , \quad (3.2)$$

where  $\rho$  is the soil bulk density [ $\text{M L}^{-3}$ ] and  $S$  is the sorbed solute concentration [ $\text{M M}^{-1}$ ].

### 3.2.1 Sorption models

Various sorption concepts are available to describe the interaction of dissolved substances with the soil material. These sorption models differ with respect to the type of sorption isotherm (linear or non-linear), the assumptions made concerning the time-dependency (instantaneous or rate-limited) and reversibility of the sorption process (reversible or irreversible). Up to three sorption regions were considered in our study. We compare the isotherm-based distribution models to the attachment/detachment approach. Whereas the former approach describes the equilibrium distribution between phases by an adsorption isotherm, the latter is based on multiple kinetic processes. It was introduced to describe the transport of small particles or bacteria through porous media (e.g. *Schijven and Hassanizadeh, 2000; Bradford et al., 2003*). The solute-soil-water distribution models considered in this study are summarized in Figure 3.1.

### 3.2.2 Isotherm-based models

A comprehensive mathematical derivation of the applied sorption models is given elsewhere in detail (e.g. *Streck et al., 1995*). Therefore, we give here only their implementation into the solute transport equation. The combination of Equations 3.1 and 3.2 results in:

$$\theta \frac{\partial C}{\partial t} + \rho \frac{\partial S}{\partial t} = \theta D \frac{\partial^2 C}{\partial z^2} - j_w \frac{\partial C}{\partial z} \quad . \quad (3.3)$$

#### One-site equilibrium sorption

For instantaneously and reversibly sorbing substances Equation 3.3 can be rewritten as:

$$R \frac{\partial C}{\partial t} = D \frac{\partial^2 C}{\partial z^2} - v \frac{\partial C}{\partial z} \quad , \quad (3.4)$$

where  $v = j_w/\theta$  is the pore water velocity [L T<sup>-1</sup>] and  $R$  [-] is the retardation factor:

$$R = 1 + \frac{\rho}{\theta} \frac{\partial S}{\partial C} \quad , \quad (3.5)$$

where  $\partial S/\partial C$  is the first derivative of a relationship between the concentration in the solid ( $S$ ) and liquid ( $C$ ) phases, expressed by the sorption isotherm. The linear and non-linear (Freundlich) isotherms are given by:

$$S = K_d C \quad , \quad (3.6)$$

where  $K_d$  is the soil-water distribution coefficient [L<sup>3</sup> M<sup>-1</sup>] and:

$$S = K_f C^m \quad , \quad (3.7)$$

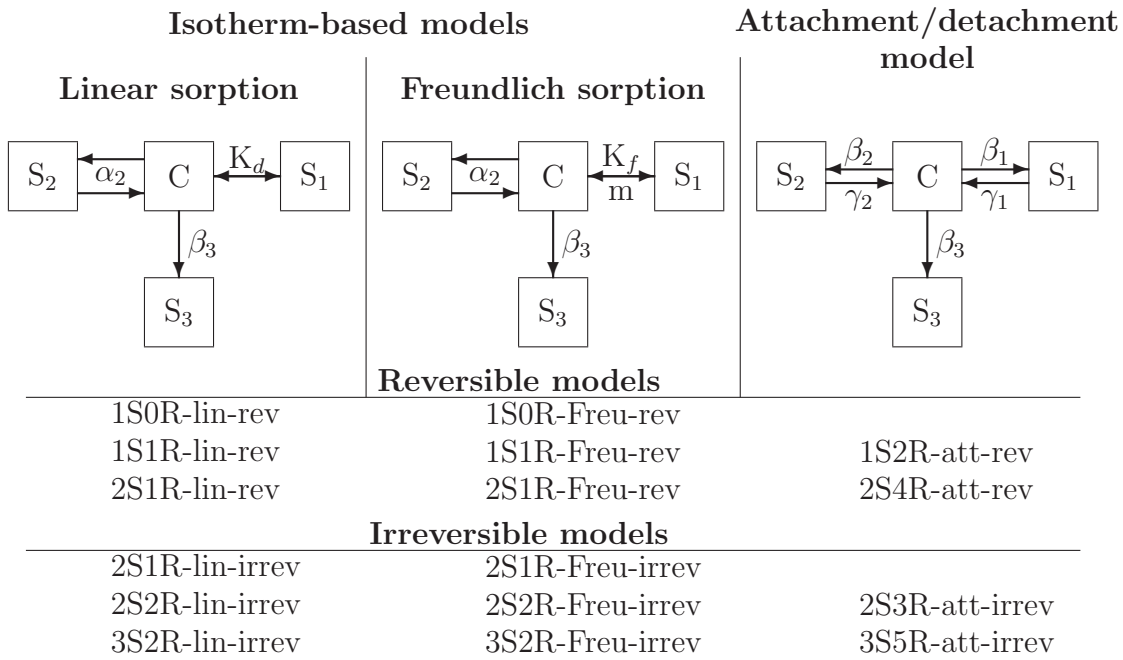


Figure 3.1: The applied solute-soil-water distribution models. The boxes labelled with  $C$  represent the liquid phase with concentration  $C$ , the boxes  $S_i$ , with  $i=1,2,3$  represent the three sorption sites with the respective concentrations  $S$ . The arrows indicate the sorption process, where  $K_d$  is the distribution coefficient,  $K_f$  and  $m$  are the Freundlich coefficient and exponent,  $\alpha_2$  is the reversible ad- and desorption rate,  $\beta_i$  and  $\gamma_i$  are the one-way attachment and detachment rates, respectively. Less complex versions of each model were derived by omitting one or two sorption sites: The possible combinations for reversible and irreversible models are given below the models. The model names are composed of the number of sites, S (1 - 3), number of rates, R (0 - 5), sorption concept (lin: linear and Freu: Freundlich sorption isotherms, att: attachment/detachment model) and reversibility (rev: reversible, irrev: irreversible).

where  $K_f$  is the Freundlich distribution coefficient [ $M_{\text{solute}}^{1-m} L^{3m} M_{\text{soil}}^{-1}$ ] and  $m$  is the dimensionless Freundlich exponent. Note that the linear isotherm is a special case of the Freundlich isotherm for  $m=1$ . The retardation factor  $R$  is given by:

$$R = 1 + \frac{\rho}{\theta} K_f m C^{m-1} \quad . \quad (3.8)$$

The 1S0R-lin-rev and 1S0R-Freu-rev models (Figure 3.1) are given by Equations 3.4 and 3.8.

### One-site, rate-limited, reversible sorption

If the equilibrium distribution of the solute between solid and liquid phases is not reached instantaneously, a kinetic term needs to be considered (*Fortin et al.*, 1997):

$$\frac{dS}{dt} = \alpha(K_f C^m - S) \quad , \quad (3.9)$$

where  $\alpha$  is the adsorption/desorption rate coefficient [ $T^{-1}$ ]. The combination of Equations 3.3 and 3.9 (*van Genuchten and Wierenga*, 1976) describe the 1S1R-lin-rev and 1S1R-Freu-rev models (Figure 3.1, the subscript 2 is dropped in the equation for simplicity in the one-site model).

### Two-site, rate-limited, reversible sorption

Two-site sorption to instantaneous ( $S_1$ ) and rate-limited sorption sites ( $S_2$ ) is described by the following set of equations (*van Genuchten and Wagenet*, 1989; *Simunek et al.*, 1998):

$$S = S_1 + S_2 \quad , \quad (3.10)$$

$$S_1 = f K_f C^m \quad , \quad (3.11)$$

$$\frac{dS_2}{dt} = \alpha_2((1-f)K_f C^m - S_2) \quad , \quad (3.12)$$

where  $f$  is the fraction of equilibrium sites ( $S_1$ ), and  $\alpha_2$  is the sorption rate coefficient [ $T^{-1}$ ]. Together with Equation 3.3 they give the 2S1R-lin-rev and 2S1R-Freu-rev models (Figure 3.1).

### Irreversible sorption

Irreversible sorption is represented as a first-order kinetic sink of solute in the water phase. This process is equivalent to the description of the first-order degradation in the water phase (*Prata et al.*, 2003) and is given by Equation 3.13, assuming that sorption sites  $S_3$  exhibit irreversible sorption:

$$\frac{\partial S_3}{\partial t} = -\frac{\theta}{\rho} \beta_3 C \quad , \quad (3.13)$$

where  $\beta_3$  is the irreversible adsorption rate coefficient [ $T^{-1}$ ]. In the three-sites two-rates irreversible sorption models (3S2R-lin-irrev and 3S2R-Freu-irrev) total sorbed concentration  $S$  is then given by:

$$S = S_1 + S_2 + S_3 \quad , \quad (3.14)$$

where sorption characteristics for  $S_1$  and  $S_2$  are described by Equations 3.11 and 3.12, respectively. In the 2S2R-lin-irrev and 2S2R-Freu-irrev models the instantaneous sorption sites  $S_1$  are omitted ( $f=0$ ), whereas the rate-limited reversible sorption sites  $S_2$  are omitted ( $f=1$ ) in the 2S1R-lin-irrev and 2S1R-Freu-irrev models.

### 3.2.3 Attachment/detachment models

In the attachment/detachment concept all processes are first-order and rate-limited. Reversible attachment/detachment processes are given by:

$$\frac{\partial S_i}{\partial t} = \frac{\theta}{\rho} \beta_i C - \gamma_i S_i \quad , i = 1, 2 \quad , \quad (3.15)$$

where  $\beta_i$  are the attachment and  $\gamma_i$  the detachment rate coefficients [ $T^{-1}$ ] for the corresponding attachment/detachment sites  $S_i$ . If detachment is omitted, the second term on the right hand side of Equation 3.15 goes to zero, thus the Equation is equivalent to Equation 3.13, i.e. it describes irreversible sorption. Equally to the isotherm-based models the total sorbed concentration is given by Equation 3.14. The attachment/detachment model with two reversible and one irreversible site (3S5R-att-irrev) is given by the combination of Equations 3.3, 3.13, 3.14, 3.15 (*Schijven and Šimůnek, 2002*). Simpler attachment/detachment models with less sites or rates are derived by setting selected rate parameters to zero:  $\beta_3=0$  in the 2S4R-att-rev model,  $\gamma_2=\beta_2=0$  in the 2S3R-att-irrev model and  $\beta_3=\gamma_2=\beta_2=0$  in the 1S2R-att-rev model.

### Comparison of isotherm-based and attachment/detachment concept

In the attachment/detachment concept the ratio of the first-order attachment and detachment rate coefficients describes the tendency of the solute to distribute in either the liquid or the solid phase. This eventually results in linear equilibrium distribution isotherms, such as the isotherm-based models with linear sorption. However, the concept of the isotherm-based and the attachment/detachment model differs in whether the interaction occurs to the bulk soil or to only one fraction ( $f$ ,  $(1-f)$ ) of the bulk soil. Despite the difference in mathematical formulation, the attachment/detachment model can be parameterized in such a way, that it is equivalent to the linear sorption model with a similar number of rate-limited sorption sites (e.g. 1S1R-lin-rev equals 1S2R-att-rev, and 2S2R-lin-irrev equals 2S3R-att-irrev). If the attachment and detachment rates in one sorption site are much faster compared to the other processes, it can be described as instantaneous. In this case the

Table 3.1: Experimental conditions of the column experiments.

soil column	$C_0^\dagger$ mg L <sup>-1</sup>	$V_{in}^\ddagger$ L	$\Delta t_{in}^\S$ h	$m_{in}^\P$ mg	$M_{app}^\#$ g m <sup>-2</sup>	$j_w^{\dagger\dagger}$ cm h <sup>-1</sup>
A	5.70	1.047	67.8	5.97	1.052	0.266
B	0.57	1.032	68.0	0.526	0.093	0.260
C	5.70	0.094	7.0	0.539	0.095	0.262

<sup>†</sup>SDZ concentration in the application solution, <sup>‡</sup>volume of application solution, <sup>§</sup>pulse duration, <sup>¶</sup>applied mass, <sup>#</sup>applied mass per soil surface area, <sup>††</sup>irrigation rate.

models 2S1R-lin-rev and 2S4R-att-rev as well as 3S2R-lin-irrev and 3S5R-att-irrev are equivalent, too. However, the 3S5R-att-irrev model is more flexible than the 3S2R-lin-irrev model because it considers all sorption processes to be rate-limited.

### 3.3 Materials and Methods

All transport experiments were done with the anti-microbial substance sulfadiazine (IUPAC-name: 4-amino-N-pyrimidin-2-yl-benzenesulfonamide). Selected physico-chemical properties are listed in Appendix A. The transport studies were conducted in repacked soil columns near water saturation to assess the mobility of SDZ in the soil. Three experiments with different input scenarios (A, B, C) were performed in order to investigate the effect of concentration and pulse duration on the fate of SDZ (Table 3.1). Whereas in experiments A and B solute was applied for a long pulse duration, solute was applied with a short pulse in experiment C. High solute concentrations were applied in experiments A and C. Only about one tenth of that concentration was applied in experiment B. Thus, the total applied solute masses were approximately equal for experiments B and C.

#### 3.3.1 Soil columns

The soil material was collected from the upper 30 cm of an Eutric Cambisol which was used as grassland in the past. The soil properties are described in Appendix B. Field moist soil was sieved (2 mm) and stored at 4 °C in the dark until usage.

The columns were made of stainless steel (inner diameter and height were 8.5 cm and 10 cm, respectively). They were mounted on a porous ceramic plate (high flow, air-entry point > 1 bar). The outflow was connected to a fraction collector. An irrigation device with 12 glass needles was placed on top of the column. An HPLC-pump (high performance liquid chromatography) supplied a constant irrigation from a reservoir.

Wet soil (gravimetric water content of 40 %) was packed in the columns in small increments, each compacted with a metal stick, up to a total height of 9 cm. Due to



Table 3.2: Properties of the soil columns and the experimental conditions. The irrigation rate,  $j_w$ , and the soil bulk density,  $\rho$ , were determined experimentally. The pore water velocity,  $\nu$ , and the dispersion coefficient,  $D$ , were fitted to the BTCs of chloride. The volumetric water content,  $\theta$ , and the dispersivity,  $\lambda$ , were calculated.

soil column	$j_w$ cm h <sup>-1</sup>	$\rho$ g cm <sup>-3</sup>	$\nu$ cm h <sup>-1</sup>	$\theta$ cm <sup>3</sup> cm <sup>-3</sup>	$D$ cm <sup>2</sup> h <sup>-1</sup>	$\lambda$ cm	$R^{2\dagger}$
A	0.266	0.89	0.437	0.609	0.580	1.329	0.990
B	0.260	0.99	0.492	0.528	0.191	0.388	0.997
C	0.262	0.84	0.543	0.483	0.258	0.475	0.983

<sup>†</sup>Coefficient of determination of the regression between the observed and predicted BTCs.

the sticky properties of the fine textured soil, the wet soil could not be compacted to a typical field soil bulk density. A density of about 1 g cm<sup>-3</sup> (Table 3.2) assured the maintenance of constant flow rates. A 0.5 cm thick layer of coarse quartz sand was put on top of the packed soil in order to provide a more uniform distribution of water and to prevent splashing of the soil material. This sand was burnt in an oven at 450 °C for 24 h to remove any organic contamination. The soil columns were saturated from the bottom with a 0.01 M CaCl<sub>2</sub> solution for three days.

### 3.3.2 Transport experiments

The soil columns were irrigated at a constant rate of approximately 0.26 cm h<sup>-1</sup> for four days to establish steady state flow conditions. The pistons of the pump were flushed with water once a day to prevent salt precipitation and drying. Although the flow rate was regulated by the HPLC-pump, it was additionally controlled by weighing the solution loss from the reservoir per unit time as well as the leached volume in the single fractions.

A defined volume of the application solution of chloride or SDZ was irrigated on top of the column and subsequently leached with the 0.01 M CaCl<sub>2</sub> solution at the same flow rate. The applied volume was determined by the mass difference in the reservoir.

Measured concentrations in single fractions of the leachate were corrected for evaporation losses (approximately  $4.5 \times 10^{-6}$  L h<sup>-1</sup>) during the open sample storage in the fraction collector. For a better comparison between the experiments, concentrations in the outflow were normalized to their corresponding input concentrations ( $C_0$ ).

## Chloride

A breakthrough curve of chloride as a non-reactive tracer was determined for each packed soil column to characterize the flow behavior of water itself. The chloride was applied as a 2-hour pulse with an input concentration  $C_0(\text{Cl}^-)$  of  $1.0 \text{ g L}^{-1}$  as  $\text{CaCl}_2$ . The leachate was collected in hourly fractions of approximately 15 mL for analysis until a constant background level was reached.

The chloride concentration in the leachate was determined by measuring the electrical conductivity. The electrical conductivity linearly correlates with the concentration of  $\text{CaCl}_2$  within the concentration range of the samples. Solutions with known concentrations of  $\text{CaCl}_2$  were used to determine the calibration curve.

## Sulfadiazine

The application solution of SDZ was prepared in 0.01 M  $\text{CaCl}_2$  solution by addition of the appropriate amount of stock solution ( $500 \text{ mg SDZ L}^{-1}$  dissolved in acetonitrile). For experiment A  $^{14}\text{C}$ -labelled SDZ and non-labelled SDZ were mixed (1:4, m:m) to reduce the consumption of the labelled compound. In experiments B and C the  $^{14}\text{C}$ -labelled SDZ was not diluted with non-labelled SDZ to ensure adequate sample concentrations for analysis. The SDZ input solution was applied using the same steady irrigation rate as for chloride experiments. After application SDZ was eluted for 500 h, which corresponds to approximately 20 pore volumes. Detailed information about the experimental conditions are listed in Table 3.1.

The concentration of SDZ in the outflow was determined by measuring its  $^{14}\text{C}$ -radio-activity according to Appendix C. The soil was sliced at 0.5 or 1 cm depth intervals at the end of each leaching experiment to determine the concentration distribution of the remaining SDZ in the column. For all samples wet and oven-dry weights were measured to determine the water content. Prior to analysis the dry soil samples were ground and homogeneously mixed. The SDZ concentration in soil was determined by measuring the  $^{14}\text{C}$ -radioactivity according to Appendix D.

### 3.3.3 Parameter estimation

Water flow and solute transport in the soil columns were treated as one-dimensional problems in mathematical simulations. The water content was assumed to be constant in space and time throughout the experiment. The columns were assumed to be initially solute free ( $\text{Cl}^-$  or SDZ). A flux concentration boundary was applied at the top and a zero concentration gradient at the bottom of the column.

#### Conservative tracer - Chloride

The transport parameters  $\nu$  and  $D$  were determined by fitting the analytical solution of the CDE (Equation 3.4 with  $R=1$ ) with appropriate initial and boundary conditions to the observed BTC using the CXTFIT code (*Toride et al.*, 1999). To account for variations in mass balance, the input concentration was also allowed to

be adjusted. From  $D$ ,  $\nu$  and  $j_w$  the volumetric water content  $\theta = j_w/\nu$  and the dispersivity  $\lambda = D/\nu$  were calculated and used to fix the water flow for the transport simulations with the reactive tracer SDZ.

### Reactive tracer - SDZ

Since SDZ exhibits non-linear sorption and no analytical solution exists for such transport behavior, we used the numerical *HYDRUS-1D* software package (*Simunek et al.*, 1998) to describe the transport experiments. *HYDRUS-1D* is a finite element code that provides numerical solutions for various transport models described above. The Galerkin finite element method with a Crank-Nicolson time weighting scheme was used to solve the governing solute transport equations. *HYDRUS-1D* includes an inverse optimization method based on the Levenberg–Marquardt algorithm. For the numerical calculations the soil profile was discretized into 101 evenly distributed nodes. The maximum time step was chosen small enough to assure a mass balance error smaller than 1 %. The model was run under saturated conditions with a gravity driven flow. The saturated hydraulic conductivity was set equal to the irrigation rate  $j_w$ .

*HYDRUS-1D* was used either in a predictive manner with fixed transport parameters or in an inverse mode to fit one or more parameters of a sorption model to the given experimental data. In the latter case the experimental data of the BTC were in selected cases internally  $\log_{10}$ -transformed to increase the weighting on the BTC tailing. The soil concentration profile data were not transformed. Unit weights were assigned to all residuals. Either BTC-, profile- or both data sets were used in the fitting procedure.

Because transformation reactions can not be ruled out during our experiments, we focused on an effective transport description for the sum of SDZ and possible transformation products. However, as the identity and fate of the possible transformation products are still unknown, the sum of SDZ and potentially active or re-transferable transformation products is of environmental concern. This lumped characterization can be used for a first risk assessment. This was previously done by *Prata et al.* (2003) and *Casey et al.* (2004), who also used  $^{14}\text{C}$ -labelled compounds for their experiments. Despite the determination of transformation products in the leachate, they applied their models to the measured  $^{14}\text{C}$ -data and the modelling resulted in an effective description of the transport behavior of the parent substance and its transformation products.

## 3.4 Results

### 3.4.1 Transport and breakthrough curves of chloride

The transport parameters  $D$  and  $\nu$  that were fitted to the chloride BTCs are listed in Table 3.2. Although the obtained parameters were not identical for all three columns, the physical equilibrium CDE was able to describe all BTCs (Figure 3.2).

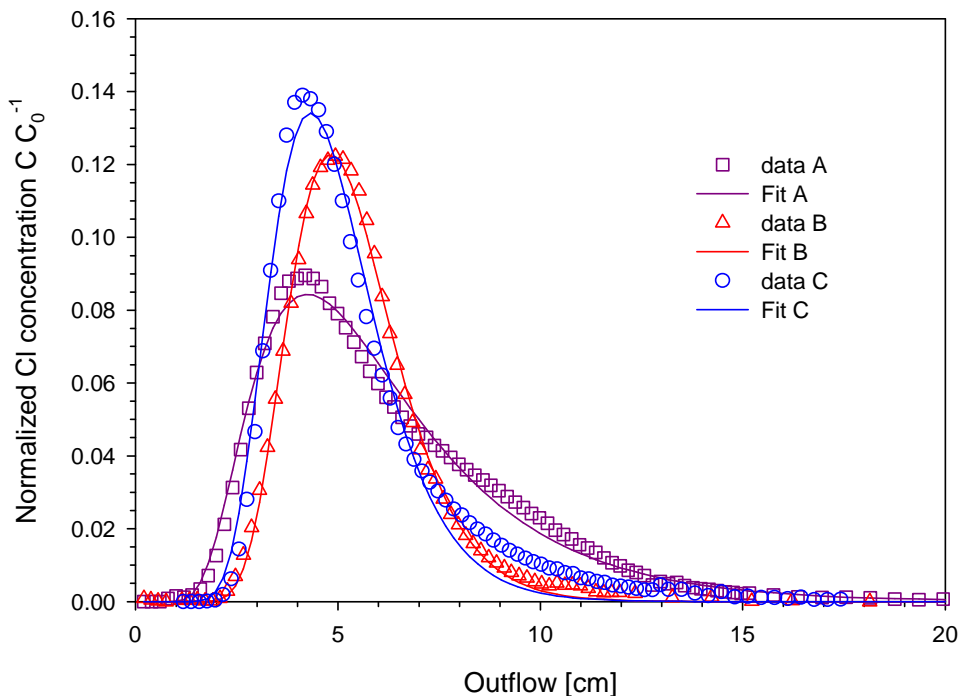


Figure 3.2: Breakthrough curves of chloride in the three columns with the fitted physical equilibrium curves.

It was, thus, concluded that no non-equilibrium processes affected the chloride transport and that all water participated in the convective flow. Relatively large differences in water contents between the three columns were likely due to the packing procedure that was difficult to standardize. To account for these variations in the flow field between columns, the transport parameters were individually determined for each column.

### 3.4.2 Transport of SDZ - experimental results

The peak maxima of different treatments were delayed relative to chloride by a factor of 2 to 5 (Figure 3.3). The decreasing limb of each BTC is characterized by an extended tailing that exhibits a rather constant slope after about 60 cm of cumulative outflow in the semi-log plot (Figure 3.3b). The BTCs differed in the maximum concentrations as well as the eluted mass fractions (from 18 % to 83 %, Table 3.3). From the pronounced tailing it can be concluded that a complete breakthrough could not be achieved within a reasonable time frame. The way of application determined the fate of SDZ: (i) the longer the pulse duration and the higher the applied concentration, the more mass was leached, and (ii) the more mass was leached the later the peak concentration arrived.

Concentration profiles of SDZ for the columns with the long pulse applications

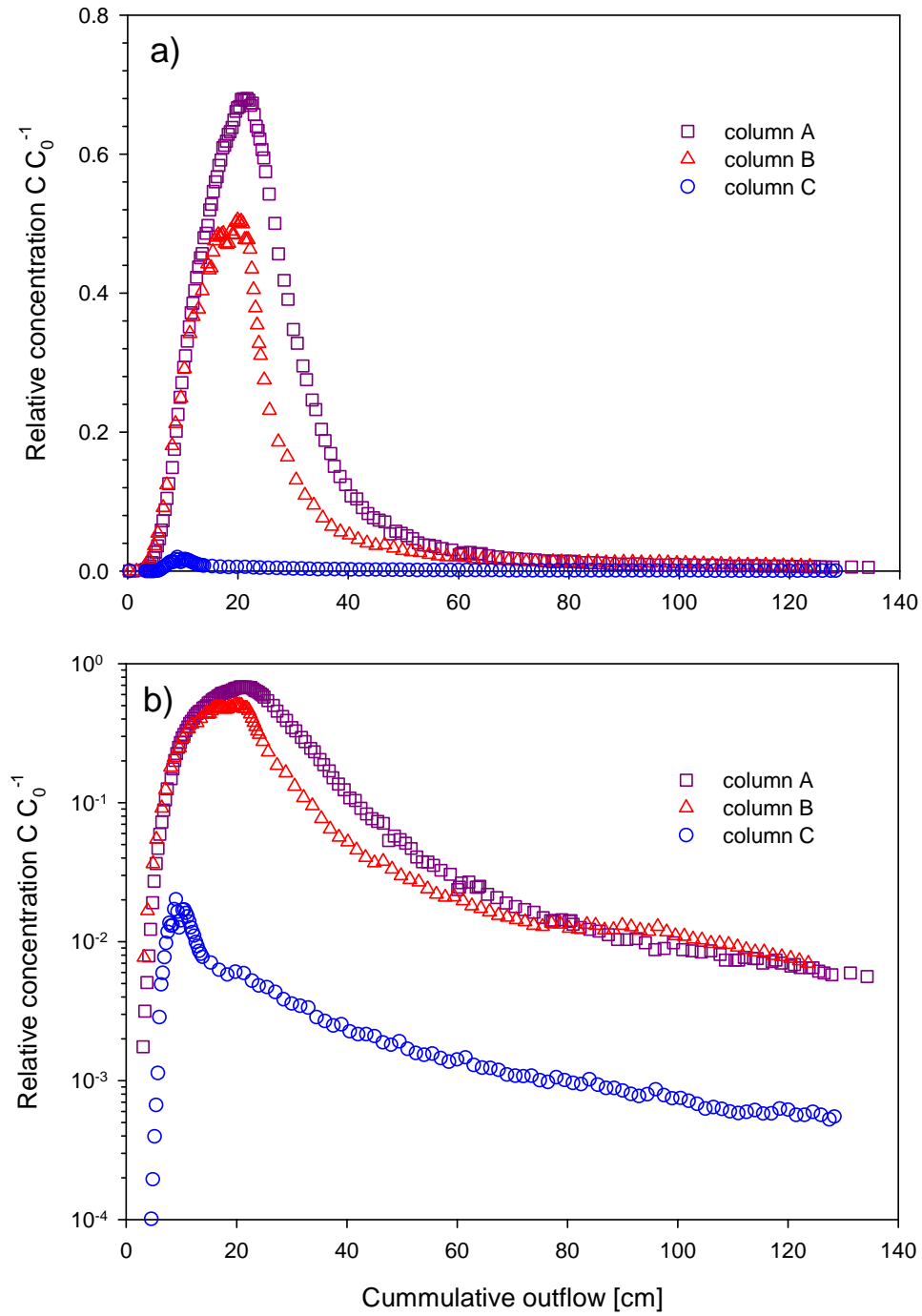


Figure 3.3: Breakthrough curves of SDZ in the three columns plotted on a linear (a) and a logarithmic (b) scale.

Table 3.3: Mass recovery of SDZ after the column experiments.

soil column	in leachate % <sup>†</sup>	in soil column %	total recovery %
A	82.7	14.5	97.2
B	60.7	38.3	99.0
C	17.8	81.8	99.6

<sup>†</sup> Mass fractions are given in percent of the applied mass,  $m_{in}$  (Table 3.1).

(A, B) showed the highest concentrations at the top of the column, with concentrations steadily decreasing towards the bottom (Figure 3.4). In the column with the short pulse application (C) solute concentrations were relatively uniformly distributed. Concentrations were slightly higher between 2 and 6 cm depth of the column. The difference between the applied and the recovered mass was less than 3 % of the applied mass for all experiments (Table 3.3).

### 3.4.3 Transport of SDZ - modelling results

The breakthrough curves of SDZ were fitted using *HYDRUS-1D* assuming different solute-soil-water interaction concepts. The various transport models and their corresponding fits are discussed below in detail for column A. The model complexity was increased from one-site equilibrium models to more complex multiple-site models with reversible or irreversible sorption. The fitted parameters and further details are given in Table 3.4.

**One-site sorption models:** Figure 3.5 shows the fit of the various one-site models in normal and semi-log representation. In general all one-site sorption models overestimated the leaching of SDZ. They could not account for the mass remaining in the soil column at the end of the experiment (Table 3.4). Notice that if sorption was assumed to be rate-limited and reversible, the predicted curves with the linear sorption (1S1R-lin-rev) and the kinetic attachment/detachment model (1S2R-att-rev) are almost identical since the models are mathematically equivalent. Only the curve fitted with the Freundlich rate-limited reversible sorption (1S1R-Freu-rev) described approximately the main features of the observed BTC. Although the maximum peak concentration and the decreasing limp were only slightly overestimated the difference in the mass balance was still relatively large (14 %, Table 3.4). Both models involving Freundlich sorption isotherms were fitted to the  $\log_{10}$ -transformed data, which gives more weight to the lower concentrations in the tailing. More weight is placed on the peak concentrations in the non-transformed data. Because the models involving kinetic sorption matched the observations better, but still not sufficiently, model complexity should be enhanced to reflect all observed features of

Table 3.4: Fitting parameters of the different isotherm-based (upper part) and attachment/detachment (lower part) models for column A. The eluted mass fraction in the experiment was 82.7 %.

model	fit <sup>†</sup>	$K_f$ $\text{kg}^{-1}\text{L}^{3m}\text{mg}^{1-m}$	m	$\alpha_2$ $\text{h}^{-1}$	f	$\beta_3$ $\text{h}^{-1}$	$R^{2\dagger}$	SSQ <sup>§</sup>	eluted <sup>¶</sup> %
<b>linear sorption models</b>									
1S0R-lin-rev	lin	1.13	1 <sup>#</sup>	0 <sup>#</sup>	1 <sup>#</sup>	0 <sup>#</sup>	0.953	42.1	99
1S1R-lin-rev	lin	1.25	1 <sup>#</sup>	$8.67 \times 10^{-2}$	0 <sup>#</sup>	0 <sup>#</sup>	0.971	13.7	99
2S1R-lin-rev	lin	4.39	1 <sup>#</sup>	$3.19 \times 10^{-3}$	0.20	0 <sup>#</sup>	0.996	1.30	89
2S1R-lin-rev	log	1.54	1 <sup>#</sup>	$6.55 \times 10^{-3}$	0.58	0 <sup>#</sup>	0.997	21.2	98
2S1R-lin-irrev	lin	0.91	1 <sup>#</sup>	0 <sup>#</sup>	1 <sup>#</sup>	$1.40 \times 10^{-2}$	0.994	2.80	73
2S2R-lin-irrev	lin	0.95	1 <sup>#</sup>	$3.76 \times 10^{-1}$	0 <sup>#</sup>	$1.17 \times 10^{-2}$	0.995	1.89	77
3S2R-lin-irrev	log	1.61	1 <sup>#</sup>	$7.08 \times 10^{-3}$	0.55	$4.67 \times 10^{-3}$	0.997	4.12	88
<b>Freundlich sorption models</b>									
1S0R-Freu-rev	log	0.76	0.50	0 <sup>#</sup>	1 <sup>#</sup>	0 <sup>#</sup>	0.588	228	99
1S1R-Freu-rev	log	2.48	0.53	$8.12 \times 10^{-2}$	0 <sup>#</sup>	0 <sup>#</sup>	0.991	6.22	97
2S1R-Freu-rev	lin	4.55	0.95	$3.32 \times 10^{-3}$	$2.00 \times 10^{-1}$	0 <sup>#</sup>	0.996	1.22	88
2S1R-Freu-rev	log	2.40	0.33	$1.09 \times 10^{-1}$	$1.72 \times 10^{-3}$	0 <sup>#</sup>	0.743	50.6	95
2S1R-Freu-irrev	lin	1.05	0.90	0 <sup>#</sup>	1 <sup>#</sup>	$1.41 \times 10^{-2}$	0.996	2.55	73
2S2R-Freu-irrev	log	2.33	0.50	$7.78 \times 10^{-2}$	0 <sup>#</sup>	$8.96 \times 10^{-3}$	0.995	7.43	80
3S2R-Freu-irrev	log	2.33	0.49	$7.35 \times 10^{-2}$	$3.64 \times 10^{-3}$	$1.02 \times 10^{-2}$	0.995	1.35	78
<b>attachment/detachment models</b>									
model	fit <sup>†</sup>	$\beta_1$ $\text{h}^{-1}$	$\gamma_1$ $\text{h}^{-1}$	$\beta_2$ $\text{h}^{-1}$	$\gamma_2$ $\text{h}^{-1}$	$\beta_3$ $\text{h}^{-1}$	$R^{2\dagger}$	SSQ <sup>§</sup>	eluted <sup>¶</sup> %
1S2R-att-rev	lin	$1.59 \times 10^{-1}$	$8.74 \times 10^{-2}$	0 <sup>#</sup>	0 <sup>#</sup>	0 <sup>#</sup>	0.971	137	99
2S3R-att-irrev	lin	$5.44 \times 10^{-1}$	$3.94 \times 10^{-1}$	0 <sup>#</sup>	0 <sup>#</sup>	$1.18 \times 10^{-2}$	0.995	1.90	77
2S4R-att-rev	lin	$8.82 \times 10^{-1}$	$6.76 \times 10^{-1}$	$1.44 \times 10^{-2}$	$2.44 \times 10^{-3}$	0 <sup>#</sup>	0.997	1.00	88
2S4R-att-rev	log	$5.13 \times 10^{+2}$	$3.94 \times 10^{+2}$	$6.22 \times 10^{-3}$	$6.95 \times 10^{-3}$	0 <sup>#</sup>	0.998	21.6	98
3S5R-att-irrev	lin	$3.05 \times 10^{+0}$	$2.53 \times 10^{+0}$	$1.17 \times 10^{-2}$	$1.41 \times 10^{-2}$	$7.68 \times 10^{-3}$	0.998	0.61	83
3S5R-att-irrev	log	$2.42 \times 10^{+2}$	$1.89 \times 10^{+2}$	$7.59 \times 10^{-3}$	$7.17 \times 10^{-3}$	$5.20 \times 10^{-3}$	0.998	0.65	87

<sup>†</sup>denotes whether the model was fitted to the non-transformed (lin) or  $\log_{10}$ -transformed concentration data (log); <sup>‡</sup>Regression coefficient; <sup>§</sup>Sum of squares, calculated for non-transformed data, even for the log-fits; <sup>¶</sup>leached mass fraction; <sup>#</sup>fixed parameters.

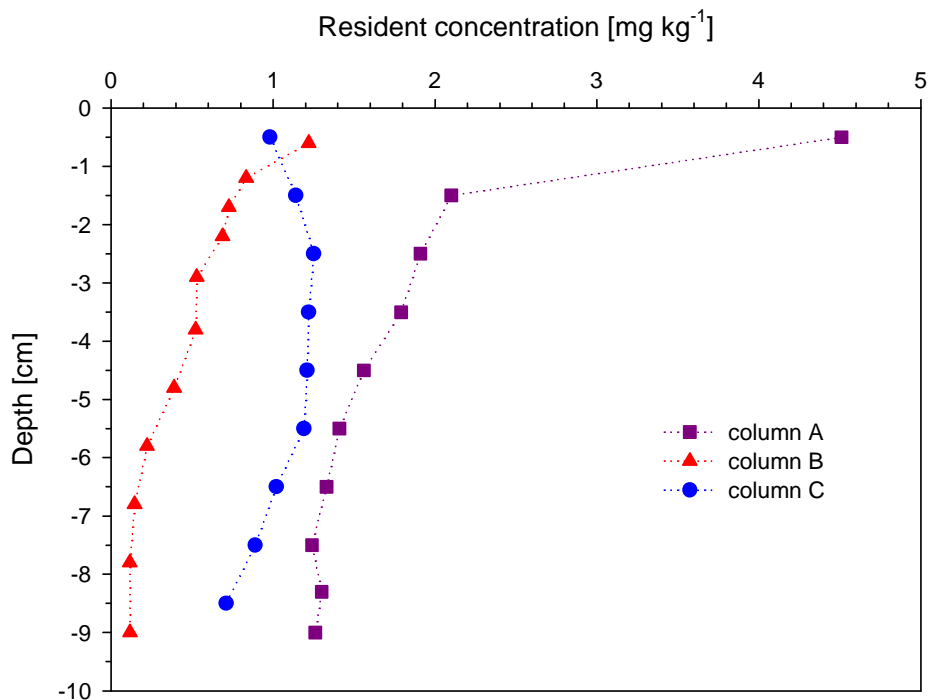


Figure 3.4: Soil concentration profiles of resident  $^{14}\text{C}$  concentrations in the three columns.

the BTC. Therefore, an additional site with kinetic reversible sorption was included in the following models.

**Two-site reversible sorption models:** The curves fitted to both, the  $\log_{10}$ - and non-transformed data using the two-site reversible sorption models are plotted in Figure 3.6a. Only the semi-log plot is given because the description of the tailing is especially interesting. The performance of all models was rather similar. The models fitted to the non-transformed data matched well the peak, but overestimated the tailing, whereas the models fitted to the  $\log_{10}$ -transformed data overestimated the peak concentrations, but described the tailing well. Similarly as for the one-site models, the linear sorption model 2S1R-lin-rev and the attachment/detachment model 2S4R-att-rev provided almost identical fits. This indicates that the attachment/detachment rates on one fraction of sorption sites are fast compared to the transport velocity and can thus be approximated by instantaneous sorption. However, the leached mass fraction was still overestimated in all two-site rate-limited reversible sorption models. At least one process is, thus missing that can account for the solute mass remaining in the soil column. While sorption is often assumed to be a reversible process, desorption kinetics may be very slow compared to the duration of the experiment and sorption may then appear to be irreversible. Whether irreversible sorption processes can account for the mass remaining in the soil column and describe the observed BTC was tested with the following models that consider



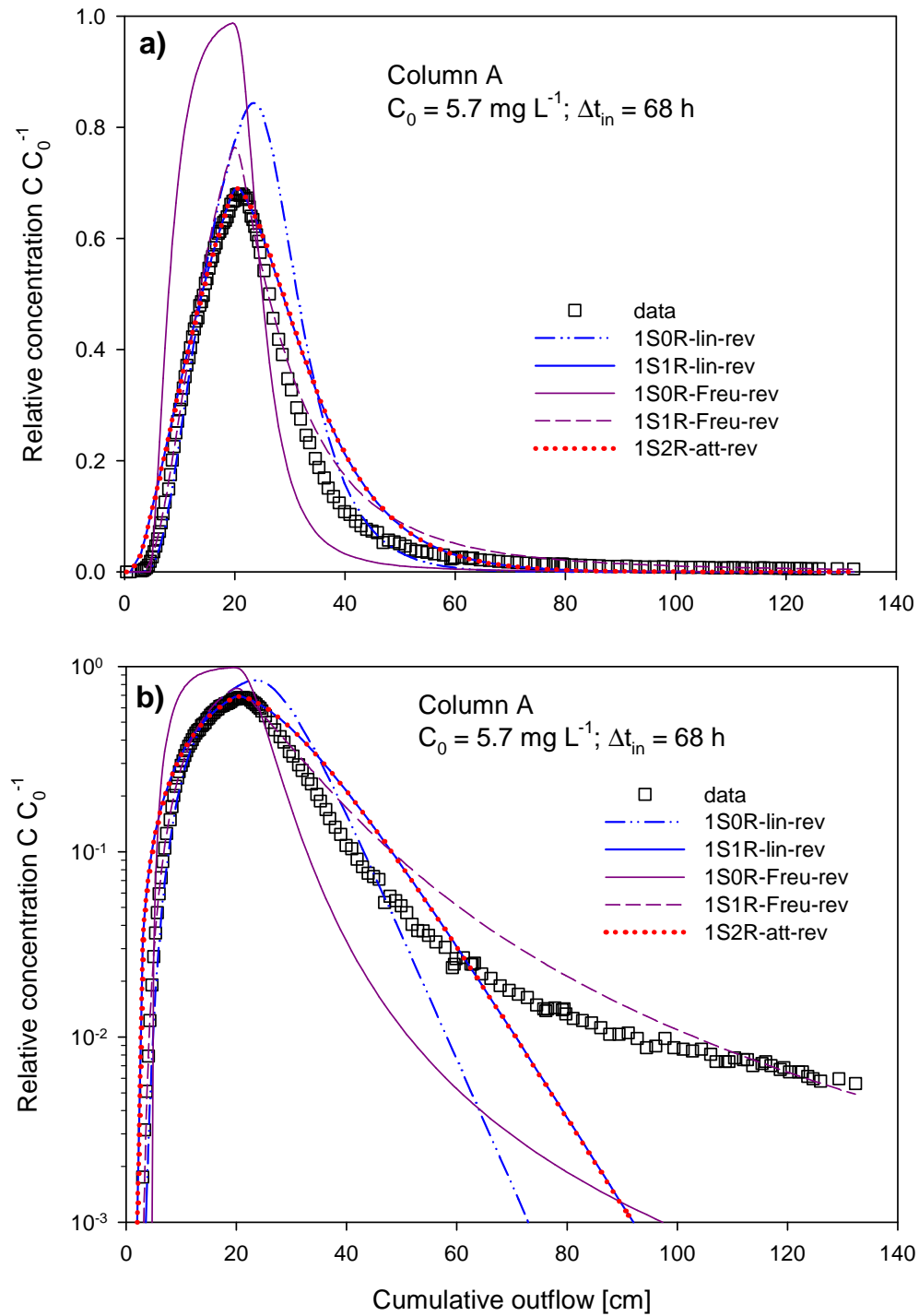


Figure 3.5: Normal (a) and semi-log (b) plots of the BTC for column A and different fits of the one-site models. The models with Freundlich sorption were fitted to the  $\log_{10}$ -transformed data.

irreversible sorption.

**Two- or three-site irreversible sorption models:** The curves fitted with models considering two or three sorption sites with one site being irreversible are presented in Figure 3.6b. The optimized parameters are given in Table 3.4. The peak concentrations were well described by all irreversible models. However, all two-site models except the 2S2R-Freu-irrev model failed to predict the extended tailing (Figure 3.6b) and underestimated the leached mass fraction (Table 3.4). The simulated curves of the 2S2R-lin-irrev and the 2S3R-att-irrev model were identical, as expected. In case of the Freundlich sorption (2S2R-Freu-irrev), the observed and predicted BTCs were in close agreement, apart from a slight underestimation of concentrations in the beginning of the decreasing limb. The calculated eluted mass fraction (80 %) was close to the observed fraction, too. An additional instantaneous sorption site (3S2R-Freu-irrev) did not further improve the model performance.

The additional sorption site in the three-site model with linear sorption (3S2R-lin-irrev) and the attachment/detachment model (3S5R-att-irrev) resulted in a very good fit of the tailing and only a slight overestimation of the peak concentrations. Both predicted curves were nearly identical with a leached mass fraction of about 88 %. In general, the long tailing characterized by two distinct slopes of the measured BTC required a model that either considered two sorption sites with kinetic desorption, such as 3S2R-lin-irrev or 3S5R-att-irrev, or one kinetic desorption site combined with non-linear sorption/desorption, such as 2S2R-Freu-irrev or 3S2R-Freu-irrev.

In terms of  $R^2$  and SSQ, the 3S5R-att-irrev model performed slightly better than models with three-site isotherm-based irreversible sorption and the 2S2R-Freu-irrev model. But from only one measured BTC it cannot be decided whether (i) sorption is linear or non-linear, nor (ii) if two or three kinetic sorption sites are required, nor (iii) whether the fast sorption process can be approximated by instantaneous sorption. Therefore, the ability of the four models, which performed best for experiment A, was tested to describe the two BTCs measured under different application scenarios.

### Model description for different application scenarios

Model fits and their parameters for experiment B are given in Figure 3.7a and Table 3.5, respectively. The 2S2R-Freu-irrev model described the peak of the BTC well, but underestimated the tailing and, thus, the eluted mass fraction. Out of the three-site models only the 3S5R-att-irrev model matched the observed BTC as well as the eluted mass fraction (52 %). The other three-site models either failed to describe the shape of the peak (3S2R-Freu-irrev) or the tailing (3S2R-lin-irrev). Since the 3S5R-att-irrev differs from the 3S2R-lin-irrev model, attachment/detachment rates on the fast kinetic sites was too slow to be approximated by instantaneous sorption.

The simulated BTCs for experiment C with the short application pulse are plotted in Figure 3.7b. The three-site models are nearly identical, and all curves roughly

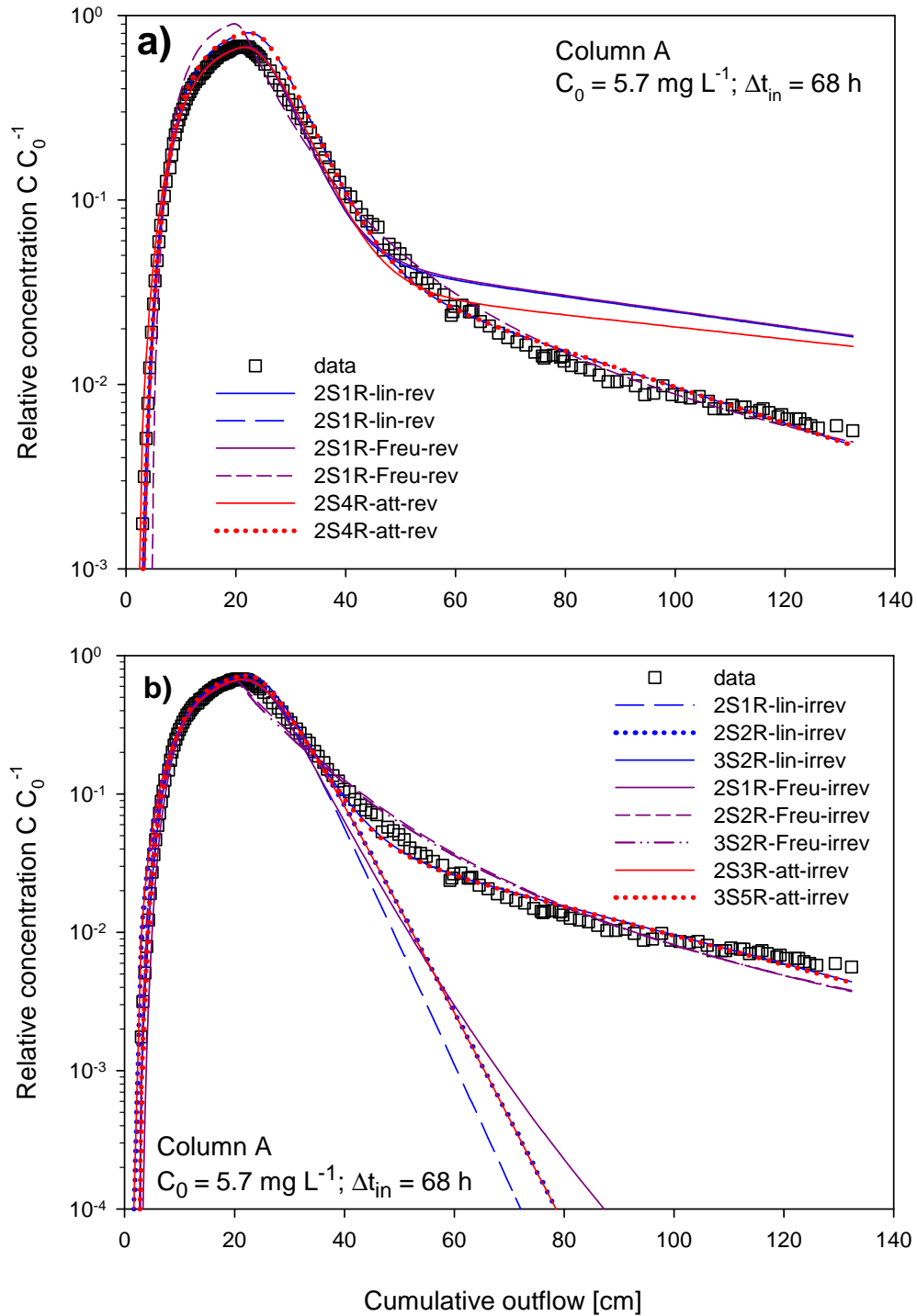


Figure 3.6: Semi-log plot of the BTC of column A and different model fits with a) two-site reversible and b) two- or three-site irreversible sorption models. For each model in Figure 3.6a both fits to the non-transformed (solid lines) and to the  $\log_{10}$ -transformed (dashed or dotted lines) are given. In Figure 3.6b the 2S1R-lin-irrev, 2S2R-lin-irrev, 2S1R-Freu-irrev, 2S3R-att-irrev models were fitted to the non-transformed data, the other four models to the  $\log_{10}$ -transformed data.

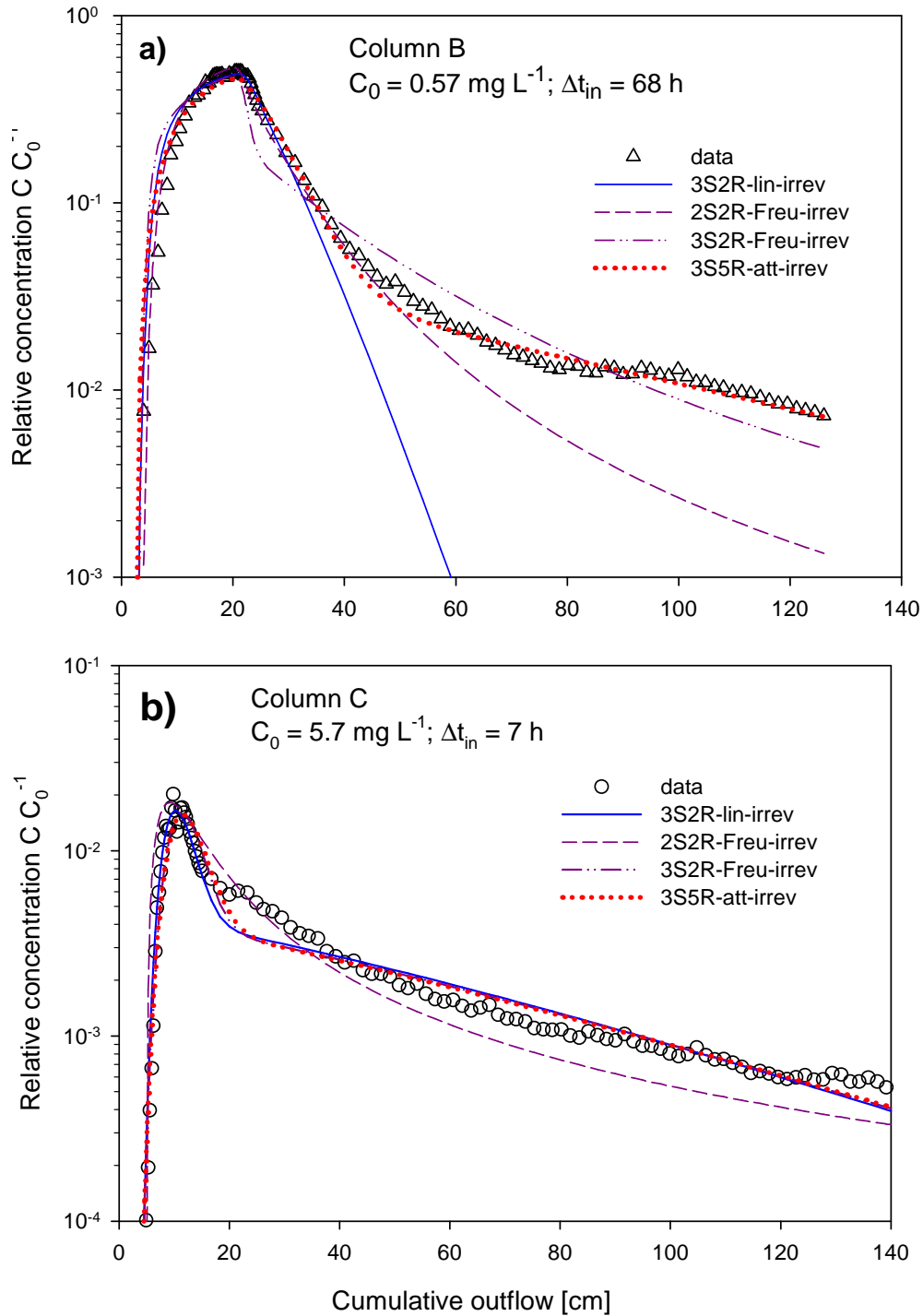


Figure 3.7: Semi-log plot of the BTC of column B (a) and C (b) and different fits of two- or three-site irreversible models. For column B (a) the 3S2R-Freu-irrev and the 3S5R-att-irrev models were fitted to the  $\log_{10}$ -transformed data, while the other two models to the non-transformed data. For column C (b) the models 2S2R-lin-irrev and 2S3R-att-irrev were fitted to the non-transformed data, while the other two models to the  $\log_{10}$ -transformed data.

described the observed BTC. The highest peak concentration and concentrations in the beginning of the tailing (between 20 and 40 cm of cumulative outflow) were underestimated. The 2S2R-Freu-irrev model predicted the latter part better, but underestimated the concentrations in the tailing. As was observed for experiment A with the same input concentration, the fast attachment/detachment process in the 3S5R-att-irrev model could be approximated by instantaneous sorption (3S2R-lin-irrev). Because the fitted Freundlich exponent was close to 1, the simulated curve with the 3S2R-Freu-irrev model was almost identical to the latter two models.

Thus, only the 3S5R-att-irrev model was flexible enough to predict the observed BTCs of all three experiments. The results show that experiments with different boundary conditions are necessary to identify the relevant sorption processes. However, the optimal parameter sets differed widely between the three experiments. Variation of other boundary conditions, such as irrigation rate, might help to further elucidate possible sorption processes.

**Concentration profiles:** Simulated concentration profiles for the different sorption models are given in Figures 3.8 and 3.9. None of the simulated profiles matched the measurements, despite good fits for the BTCs. Including observed concentration profile data in the numerical inversion of models with irreversible sorption did not result in a parameter set that could considerably better simulate the measured soil concentration profiles (data not shown).

The first-order irreversible sorption process results in an exponential decrease in the soil resident concentration profile. However, no parameter combination was found for experiments A and B to match all features of the profile concentrations under the prevailing boundary conditions, i.e. the high concentrations in the upper part followed by the steep concentration gradient and the constant concentration level in the lower part of the column. Still, only models involving irreversible sorption processes were able to predict higher resident concentrations at the top than at the bottom of the column (Figures 3.8a and b) after long leaching periods.

In experiment C a more uniform soil concentration distribution was observed (Figure 3.9b). To account for the large mass fraction remaining in the column, the fitted irreversible sorption rate was larger in all models than for experiments A or B. However, the modelled soil concentration gradient was steepest for this set of parameters, and did not match the observed shape.

**Parameter comparison and predictability:** Although the 3S5R-att-irrev model might not be the adequate process description, the optimized parameter values for the different experiments (Tables 3.4, 3.5 and 3.6) showed some trends. Since most mass was retained in the soil in experiment C parameter  $\beta_3$  and sorption affinity were both the highest for this experiment. The attachment rate coefficient towards the irreversible sorption site  $\beta_3$  irreversibly removes solute mass from the transport domain. Sorption affinity reduces the solute transport velocity compared to the water flow and can be estimated from the ratio between the attachment and the detachment rate coefficients ( $\beta_i/\gamma_i$ ). The slow reversible attachment/detachment

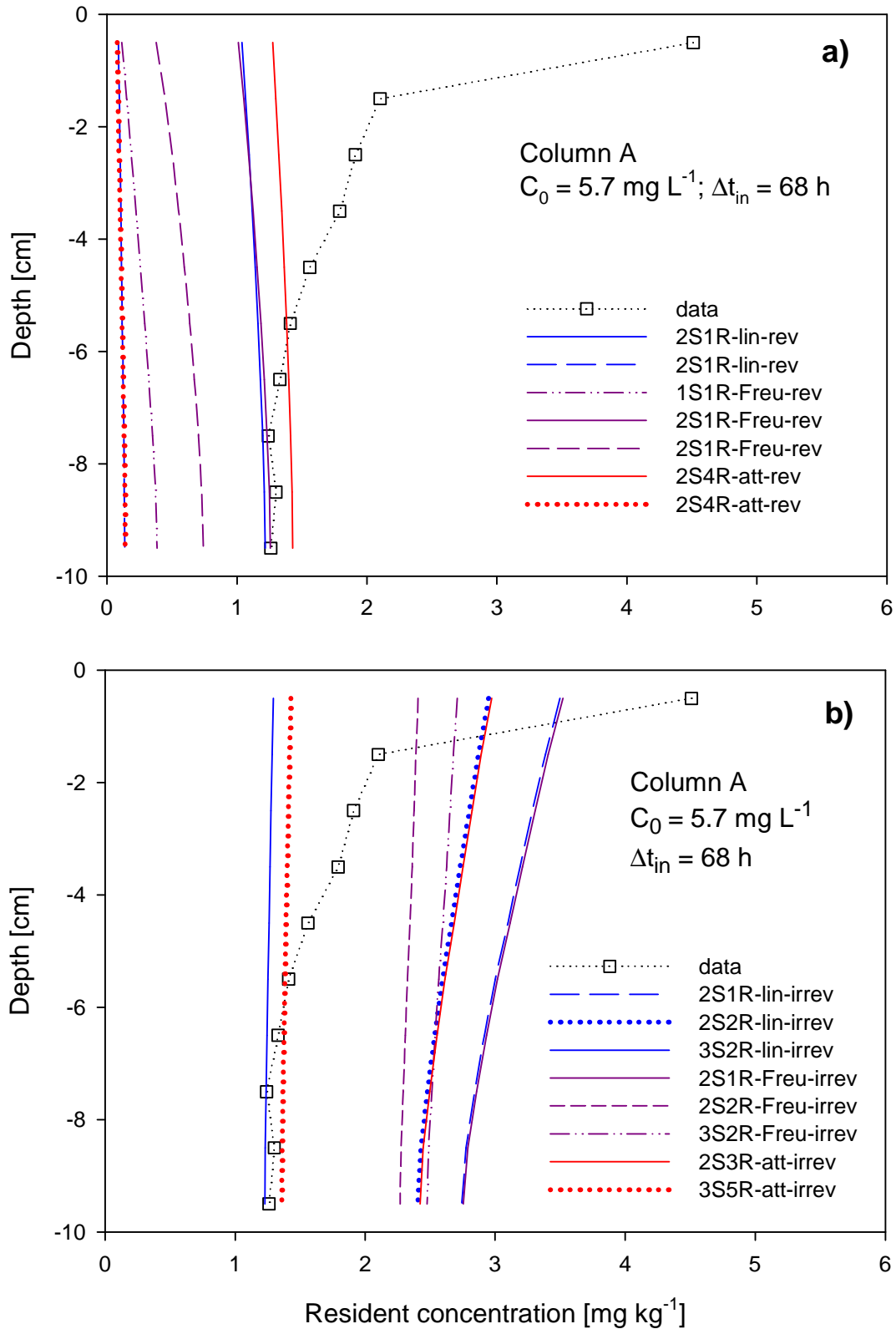


Figure 3.8: Measured and modelled soil profiles of resident  $^{14}\text{C}$  concentrations in column A. The reversible models are given in Figure 3.8a, the irreversible models in Figure 3.8b.

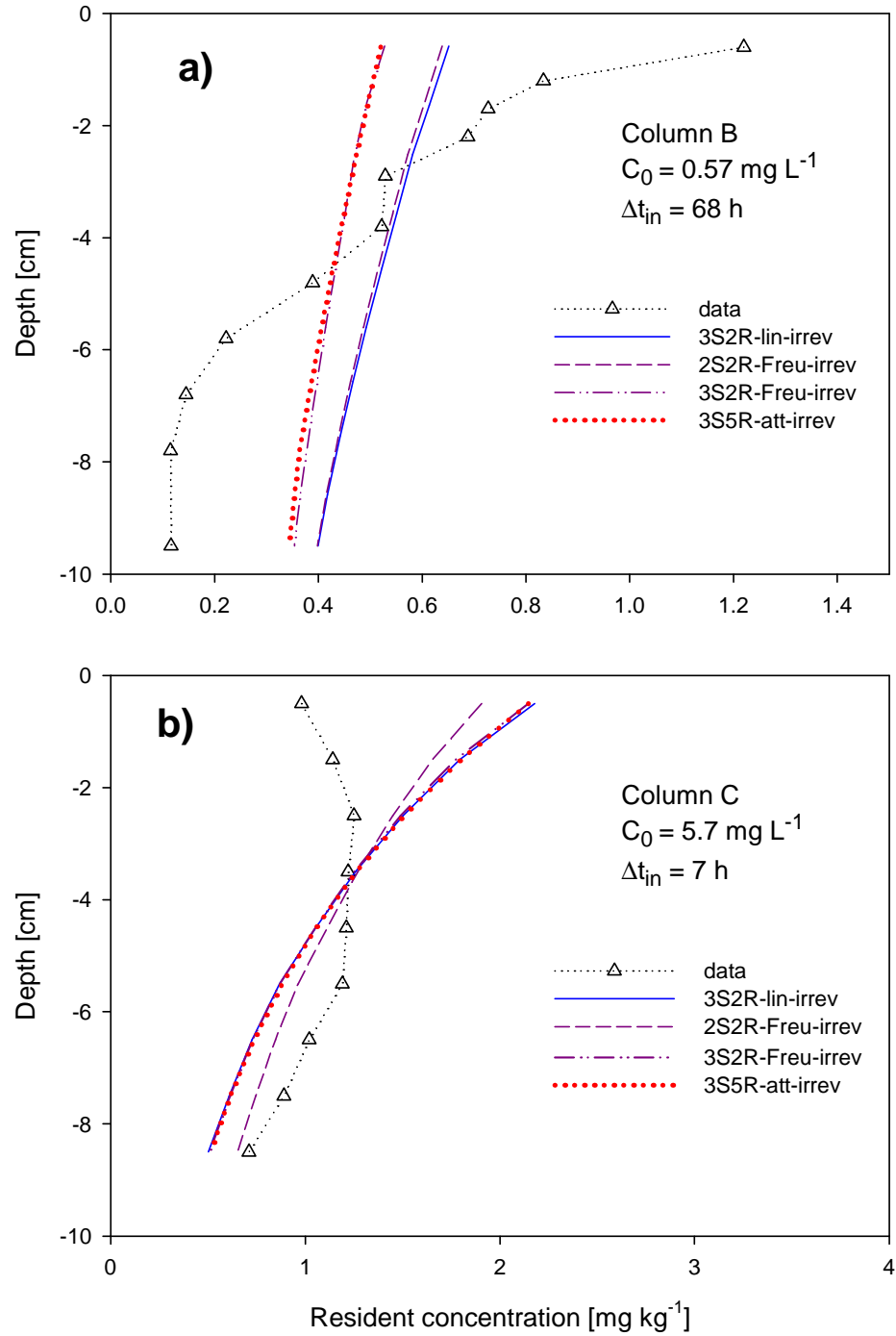


Figure 3.9: Measured and modelled soil profiles of resident  $^{14}\text{C}$  concentrations in column B (a) and C (b).

rate coefficients were within the same range, whereas the rate coefficients for the fast sorption site differed by three orders of magnitude, with the largest values for experiment A and smallest for experiment B.

However, if the 3S5R-att-irrev model included all relevant processes occurring during the experiments and if its parameters were constant (i.e. concentration independent), the optimal parameters for all experimental conditions should be identical. The predictive power of the 3S5R-att-irrev model was tested to describe the BTCs. The optimal parameter set for one experiment was used to predict the BTC for the other two application scenarios (Figure 3.10). The earliest breakthrough was always predicted using the parameters of experiment B, the latest using the parameters of experiment C. The observed peak concentrations and the eluted mass fractions were never met by the forward calculations, because the values of  $\beta_3$  were too different. However, the tailing is described well by all parameter combinations (Figure 3.10). The tailing of the BTC cannot proceed faster than  $\exp(-\alpha_{\text{slow}}t)$ , suggesting that it drops with  $\exp(-\beta t)$ , where  $\beta = \alpha_{\text{slow}} - \delta$  with  $\delta > 0$  (Vereecken *et al.*, 1999). Here  $\beta$  is the slope of the tailing in the semi-log plot for two-site-kinetic sorption models (equivalent to the 2S2R-lin-rev or 2S4R-att-rev models) and  $\alpha_{\text{slow}}$  is the smallest sorption rate coefficient. For the 3S5R-att-irrev model the determining rate coefficient for the tailing is the smallest desorption rate  $\gamma_2$ , because the irreversible sorption process does not influence the slope of the tailing. For all sets of parameters, the values of  $\gamma_2$  are in the same order and thus the slopes of the tailing are expected to be similar, too.

### 3.5 Discussion

Incomplete breakthrough of sulfonamides has previously been reported during transport of SDZ (Kreuzig and Hölting, 2005), sulfachloropyridazine (Boxall *et al.*, 2002; Kay *et al.*, 2005b) and sulfamethoxazole (Drillia *et al.*, 2005). However, the effect of the application mode on the transport was not yet investigated. Kreuzig and Hölting (2005) found only 4 % of the applied SDZ in the leachate compared to 43 % of a simultaneously applied conservative tracer. They also found more than 60 % of the applied  $^{14}\text{C}$ -labelled SDZ as non-extractable residues in the upper 5 cm of the column after 6 days of irrigation. The resulting concentration profile is in accordance with our studies, although detailed information about the BTCs was lacking. Low recoveries were shown for SDZ by Kreuzig *et al.* (2003) or Hamscher *et al.* (2005), especially for aged soil residues. Because of the lack of proved degradation products, the missing mass may as well be non-extractable, apparently irreversibly sorbed parent substance. The model concept proposed to describe the transport of sulfamethoxazole included non-linear Freundlich sorption as well as a rate-limited mass transfer between the flowing bulk liquid phase and a stagnant water film attached to the soil particles (Drillia *et al.*, 2005). However, for soils with little organic material, a strong sorption hysteresis was also observed, which might be described by a second, slower reversible or even an irreversible sorption process (Drillia *et al.*, 2005).



Table 3.5: Fitting parameters of the different isotherm-based (upper part) and attachment/detachment (lower part) models for column B. The eluted mass fraction in the experiment was 60.7 %.

model	fit <sup>†</sup>	$K_f$ $\text{kg}^{-1}\text{L}^{3m}\text{mg}^{1-m}$	m	$\alpha_2$ $\text{h}^{-1}$	f	$\beta_3$ $\text{h}^{-1}$	$R^{2\dagger}$	SSQ <sup>§</sup>	eluted <sup>¶</sup> %
<b>linear sorption models</b>									
2S2R-lin-irrev	lin	0.59	1 <sup>#</sup>	$1.33 \times 10^{-1}$	0 <sup>#</sup>	$3.41 \times 10^{-2}$	0.989	0.018	52
3S2R-lin-irrev	lin	0.65	1 <sup>#</sup>	$7.53 \times 10^{-2}$	$2.46 \times 10^{-1}$	$3.29 \times 10^{-2}$	0.987	0.016	59
<b>Freundlich sorption models</b>									
2S2R-Freu-irrev	lin	0.46	0.50	$7.80 \times 10^{-2}$	0 <sup>#</sup>	$2.80 \times 10^{-2}$	0.994	0.009	56
3S2R-Freu-irrev	log	0.61	0.45	$2.76 \times 10^{-2}$	$2.10 \times 10^{-3}$	$2.53 \times 10^{-2}$	0.792	0.096	59
<b>attachment/detachment models</b>									
model	fit <sup>†</sup>	$\beta_1$ $\text{h}^{-1}$	$\gamma_1$ $\text{h}^{-1}$	$\beta_2$ $\text{h}^{-1}$	$\gamma_2$ $\text{h}^{-1}$	$\beta_3$ $\text{h}^{-1}$	$R^{2\dagger}$	SSQ <sup>§</sup>	eluted <sup>¶</sup> %
2S3R-att-irrev	lin	$41.49 \times 10^{-1}$	$1.34 \times 10^{-1}$	0 <sup>#</sup>	0 <sup>#</sup>	$3.41 \times 10^{-2}$	0.989	0.0176	52
3S5R-att-irrev	log	$1.37 \times 10^{-1}$	$1.10 \times 10^{-1}$	$1.29 \times 10^{-2}$	$4.66 \times 10^{-3}$	$2.49 \times 10^{-2}$	0.870	0.026	59

<sup>†</sup>denotes whether the model was fitted to the non-transformed (lin) or  $\log_{10}$ -transformed concentration data (log); <sup>‡</sup>Regression coefficient; <sup>§</sup>Sum of squares, calculated for non-transformed data, also for the log-fits; <sup>¶</sup>leached mass fraction; <sup>#</sup>fixed parameters.

Table 3.6: Fitting parameters of the different isotherm-based (upper part) and attachment/detachment (lower part) models for column C. The eluted mass fraction in the experiment was 17.8%.

model	fit <sup>†</sup>	$K_f$ $\text{kg}^{-1}\text{L}^{3m}\text{mg}^{1-m}$	m	$\alpha_2$ $\text{h}^{-1}$	f	$\beta_3$ $\text{h}^{-1}$	$R^{2\dagger}$	SSQ <sup>§</sup>	eluted <sup>¶</sup> %
<b>linear sorption models</b>									
2S2R-lin-irrev	lin	1.12	1 <sup>#</sup>	$1.86 \times 10^{+0}$	0 <sup>#</sup>	$1.70 \times 10^{-1}$	0.911	0.014	7
3S2R-lin-irrev	lin	4.51	1 <sup>#</sup>	$1.41 \times 10^{-1}$	0.23	$1.08 \times 10^{-1}$	0.977	0.002	17
<b>Freundlich sorption models</b>									
2S2R-Freu-irrev	log	0.86	0.20	$1.99 \times 10^{-1}$	0 <sup>#</sup>	$8.63 \times 10^{-2}$	0.874	0.023	19
3S2R-Freu-irrev	log	7.07	1.06	$8.22 \times 10^{-3}$	0.17	$1.06 \times 10^{-1}$	0.811	0.007	17
<b>attachment/detachment models</b>									
model	fit <sup>†</sup>	$\beta_1$ $\text{h}^{-1}$	$\gamma_1$ $\text{h}^{-1}$	$\beta_2$ $\text{h}^{-1}$	$\gamma_2$ $\text{h}^{-1}$	$\beta_3$ $\text{h}^{-1}$	$R^{2\dagger}$	SSQ <sup>§</sup>	eluted <sup>¶</sup> %
<b>attachment/detachment models</b>									
2S3R-att-irrev	lin	4.18	2.15	0 <sup>#</sup>	0 <sup>#</sup>	$1.71 \times 10^{-1}$	0.912	0.014	7
3S5R-att-irrev	log	5.91	2.81	$7.45 \times 10^{-2}$	$8.51 \times 10^{-3}$	$1.05 \times 10^{-1}$	0.811	0.007	18

<sup>†</sup>denotes whether the model was fitted to the non-transformed (lin) or  $\log_{10}$ -transformed concentration data (log); <sup>‡</sup>Regression coefficient; <sup>§</sup>Sum of squares, calculated for non-transformed data, also for the log-fits; <sup>¶</sup>leached mass fraction; <sup>#</sup>fixed parameters.

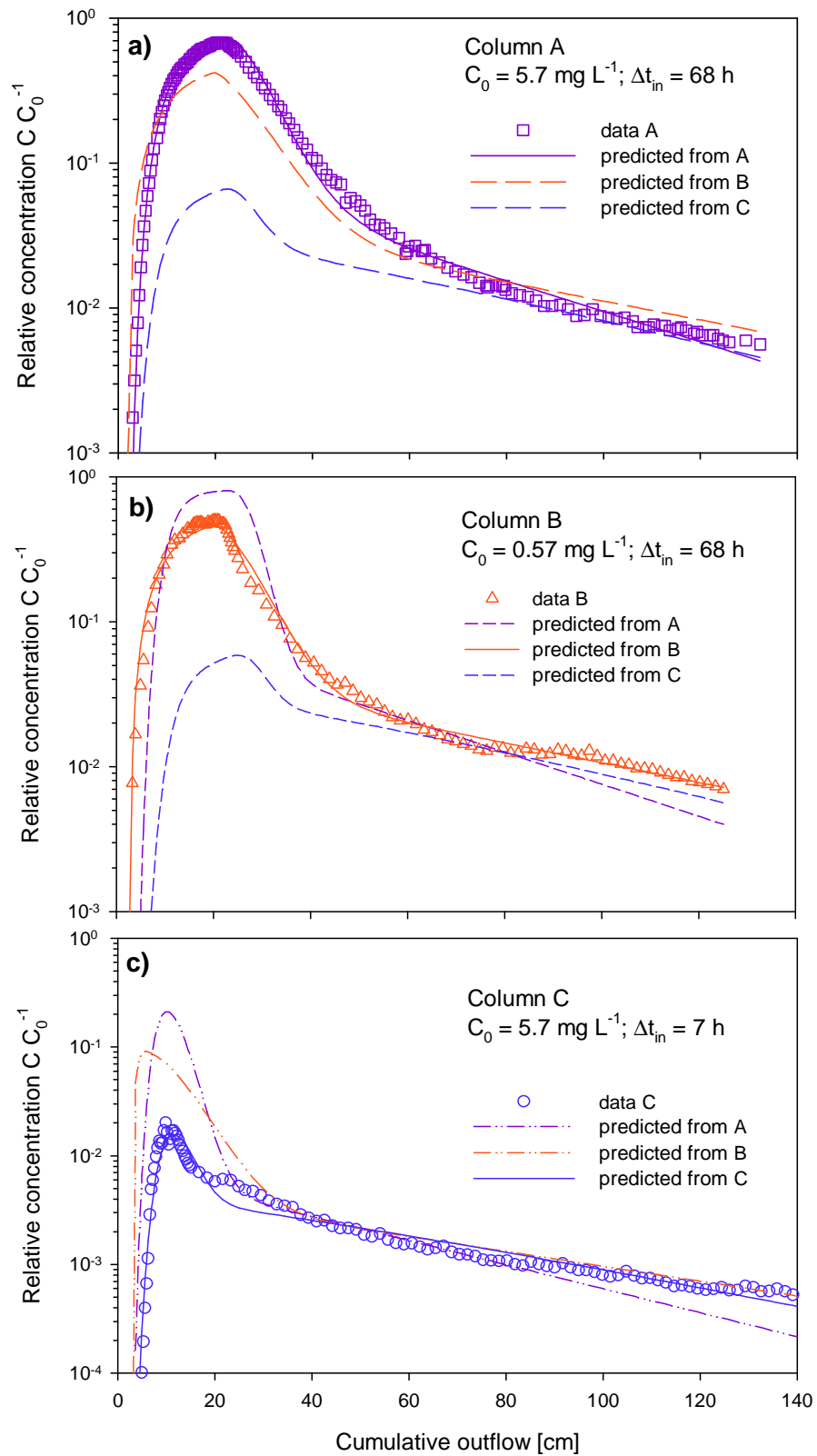


Figure 3.10: Measured, fitted and predicted BTCs with the 3S5R-att-irrev model for experimental conditions A (a), B (b) and C (c).

Although process-oriented transport studies for veterinary pharmaceuticals are still rare, comparable experimental protocols are commonly used for the estimation of the transport parameters for other environmental pollutants, such as pesticides or bacteria. *Prata et al.* (2003) described the BTC of the herbicide atrazine in repacked soil columns well with the 3S2R-lin-irrev model. The irreversible sorption process accounted for 40 to 50 % of the applied mass remaining in the soil column after the leaching period, while even the concentration profile was relatively well reproduced. A similar long tailing due to chemical non-equilibrium sorption was observed for the hormone testosterone in repacked soil columns (*Casey et al.*, 2004). They successfully described the observed BTCs with a one-site kinetic Freundlich sorption model, having a first-order degradation in the solid phase.

The attachment/detachment concept gave the best predictions for all experiments. This approach is commonly used to describe the transport of small particles such as bacteria or viruses in soils or aquifers (*Schijven and Hassanizadeh*, 2000). In these studies the characteristic soil concentration profiles and the extended tailing are often observed (*Bradford et al.*, 2002, 2003; *Schijven et al.*, 2002). However, in particle transport studies additional processes, such as blocking, filtration or straining are included to describe how the size of the particles and their surface properties affect the transport behavior. The required parameters can even be determined independently (*Bradford et al.*, 2002, 2003). These authors considered, for example, blocking as depth-dependent. This concept results in high resident concentrations near the source of the particle release, i.e. the top of the column with very steep concentration gradients.

However, a depth-dependent process, which might better describe the observed soil concentration profiles in this study, cannot be justified for a solute such as SDZ. Nevertheless, the poor model performance for the concentration profiles is a hint that at least one process is lacking in the model. Since our chemical analysis of SDZ was restricted to  $^{14}\text{C}$  only, we have no information available on possible transformation reactions of the  $^{14}\text{C}$ -labelled parent compound and its daughter products in the leachate or the soil. The transformation products can each have very different sorption and transport behavior than the parent compound. The combination of multiple sorption characteristics can lead to different profile concentrations and BTCs than the effective description of  $^{14}\text{C}$  with the assumption of equal sorption characteristics of all species or a lumped parametrization.

## 3.6 Conclusions

We showed that the transport of SDZ depends on the application scenario of the solute, i.e. the input concentration and the pulse duration. The observation of low concentrations in the tailing and the determination of soil resident concentrations was only possible due to the  $^{14}\text{C}$ -analysis. The observed differences in peak concentrations and eluted mass fraction are caused by time- and concentration-dependent sorption processes. Only the complex three-site kinetic sorption model with two reversible and one irreversible sorption site was flexible enough to describe

the complete observed BTCs for the various application scenarios. Despite the good agreement for the BTCs, the observed and modelled concentration profiles in the soil differed substantially. Therefore, common approaches for process identification on the basis of the main peak breakthrough without the observation of the tailing and the concentration profile are precarious. Reasons for the discrepancy between observations and model predictions might be: (i) possible transformation reactions, which were out of the scope of the experimental and model investigations, (ii) inappropriate mathematical concepts for the sorption processes, i.e. isotherms and rate-laws and (iii) the assumption of sorption irreversibility. Although SDZ reaches the soil environment typically as ingredient of manure, the results imply that leaching of SDZ might be enhanced if applied in higher concentrations on soils near water saturation shortly before the next rain event.



# Chapter 4

## Sorption, transformation and transport of sulfadiazine in soil columns - experiments and modelling approaches

### 4.1 Introduction

Antibiotic substances such as sulfadiazine (SDZ) are commonly used in intensive livestock production to treat and prevent diseases. The administered drugs are not completely resorbed by the animals, but are excreted as parent compounds or their metabolites (*Kroger, 1983*). Dung and manure containing these substances are applied onto agricultural soils as fertilizers (*Jørgensen and Halling-Sørensen, 2000*). The fate of pharmaceuticals and the corresponding transformation products in soils and the effects of these compounds on the environment are not yet well understood. However, this knowledge is essential to assess possible adverse effects on soil flora and fauna, and possible contamination of crops or groundwater. Processes affecting the fate of pharmaceuticals in soil may be biotic or abiotic transformations, degradation or mineralization of the substance, sorption onto the soil matrix or uptake by plants or microorganisms. These processes determine to what extent the substance or its transformation products are transported towards deeper soil layers with the percolating water. Thus, an understanding of the governing processes is necessary for risk assessment.

Up to four transformation products of SDZ were found in soil extracts by *Kreuzig and Höltge (2005)* using radio thin layer chromatography. However, the transformation products remained unidentified in their study. We also detected up to three transformation products in our own batch-type studies (Appendix G). Two of these were identified as Acetyl- and Hydroxy-SDZ, respectively, the other remained unidentified. During the metabolism in treated pigs, SDZ is transformed to N4-acetyl-sulfadiazine and both substances are consequently found in pig manure (*Kroger, 1983; Grote et al., 2004*). The acylation of SDZ is reversible in stored ma-

nure (*Berger et al.*, 1986; *Grote et al.*, 2004). Although these studies focused on the metabolism in manure, the results of *Kreuzig and Höltge* (2005) and our separate experiments indicate that transformation reactions might also occur in soils. It is therefore essential to investigate the fate of both, the parent and possible transformation products, in case of re-transformation.

Little is known about the various processes affecting the fate of SDZ in soils. Since the identity, fate and effects of the transformation products are still not well understood, these substances must be included in the environmental risk assessment. The use of  $^{14}\text{C}$ -labelled SDZ allows to follow all compounds (SDZ and its transformation products) simultaneously in batch and column studies. Although the detection of the single compounds requires advanced analytical methods and is often limited to relatively high concentrations, the measurement of total  $^{14}\text{C}$  is insensitive to matrix effects and can be applied in a wide concentration range. In contrast to experiments with the non-labelled compound, the experiments with the  $^{14}\text{C}$ -labelled SDZ are accompanied by closed mass balances at all times. Since the  $^{14}\text{C}$ -labelling is placed at a presumably stable position within the molecule, it is likely to remain in the transformation products. The approach chosen in the sorption and transport section of this thesis (Chapters 2 and 3) was to lump all solutes (SDZ and its transformation products) in the experimental analysis by total  $^{14}\text{C}$ -radioactivity measurements. The worst case scenario, occurring in case the transformation products travel faster through the soil than the parent compound, can also be determined using this method. However, there is a risk to overlook unknown transformation products, if trace analytical methods are applied.

Multiple-site sorption models that do not consider transformations of the parent compound were used to characterize sorption and transport of  $^{14}\text{C}$ -SDZ in the previous transport and sorption Sections 2 and 3. The sorption parameters in these models lump the sorption characteristics of all solutes. However, this approach may be deficient, because each species exhibits its own sorption properties in soils. Assuming that transformation is a time-dependent process, the solute composition will change with respect to time. Therefore, the combined sorption characteristics of all solutes will also change in time. In case sorption of a solute undergoing transformation is described with a lumped approach, the sorption parameters will represent averaged values for all species. Although the lumped approach can successfully describe sorption and transport of solutes with slow transformation rates or if all species (parent and transformation products) have similar (linear) sorption characteristics (e.g. *Prata et al.*, 2003), this may not be the case for the sulfadiazine-soil-water system.

Transformation of organic trace contaminants in soils is frequently assumed to follow first-order kinetics (*Guo and Wagenet*, 1999). Transformation may occur in the dissolved and on the sorbed phases at equal or different rates. However, the experimental verification of the individual processes is impossible (*Gamerdingner et al.*, 1991). Therefore, inverse modelling techniques are used for the simultaneous estimation of sorption and transformation parameters (e.g. *Casey and Šimínek*, 2001). However, sorption affinity and sorption kinetics may influence the transformation



in case of different transformation velocities in the liquid and sorbed phases (*Guo et al.*, 2000). Model calculations for the pesticide 2,4-D (assuming higher degradation rates in the liquid than in the sorbed phase) showed that non-equilibrium sorption will initially favor degradation; however, for the long term, degradation will decrease when desorption kinetics becomes the limiting factor (*Guo et al.*, 2000). For the pesticide alachlor degradation was faster under transport conditions than in batch-systems, indicating that non-equilibrium transport favored alachlor degradation (*Guo and Wagenet*, 1999). Since sorption and transformation both reduce the concentration of the parent compound in the liquid phase, the simplified assumption of equilibrium sorption characteristics during parameter estimation results in erroneous estimates of the transformation rate coefficients (*Guo et al.*, 1999).

*Casey and Šimůnek* (2001) successfully described the transport of chlorinated hydrocarbons using a model considering linear non-equilibrium sorption of multiple solutes involved in sequential decay. The authors restricted the analysis to the breakthrough curves (BTCs). During the transport of  $^{14}\text{C}$ -testosterone through soil columns transformation and sorption occurred simultaneously (*Casey et al.*, 2004). Inverse parameter estimation was used to characterize the kinetic Freundlich sorption and transformation kinetics based on  $^{14}\text{C}$ -BTC data.

*Casey et al.* (2003, 2005) studied the transport behavior of  $^{14}\text{C}$ -labelled  $17\beta$ -estradiol in soil. The parent substance transformed readily into two daughter products, which were further degraded. One transformation product was detected in the leachate, another sorbed strongly and remained in the soil column. The experimental observations were described with two model approaches. The first approach considered no transformation of  $^{14}\text{C}$ - $17\beta$ -estradiol versus sequential transformation of the parent compound in the second approach. Both models could equally well describe either the BTCs or the soil concentration profiles of  $^{14}\text{C}$  in various soil materials. The parameter estimates of the first approach were more reliable (smaller confidence intervals) due to fewer fitting parameters. However, the second model is physicochemically more realistic. The second model was also applied to predict the BTC of  $17\beta$ -estradiol and its transformation product estrone. The estimated sorption and transformation parameters could relatively well describe the BTCs of both solutes and predict the resident concentration profiles, although the latter were not considered in the objective function.

The objective of this study was to evaluate the effect of possible transformation pathways on the transport behavior of SDZ. Additional analysis of the leachate was performed in order to characterize the identity of the total  $^{14}\text{C}$ -radioactivity and to quantify the transformation products. Different model approaches, involving non-equilibrium and irreversible sorption and transformation were tested to describe the observed transport behavior of SDZ and its transformation products.

## 4.2 Materials and Methods

### 4.2.1 Experiments

The transport experiments are described in detail in the transport Section 3.3. Additional to the  $^{14}\text{C}$ -radioactivity measurements in the leachate, selected samples were analyzed by radio-HPLC to characterize the identity of the  $^{14}\text{C}$ . The HPLC-method is described in detail in Appendix E.1 (method II). This method can differentiate between the parent compound SDZ and three of its transformation products by chromatographic separation. Since we employed a reversed phase chromatography column, the substance eluting first had the highest polarity. The most polar substance is still unidentified and is named "MB1" throughout the thesis. The second peak in the radio-HPLC chromatogram is Hydroxy-SDZ followed by SDZ itself. Acetyl-SDZ is slightly less polar than SDZ and was eluted as the last substance in this chromatographic method. According to the detection limit of the radio-HPLC method, only samples with a total  $^{14}\text{C}$ -radioactivity higher than  $800 \text{ kBq L}^{-1}$  (equivalent to  $0.92$  and  $0.23 \text{ mg L}^{-1}$  mass equivalents of SDZ in experiment A and B, respectively) could be characterized. Information about the presence of transformation products is therefore restricted to the main peaks of the BTCs of experiments A and B.

The soil resident concentrations were only measured as total  $^{14}\text{C}$ -radioactivity. An extraction method is required to determine and quantify the different species in soil. However, the extraction efficiency of the available microwave extraction procedure is as low as 10 to 20 % for total  $^{14}\text{C}$ -radioactivity in aged soil samples. This was considered to be insufficient for our purposes, as the majority of the sorbed  $^{14}\text{C}$ -residues in soil would remain uncharacterized. Moreover, the extraction efficiencies of the various species is unknown and is likely to differ between the species.

### 4.2.2 Model approaches

The theory of solute transport under steady state conditions and physical equilibrium is given in the transport Section 3.2 of this thesis. In this section we will restrict to describe the implementation of the transformation processes in the previously used model concepts. All transformation reactions are considered to follow first-order kinetics and take place either in the liquid or the sorbed phases. Our separate batch-type experiments show that transformation products do not appear in the soil solution but additionally require the presence of soil (Appendix G). Therefore, we consider in the model approaches that the transformation reactions occur only in the sorbed phases. The generated transformation product appears in the liquid phase and is there subjected to further sorption and transformation processes. Sorption can either be described by linear or Freundlich isotherms, or by the attachment/detachment approach.

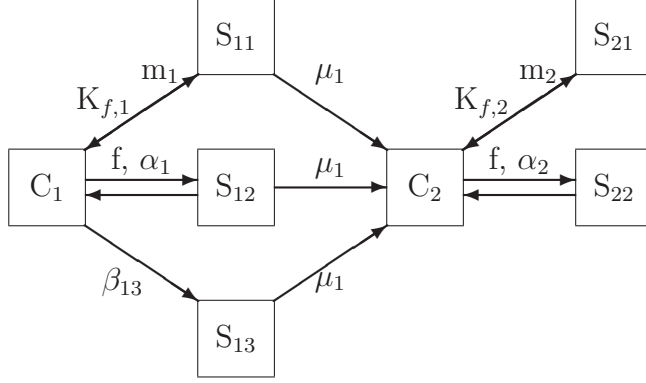


Figure 4.1: Conceptual model involving isotherm-based sorption. The boxes labelled with  $C_i$  represent the liquid phase concentration  $C$ , the boxes  $S_{ij}$  represent the sorbed concentrations at the separate sorption sites. The index  $i = 1, 2$  indicates the solute number, the index  $j = 1, 2, 3$  the sorption sites number.  $K_{f,i}$  and  $m_i$  are the Freundlich distribution coefficient and the Freundlich exponent, respectively,  $f$  indicates the fraction of equilibrium sorption sites,  $\alpha_i$  is the kinetic sorption rate coefficient,  $\beta_{13}$  is the irreversible sorption rate coefficient and  $\mu_1$  is the transformation rate coefficient.

### Isotherm-based transport of two solutes

The concept of the isotherm-based sorption and transport model is illustrated in Figure 4.1. The transport equations for the parent solute (index 1) and its transformation product (index 2) are given by:

$$\theta \frac{\partial C_1}{\partial t} + \rho \frac{\partial S_1}{\partial t} = D\theta \frac{\partial^2 C_1}{\partial z^2} - j_w \frac{\partial C_1}{\partial z} - \mu_1 \rho S_1 \quad (4.1)$$

$$\theta \frac{\partial C_2}{\partial t} + \rho \frac{\partial S_2}{\partial t} = D\theta \frac{\partial^2 C_2}{\partial z^2} - j_w \frac{\partial C_2}{\partial z} + \mu_1 \rho S_1 \quad , \quad (4.2)$$

where  $\mu_1$  is the transformation rate coefficient [ $T^{-1}$ ].

Sorption is considered to follow Freundlich characteristics and can be both, instantaneous ( $S_{11}$  and  $S_{21}$ ) or rate-limited ( $S_{12}$  and  $S_{22}$ ). The parent compound can additionally sorb irreversibly following a first-order kinetic ( $S_{13}$ ). Total sorbed concentrations of the first and second solute are given by:

$$S_i = S_{i1} + S_{i2} + S_{i3} \quad , \quad (4.3)$$

where  $i = 1, 2$  indicates the solute number. Notice that there is no irreversible sorption for the second solute ( $S_{23} = 0$ ). The total sorbed concentration is:

$$S = S_1 + S_2 \quad . \quad (4.4)$$

Transformation of the parent compound occurs at all three sorption sites at the same rate  $\mu_1$ . No transformation is considered for the second compound. The sorption parameters of the two solutes are different. Only the parameter  $f$ , which determines the fraction of equilibrium sorption sites, is assumed to be identical for both solutes. Sorption at the equilibrium sorption sites is given by:

$$S_{i1} = fK_{f,i}C_i^{m_i} \quad , \quad (4.5)$$

for sorption of the parent ( $i = 1$ ) and the transformation product ( $i = 2$ ).  $K_{f,i}$  is the Freundlich distribution coefficient [ $M_{\text{solute}}^{1-m_i} L^{3m_i} M_{\text{soil}}^{-1}$ ] and  $m_i$  is the dimensionless Freundlich exponent. Note that linear sorption is a special case of Freundlich sorption with  $m_i=1$ . Sorption at the kinetic sorption sites is given by:

$$\frac{\partial S_{i2}}{\partial t} = \alpha_i[(1-f)K_{f,i}C_i^{m_i} - S_{i2}] - \mu_i S_{i2} \quad , \quad (4.6)$$

where  $\alpha_i$  is the sorption rate coefficient [ $T^{-1}$ ]. The second solute is not transformed ( $\mu_2 = 0$ ). The irreversible sorption of the parent compound is given by:

$$\frac{\partial S_{13}}{\partial t} = \beta_{13} \frac{\theta}{\rho} C_1 - \mu_1 S_{13} \quad , \quad (4.7)$$

where  $\beta_{13}$  is the irreversible sorption rate coefficient [ $T^{-1}$ ].

### Attachment/detachment-based transport of two solutes

If the sorption of the parent compound and the degradation product is described by the attachment/detachment concept, the transport equations are identical to Equations 4.1 and 4.2. The sorbed species in Equation 4.3 are then:  $S_{i1}$  and  $S_{i2}$  are the sorbed concentrations for solute 1 and 2 at the fast and slow attachment/detachment sites, respectively and  $S_{13}$  is the sorbed concentrations for solute 1 at the irreversible sorption sites. Figure 4.2 illustrates the model concept. The attachment/detachment processes for each solute at different sorption sites are described as:

$$\frac{\partial S_{ij}}{\partial t} = \frac{\theta}{\rho} \beta_{ij} C_i - \gamma_{ij} S_{ij} - \mu_i S_{ij} \quad , \quad (4.8)$$

where  $\beta_{ij}$  and  $\gamma_{ij}$  are the attachment and detachment rate coefficients [ $T^{-1}$ ], respectively. The index  $i = 1, 2$  indicates the solute number, whereas the index  $j = 1, 2, 3$  indicates the sorption sites number. Note that coefficients  $\gamma_{13}$  and  $\mu_2$  are equal to zero in this conceptual model.

In the above models the transformation process was assumed to occur at the same rate at all sorption sites. However, if the transformation from certain sorption sites is prevented, this conceptual model may not be appropriate. In the next model approach, transformation was not allowed at the irreversible sorption sites. The sorption equations (Equation 4.7 and 4.8) for the irreversible sorption sites then reduces to:

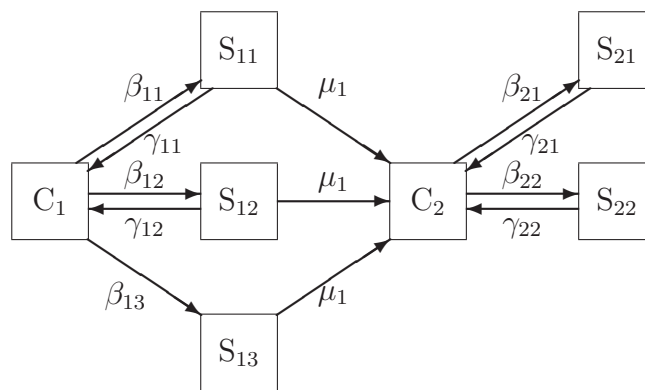


Figure 4.2: Conceptual model involving attachment/detachment-based sorption. The boxes labelled with  $C_i$  represent the liquid phase concentration  $C$ , the boxes  $S_{ij}$  represent the sorbed concentrations at the separate sorption sites. The index  $i = 1, 2$  indicates the solute number, the index  $j = 1, 2, 3$  the attachment/detachment sites number. Parameters  $\beta_{ij}$  and  $\gamma_{ij}$  are the attachment and detachment rate coefficients of solute  $i$  at sorption sites  $j$ , respectively, and  $\mu_1$  is the transformation rate coefficient.

$$\frac{\partial S_{13}}{\partial t} = \frac{\theta}{\rho} \beta_{13} C_1 \quad . \quad (4.9)$$

Equation 4.3 then changes to:

$$S_1 = S_{1,rev} + S_{13} \quad , \quad S_{1,rev} = S_{11} + S_{12} \quad , \quad (4.10)$$

where  $S_{1,rev}$  represents the sorbed concentration of solute 1 with reversible sorption where transformation occurs. Consequently, the third term on the right hand side of Equations 4.1 and 4.2 changes to  $\mu_1 \rho S_{1,rev}$ .

### Attachment/detachment-based transport of three solutes

Because there was experimental evidence of more than one transformation product, a third solute was included into the model (Figure 4.3). The three solutes are included as a sequential reaction, from the first to the second and from the second to the third solute. All solutes exhibit their own attachment/detachment characteristics at the two possible sorption sites. Transformation occurs only at one of these sorption sites. The transport equations for the three solutes are:

$$\theta \frac{\partial C_1}{\partial t} + \rho \frac{\partial S_1}{\partial t} = D \theta \frac{\partial^2 C_1}{\partial z^2} - j_w \frac{\partial C_1}{\partial z} - \mu_1 \rho S_{11} \quad (4.11)$$

$$\theta \frac{\partial C_2}{\partial t} + \rho \frac{\partial S_2}{\partial t} = D \theta \frac{\partial^2 C_2}{\partial z^2} - j_w \frac{\partial C_2}{\partial z} - \mu_2 \rho S_{21} + \mu_1 \rho S_{11} \quad (4.12)$$

$$\theta \frac{\partial C_3}{\partial t} + \rho \frac{\partial S_3}{\partial t} = D \theta \frac{\partial^2 C_3}{\partial z^2} - j_w \frac{\partial C_3}{\partial z} + \mu_2 \rho S_{21} \quad , \quad (4.13)$$

where  $\mu_i$  is the transformation rate coefficients [ $T^{-1}$ ] of solute 1 ( $i = 1$ ) and solute 2 ( $i = 2$ ). Sorbed concentrations are given by:

$$S_i = S_{i1} + S_{i2} \quad . \quad (4.14)$$

The sorption equation for the sorption sites, where transformation occurs is given for all solutes by:

$$\frac{\partial S_{i1}}{\partial t} = \frac{\theta}{\rho} \beta_{i1} C_i - \gamma_{i1} S_i - \mu_i S_{i1} \quad . \quad (4.15)$$

Note that there is no transformation of the third solute and, thus,  $\mu_3 = 0$ . The sorption equation for the sorption sites without transformation is given by:

$$\frac{\partial S_{i2}}{\partial t} = \frac{\theta}{\rho} \beta_{i2} C_i - \gamma_{i2} S_i \quad . \quad (4.16)$$

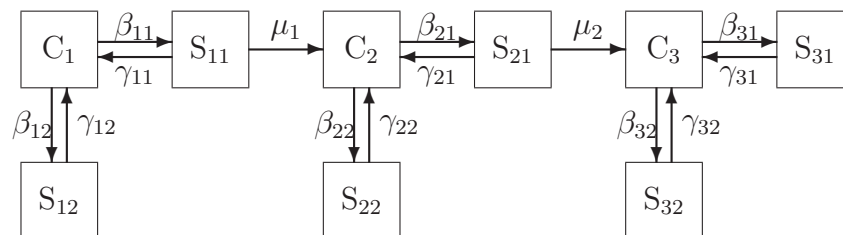


Figure 4.3: Conceptual model involving attachment/detachment-based sorption and three solutes. The boxes labelled with  $C_i$  represent the liquid phase concentration of solute  $i$ , the boxes  $S_{ij}$  represent the sorbed concentration of solute  $i$  at the separate sorption sites  $j$ . Parameters  $\beta_{ij}$  and  $\gamma_{ij}$  are the attachment and detachment rate coefficients of solute  $i$  at sorption sites  $j$ , respectively, and  $\mu_i$  is the transformation rate coefficient of solute  $i$ .

### Parameter estimation

The sorption and transformation models were implemented into the *HYDRUS-1D* software package (version 3.0, *Simunek et al. (2005)*). Simulations were run according to the descriptions given in the transport section (Section 3.3). The objective function of the inverse solution mode was adapted to the available experimental data. Total  $^{14}\text{C}$ -radioactivity data of both the BTC and the resident soil concentration profile were assumed to be the sum of all solutes,  $C_1 + C_2 + C_3$  and  $S_1 + S_2 + S_3$ , respectively. The dissolved solute masses were neglected in the calculation of the soil resident concentrations. This was justified by the low leachate concentrations at the end of the experiment. In addition to the total  $^{14}\text{C}$ -concentration in the BTC, the concentrations of the parent compound (SDZ) are included in the objective function. BTC data could be internally  $\log_{10}$ -transformed in the optimization procedure to put more weight on the low concentrations in the tailing.

The models described above are the most complex concepts considered in the *HYDRUS-1D*-code. The aim was to find the simplest model that can describe the experimental data. This model requires the fewest number of fitting parameters; additional parameters will not improve the goodness of the fit. These less complex models were defined by considering less sorption sites or simpler sorption isotherm assumptions, i.e. setting selected parameters equal to zero.

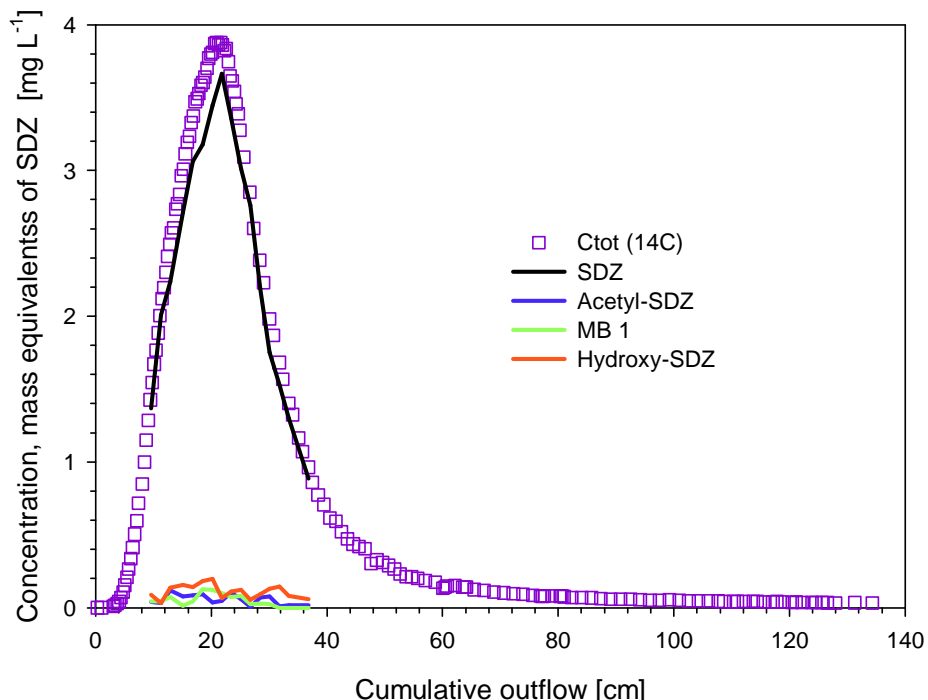


Figure 4.4: BTCs of total  $^{14}\text{C}$ , SDZ and its transformation products in column A.

## 4.3 Results

### 4.3.1 Experimental results

Up to three transformation products were detected in the leachate of the experiments A and B during the breakthrough of the peak (Figures 4.4 and 4.5). The  $^{14}\text{C}$ -concentrations in the BTC of column C were lower than the detection limit of the radio-HPLC method. Within the measured samples the fraction of SDZ on the total  $^{14}\text{C}$ -radioactivity was equal or higher than 88 % or 57 % for experiments A and B, respectively. The remaining  $^{14}\text{C}$ -radioactivity was attributed to the three transformation products. Although the concentration data show a pronounced scattering, some general trends were observed: In both columns Hydroxy-SDZ had slightly higher concentrations than MB1 and Acetyl-SDZ. Whereas the more polar substances MB1 and Hydroxy-SDZ arrived simultaneously with SDZ, the less polar Acetyl-SDZ appears later than the other substances in the effluent of column B. As was also observed in the batch-type experiments (Appendix G), the fraction of transformation products seems to increase with decreasing concentrations of total  $^{14}\text{C}$ .



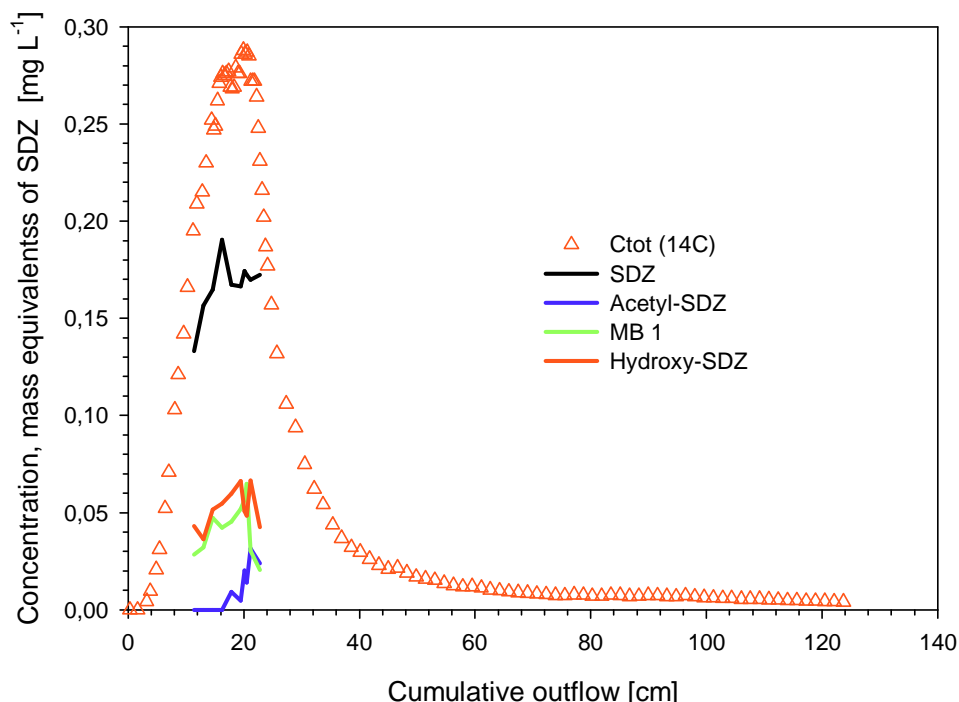


Figure 4.5: BTCs of total  $^{14}\text{C}$ , SDZ and its transformation products in column B.

### 4.3.2 Modelling results

We tested different sorption and transformation models on their ability to describe the observed BTCs of SDZ and the total  $^{14}\text{C}$ -radioactivity and the soil resident concentration profiles. Transformation was assumed to follow first-order kinetics and to occur in the sorbed phases. Models that consider the transformation of irreversibly sorbed solute were not able to describe the experimental data. Thus, no transformation occurs on the irreversible sorption sites in the models discussed below.

#### Description of the BTCs

**Isotherm-based models** The BTCs of SDZ and the total  $^{14}\text{C}$ -radioactivity in experiment A were well described with a model considering Freundlich equilibrium sorption for two solutes with transformation in the sorbed phase (Figure 4.6). The model assumptions and fitted parameter values of this one-site equilibrium sorption and transformation model (I) are given in Tables 4.1 and 4.2. Note that only the data of the BTCs were used in the objective function. In the model calculations the first solute arrived well before the second in the leachate and accounted for most of the peak breakthrough. Due to a higher sorption affinity and a more pronounced non-linearity, the second solute arrived much later and accounted completely for the tailing of the  $^{14}\text{C}$ -BTC.

Table 4.1: Model assumptions for the isotherm-based (upper part) and the attachment/detachment-based (lower part) sorption and transformation models for two solutes. The relevant equations as well as the assumptions for the involved parameters are given.

model	Equations	$K_{f,1}$	$m_1$	$\alpha_1$	$f$	$\beta_{1,3}$	$\mu_1$	$K_{f,2}$	$m_2$	$\alpha_2$	transformation in $S_{1,3}$	
I	1, 2, 3, 4, 5	fit	fit	0	1	0	fit	fit	fit	0	no $S_{1,3}$	
<b>equilibrium models</b>												
II	1, 2, 3, 4, 5, 6	fit	fit	fit	0	0	fit	fit	fit	fit	no $S_{1,3}$	
<b>kinetic model</b>												
model	Equations	$\beta_{1,1}$	$\gamma_{1,1}$	$\beta_{1,2}$	$\gamma_{1,2}$	$\beta_{1,3}$	$\mu_1$	$\beta_{2,1}$	$\gamma_{2,1}$	$\beta_{2,2}$	$\gamma_{2,2}$	transformation in $S_{1,3}$
<b>attachment/detachment models</b>												
III	1, 2, 4, 9, 10	fit	0	0	0	fit	fit	fit	fit	0	0	no
IV	1, 2, 4, 9, 10	fit	fit	0	0	fit	fit	fit	fit	0	0	no

Table 4.2: Fitting parameters of the different isotherm-based (upper part) and attachment/detachment-based (lower part) sorption and transformation models for two solutes.

experiment	model	fit <sup>†</sup>	objective function <sup>¶</sup>		$K_{f,1}$ kg <sup>-1</sup> L <sup>3m</sup> mg <sup>1-m</sup>	$m_1$	$\alpha_1$ h <sup>-1</sup>	$f$	$\mu_1$ h <sup>-1</sup>	$K_{f,2}$ kg <sup>-1</sup> L <sup>3m</sup> mg <sup>1-m</sup>	$m_2$	$\alpha_2$ h <sup>-1</sup>
			BTC	profile								
A	I	lin	<sup>14</sup> C, SDZ	0	$9.51 \times 10^{-1}$	0.95	0 <sup>#</sup>	1 <sup>#</sup>	$1.24 \times 10^{-2}$	$4.02 \times 10^{+0}$	0.18	0 <sup>#</sup>
B	I	lin	<sup>14</sup> C	0	$4.29 \times 10^{-1}$	0.93	0 <sup>#</sup>	1 <sup>#</sup>	$4.74 \times 10^{-2}$	$7.59 \times 10^{-1}$	0.10 <sup>‡</sup>	0 <sup>#</sup>
B	II	lin	<sup>14</sup> C, SDZ	<sup>14</sup> C	$1.46 \times 10^{+0}$	0.76	$3.71 \times 10^{-2}$	0 <sup>#</sup>	$2.20 \times 10^{-2}$	$7.73 \times 10^{+0}$	0.54	$3.05 \times 10^{-3}$

experiment	model	fit <sup>†</sup>	objective function		$\beta_{11}$ h <sup>-1</sup>	$\gamma_{11}$ h <sup>-1</sup>	$\beta_{13}$ h <sup>-1</sup>	$\mu_1$ h <sup>-1</sup>	$\beta_{21}$ h <sup>-1</sup>	$\gamma_{21}$ h <sup>-1</sup>
			BTC	profile						
A	III	lin	<sup>14</sup> C, SDZ	<sup>14</sup> C	$1.50 \times 10^{+0}$	0 <sup>#</sup>	$6.51 \times 10^{-2}$	$3.15 \times 10^{-2}$	$8.37 \times 10^{-3}$	$7.72 \times 10^{-4}$
A	III	log	<sup>14</sup> C, SDZ	<sup>14</sup> C	$1.72 \times 10^{-2}$	0 <sup>#</sup>	$9.01 \times 10^{-3}$	$1.51 \times 10^{-2}$	$1.91 \times 10^{-2}$	$6.79 \times 10^{-3}$
B	IV	lin	<sup>14</sup> C, SDZ	<sup>14</sup> C	$3.76 \times 10^{+0}$	$3.55 \times 10^{+0}$	$6.10 \times 10^{-2}$	$6.12 \times 10^{-2}$	$6.46 \times 10^{-2}$	$5.58 \times 10^{-2}$
B	IV	log	<sup>14</sup> C, SDZ	<sup>14</sup> C	$1.40 \times 10^{-1}$	$7.56 \times 10^{-2}$	$3.73 \times 10^{-2}$	$1.73 \times 10^{-2}$	$5.58 \times 10^{-2}$	$6.52 \times 10^{-3}$
C	IV	lin	<sup>14</sup> C	<sup>14</sup> C	$2.63 \times 10^{+0}$	$1.09 \times 10^{+0}$	$3.96 \times 10^{-2}$	$6.81 \times 10^{-2}$	$5.27 \times 10^{-1}$	$4.98 \times 10^{-3}$

<sup>†</sup>denotes whether the model was fitted to the non-transformed (lin) or log<sub>10</sub>-transformed concentration data (log); <sup>¶</sup> data used in the objective function; <sup>‡</sup>lower limit in parameter estimation procedure; <sup>#</sup>fixed parameters.

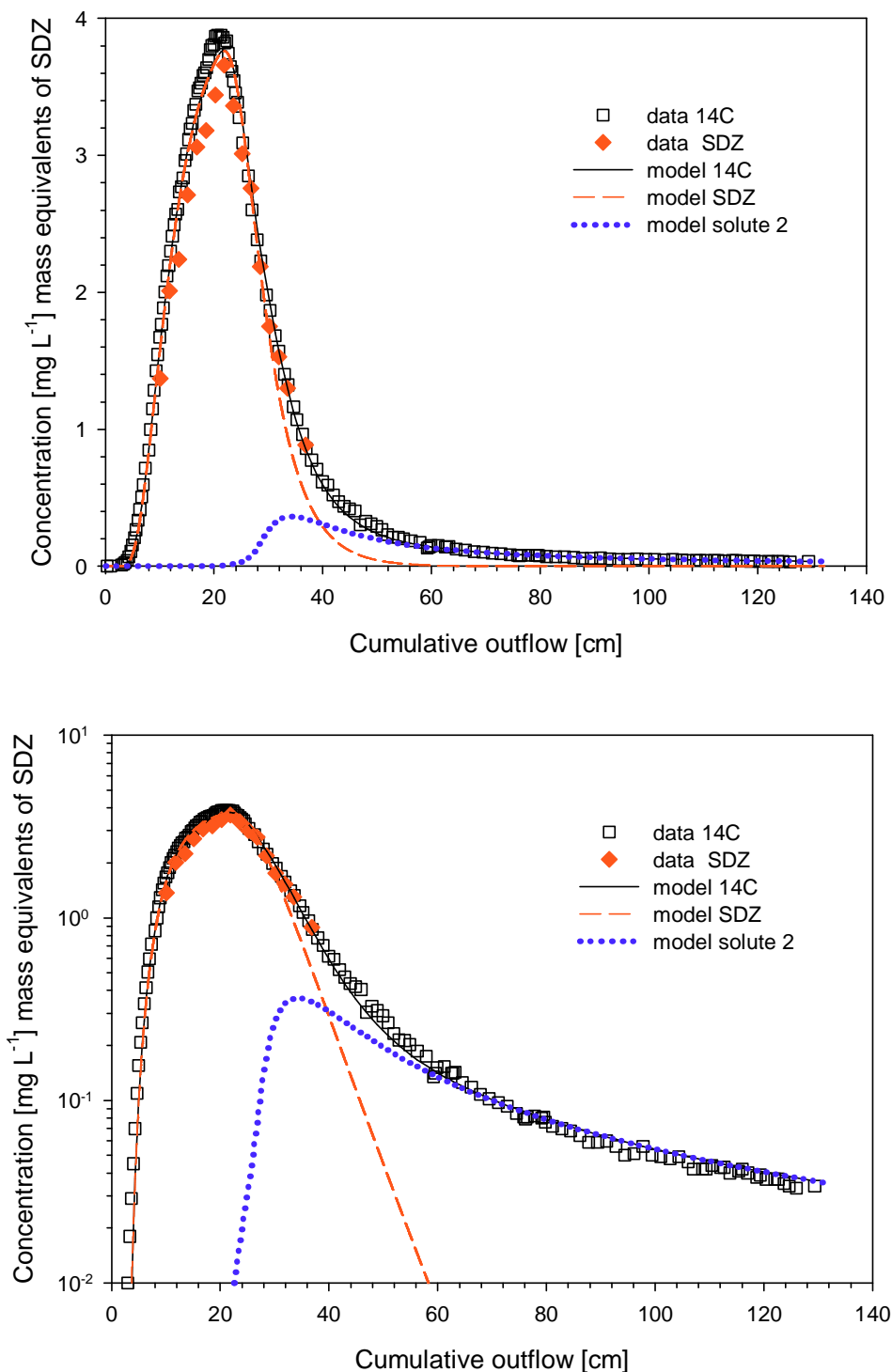


Figure 4.6: Breakthrough curves of total <sup>14</sup>C, SDZ and one transformation product in column A. The symbols represent measurements and the lines (solid, dashed and dotted) model calculations. The Freundlich equilibrium sorption model (model I in Table 4.1) was fitted to the BTC data. The corresponding soil concentration profiles are given in Figure 4.14.

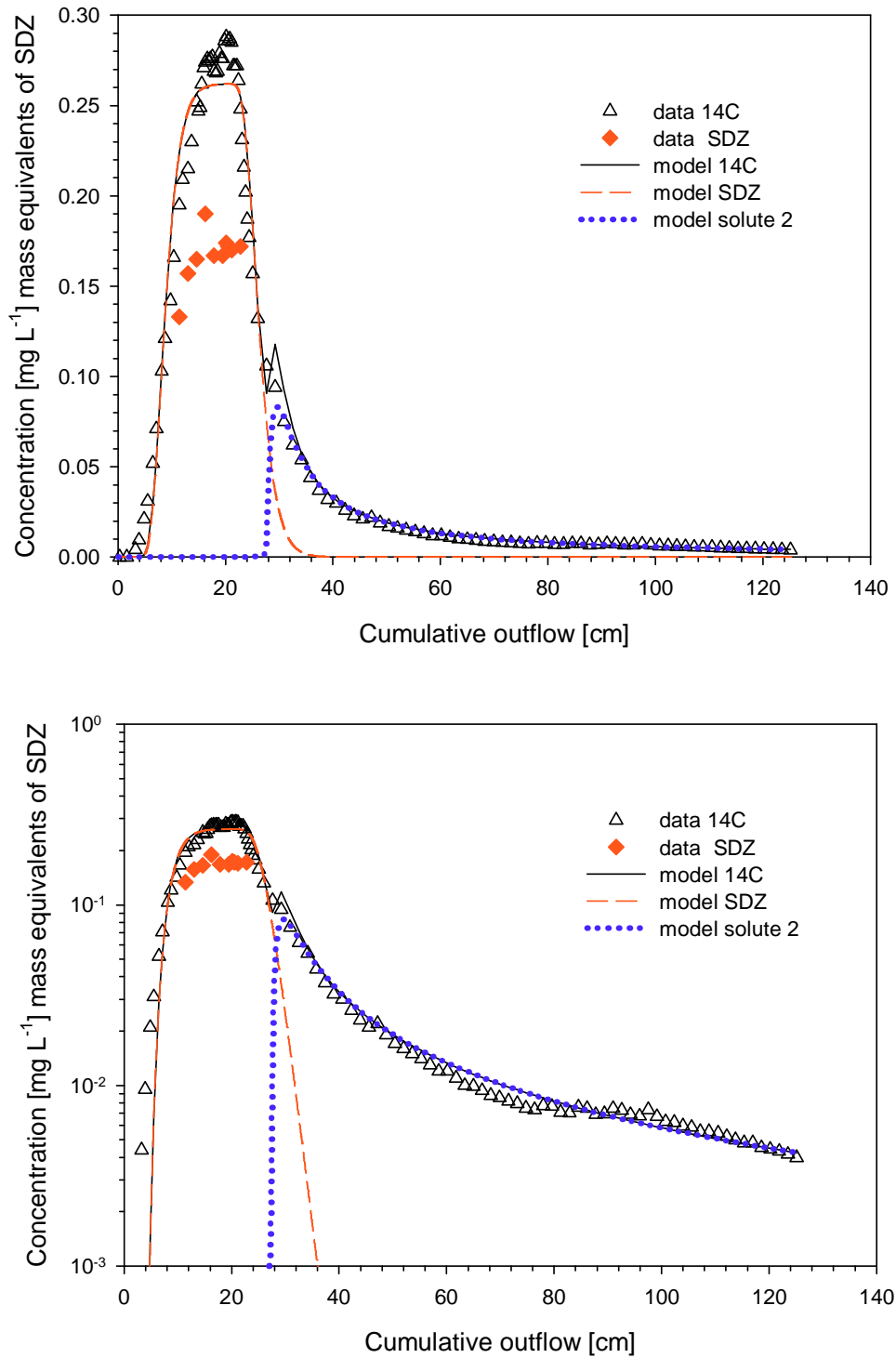


Figure 4.7: Breakthrough curves of total  $^{14}\text{C}$ , SDZ and one transformation product in column B. The symbols represent measurements and the lines (solid, dashed and dotted) model calculations. The Freundlich equilibrium sorption model (model I in Table 4.1) was fitted only to the  $^{14}\text{C}$  BTC data. The corresponding soil concentration profiles are given in Figure 4.15.

No parametrization was found to describe both the BTC of  $^{14}\text{C}$  and SDZ of experiment B using the model concept I. In Figure 4.7 model I was fitted only to the total  $^{14}\text{C}$ -BTC data. As for column A, the total  $^{14}\text{C}$ -BTC was well described by the sum of the two non-linear sorbing solutes. Since the first solute accounts for the main peak breakthrough, the calculated concentrations are much higher than the measured SDZ concentrations. The sorption of the second solute was again highly non-linear (Table 4.2). This resulted in a large retardation for low concentrations and a pronounced tailing, which accounted perfectly for the measured tailing of the  $^{14}\text{C}$ -BTC.

A more complex model was required for the description of the SDZ BTC in experiment B (model II in Table 4.1). A good fit of both BTCs was obtained assuming kinetic Freundlich sorption instead of equilibrium Freundlich sorption for both solutes (Figure 4.8). The peak of both solutes arrived after leaching of approximately the same amount of cumulative outflow. The first solute appeared slightly earlier in the leachate and concentrations decreased rapidly after the peak breakthrough. The combination of non-linear sorption and a lower sorption rate coefficient, resulted in a pronounced tailing for the second solute; the tailing at the end of the experiment was slightly overestimated.

**Attachment/detachment-based models** The model with the fewest parameters that was able to describe the  $^{14}\text{C}$ -BTC of experiment A considered attachment of the first solute towards two separate sorption sites, but no detachment from these sites (model III in Table 4.1). Whereas the solute at the second sorption sites remained irreversibly sorbed, the solute at the first sorption sites was transformed into the second solute. The second solute was attached and detached at one type of sorption sites. While the  $^{14}\text{C}$ -BTC was described well, the first solute did not leach contrary to the observations (Figure 4.9). The second solute accounted completely for the breakthrough. The concentrations in the tailing of the BTC were slightly underestimated. Both solutes leached if more weight is put on the tailing in the fitting procedure by a  $\log_{10}$ -transformation of the BTC data. Whereas the tailing was now well-described by the second solute, the peak shape of the fitted BTCs did not match the observations (Figure 4.10). The first solute arrived too early in the leachate and its concentrations dropped rapidly. Predicted peak concentrations of the second solute arrived simultaneously to the observed peak of total  $^{14}\text{C}$ .

The best model that was able to describe the observed data of experiment B considered reversible sorption of the first solute at the first sorption sites (model IV in Table 4.1). The model performance also depended on the  $\log_{10}$ -transformation of the BTC-data (Figures 4.11 and 4.12). In case the data were not transformed and unit weight was assigned to all data points (BTCs and profile), the best model fit is given in Figure 4.11. In the leachate the second solute arrived shortly before the first solute and the peak of both BTCs appeared at about the same time as the peak of total  $^{14}\text{C}$ . The concentrations of the first solute were about one fourth of the concentrations of the second solute and also only about one third of the measured SDZ concentrations. The observed tailing for the  $^{14}\text{C}$ -BTC was not described by the

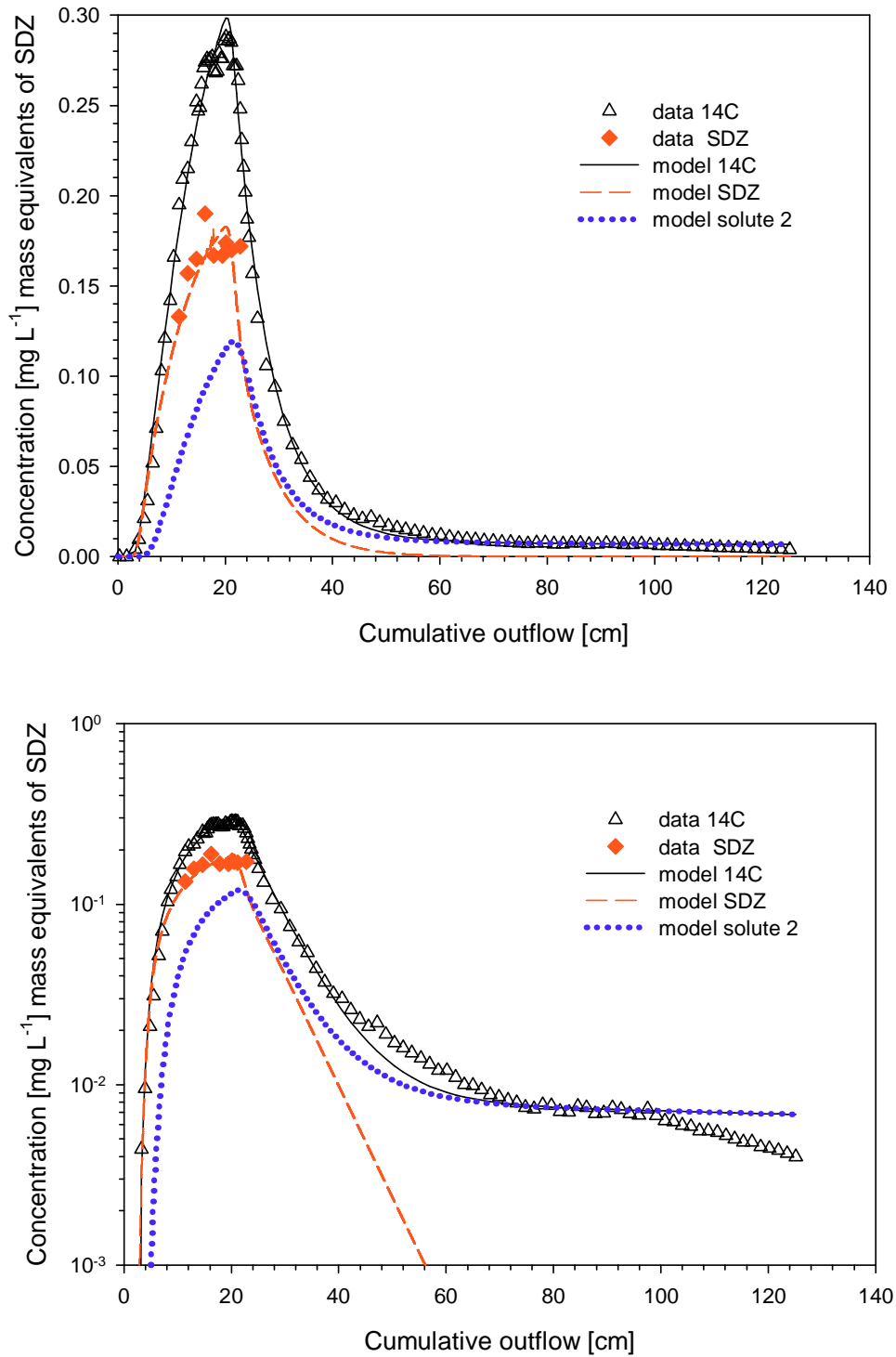


Figure 4.8: Breakthrough curves of total  $^{14}\text{C}$ , SDZ and one transformation product in column B. The symbols represent measurements and the lines (solid, dashed and dotted) model calculations. The kinetic Freundlich sorption model (model II in Table 4.1) was fitted to the BTC and profile data. The corresponding soil concentration profiles are given in Figure 4.16.

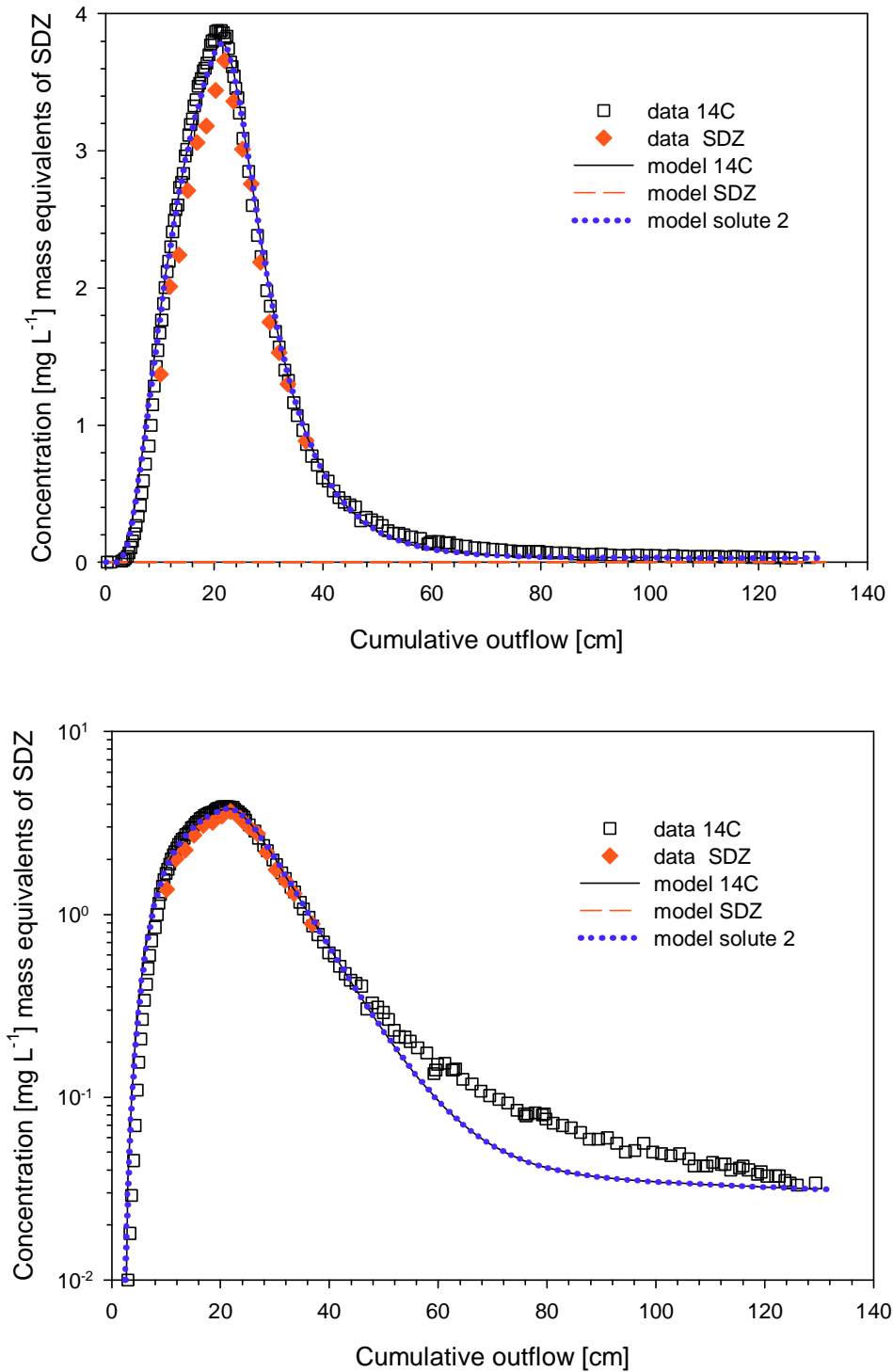


Figure 4.9: Breakthrough curves of total  $^{14}\text{C}$ , SDZ and one transformation product in column A. The symbols represent measurements and the lines (solid, dashed and dotted) model calculations. The attachment/detachment sorption model (model III in Table 4.1) was fitted to the BTC and profile data. The corresponding soil concentration profiles are given in Figure 4.17.



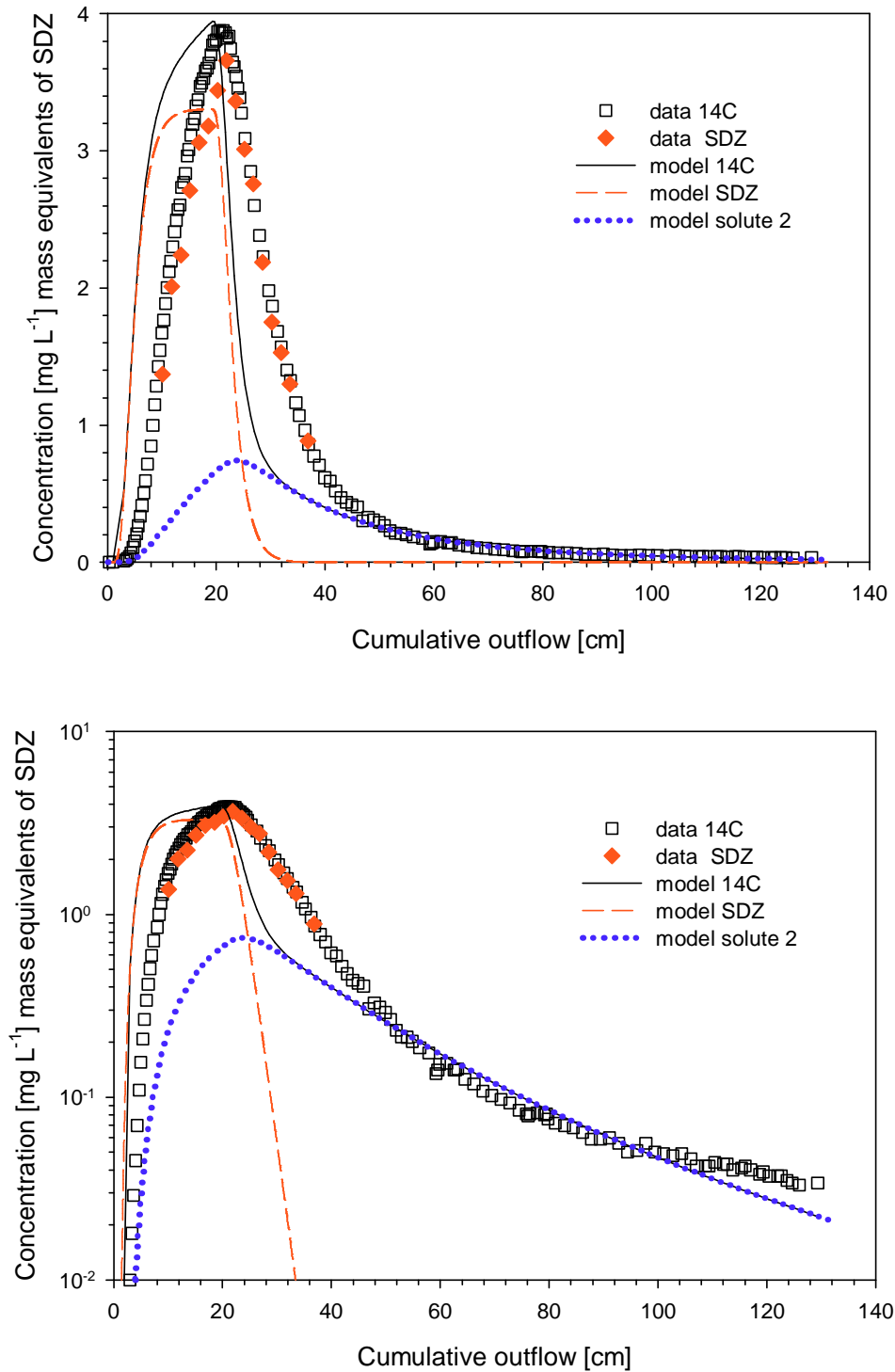


Figure 4.10: Breakthrough curves of total  $^{14}\text{C}$ , SDZ and one transformation product in column A. The symbols represent measurements and the lines (solid, dashed and dotted) model calculations. The attachment/detachment sorption model (model III in Table 4.1) was fitted to the profile and  $\log_{10}$ -transformed BTC data. The corresponding soil concentration profiles are given in Figure 4.18.

rather steep decreasing limbs of the BTCs of both solutes. After  $\log_{10}$ -transformation of the BTC data the model fit resulted in a correct description of the tailing and SDZ itself (Figure 4.12). Due to the slower attachment/detachment kinetics of the first solute at the first sorption sites, leachate concentrations were higher and matched the observed values of SDZ. The second solute arrived later in the leachate and did not reach concentrations as high as calculated for the first solute. The BTC of the sum of both solutes slightly underestimated the observed peak concentrations and the eluted mass fraction.

Despite there were no concentration data available for the separate solute species in experiment C, the model concept IV was fitted to the  $^{14}\text{C}$  BTC and profile data (Figure 4.13). The main peak breakthrough was well described with the attachment/detachment model for two solutes. Both solutes arrived at approximately the same time in the leachate and reached their maximum concentration simultaneously. However, the tailing of the total  $^{14}\text{C}$  could not be described with this model, independent of the transformation of the BTC data.

### Description of the soil concentration profiles

In this section the model performance of the above-mentioned models is discussed with respect to the soil concentration profiles. For all parameter combinations in Table 4.2 the soil concentration profiles were also calculated (Figures 4.14 - 4.19).

**Isotherm-based models** The soil concentration profiles predicted from the equilibrium or kinetic Freundlich sorption models (models I or II in Table 4.1, Figures 4.14, 4.15 and 4.16) were characterized by increasing concentrations with profile depth contradictory to the experimental data. Since the first solute was either leached or transformed into the second solute, only the second solute accounted for the soil resident concentrations at the end of the experiment. Notice that the resident concentration profiles were not considered in the objective function of the equilibrium model (Table 4.2). However, reversible sorption concepts are not able to predict decreasing resident concentrations with profile depth and tailing.

**Attachment/detachment-based models** The resident concentration profiles of all experiments were well described, assuming attachment/detachment of both solutes. Assigning unit weight to the experimental data of experiment A ( $^{14}\text{C}$  and SDZ BTC and  $^{14}\text{C}$  concentration profile), the soil concentration profile was perfectly described (Figure 4.17). The irreversibly sorbed fraction of the first solute accounted for the high concentrations at the top of the soil column. The second solute accounted for the evenly distributed resident concentrations in the lower part of the soil concentration profile. In case the BTC data were  $\log_{10}$ -transformed in the fitting procedure, the high concentration at the top of the soil column was not correctly predicted (Figure 4.18). However, resident concentrations below 1-cm depth were well predicted and were mostly composed of the irreversibly sorbed fraction of the first solute.

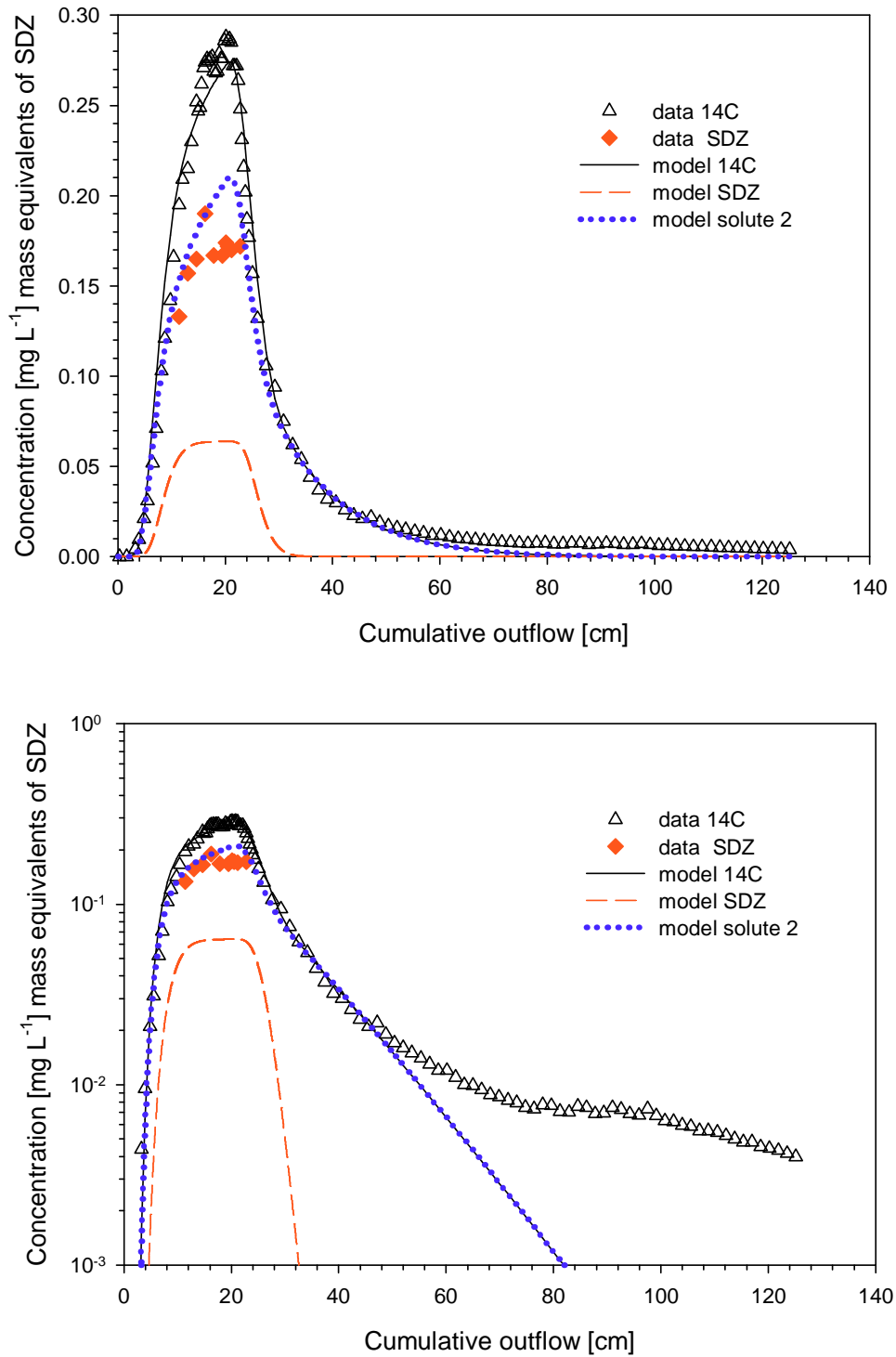


Figure 4.11: Breakthrough curves of total <sup>14</sup>C, SDZ and one transformation product in column B. The symbols represent measurements and the lines (solid, dashed and dotted) model calculations. The attachment/detachment sorption model (model IV in Table 4.1) was fitted to the BTC and profile data. The corresponding soil concentration profiles are given in Figure 4.20.

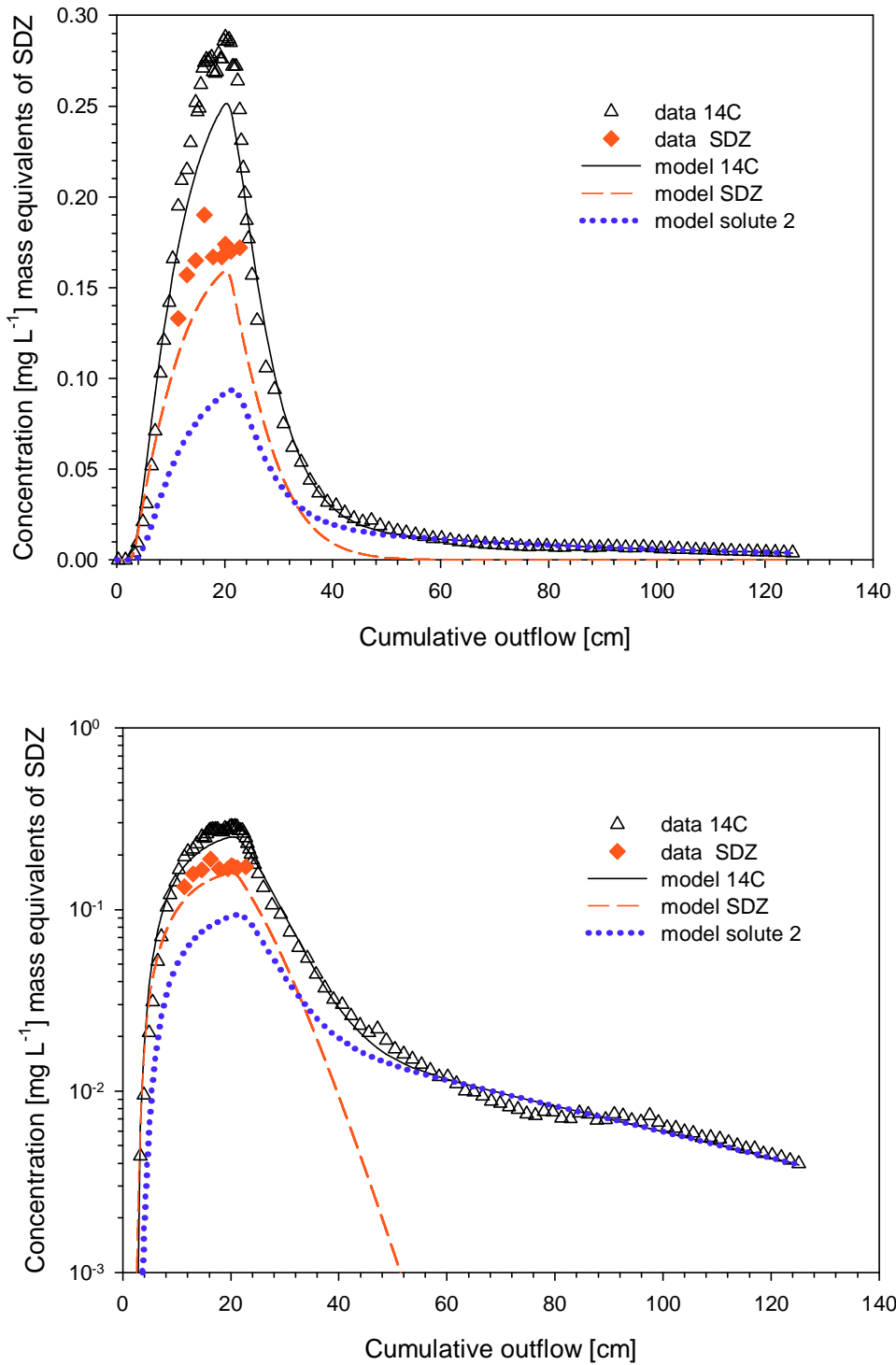


Figure 4.12: Breakthrough curves of total  $^{14}\text{C}$ , SDZ and one transformation product in column B. The symbols represent measurements and the lines (solid, dashed and dotted) model calculations. The attachment/detachment sorption model (model IV in Table 4.1) was fitted to the profile and  $\log_{10}$ -transformed BTC data. The corresponding soil concentration profiles are given in Figure 4.21.

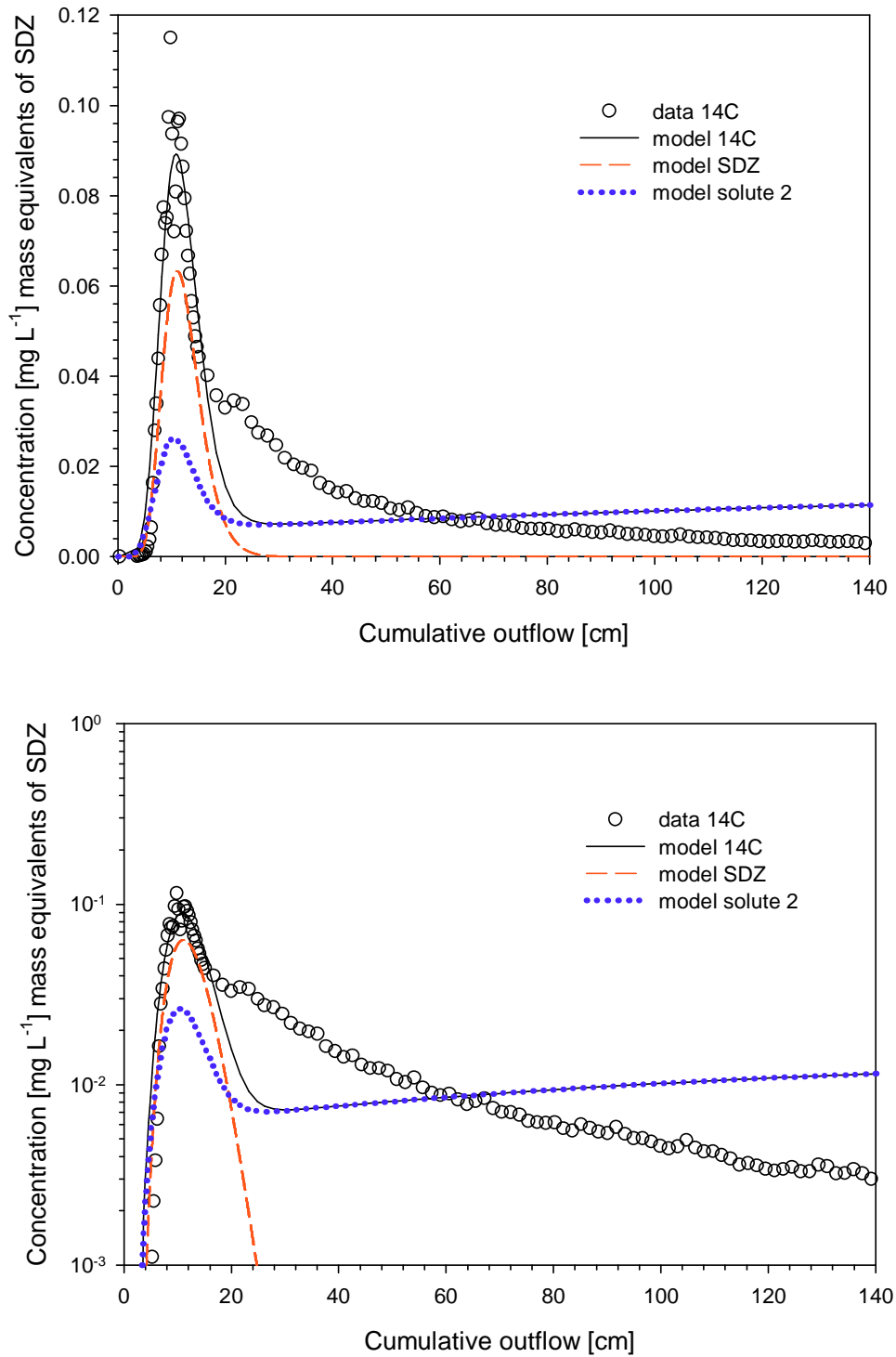


Figure 4.13: Breakthrough curves of total  $^{14}\text{C}$ , SDZ and one transformation product in column C. The symbols represent measurements and the lines (solid, dashed and dotted) model calculations. The attachment/detachment sorption model (model IV in Table 4.1) was fitted to the BTC and profile data. The corresponding soil concentration profiles are given in Figure 4.19.

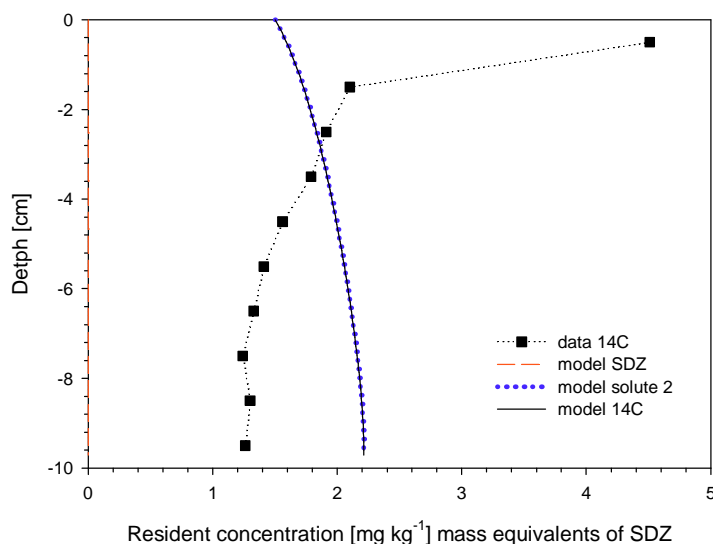


Figure 4.14: Resident soil concentration profiles of total <sup>14</sup>C, SDZ and one transformation product in column A. The symbols represent measurements and the lines (solid, dashed and dotted) model calculations. The Freundlich equilibrium sorption model (model I in Table 4.1) was fitted to the BTC data.

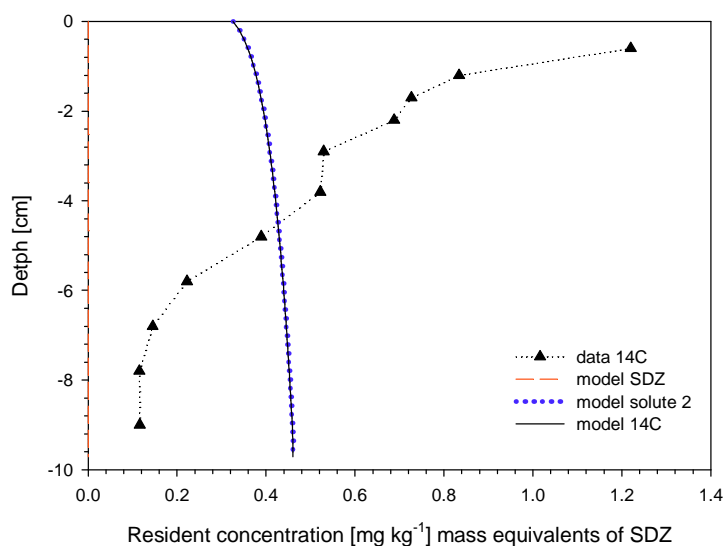


Figure 4.15: Soil resident concentration profiles of total <sup>14</sup>C, SDZ and one transformation product in column B. The symbols represent measurements and the lines (solid, dashed and dotted) model calculations. The Freundlich equilibrium sorption model (model I in Table 4.1) was fitted only to the <sup>14</sup>C BTC data.

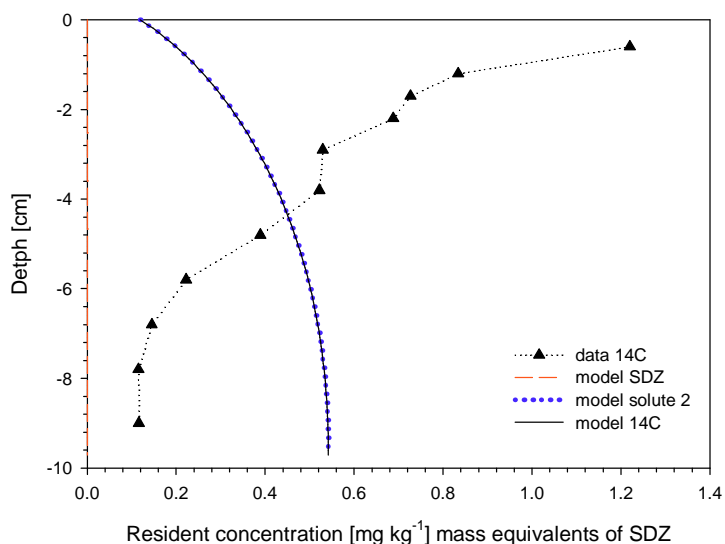


Figure 4.16: Soil resident concentration profiles of total  $^{14}\text{C}$ , SDZ and one transformation product in column B. The symbols represent measurements and the lines (solid, dashed and dotted) model calculations. The kinetic Freundlich sorption model (model II in Table 4.1) was fitted to the BTC and profile data.

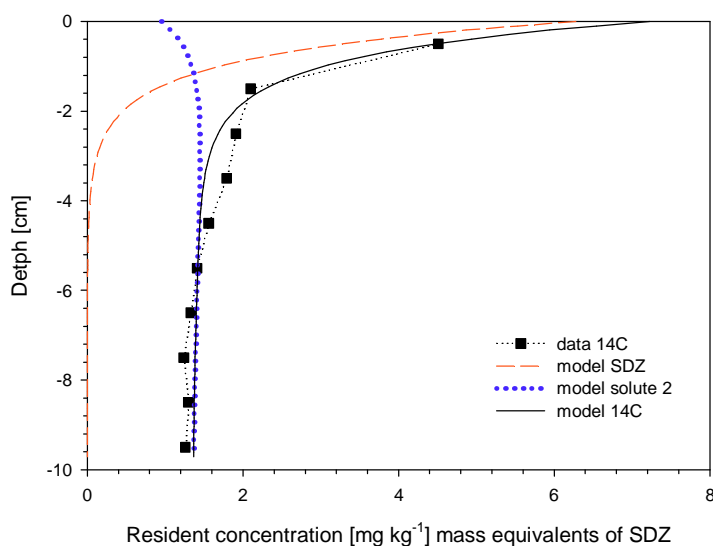


Figure 4.17: Soil resident concentration profiles of total  $^{14}\text{C}$ , SDZ and one transformation product in column A. The symbols represent measurements and the lines (solid, dashed and dotted) model calculations. The attachment/detachment sorption model (model III in Table 4.1) was fitted to the BTC and profile data.

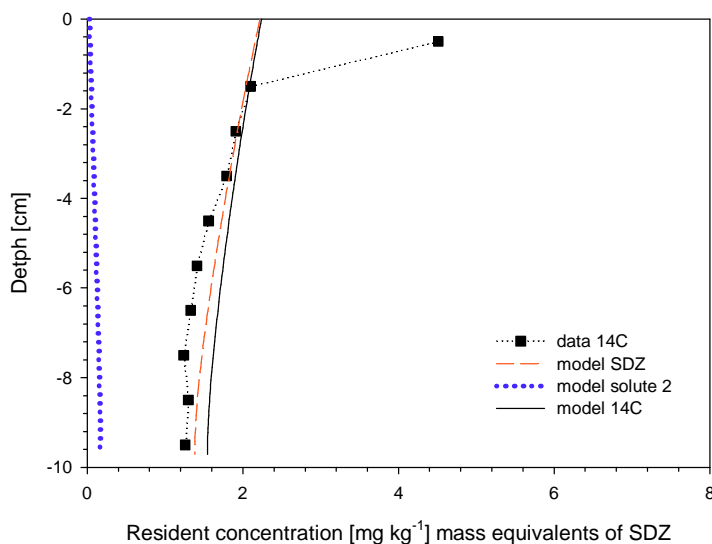


Figure 4.18: Soil resident concentration profiles of total  $^{14}\text{C}$ , SDZ and one transformation product in column A. The symbols represent measurements and the lines (solid, dashed and dotted) model calculations. The attachment/detachment sorption model (model III in Table 4.1) was fitted to the profile and  $\log_{10}$ -transformed BTC data.

The soil resident concentrations of experiment B were also best fitted with the attachment/detachment model for two solutes, if unit weight was assigned to all data points (Figure 4.20). The irreversibly sorbed fraction of the first solute accounted for the total concentration profile. If the BTC data were  $\log_{10}$ -transformed, the calculated concentration profile was not as steep as the observed data (Figure 4.21).

Even the soil concentration profile for experiment C was well described by the attachment/detachment model for two solutes (Figure 4.19). Modelled resident concentrations at the top of the column mainly consisted of the irreversibly sorbed fraction of the first solute, whereas the second solute accounted for the lower part of the soil concentration profile. The  $\log_{10}$ -transformation of the BTC data did not improve the description of the tailing and additionally failed to match of the profile (data not shown).

### Attachment/detachment-based sorption and transformation models (3 solutes)

No parametrization was found for the attachment/detachment model considering three solutes that described the experimental data better than the previous models; the description of the  $^{14}\text{C}$ -data was equally good but required additional parameters. Only a fast irreversible sorption process of the first solute can cause the experimentally determined high resident concentrations in the upper part of the soil column in experiment A in case of the above two-solute attachment/detachment model. In the



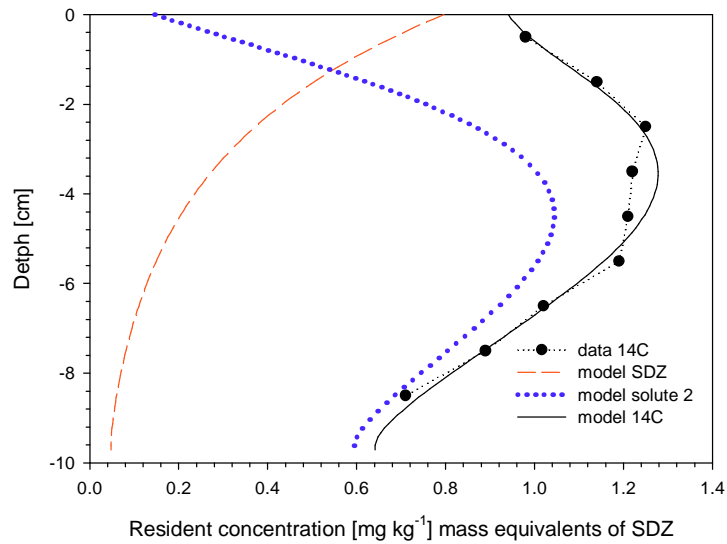


Figure 4.19: Soil resident concentration profiles of total  $^{14}\text{C}$ , SDZ and one transformation product in column C. The symbols represent measurements and the lines (solid, dashed and dotted) model calculations. The attachment/detachment sorption model (model IV in Table 4.1) was fitted to the BTC and profile data.

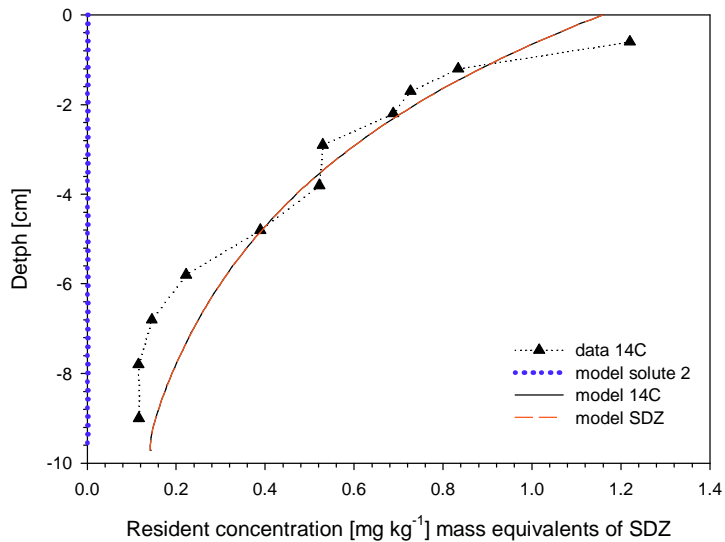


Figure 4.20: Soil resident concentration profiles Breakthrough curves of total  $^{14}\text{C}$ , SDZ and one transformation product in column B. The symbols represent measurements and the lines (solid, dashed and dotted) model calculations. The attachment/detachment sorption model (model IV in Table 4.1) was fitted to the BTC and profile data.

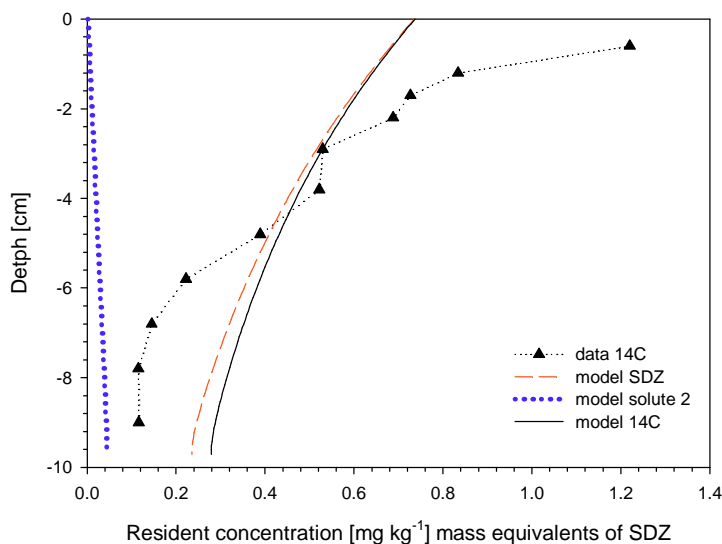


Figure 4.21: Soil resident concentration profiles of total  $^{14}\text{C}$ , SDZ and one transformation product in column B. The symbols represent measurements and the lines (solid, dashed and dotted) model calculations. The attachment/detachment sorption model (model IV in Table 4.1) was fitted to the profile and  $\log_{10}$ -transformed BTC data.

model considering three solutes, the second solute of the sequential transformation may account for the high resident concentration at the top of the soil column by fast irreversible sorption. This then allowed leaching of the first solute. However, the high resident concentrations require a very fast irreversible sorption process. Since the second solute is only a transformation product, sorption and transformation of the first solute need also to be fast. These high sorption and transformation rates reduce the leaching of the first solute. The resulting BTC concentrations of the first solute are lower than observed for SDZ.

Thus, an additional solute involved in sequential decay in the attachment/detachment concept did not explain the experimental observations. Nevertheless, it should be noted that an additional solute in the conceptual model increased the number of fitting parameters. Despite enhancing the model flexibility, this also results in high correlations between the parameters and reduces the accuracy of the estimated parameters. Additionally the analytical results hint towards independent transformation products. Thus, sequential decay, as it was considered in the presented model concept, may not be the true transformation pathway.

### Model and parameter comparison

The applied sorption and transformation models for two solutes required five to seven fitting parameters (Table 4.2). Only five parameters were involved in the equilibrium Freundlich sorption model and the attachment/detachment model ap-

plied for experiment A. In the kinetic Freundlich sorption model for the description of experiment B seven parameters were fitted. The fitted transformation rate coefficient was within the range from  $1.24 \times 10^{-2}$  to  $6.81 \times 10^{-2} \text{ h}^{-1}$  for SDZ for all models and experiments. This is equivalent to a half live time of 0.4 to 2.3 days for the parent compound. Since the sorbed concentration, which is the source for transformation, was determined by different sorption models, the comparability of the transformation rate parameters is limited.

For the equilibrium and the kinetic Freundlich sorption models, the fitted Freundlich coefficients for the first solute were smaller than for the second. The Freundlich exponents were smaller for the second solute, indicating a stronger sorption of the second solute especially in the lower concentration range. The sorption rate of the first solute in case of the kinetic sorption is within the same order of magnitude as the transformation rate and one order of magnitude higher than the sorption rate of the second solute.

The fitted parameters differed between the experiments, when the attachment/detachment concept was applied. Additionally the inverse solution was sensitive to the  $\log_{10}$ -transformation of the BTC-data. Attachment of the first solute towards the first sorption sites was generally faster than towards the irreversible sorption sites ( $\beta_{11} > \beta_{13}$ , Table 4.2) and also faster than attachment/detachment of the second solute ( $\beta_{11} > \beta_{21}$ ). Since the ratio of the attachment/detachment rate coefficients ( $\beta_{i1}/\gamma_{i1}$ ) was smaller for the first than for the second solute in experiments B and C, sorption of the second solute is stronger. The irreversible sorption coefficients of the first solute were within the same range as the transformation coefficients. Notice that transformation occurred in the sorbed phases while irreversible sorption is related to the dissolved concentrations.

Despite the limitations in the simultaneous description of the BTCs and the soil concentration profiles, the applied model concepts were able to describe some features observed in the transport experiments with SDZ. The observed soil concentration profiles were described by a model that considers two solutes which are involved in sequential transformation and exhibit different sorption characteristics. This was not possible with the lumped model approach discussed in the transport section.

## 4.4 Discussion

The  $^{14}\text{C}$ -BTCs were well described with the three-sites-irreversible sorption model (3S5R-att-irrev) considering lumped sorption characteristics for one solute. However, the HPLC-analyses hint towards considerable transformation of SDZ, which may not be neglected in the process description. The need for the complexity of the 3S5R-att-irrev model may be due to neglecting the transformation process in this conceptual model. In contrast to the lumped sorption models in the transport section (with five fitting parameters, Section 3.4.3) the attachment/detachment model considering two solutes was able to describe the observed soil concentration profiles.

The applied model concepts are restricted to two or three solutes subjected to

sequential transformation, despite the experimental evidence that three independent transformation products were found in the effluent. The transformation is not likely to be sequential, because both identified transformation products are chemically independent. Since de-acylation of the acetyl-SDZ is possible in manure, reversible transformation reactions need consideration. We were not able to validate more complex model concepts due to the lack of information on the transformation pathways, the properties of the transformation products and the concentrations in the tailing of the BTCs and in the soil columns. Since the identity of the soil residues remains unknown, the occurrence of further transformation products can not be excluded. A quickly generated and strongly sorbed solute can account for the non-eluted mass fractions and possibly explain the soil concentration profiles.

The non-equilibrium characteristics of the observed BTCs and soil concentration profiles may also be caused by a combination of chemical and physical non-equilibrium. Solute transported within the faster flow region is then eluted first in relatively high concentrations and accounts for the main breakthrough. Since the residence time of solute in the slow flow regions is longer, more time is available for sorption, resulting in a larger retardation and in lower solute concentrations in the leachate. The solute fraction transported within the slower flow regions then accounts for the tailing in the BTC and the solute mass remaining in the soil column. However, the assumption of physical non-equilibrium is not justified by the BTCs of the conservative tracer chloride (Section 3.4.1). Furthermore, this model concept would involve many parameters to describe the various non-equilibrium processes, which are difficult to determine experimentally.

## 4.5 Conclusions

We showed that the consideration of common transformation assumptions in the sorption and transport model did not allow the simultaneous description of the BTCs and resident concentration profiles of SDZ, yet either of them can be predicted. Despite the high flexibility of the applied models, other model concepts need to be developed. This is, however, only possible, after further experimental investigation of the transformation and sorption processes of SDZ in soil.

Existing analytical methods (radio-HPLC, LC-MS-MS) should be further developed to enable the quantification of all, SDZ and its transformation products, at low concentration levels in both liquid and solid samples. The latter would require an extraction method for the soil residues, which allows no transformation of the substances during the extraction procedure. More advanced experimental and analytical methods are needed to identify and quantify the sorption and transformation processes of SDZ in the soil environment. These methods should be able to experimentally differentiate between sorption and transformation processes and to independently determine the governing rate laws. Finally, reaction hypothesis for the pathways of the transformation are required to develop appropriate model concepts. The chemical identification of MB1 would be crucial to reach that goal.

# Chapter 5

## Final remarks

### 5.1 Synthesis of results

Sorption and transport of  $^{14}\text{C}$ -SDZ were investigated with batch and column experiments (Chapter 2 and 3). The results of both approaches are based on  $^{14}\text{C}$ -analysis and thus, do not differentiate between SDZ and its transformation products. To elucidate relevant processes, various model concepts were tested. Models involving similar sorption processes were necessary to describe the characteristic features of the batch and transport experiments. The non-linear sorption behavior observed in the sorption experiments was best described by the Freundlich sorption isotherm. It was included in all investigated sorption models and in some of the transport models. Non-linear sorption (Freundlich exponent  $m < 1$ ) may also be one reason for the pronounced tailing of the BTCs in the transport experiments. The rate-limited sorption accounts for the slow attainment of apparent sorption equilibrium during the batch experiments and can also contribute to the tailing of the BTCs. However, sorption sites exhibiting instantaneous equilibrium sorption were required in addition to the kinetic sorption to describe both, the one-day adsorption and the BTCs for two out of three column experiments (B and C). Only the consideration of irreversible sorption enabled the description of the very slow desorption at the various experimental time scales as well as the description of the retained mass in the columns. Three site sorption models exhibiting fast and slow equilibrium sorption as well as irreversible sorption were required for the description of the batch and transport experiments.

The various sorption experiments were best described with the 3S2Rirrev model (three sorption sites exhibiting non-linear equilibrium or rate-limited sorption or linear, first-order irreversible sorption). This model is equivalent to the 3S2R-Freuirrev model in the transport section, which was suitable to reasonably well describe the BTCs of the column experiments. The best fit parameters for the sorption experiment were used to predict the transport experiments. The results of these simulations are presented in Figure 5.1. The best fit parameters for the sorption and the transport experiments are additionally compiled in Table 5.1.

The BTC of the high concentration, long pulse transport experiment A was relatively well predicted with the parameters derived from the batch experiments. For

Table 5.1: Best fit parameters for the sorption experiments A-E and column experiments A, B, C using the 3S2Rirrev or 3S2R-Freu-irrev model, respectively.

Experiment	$\alpha_{\text{rev}}^{\dagger}$	$\alpha_{\text{irrev}}^{\ddagger}$	$g^{\S}$	$m$	$K_f$
	h <sup>-1</sup>				mg <sup>1-m</sup> L <sup>m</sup> kg <sup>-1</sup>
sorption <sup>¶</sup>	$4.0 \times 10^{-3}$	$1.3 \times 10^{-3}$	$2.0 \times 10^{-1}$	0.53	$6.4 \times 10^{+0}$
column A	$7.4 \times 10^{-2}$	$1.0 \times 10^{-2}$	$3.6 \times 10^{-3}$	0.49	$2.3 \times 10^{+0}$
column B	$2.8 \times 10^{-2}$	$2.5 \times 10^{-2}$	$2.1 \times 10^{-3}$	0.45	$6.1 \times 10^{-1}$
column C	$8.2 \times 10^{-3}$	$1.1 \times 10^{-1}$	$1.7 \times 10^{-1}$	1.06	$7.1 \times 10^{+0}$

<sup>†</sup>equals  $\alpha_2$  in notation of 3S2R-Freu-irrev; <sup>‡</sup>equals  $\beta$  in notation of 3S2R-Freu-irrev; <sup>§</sup>equals  $f$  in notation of 3S2R-Freu-irrev; <sup>¶</sup>the model was fitted to experiments A-E.

the low concentration, long pulse transport experiment B SDZ was expected to arrive much later in the outflow than it was observed. The simulated peak concentrations were also lower, however the concentrations in the tailing were overestimated. The first appearance of SDZ in the outflow was well predicted in the high concentration, short pulse experiment C. However, the observed and simulated peak concentrations differed by approximately one order of magnitude. The concentrations in the modelled BTC decreased rapidly and were lower than the observed concentrations in the tailing towards the end of the experiment. The leached mass fraction was overestimated for the short pulse transport experiment. None of the predicted soil concentration profiles matched the observations (Figure 5.1). This could have been expected since the 3S2R-Freu-irrev model was not able to describe the observed soil concentration profiles in the inverse simulation mode (Section 3).

The BTCs of the transport experiments were best described with the 3S5R-att-irrev model (three sorption sites exhibiting fast or slow reversible linear sorption or linear irreversible sorption). This model concept can not describe non-linear sorption isotherms and was thus, not suitable for the description of the batch experiments. Furthermore, the attachment/detachment model and its fitting parameters are not readily applicable to data observed under varying experimental conditions since the model rate parameters depend on the soil-water ratio.

Transformation of SDZ was discussed as a possible explanation for the limitations in process description of the lumped model approaches. Common first-order transformation assumptions were coupled to various sorption concepts to overcome the shortages in the description of the transport experiments (Section 4). Despite their high flexibility, these model approaches could not simultaneously describe the BTCs of SDZ and total <sup>14</sup>C-radioactivity and the resident concentration profiles. However, these models were able to describe the BTCs or the soil concentrations separately.

The chemical analysis of selected samples showed that transformation of SDZ into three transformation processes occurs (Appendix G) in soil-water systems. Two transformation products were identified as acetyl-SDZ and hydroxy-SDZ, the third

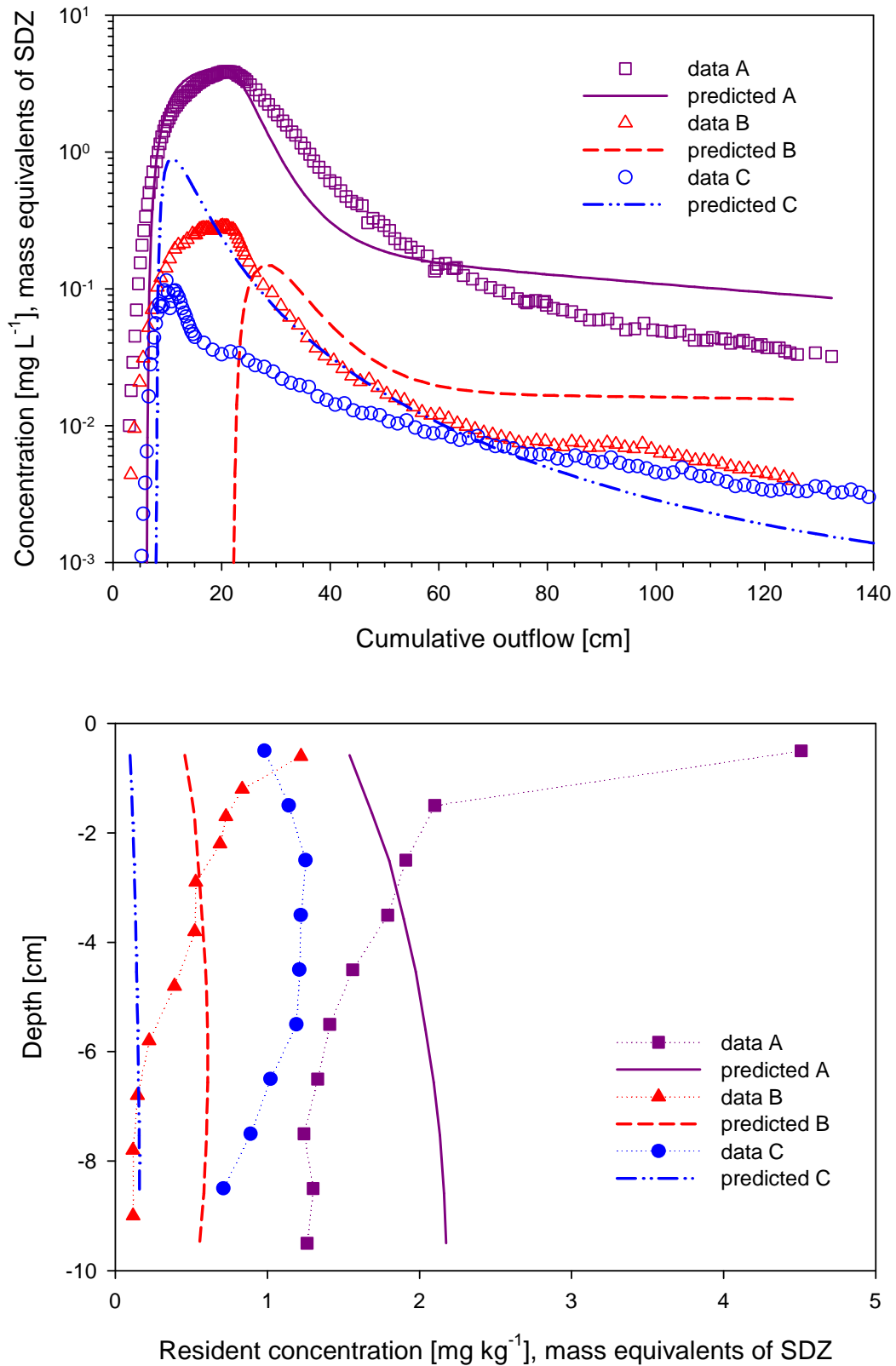


Figure 5.1: Measured and predicted BTCs and soil concentration profiles. The applied model was the 3S2Rirrev with the sorption parameters gained from fitting the model to the sorption experiments A, B, C, D and E.

transformation product is still unidentified and shows a higher polarity compared to the other species and SDZ. Little is known about the transformation pathways. Our experiments hint towards partially abiotic and surface-dependent processes. The formation of transformation products tends to increase with time and decreasing concentration level. Since sorption and transformation processes occurred only simultaneously, the investigation and quantification of the underlying processes is additionally impeded.

## 5.2 General conclusions

The fate of  $^{14}\text{C}$ -labelled SDZ in soil depends on various interconnected processes. Sorption and transformation of SDZ occurred simultaneously. Both processes seemed to be time- and concentration-dependent. The sorption affinity of  $^{14}\text{C}$ -SDZ was lower in annealed soil and was therefore assumed to be enhanced by soil organic matter. The experimental results hint towards abiotic and surface-dependent transformation processes. Although two of the transformation products were identified, the transformation pathways and the fate and effects of the transformation products in the soil environment remained unknown. Therefore, the lumped behavior of SDZ and its transformation products was investigated using  $^{14}\text{C}$ -labelled SDZ and various model approaches.

$^{14}\text{C}$ -SDZ showed non-linear sorption with slow kinetics. An apparent sorption equilibrium was reached after approximately 20 days in continuously shaken batch systems. Desorption appeared to be much slower. The strong binding of  $^{14}\text{C}$ -SDZ in soil was not only observed during the long-term desorption experiment (270 days), but also the extractability of aged soil residues decreased rapidly (within 20 days) to about 20 % (microwave extraction with organic solvents). Despite the non-linear sorption isotherms observed in the batch experiments,  $^{14}\text{C}$ -SDZ arrived nearly simultaneously in the leachate independent of the applied concentration. Compared to a conservative tracer, the  $^{14}\text{C}$ -SDZ peak maximum of all BTCs was only slightly retarded during the transport through the soil columns near saturation. However, unlike the conservative tracer all BTCs were characterized by an extended tailing. Between 15 and 82 % of the applied  $^{14}\text{C}$ -SDZ remained in the soil column after leaching with approximately 20 pore volumes, depending on the application mode.

Various experimental conditions (duration, concentration, application mode) were necessary to elucidate the characteristic and complex behavior of SDZ during both, batch and column experiments. Commonly conducted short-term adsorption experiments would have underestimated the overall sorption affinity and the slow kinetics of the sorption processes. One column experiment was also insufficient to find an appropriate model concept for the transport of  $^{14}\text{C}$ -SDZ. However, despite the high complexity of the proposed three site, variable rate reversible and irreversible sorption models, they were not flexible enough to describe all experimental observations simultaneously. Also the consideration of common sequential transformation assumptions in combination with multiple compartment sorption could not describe all experimental data with one set of parameters.



The application of  $^{14}\text{C}$ -labelled SDZ and the respective analytical methods enabled to track the total applied mass during the course of the experiments. The determination of the mineralization, the non-desorbable residues in soil as well as the soil resident concentrations in the soil columns and the low concentrations in the soil solution would not have been possible without the applied  $^{14}\text{C}$ -tracer technique. However trace analytical methods would have been desirable for the quantification of the transformation products in the lower concentration ranges of water samples as well as for their determination in soil samples.

The overall conclusion of the presented thesis is that we do not yet fully understand the fate of SDZ in the soil environment. This demonstrates the need for further research, since we employed relatively simple experimental systems under constant boundary conditions on the one hand side but applied very sophisticated model approaches on the other hand side. The fate of SDZ is expected to depend on additional environmental conditions in the field, such as temperature, water content, pH-value and the presence of manure as the typical matrix in which veterinary pharmaceuticals reach the environment. Thus, further research is required to determine the relevant sorption and transformation processes for a successful environmental risk assessment.

### 5.3 Outlook

The characterization of the sorption behavior of SDZ requires further knowledge of the transformation processes. The identification of the transformation products, the reaction pathways and the corresponding reaction rates is crucial for the characterization of the transformation. As a prerequisite for further experiments, improved analytical methods are required for the quantification of SDZ and its transformation products in soil and water. Based on the experimental results, more complex model concepts may be developed and validated, regarding the interaction of sorption and transformation processes and the relevant environmental conditions.



# Bibliography

- Addiscott, T., J. Smith, and N. Bradbury, Critical evaluation of models and their parameters, *Journal of Environmental Quality*, *24*, 803–807, 1995.
- Ahmad, R., R. Kookana, A. Alston, and J. Skjemstad, The nature of soil organic matter affects sorption of pesticides. 1. Relationships with carbon chemistry as determined by  $^{13}\text{C}$  CPMAS NMR spectroscopy, *Environmental Science and Technology*, *35*, 878, 2001.
- Altfelder, S., T. Streck, and J. Richter, Nonsingular sorption of organic compounds in soil: the role of slow kinetics, *Journal of Environmental Quality*, *29*, 917–925, 2000.
- Altfelder, S., T. Streck, M. Maraqua, and T. Voice, Nonequilibrium sorption of dimethylphthalat - compatibility of batch and column techniques, *Soil Science Society America Journal*, *65*, 102–111, 2001.
- Baek, D.-S., S.-B. Kim, and D.-J. Kim, Irreversible sorption of benzene in sandy aquifer materials, *Hydrological Processes*, *17*, 1239–1251, 2003.
- Berger, K., B. Petersen, and H. B. Pfaue, Persistenz von Gülle-Arzneistoffen in der Nahrungskette, *Archiv für Lebensmittelchemie*, *37*, 99–102, 1986.
- Boxall, A. B. A., P. Blackwell, R. Cavallo, P. Kay, and J. Tolls, The sorption and transport of a sulfonamide antibiotic in soil systems, *Toxicology Letters*, *131*, 19–28, 2002.
- Boxall, A. B. A., L. A. Fogg, P. A. Blackwell, P. Kay, E. J. Pemberton, and A. Croxford, Veterinary medicines in the environment, *Reviews of Environmental Contamination and Toxicology*, *180*, 1–91, 2004.
- Bradford, S. A., S. Yates, M. Betthar, and J. Simunek, Physical factors affecting the transport and fate of colloids in saturated porous media, *Water Resources Research*, *38*, doi:10.1029/2002WR001340, 2002.
- Bradford, S. A., J. Simunek, M. Betthar, M. T. van Genuchten, and S. Yates, Modeling colloid attachment, straining, and exclusion in saturated porous media, *Environmental Science and Technology*, *37*, 2242–2250, 2003.

- Brumhard, B., Lysimeterversuche zum Langzeitverhalten der Herbizide Metamitron (GOLTIX<sup>R</sup>) und Methabenzthiazuron (TRIBUNIL<sup>R</sup>) in einer Parabraunerde mit besonderer Berücksichtigung der Transport- und Verlagerungsprozesse unter Einbeziehung von Detailuntersuchungen, *Dissertation an der Universität Bonn*, 1991.
- Brusseau, M. L., Nonequilibrium sorption of organic chemicals: Elucidation of rate-limiting processes, *Environmental Science and Technology*, *25*, 134–142, 1991.
- Brusseau, M. L., R. Jessrup, and P. Rao, Modelling transport of solutes influenced by multiprocess nonequilibrium, *Water Resources Research*, *25*, 1971–1988, 1989.
- Burkhardt, M., C. Stamm, C. Waul, H. Singer, and S. Müller, Surface runoff and transport of sulfonamide antibiotics and tracers on manured grassland, *Journal of Environmental Quality*, *34*, 1363–1371, 2005.
- Cameron, C. R., and A. Klute, Convective-dispersive solute transport with a combined equilibrium and kinetic adsorption model, *Water Resources Research*, *13*, 183–188, 1977.
- Casey, F. X. M., and J. Šimunek, Inverse analysis of transport of chlorinated hydrocarbons subject to sequential transformation reactions, *Journal of Environmental Quality*, *30*, 1354–1360, 2001.
- Casey, F. X. M., G. Larsen, H. Hakk, and J. Simunek, Fate and transport of 17 $\beta$ -estradiol in soil-water systems, *Environmental Science and Technology*, *37*, 790–798, 2003.
- Casey, F. X. M., H. Hakk, J. Simunek, and G. Larsen, Fate and transport of testosterone in agricultural soils, *Environmental Science and Technology*, *38*, 2400–2409, 2004.
- Casey, F. X. M., J. Simunek, J. Lee, G. E. Larsen, and H. Hakk, Sorption, mobility, and transformation of estrogenic hormones in natural soil, *Journal of Environmental Quality*, *34*, 1372–1379, 2005.
- Christian, T., R. J. Schneider, H. A. Färber, D. Skutlarek, M. T. Meyer, and H. E. Goldbach, Determination of antibiotic residues in manure, soil and surface waters, *Acta hydrochimica et hydrobiologica*, *31*, 36–44, 2003.
- Deutsche-Arzneibuch-Kommission, *Deutsches Arzneibuch*, Deutscher Apotheker Verlag, Stuttgart, 2002.
- Drillia, P., K. Stamatelatos, and G. Lyberatos, Fate and mobility of pharmaceuticals in solid matrices, *Chemosphere*, *60*, 1034–1044, 2005.
- EMA, Guideline on environmental impact assessment (EIAS) for veterinary medicinal products - Phase I, *CVMP/VICH/592/98-Final*, London, 2000.

- Fortin, J., M. Flury, W. Jury, and T. Streck, Rate-limited sorption of simazine in saturated soil columns, *Journal of Contaminant Hydrology*, 25, 219–234, 1997.
- Gamerdinger, A., A. Lemley, and R. J. Wagenet, Non-equilibrium sorption and degradation of three 2-chloro-s-triazine herbicides in soil-water systems, *Journal of Environmental Quality*, 1991.
- Gamst, J., T. Olesen, H. D. Jonge, P. Moldrup, and D. E. Rolston, Nonsingularity of naphthalene sorption in soil: Observations and the two-compartment model, *Soil Science Society of America Journal*, 65, 1662–1633, 2001.
- Gamst, J., P. Moldrup, D. E. Rolston, T. Olesen, K. M. Scow, and T. Komatsu, Comparison of naphthalen diffusion and nonequilibrium adsorption-desorption experiments, *Soil Science Society of America Journal*, 67, 765–777, 2003.
- Gamst, J., P. Moldrup, D. E. Rolston, K. M. Scow, K. Henriksen, and T. Komatsu, Time-dependency of naphthalene sorption in soil: simple rate-, diffusion-, and isotherm-parameter-based models, *Soil Science*, 169, 2004.
- Gao, J., and J. A. Pedersen, Adsorption of sulfonamide antimicrobial agents to clay minerals, *Environmental Science and Technology*, 39, 9509–9516, 2005.
- Grote, M., A. Vockel, D. Schwarze, A. Mehlich, and M. Freitag, Fate of antibiotics in food chain and environment originating from pigfattening, *Fresenius Environmental Bulletin*, 13, 1214–1216, 2004.
- Guo, L., and R. J. Wagenet, Evaluation ofalachlor degradation under transport conditions, *Soil Science Society of America Journal*, 63, 443–449, 1999.
- Guo, L., R. J. Wagenet, and W. A. Jury, Adsorption effects on kinetics of aldicarb degradation: Equilibrium model and application to incubation and transport experiments, *Soil Science Society of America Journal*, 63, 1637–1644, 1999.
- Guo, L., W. A. Jury, R. J. Wagenet, and M. Flury, Dependence of pesticide degradation on sorption: nonequilibrium model and application to soil reactors, *Journal of Contaminant Hydrology*, 43, 45–62, 2000.
- Haller, M. Y., S. R. Müller, C. McArdell, A. C. Alder, and M. J.-F. Suter, Quantification of veterinary antibiotics (sulfonamides and trimethoprim) in animal manure by liquid chromatography - mass spectrometry, *Journal of Chromatography A*, 952, 111–120, 2002.
- Hamscher, G., H. T. Pawelzick, H. Höper, and H. Nau, Different behaviour of tetracyclines and sulfonamides in sandy soils after repeated fertilization with liquid manure, *Environmental Toxicology and Chemistry*, 24, 861–868, 2005.
- Hartmann, N., An extraction method to determine sulfonamide antibiotics in soil, *Diploma Thesis at the Department of Environmental Sciences ETH Zürich, done at EAWAG in Dübendorf*, 2003.

- Hillel, D., *Environmental Soil Physics*, Academic Press, San Diego, 1998.
- Hinz, C., Description of sorption data with isotherm equations, *Geoderma*, *99*, 225–243, 2001.
- Höper, H., J. Kues, H. Nau, and G. Hamscher, Eintrag und Verbleib von Tierarzneimittelwirkstoffen in Böden, *Bodenschutz*, *4*, 141–148, 2002.
- Jørgensen, S. E., and B. Halling-Sørensen, Drugs in the environment, *Chemosphere*, *40*, 691–699, 2000.
- Kahle, M., H. Singer, and C. Stamm, Sorption von Sulfathiazol an organische Substanz und Eisenoxide, *DBG*, p. personal communication, 2005.
- Kan, A. T., G. Fu, and M. B. Tomson, Adsorption/desorption hysteresis in organic pollutant and soil/sediment interaction, *Environmental Science and Technology*, *28*, 859–887, 1994.
- Kan, A. T., G. Fu, M. Hunter, and M. B. Tomson, Irreversible adsorption of naphthalen and tetrachlorobiphenyl to lua and surrogate sediments, *Environmental Science and Technology*, *31*, 2176–2185, 1997.
- Kan, A. T., G. Fu, M. A. Hunter, W. Chen, C. H. Ward, and M. B. Tomson, Irreversible sorption of neutral hydrocarbons in sediments: Experimental observations and model predictions, *Environmental Science and Technology*, *32*, 892–902, 1998.
- Kay, P., P. A. Blackwell, and A. B. Boxall, Fate of veterinary antibiotics in a macroporous tile drained clay soil, *Environmental Toxicology and Chemistry*, *23*, 1136–1144, 2004.
- Kay, P., P. A. Blackwell, and A. B. Boxall, Transport of veterinary antibiotics in overland flow following the application of slurry to arable land, *Chemosphere*, *59*, 951–959, 2005a.
- Kay, P., P. A. Blackwell, and A. B. Boxall, Column studies to investigate the fate of veterinary antibiotics in clay soils following slurry application to agricultural land, *Chemosphere*, *60*, 497–507, 2005b.
- Kleineidam, S., H. Rüniger, and P. Grathwohl, Desorption kinetics of phenanthrene in aquifer material lacks hysteresis, *Environmental Science and Technology*, *38*, 4169–4175, 2004.
- Kookana, R. S., L. A. G. Aylmoore, and R. G. Gerritse, Time dependent sorption of pesticides during transport in soils, *Soil Science*, *154*, 214–225, 1992.
- Kreuzig, R., and S. Höltge, Investigations on the fate of sulfadiazine in manured soil: Laboratory experiments and test plot studies, *Environmental Toxicology and Chemistry*, *24*, 771–776, 2005.

- Kreuzig, R., C. Kullmer, B. Matthies, S. Höltge, and H. Diekmann, Fate and behavior of pharmaceutical residues in soils, *Fresenius Environmental Bulletin*, *12*, 550–558, 2003.
- Kroker, R., Aspects of the elimination of antibiotics after treatment of domestic animals, *Wissenschaft und Umwelt*, *4*, 305–308, 1983.
- Kubiak, R., H. Ellbel, M. Lambert, and K. Eichhorn, Degradation of isoproturon in soil in relation to changes of microbial biomass and activity in small-scale laboratory and outdoor studies., *International Journal of Analytical Chemistry*, *58*, 123–132, 1995.
- Langhammer, J.-P., and H. Büning-Pfaue, Bewertung von Arzneistoffen aus der Gülle im Boden, *Lebensmittelchem. Gerichtl. Chemie*, *43*, 108, 1989.
- Larsen, T., T. H. Christensen, and M. Brusseau, Predicting nonequilibrium transport of naphthalene through aquifer materials using batch determined sorption parameters, *Chemosphere*, *24*, 141–153, 1992.
- Luthy, R. G., et al., Sequestration of hydrophobic organic contaminants by geosorbents, *Environmental Science and Technology*, *31*, 3341–3347, 1997.
- Ma, L., and H. M. Selim, Predicting the transport of atrazine in soils: Second-order and multireaction approaches, *Water Resources Research*, *30*, 3489–3498, 1994a.
- Ma, L., and H. M. Selim, Predicting atrazine adsorption-desorption in soils: A modified second-order kinetic model, *Water Resources Research*, *30*, 447–456, 1994b.
- Ma, L., and H. M. Selim, Evaluation of nonequilibrium models for predicting atrazine transport in soils, *Soil Science of America Journal*, *61*, 1299–1307, 1997.
- Ma, L., L. M. Southwick, G. H. Willis, and H. M. Selim, Hysteretic characteristics of Atrazine adsorption-desorption by a Sharkey soil, *Weed Science*, *41*, 627–633, 1993.
- Maraqa, M. A., X. Zhao, R. Wallace, and T. C. Voice, Retardation coefficients of nonionic organic compounds determined by batch and column techniques, *Soil Science Society of America Journal*, *62*, 142–152, 1998.
- Northcott, G. L., and K. C. Jones, Experimental approaches and analytical techniques for determining organic compound bound residues in soil and sediment, *Environmental Pollution*, *108*, 19–43, 2000.
- OECD, Guidline for testing chemicals: adsorption/desorption, *OECD guideline*, *106*, 1981.

- Pfeifer, T., J. Tuerk, K. Bester, and M. Spiteller, Determination of selected sulfonamide antibiotics and trimethoprim in manure by electrospray and atmospheric pressure ionization tandem mass spectrometry, *Rapid Communication in Mass Spectrometry*, *16*, 663–669, 2002.
- Pignatello, J. J., and B. Xing, Mechanisms of slow sorption of organic chemicals to natural particles, *Environmental Science and Technology*, *30*, 1–11, 1996.
- Prata, F., A. Lavorenti, J. Vanderborght, P. Burauel, and H. Vereecken, Miscible displacement, sorption and desorption of atrazine in a Brazilian Oxisol, *Vadose Zone Journal*, *2*, 728–738, 2003.
- Sabbah, I., W. P. Ball, D. F. Young, and E. J. Bouwer, Misinterpretations in the modeling of contaminant desorption from environmental solids when equilibrium conditions are not fully understood, *Environmental Engineering Science*, *22*, 350–366, 2005.
- Sander, M., and J. J. Pignatello, Characterization of charcoal adsorption sites for aromatic compounds: Insights drawn from single-solute and bi-solute competitive experiments, *Environmental Science and Technology*, *39*, 619–629, 2005a.
- Sander, M., and J. J. Pignatello, An isotope exchange technique to assess mechanisms of sorption hysteresis applied to naphthalen in kerogenous organic matter, *Environmental Science and Technology*, *39*, 7476–7484, 2005b.
- Schijven, J. F., and S. M. Hassanizadeh, Removal of viruses by soil passage: overview of modeling, processes, and parameters, *Critical Review in Environmental Science and Technology*, *30*, 49–127, 2000.
- Schijven, J. F., and J. Šimunek, Kinetic modeling of virus transport at the field scale, *Journal of Contaminant Hydrology*, *55*, 113–135, 2002.
- Schijven, J. F., S. M. Hassanizadeh, and H. de Bruin, Two-site kinetic modeling of bacteriophages transport through columns of saturated dune sand, *Journal of Contaminant Hydrology*, *57*, 259–279, 2002.
- Schwarzenbach, R. P., P. M. Gschwend, and D. M. Imboden, *Environmental organic chemistry*, 2nd ed., New York, NY: Wiley-Interscience, 2003.
- Šimunek, J., M. Šejna, and M. T. van Genuchten, *The HYDRUS-1D software package for simulating the one-dimensional movement of water, heat, and multiple solutes in variably saturated media. Version 2.0*, ICGWMC-TPS-70. International Ground Water Modeling Center, Colorado School of Mines, Golden, Colorado, 1998, pp. 202.
- Šimunek, J., M. T. van Genuchten, and M. Šejna, *The HYDRUS-1D software package for simulating the one-dimensional movement of water, heat, and multiple*



- solutes in variably-saturated media. Version 3.0*, HYDRUS Software Series 1, Department of Environmental Sciences, University of California Riverside, Riverside, California, USA, 2005, pp. 270.
- Streck, T., and H. Piehler, On field-scale dispersion of strongly sorbing solutes in soils, *Water Resources Research*, *34*, 2769–2773, 1998.
- Streck, T., and J. Richter, Field-scale study of chlortoluron movement in a sandy soil over winter: Ii. modeling, *Journal of Environmental Quality*, *28*, 1824–1831, 1999.
- Streck, T., N. N. Poletika, W. A. Jury, and W. W. Farmer, Description of simazine transport with rate-limited, two-stage, linear and nonlinear sorption, *Water Resources Research*, *31*, 811–822, 1995.
- Thiele, S., Adsorption of the antibiotic pharmaceutical compound sulfapyridine by a long-term differently fertilized loess chernozem, *Journal of Plant Nutrition and Soil Science*, *163*, 589–594, 2000.
- Thiele-Bruhn, S., Pharmaceutical antibiotic compounds in soil - A review, *Journal of Plant Nutrition and Soil Science*, *166*, 145–167, 2003.
- Thiele-Bruhn, S., Microbial inhibition by pharmaceutical antibiotics in different soils - dose-response relations determined with the iron(iii)reduction test, *Environmental Toxicology and Chemistry*, *24*, 869–876, 2005.
- Thiele-Bruhn, S., and M.-O. Aust, Effects of pig slurry on the sorption of sulfonamide antibiotics in soil, *Archives of Environmental Contamination and Toxicology*, *47*, 31–39, 2003.
- Thiele-Bruhn, S., T. Seibicke, H. Schulten, and P. Leinweber, Sorption of sulfonamide pharmaceutical antibiotics on whole soils and particle-size fractions, *Journal of Environmental Quality*, *33*, 1331–1342, 2004.
- Tolls, J., Sorption of veterinary pharmaceuticals in soils: A review, *Environmental Science and Technology*, *35*, 3397–3406, 2001.
- Toride, N., F. J. Leij, and M. T. van Genuchten, *The CXTFIT code for estimating transport parameters from laboratory or field tracer experiments. Version 2.1*, US Salinity Laboratory, Agricultural Research Service US Department of Agriculture, Riverside, California, Research Report No. 137, 1999.
- van der Zee, E. A. T. M., Reaction kinetics and transport in soil: compatibility and differences between some simple models, *Transport in Porous Media*, *6*, 703–737, 1991.
- van Genuchten, M. T., and R. J. Wagenet, Two-site/two-region models for pesticide transport and degradation: Theoretical development and analytical solutions, *Soil Science Society of America Journal*, *53*, 1303–1310, 1989.

- van Genuchten, M. T., and P. J. Wierenga, Mass transfer studies in sorbing porous media: I. Analytical solutions., *Soil Science Society of America Journal*, *40*, 473–481, 1976.
- Vereecken, H., U. Jaeckel, and A. Georgescu, Assymptotic analysis of solute transport with linear nonequilibrium sorption in porous media, *Transport in Porous Media*, *36*, 189–210, 1999.
- Zhao, D., J. J. Pignatello, J. C. White, W. Braida, and F. Ferrandino, Dual-mode modeling of competitive and concentration-dependent sorption and desorption kinetics of polycyclic aromatic hydrocarbons in soils, *Water Resources Research*, *37*, 2205–2212, 2001.

# Appendix A

## Properties of sulfadiazine

All experiments were done with the antibiotic substance sulfadiazine (SDZ), having the physicochemical properties presented in Table A.1. The molecular structure is given in Figure A.1.  $^{14}\text{C}$ -labelled SDZ with a specific radioactivity of  $3.46 \text{ MBq mg}^{-1}$  was used, with the  $^{14}\text{C}$ -label in the phenyl-ring. All, from single to sixfold labelled SDZ might be included in the substance provided by the Institute of Isotopes Co., Ltd., Budapest, Hungary. However the sixfold-labelled species is most likely, as it was the goal of the synthesis.

Table A.1: Selected physicochemical properties of sulfadiazine according to the supplier of the non-labelled SDZ, Sigma Aldrich, Taufkirchen, Germany.

molecular formula		$\text{C}_{10}\text{H}_{10}\text{N}_4\text{O}_2\text{S}$
CAS <sup>‡</sup>		68 - 35 - 9
molecular mass	[g mol <sup>-1</sup> ]	250.28
pK <sub>a1</sub> and pK <sub>a2</sub> <sup>§</sup>		1.57 and 6.50
melting point	[°C]	250
vapor pressure	[Pa]	$5.745 \times 10^{-6}$
Henry constant	[atm m <sup>3</sup> mol <sup>-1</sup> ]	$1.58 \times 10^{-10}$
solubility in water	[mg L <sup>-1</sup> ]	13 to 77
octanol/water distribution coefficient		0.76

<sup>‡</sup>Registration number of the Chemical Abstract Service; <sup>§</sup>Acidity constants.

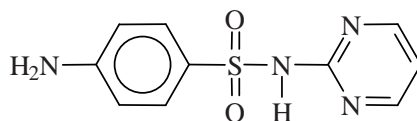


Figure A.1: Chemical structure of sulfadiazine (SDZ).

# Appendix B

## Soil properties

The sampling site was located close to lake Greifensee near Zürich, Switzerland. The soil material was collected from the upper 30 cm of an Eutric Cambisol which was used as grassland in the past. The samples were taken in October 2002 and stored field moist in plastic bags at 4 °C in the dark until further use. The soil is a silty loam and characterized as described in Table B.1. It was investigated by standard procedures at the laboratory of the LUFA (*Landwirtschaftliche Untersuchungs- und Forschungsanstalt*) in Speyer, Germany. The clay analyses were done at the Institute of Soil Science and Soil Ecology at the University of Bonn, Germany.

Table B.1: Selected physical and chemical properties of the soil material.

Parameter	Unit	Value
Texture:		
Clay (<0.002 mm)	[% weight] <sup>†</sup>	23
Fine silt (0.002 – 0.006 mm)	[% weight] <sup>†</sup>	7
Medium silt (0.006 – 0.020 mm)	[% weight] <sup>†</sup>	14
Coarse silt (0.020 – 0.063 mm)	[% weight] <sup>†</sup>	22
Fine sand (0.063 – 0.200 mm)	[% weight] <sup>†</sup>	19
Medium sand (0.200 – 0.630 mm)	[% weight] <sup>†</sup>	11
Coarse sand (0.630 – 2.000 mm)	[% weight] <sup>†</sup>	4
Clay minerals:		
Smectite	[%]	25
Illite	[%]	25
Chlorite	[%]	50
Specific surface area	[m <sup>2</sup> g <sup>-1</sup> ]	4.96
Chemical analysis:		
pH		6.1
P <sub>tot</sub> <sup>‡</sup>	[mg kg <sup>-1</sup> ]	1292
CEC <sup>§</sup>	[meq 100 g <sup>-1</sup> ]	17.4
C <sub>org</sub> <sup>¶</sup>	[% weight] <sup>‡‡</sup>	3.3
N <sub>tot</sub> <sup>‡</sup>	[% weight] <sup>‡‡</sup>	0.38
CaCO <sub>3</sub> <sup>‡‡</sup>	[% weight] <sup>‡‡</sup>	<3

Soil was air dried and sieved to 2 mm prior to analysis. <sup>†</sup>The weight fractions are based on the mass of the mineral phase. <sup>‡</sup>Total content of phosphorous, <sup>§</sup>cation exchange capacity, <sup>¶</sup>content of organic carbon, <sup>‡</sup>content of nitrogen, <sup>‡‡</sup>content of carbonate. <sup>‡‡</sup>The weight fractions are based on the total mass of soil.

## Appendix C

### Analysis of $^{14}\text{C}$ in liquid samples

The concentration of SDZ in liquid samples ( $C$  [ $\text{M L}^{-3}$ ]) was determined by measuring its  $^{14}\text{C}$ -radioactivity. Therefore an aliquot of the sample was mixed with 10 mL of an appropriate scintillation cocktail and measured by liquid scintillation counting (LSC). The detection limit of the LSC-method was at 0.25 Bq per sample. The measured volume ( $V(\text{meas})$  [ $\text{L}^3$ ]) was chosen according to the expected specific radioactivity of the sample, varying from 0.1 to 5 mL for high and low specific radioactivities, respectively. Each sample was measured in triplicate and corrected for the background radiation. The corresponding specific radioactivity ( $A_{\text{spec}}$  [ $\text{T}^{-1} \text{L}^{-3}$ ]) was calculated from the measured radioactivity ( $A$  [ $\text{T}^{-1}$ ]). The equivalent SDZ concentration of the sample was determined after division by the specific radioactivity of the applied SDZ ( $A_{\text{spec}}(\text{SDZ})$  [ $\text{T}^{-1} \text{M}^{-1}$ ]), assuming that  $^{14}\text{C}$ -radioactivity is linearly related to SDZ. If any transformation products were present, the resulting total SDZ concentrations were the sum of both, parent and transformation products, given in mass equivalents of SDZ (molecular weight=250.28  $\text{g mol}^{-1}$ ).

## Appendix D

### Analysis of $^{14}\text{C}$ in soil samples

The SDZ concentration in soil was determined by measuring the  $^{14}\text{C}$ -radioactivity after total combustion of the soil samples with the help of a biological oxidizer. Three replicates of 0.500 g of each soil sample were combusted at 900 °C. The evolving gas was washed into a scintillation cocktail. Here,  $^{14}\text{CO}_2$  was trapped and subsequently measured by LSC. The  $^{14}\text{C}$ -analysis in both, the solid and liquid phases, was insensitive to matrix effects and did not require any extraction steps prior to the trace analysis in soil.

The performance of the method was checked in each measuring series. Blanks were run before and after the samples to check for background contamination and cross contamination during the measurement. The recovery of the method is defined as the ratio of measured radioactivities in a blank sample spiked with a known amount of  $^{14}\text{C}$  prior to combustion to the radioactivity in a blank sample where  $^{14}\text{C}$  was spiked to the scintillation cocktail after combustion of an uncontaminated sample. Measurement series with a recovery < 92 % were repeated.

The total concentration of SDZ in the soil [ $\text{M}(\text{SDZ}) \text{M}^{-1}(\text{soil})$ ] is calculated from the mass of the soil, the specific radioactivity of the applied SDZ ( $A_{\text{spec}}(\text{SDZ})[\text{T}^{-1} \text{M}^{-1}]$ ), and the measured radioactivity corrected for the corresponding recovery. As discussed for the liquid phase concentrations above, SDZ concentrations in the solid phase refer to the sum of both, the parent compound and its transformation products, given in mass equivalents of SDZ. Note that the soil concentration is the sum of the sorbed and dissolved solute per unit mass of soil.

# Appendix E

## Detection and determination of transformation products of SDZ

### E.1 Detection of the transformation products by radio-HPLC

Chromatographic separation and quantification of SDZ and its transformation products in liquid samples was done by High Performance Liquid Chromatography (HPLC) and subsequent radioactivity measurement. An appropriate volume of the sample (10 to 200  $\mu\text{L}$ , depending on the  $^{14}\text{C}$ -concentration in the sample) was injected into the sample loop by an auto-sampler. The sample was then flushed through the chromatographic column with the eluent flow. The technical details of the employed chromatographic procedures are given in Table E.1. The outlet of the chromatographic column was connected to a radioactivity monitor employing an Yttrium-glass detector, which continuously measured the radioactivity in the outflow.

Each substance has a characteristic retardation time for a predefined chromatographic method. The retardation time of SDZ itself was determined by measuring the stock solution (0.5 g L<sup>-1</sup>  $^{14}\text{C}$ -labelled SDZ in acetonitrile). Radioactivity peaks appearing before or after the SDZ in sample chromatograms were attributed to transformation products of SDZ. Since a reversed phase column was employed, substances with higher polarity will elute earlier than less polar substances. However, the peaks of two or more species may overlap if the difference in retention is too small for the given chromatographic conditions.

The quantification of the various substances in one sample is done by integration of the respective peak areas in the chromatogram. The fraction of the area of one peak to the total area of all peaks gives the relative abundance of the substance in the sample. Concentrations are determined by multiplication of this fraction with the total  $^{14}\text{C}$ -concentration of the sample (measured by LSC) and the specific radioactivity of the substance. Since the transformation products are partially unknown (and, thus, their molar weight), concentrations are given as mass equivalents of SDZ. The detection limit of the radio-HPLC is at approximately 800 kBq L<sup>-1</sup>



(total  $^{14}\text{C}$ -radioactivity). It is higher in samples where the radioactivity is distributed among more substances.

Ideally, the chromatographic separation is optimized previous to the experimental sample analysis using analytical standard substances. However, the transformation products of SDZ were only discovered during the course of this study. To my knowledge the transformation products in soil were neither known nor commercially available as analytical standard substances at the beginning of our study. Although the radio-HPLC enabled the detection of unknown (transformation) products in the samples, it was of no help for their identification or characterization. The additional application of mass spectrometric methods allowed the allocation of the peaks in the radioactivity with the proposed transformation products (Section E.2).

The gain of knowledge regarding the transformation products of SDZ and their analysis is reflected in the stepwise improved chromatographic methods during our study. Method I (Table E.2, Figure E.1) was the first chromatographic attempt. It was used for the analysis of the batch samples in Appendix G. However, later analysis (Appendix E.2) showed that method I did not separate SDZ and the transformation product acetyl-SDZ. The improved HPLC-method II was used for the analysis of the BTC-samples. Subsequent trials then revealed that method III should be preferred in forthcoming investigations, because it achieves a better separation of the species (Figure E.1). Furthermore, two additional peaks appeared in method III (MB2, MB3). Since we have no information about the stability of the various species in the water samples during storage, the results of a repeated analysis of the stored samples using method III would have been questionable, and was hence omitted.

## E.2 Identification of the transformation products by LC-MS-MS

**Sample preparation** For the characterization of the transformation products separate samples were prepared with  $^{14}\text{C}$ -labelled and non-labelled SDZ. For this purpose high concentrations of the investigated substance are necessary, especially in presence of a complex sample matrix. However, previous investigations (Appendix G) indicated that higher total concentration levels do not imply higher relative concentrations of the transformation products. Therefore, samples were prepared at five concentration levels (3, 6, 12, 18, 24 mg L $^{-1}$  initial concentration in the liquid phase, sorbed concentrations initially zero).

Field moist soil and 0.01 M CaCl $_2$  solution were mixed (2.3 g dry soil + 23 mL solution) and spiked with the appropriate amount of stock solution of SDZ (0.5 g L $^{-1}$  in acetonitrile). The batch systems were shaken in the dark for five days before centrifugation and sampling of the liquid phase. Samples of the batch systems containing the  $^{14}\text{C}$ -labelled substance were analyzed by LSC (Appendix C) and radio-HPLC (method I, Appendix E.1). According to these results the batch systems with the highest concentration of the non-labelled transformation products were chosen for subsequent measurements in LC-MS-MS.

Table E.1: HPLC-methods for chromatographic separation of SDZ and its transformation products. Methods I and II were routinely applied for the sample analysis of the batch and BTC samples, respectively, method III should be considered for further investigations.

	Method I			Method II			Method III		
	Pre-column	Column	Flow rate	Pre-column	Column	Flow rate	Pre-column	Column	Flow rate
Pre-column	4 × 4 mm, Select B, Merck	4 × 4 mm, Select B, Merck	0.7 mL min <sup>-1</sup>	4 × 4 mm, Select B, Merck	4 × 4 mm, Select B, Merck	1.0 mL min <sup>-1</sup>	4 × 4 mm, Select B, Merck	4 × 4 mm, Select B, Merck	1.0 mL min <sup>-1</sup>
Column	Lichrosphere, RP, Select B 250 × 4.00 mm 5 μm	LUNA, Phenomenex 150 × 4.60 mm 5 μm Ultracarb ODS (30)	0.7 mL min <sup>-1</sup>	LUNA, Phenomenex 150 × 4.60 mm 5 μm Ultracarb ODS (30)	LUNA, Phenomenex 150 × 4.60 mm 5 μm Ultracarb ODS (30)	1.0 mL min <sup>-1</sup>	MZ Target SIL 125 × 4.60 mm 3 μm Gr 07	MZ Target SIL 125 × 4.60 mm 3 μm Gr 07	MZ Target SIL 125 × 4.60 mm 3 μm Gr 07
Temperature	25 °C	25 °C	25 °C	25 °C	25 °C	25 °C	25 °C	25 °C	25 °C
Eluent A	H <sub>2</sub> O + 0.1 % (v) H <sub>3</sub> PO <sub>4</sub> , pH = 2.5	H <sub>2</sub> O + 0.1 % (v) H <sub>3</sub> PO <sub>4</sub> , pH = 2.5	0.7 mL min <sup>-1</sup>	H <sub>2</sub> O + 0.1 % (v) H <sub>3</sub> PO <sub>4</sub> , pH = 2.5	H <sub>2</sub> O + 0.1 % (v) H <sub>3</sub> PO <sub>4</sub> , pH = 2.5	1.0 mL min <sup>-1</sup>	H <sub>2</sub> O (25 mmol L <sup>-1</sup> KH <sub>2</sub> PO <sub>4</sub> + 2 % (v) Methanol, pH = 3 with H <sub>3</sub> PO <sub>4</sub> )	H <sub>2</sub> O (25 mmol L <sup>-1</sup> KH <sub>2</sub> PO <sub>4</sub> + 2 % (v) Methanol, pH = 3 with H <sub>3</sub> PO <sub>4</sub> )	H <sub>2</sub> O (25 mmol L <sup>-1</sup> KH <sub>2</sub> PO <sub>4</sub> + 2 % (v) Methanol, pH = 3 with H <sub>3</sub> PO <sub>4</sub> )
Eluent B	Acetonitrile	Acetonitrile	0.7 mL min <sup>-1</sup>	Acetonitrile	Acetonitrile	1.0 mL min <sup>-1</sup>	Methanol	Methanol	Methanol
Gradient	time [min]	time [min]	time [min]	time [min]	time [min]	time [min]	time [min]	time [min]	time [min]
	A [%]	B [%]	A [%]	A [%]	B [%]	A [%]	A [%]	B [%]	B [%]
	0	30	0	100	0	0	0	100	0
	10	70	3	100	0	3	100	100	0
	15	64	11	80	20	23	43	57	57
	21	52	13	10	90	28	0	100	100
	23	25	21	10	90	32	0	100	100
	29	10	25	50	50	35	100	0	0
	32	70	28	100	0	45	100	0	0
	40	70	45	100	0				

Table E.2: Retention time (given in minutes after injection) of SDZ and its transformation products during HPLC.

Substance	Method I	Method II	Method III
MB1	3.0	2.7	3.7
Hydroxy-SDZ	4.2	11.7	13.3
SDZ	5.7 <sup>†</sup>	13.5	14.4
Acetyl-SDZ	5.7 <sup>†</sup>	14.8	18.0
MB2 <sup>‡</sup>	-	-	10.7
MB3 <sup>‡</sup>	-	-	16.7

<sup>†</sup>Acetyl-SDZ and SDZ were not separated by method I.

<sup>‡</sup>MB2 and MB3 were only detected with method III. However, at the time of measurement the samples were already stored for approximately one year.

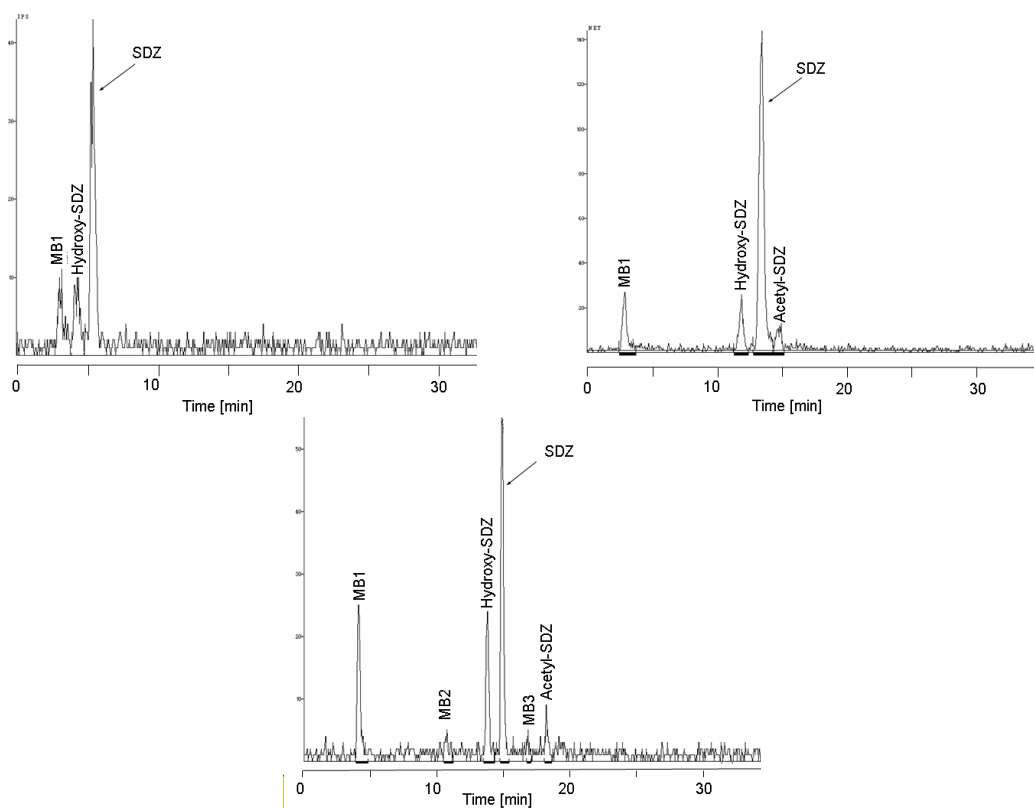


Figure E.1: Radio-HPLC-chromatograms of selected samples determined with method I (top left), method II (top right) and method III (bottom).

**Substance identification** The identification of the transformation products was kindly done by Prof. M. Spiteller and Sebastian Zühlke at the Institute of Environmental Research, University of Dortmund, Germany. They applied the LC-MS-MS (liquid chromatography coupled on tandem mass spectrometry) method of Pfeifer *et al.* (2002) and used full-scan, SIM (single ion monitoring) and SRM (selected reaction mode) modi for the identification of the substances. Due to the lack of analytical standard substances, a quantification of the transformation products was impossible.

Two transformation products were identified using LC-MS-MS. One is acetyl-SDZ, where an acetyl-group is attached to the amino-group connected to the phenyl-ring (Figure E.2). The other is hydroxy-SDZ, where a hydroxy-group is attached to the diazine-ring (Figure E.2). Its position was not further specified. Both substances were determined because of their characteristic fragment ions in tandem mass spectrometry (Table E.3).

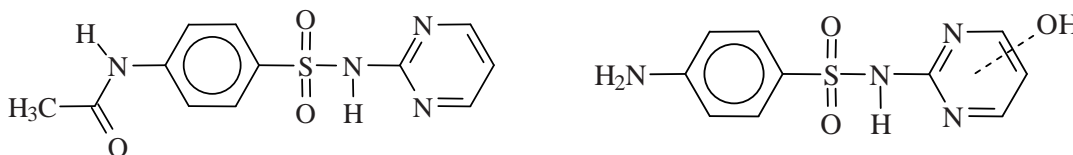


Figure E.2: Chemical structure of the identified transformation products of sulfadiazine, <sup>4</sup>N-acetylsulfadiazine (top) and hydroxy-sulfadiazine (bottom).

**Allocation of identified substances to peaks in radio-HPLC** Since the chromatographic conditions in the LC-MS-MS were different from the conditions in the radio-HPLC, further investigations were required to match the identified species with the peaks observed in the radio-HPLC. This was done by fractionation of the samples. 200  $\mu$ L of the sample exhibiting a high abundance of one species were injected into the HPLC-system. After the passage of the measuring cell, the outflow was collected during the expected time interval of the peak. The procedure was repeated several times to gain enough sample volume for the identification of the substance.

The sample fraction containing the first compound (3.0 minutes retardation time, method I) did not contain any of the identified substances and remained unidentified. The compound with the retardation time of 4.2 minutes (method I) was determined to be hydroxy-SDZ. Acetyl-SDZ was determined in the fraction which was expected to contain only SDZ (5.7 minutes retardation time, method I). Hence it was concluded that method I did not separate SDZ and acetyl-SDZ, and the chromatographic procedure was improved.

Table E.3: Characteristic fragment ions of SDZ, acetyl-SDZ and hydroxy-SDZ for tandem mass spectrometry and the respective collision energies.

Compound	$[M + H]^+$ † [u]‡	Fragment ions [ $m/z$ ]§	Collision energy [eV]¶
SDZ	251	92	36
		96	36
		156	22
		158	22
Acetyl-SDZ	293	65	44
		108	36
		134	30
		198	22
Hydroxy-SDZ	268	92	30
		113	26
		156	22
		175	22

†mass of ionized parent compound; ‡atomic mass unit; §ratio of fragment mass ( $m$ ) and charge ( $z$ ); ¶energy given in electron volt.

### E.3 Conclusions

The radio-HPLC and mass spectrometric methods were successfully combined to detect and partially identify three transformation products of SDZ. The use of  $^{14}\text{C}$ -labelled SDZ and radio-HPLC allowed the detection of unknown transformation products. Replicate samples with non-labelled SDZ allowed the LC-MS-MS identification of two out of three transformation products. This information was not only of primary interest but was also essential to improve the chromatographic separation of SDZ and the transformation products during HPLC. However, the application of method II for routine sample analysis was still bound to the detection limit of the radio-HPLC measurement, which was too high for the analysis of most samples. To overcome this limitation, an automated method might be established to fractionate the samples after the passage of the HPLC according to the characteristic retardation time of the compounds. These fractions may be measured subsequently by LSC, where the detection limit is lower.

LC-MS-MS is also applicable for the quantification of the various chromatographically separated substances in a sample. Quantification is usually done according to the ratio of the abundances of the substance to the corresponding internal standard. Deuterized  $\text{D}_4$ -SDZ was employed in our laboratory for the quantification of non-labelled SDZ. However, this method was not suitable for the  $^{14}\text{C}$ -labelled SDZ because of the variable  $^{14}\text{C}$ -labelling (Appendix A). The parent mass of the  $^{14}\text{C}$ -SDZ standard substance can range from 250 u (non-labelled substance) to 262 u (sixfold

labelled) in increments of 2 u. Hence, the masses of the twofold labelled species and the D<sub>4</sub>-SDZ were equivalent. Since all experiments were conducted with the <sup>14</sup>C-labelled SDZ, LC-MS-MS could not be used as a routine method of quantification of the parent compound.

# Appendix F

## Mineralization of $^{14}\text{C}$ -SDZ in wet soil

### F.1 Experimental setup

A microcosm study was conducted to investigate the mineralization of  $^{14}\text{C}$ -SDZ in wet soil under laboratory conditions. The initial SDZ concentration was  $100\ \mu\text{g}\ \text{kg}^{-1}$  dry soil. The experiment was conducted at  $20\ ^\circ\text{C}$  in the dark and at a constant gravimetric water content of 30 % during 105 days. The experimental setup was adopted according to *Kubiak et al.* (1995).

59 g of field moist soil (18 % gravimetric water content, soil properties given in Appendix B) were weighted into Erlenmeyer flasks. Each system was closed with a soda lime  $\text{CO}_2$ -trap. These  $\text{CO}_2$ -traps were glass tubes filled with two layers of granular  $\text{Na}_2\text{CO}_3$ , which were supported and separated by glass wool plugs. The lower soda lime fraction (10 g) was meant to absorb the evolving  $\text{CO}_2$  from the system, whereas the upper fraction (4 g) should absorb entering  $\text{CO}_2$  from the atmosphere. The systems were sealed airtight at the connection to the trap, so that an air exchange with the surroundings was only possible through the soda lime trap.

The soil in each system was spiked with 3 mL of a  $1.67\ \text{mg}\ \text{L}^{-1}$   $^{14}\text{C}$ -SDZ application solution. This application solution was prepared by diluting the appropriate volume of stock solution ( $0.5\ \text{g}\ \text{L}^{-1}$  in acetonitrile) with distilled water. The soil was then mixed with a stainless steel spatula to get a homogeneous distribution of SDZ. Finally, distilled water was added drop-wise to adjust the gravimetric water content to 30 %, which was controlled by weighting. The water was simultaneously used to wash off any soil sticking onto the spatula into the system to prevent soil and  $^{14}\text{C}$ -SDZ mass losses. The systems were then placed in a temperature controlled chamber at  $20\ ^\circ\text{C}$ .

The water loss due to evaporation was determined by weight loss and compensated weekly with distilled water. Before opening the systems for the water application, they were purged with nitrogen gas for three minutes, to flush the air in the system through the  $\text{CO}_2$ -trap and, thus, trap the  $^{14}\text{CO}_2$  quantitatively.

## F.2 Sampling and analysis

Sampling was done at 0, 7, 14, 21, 28, 42, 56, 77 and 105 days after spiking to determine the mineralized radioactivity in the soda lime traps as well as the  $^{14}\text{C}$  remaining in the soil as extractable or non-extractable residues. At each sampling time, three systems were dismantled. After purging the systems, the soda lime  $\text{CO}_2$ -traps were taken off and stored at  $-20\text{ }^\circ\text{C}$  until further analysis. The radioactivity in the soda lime was analyzed according to *Brumhard* (1991). The water content of the soil was determined by weighting before and after drying at  $105\text{ }^\circ\text{C}$ . The total  $^{14}\text{C}$ -concentration in the soil was determined after thorough homogenization and grinding according to the procedure described in Appendix D.

The extractable fraction of soil-bound radioactivity was determined immediately after sampling by microwave extraction. The microwave extraction was done with a solvent mixture of acetonitrile and water (8:2, v:v) adjusted to pH 2.2 using  $\text{H}_3\text{PO}_4$ . 5 g of the wet soil were extracted with 10 mL of the solvent at  $100\text{ }^\circ\text{C}$  for 30 minutes (heating time 10 minutes) in closed vessels in the microwave. After cooling down, the soil and the supernatant were separated by filtration. The extracted soil and the walls of the extraction vessel were rinsed once with 10 mL of solvent. The  $^{14}\text{C}$ -activity was determined in the solvent extract as well as in the extracted soil using the methods given in the Appendices C and D, respectively.

## F.3 Results

$^{14}\text{CO}_2$  was formed during the initial 42 days of the microcosm experiment (Figure F.1a). After this time, the fraction of mineralized  $^{14}\text{C}$ -SDZ remained constant at approximately 0.3 % of the applied radioactivity. The variation coefficient between the three replicates was 16 %. The total recovered  $^{14}\text{C}$ -radioactivity in the soil samples was between 91 % and 97 % of the calculated applied radioactivity, leaving up to 9 % of  $^{14}\text{C}$  non-recovered. This can be attributed to uncertainties in the total applied radioactivity during spiking, losses due to sorption on the spatula and the glass walls, losses of  $^{14}\text{CO}_2$  during short-term opening for water application, incomplete  $^{14}\text{CO}_2$  absorption by the soda lime trap during the initially fast mineralization, uncertainties in the water content or inhomogeneous SDZ distribution within the soil.

The extractable fraction of  $^{14}\text{C}$ -SDZ residues decreased from initially 70 % to approximately 20 % of the applied radioactivity within 20 days (Figure F.1b). Due to the low extraction efficiency for the aged soil residues and because of analytical difficulties, there is no reliable information on the presence of transformation products in the extractable  $^{14}\text{C}$  fraction. However, the occurrence of  $^{14}\text{CO}_2$  due to mineralization of  $^{14}\text{C}$ -SDZ hints towards transformation or degradation of SDZ. The intermediate products of these processes might be present in soil or soil solution.



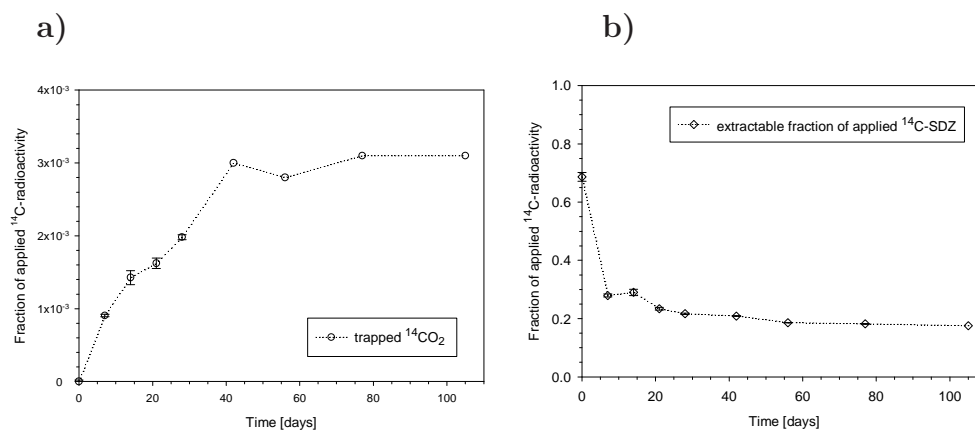


Figure F.1: Mineralization of  $^{14}\text{C}$ -SDZ in wet soil (Figure a). Decrease of extractable fraction of  $^{14}\text{C}$  residues in wet soil (Figure b). Vertical bars indicate the standard error of the three replicates.

## F.4 Conclusions

Mineralization of  $^{14}\text{C}$ -SDZ plays a minor role as potential sink of SDZ in moist soil under the prevailing laboratory conditions. Since mineralization occurs, intermediate products may persist in soil or soil water. However, the quantification and characterization of these transformation products is difficult, because the extractability of SDZ residues in soil decreases rapidly with time to approximately 20 %. The low extraction efficiency for aged SDZ residues hints either towards strong or irreversible sorption or an unsuitable extraction method.

# Appendix G

## Occurrence of the transformation products in soil-water systems

### G.1 Experimental setup

Batch sorption experiments were conducted to investigate the influence of time, total solute concentration and microbial activity on the occurrence of transformation products. To check the chemical stability of  $^{14}\text{C}$ -SDZ, control experiments were conducted in 0.01 M  $\text{CaCl}_2$  solution and in diluted soil solution. The experimental procedure is described in more detail in Section 2.3. Field moist soil and 0.01 M  $\text{CaCl}_2$  solution (8.5 g dry mass + 24 mL) were equilibrated for one week and spiked at four concentration levels (3.0, 1.5, 0.5, 0.25  $\text{mg L}^{-1}$ ) with  $^{14}\text{C}$ -SDZ.

Experiments with untreated, moist soil (equals experiment E, Section 2) were compared to experiments conducted using sterilized soil in order to investigate the influence of microbial activity on transformation. Sterilization was done by  $\gamma$ -irradiation (35 kilo Gray for 24 hours) at maximal 45 °C at the Research Reactor Division, Research Center Jülich GmbH. The sterility of the soil samples was tested at the beginning of the experiment according to the sterility test V.2.1.1 (*Deutsche-Arzneibuch-Kommission*, 2002). Since the batch systems were closed apart from the spiking and sampling times, colonization by microorganisms was assumed to be limited and no further test of sterility was performed. To check the stability of SDZ within the experimental time frame two control systems, which contained only 0.01 M  $\text{CaCl}_2$  with 3  $\text{mg L}^{-1}$   $^{14}\text{C}$ -SDZ, were run in parallel.

A separate experiment was conducted to assess whether the transformation of SDZ in soil-water batch systems occurs rather in the solid or the liquid phase. Since the analysis of the transformation products was restricted to liquid samples, the transformation of SDZ was investigated only in the soil solution. In comparison to the  $\text{CaCl}_2$ -solution control systems, the soil solution contained dissolved organic matter, salts and microorganisms. The diluted soil solution was prepared by continuously shaking 30 g (dry weight) of soil with 200 mL of a 0.01 M  $\text{CaCl}_2$  solution in the dark for two days and subsequent filtration. 25 mL of this diluted soil solution were spiked with  $^{14}\text{C}$ -SDZ to a final concentration of 2.1  $\text{mg L}^{-1}$ .

After spiking, all batch systems were shaken in the dark at 20 °C for 40 days.

Sampling of the soil solutions was done after centrifugation. Additionally to the quantification of the  $^{14}\text{C}$ -radioactivity by LSC (Appendix C) the transformation products were analyzed by radio-HPLC (method I, Appendix E.1). However, the applied method did not separate SDZ and the transformation product acetyl-SDZ.

## G.2 Results

Figure G.1 presents the concentrations of SDZ and its transformation products in the liquid phase for the various batch systems containing soil. SDZ concentrations of the batch systems with the lowest concentration level ( $0.5\text{ mgL}^{-1}$  for both, and  $1\text{ mgL}^{-1}$  for the sterile version) were below the detection limit of the radio-HPLC. The concentration of total  $^{14}\text{C}$  in the liquid phases of all batch systems decreased with increasing time due to slow sorption kinetics (Section 2). After about 15 days approximately constant  $^{14}\text{C}$ -concentrations were reached. This apparent equilibrium concentration is higher in non-treated soil than in the sterilized soil. This change in sorption affinity may hint towards changes of the soil structure during the exposure to  $\gamma$ -irradiation.

The transformation products of SDZ were rapidly formed in all systems. Only in the sterile systems, MB1 was not present after one day of incubation. In the fresh soil systems Hydroxy-SDZ amounted to 18 to 23 % of the total radioactivity one day after spiking, whereas its fraction was lower (5 to 8 %) in the sterile soil systems. The concentrations of the transformation products showed some changes with time. However, the concentration of SDZ and acetyl-SDZ decreased, thus, the fraction of MB1 and hydroxy-SDZ on total radioactivity increased during the course of the experiment. Additionally, the relative abundance of the transformation products seems to increase at lower total concentration in the system. The fraction of MB1 and hydroxy-SDZ on total radioactivity was initially smaller in the sterile batch systems. However, it was higher in the sterile than in the fresh soil systems 40 days after application (initial concentration  $5\text{ mg L}^{-1}$ ).

In the systems without soil material (soil solution or  $0.01\text{ M CaCl}_2$ ) no transformation products were detected within the experimental time frame. The particle surfaces of the soil material seem to be essential for the transformation processes.

## G.3 Conclusion

The experiments hint towards a fast transformation of SDZ in the soil environment. Since the transformation products were also present in the sterile batch systems shortly after contamination, the transformation process is at least partially abiotic. The abundance of the transformation products depends on the incubation time and on the total concentration in the system. Since transformation and sorption/desorption processes occur simultaneously in the soil-water systems, the interpretation of the experimental data is complicated. Additionally, transformation occurred only in the presence of soil particles. Thus, the processes of sorption and transformation cannot be separated for an experimental process investigation.

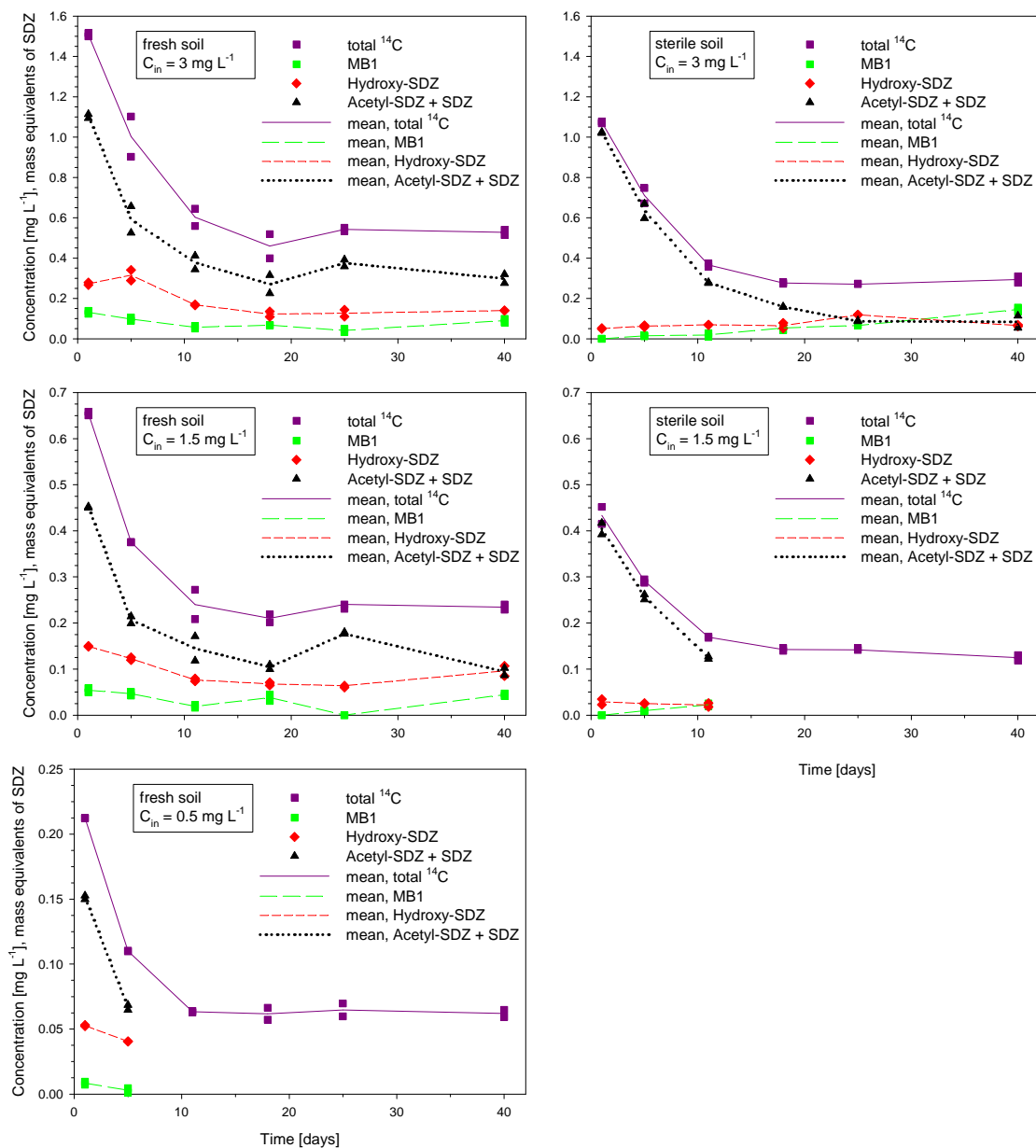


Figure G.1: Transformation of SDZ in batch systems with fresh and sterilized soil. The symbols indicate the two replicates, the lines the respective mean values.  $C_{in}$  is the initial concentration in the liquid phase in the batch systems (solid phase concentrations are initially zero). No radio-HPLC data are available in the lower concentration range.

# Appendix H

## Chemicals and Instruments

### H.1 Chemicals

acetonitrile	Merck KGaA, Darmstadt, Germany
acetonitrile (HPLC)	Economy Grade, LGC-Promochem, Wesel, Germany
CaCl <sub>2</sub>	Merck KGaA, Darmstadt, Germany
KH <sub>2</sub> PO <sub>4</sub>	Merck KGaA, Darmstadt, Germany
liquid scintillation cocktail	Instant Scint-Gel Plus, Canberra Packard GmbH, Dreieich, Germany
liquid scintillation cocktail	Oxysolve C-400, Zinsser Analytics, Germany
methanol	Merck KGaA, Darmstadt, Germany
methanol (HPLC)	Economy Grade, LGC-Promochem, Wesel, Germany
millipore water	Milli-Q Plus 185 with QPAK2, Millipore, Eschborn, Germany
Na <sub>2</sub> CO <sub>3</sub>	Merck KGaA, Darmstadt, Germany
phosphoric acid (25 %)	Grüssing Diagnostika, Filsum, Germany
SDZ	Sigma Aldrich, Taufkirchen, Germany
<sup>14</sup> C-SDZ	Institute of Isotopes Co. Ltd., Budapest, Hungary
D <sub>4</sub> -SDZ	Toronto Research Chemicals, Toronto, Canada

## H.2 Instruments

analytical balance	BP211D, Sartorius, Göttingen, Germany
annealing oven	Herareus, Germany
balance	PG 5002-S, Mettler Toledo, Giessen, Germany
biological oxidizer	Robox 192, Zinsser Analytik GmbH, Frankfurt, Germany
centrifuge	J2-21, Beckmann, Palo Alto, US
centrifuge	Allegra 6KR, Beckmann-Coulter, Palo Alto, US
conductivity meter	Inolab, WTW, Weilheim, Germany
drying oven	Tv 30b, Memmert, Schwabach, Germany
fraction collector	RF-III, Köhler Technik, Neulussheim, Germany
horizontal shaker	SM-25, SM-30, Edmund Bühler GmbH, Tübingen, Germany
liquid scintillation counter	2500 TR, Packard Bioscience GmbH, Dreieich, Germany
microwave	MLS Ethos 1600, MLS Leutkirch, Germany
pH-meter	MP 230, Mettler Toledo, Giessen, Germany
planetary ball mill	PM400, Retsch, Haan, Germany
pump (transport experiments)	HPLC-pump K-500, Knauer, Berlin, Germany
sieve for analytics	2 mm sieve, Retsch, Haan, Germany Radio-HPLC
pump	PU1580, Jasco, Gross-Umstadt, Germany
autosampler	Gina 50, Gynkotec, Germering, Germany
column oven	ST585, Gynkotec, Germering, Germany
radio detector	LB506-C, YG-150U4D, Berthold, Bad Wildbad, Germany LC-MS-MS
pump and column oven	Agilent 1100, Agilent, Waldbronn, Germany
autosampler	HTC PAL, CTC Analytics, Chromtec, Germany
ESI, MS-MS	TSQ-Quantum, Thermofinnigan, Dreieich, Germany

## Acknowledgements

This work benefited tremendously from the expert attention it received from numerous individuals. First I want to thank my referee Prof. Harry Vereecken, head of the ICG-IV, Agrosphere, Forschungszentrum Jülich GmbH, and Dr. Joost Groeneweg, head of the project "Veterinary pharmaceuticals in soils", for the chance to conduct this research at their institute.

This undertaking would have gone nowhere without the considerable assistance from many colleagues of the Agrosphere and the nice working atmosphere. For numerous discussions in our project I am grateful to Yvonne Zielesny, Joost Groeneweg, Wolfgang Tappe and Dr. Narres. Thanks to Erwin Klumpp and Attila Bota who substantially supported the organization of the  $^{14}\text{C}$ -labelled substance. For their explanation and discussion regarding the  $^{14}\text{C}$ -tracer technique I am grateful to Martina Krause, Ulrike Langen, Anne Berns, Frauke Schnitzler and Werner Mittelstädt. I am indebted to Anna Galinski, Christian Reimers and Armin Arnecke for their splendid help in the lab and the cheerful atmosphere. Stephan Köppchen did an excellent job at the radio-HPLC and the LC-MS-MS and I am grateful for his patience with my non-standard questions and applications. A special thanks to Jürgen Höltkemeier for his endless treasure of tricks to circumvent technical problems as well as his good spirits. Anke Langen and Odilia Esser greatly contributed to this work with the chloride analysis. Thanks to Swen Gottschalk, whose Maple-support made maths so much easier.

For his expert advise and his kind way to encourage and challenge me and my work alike I am especially indebted to Roy Kasteel. He kept an eye on my work and his door and mind were always open for my latest questions.

My research was informed by the work of fellow colleagues in the group Water and Agriculture at the EAWAG, Switzerland, Maren Kahle, Michael Burkhardt, Krispin Stoob, Heinz Singer and Christian Stamm. They did not only supply the soil of investigation but provided analytical experience, inspiration and discussion during several fruitful meetings.

I gratefully acknowledge the contribution of Dr. Sebastian Zühlke and Prof. Spittler, University Dortmund, for their analytical expertise and the identification of the transformation products.

I owe a special thanks to Prof. Thilo Streck, who was always interested in my work and provided not only the *fithyst*-model and its modifications but also valuable comments. Sven Altfelder was of considerable help during the first modelling exercises and kindly provided explanations and discussion when needed.

For adapting the *HYDRUS-1D*-code to my needs, his immediate and patient e-mail consultancy, the sunny autumn in his group and fruitful discussions I am especially thankful to Prof. Jirka Simunek.

I am grateful to Maren Kahle, Roy Kasteel, Joost Groeneweg, Harry Vereecken and Jirka Simunek for reading early and partial drafts of the manuscript and providing helpful feedback.

Thanks to Eva, Andrea, Anne, Kerstin, Thomas, Lutz, Ferdi and Alex for companionship and training my stamina during the lunchtime-running. Last but not least, a special thanks to my parents, family and friends who always gave encouragement and counsel when needed.